

**BEHAVIOUR OF SAND IN MONOTONIC AND CYCLIC SIMPLE SHEAR LOADING
AT LOW-STRESS LEVEL**

by

© Mahmud Amer Al Tarhouni

A Thesis submitted to the

School of Graduate Studies

in partial fulfillment of the requirements for the degree of

Doctor of Philosophy

Faculty of Engineering and Applied Science

Memorial University of Newfoundland

January 2021

St. John's

Newfoundland

Canada

ABSTRACT

Geotechnical engineers deal with sands of varying in-situ (initial) conditions that develop through the process of land formation in natural environments and geotechnical constructions, such as compaction. The formation and construction processes can give different sand particle arrangement (fabric), which could significantly influence the behaviour of sand in subsequent loading. Geotechnical properties of sand are generally obtained from laboratory tests on reconstituted samples because of difficulties in collecting undisturbed sand samples from the field. The sample is sheared typically in direct shear and triaxial conditions, and in simple shear mode in some advanced laboratories. Soil strength depends on effective stress. In the field, sometimes the effective stress could be very low, in the order of 10–30 kPa, such as the soil around buried pipelines and near the seabed surface; however, in many cases, such as the soil around shallow and pile foundations, medium to high effective stresses are encountered.

In the present study, the monotonic and cyclic behaviour of sand is investigated for simple shear loading conditions with a particular focus on the behaviour at low-stress levels. The laboratory tests were conducted using a combined advanced dynamic cyclic simple shear apparatus with a high-precision feedback system for controlling and measuring the forces and displacements while maintaining a high level of accuracy, which is essential, especially for tests at low normal stresses. The direct simple shear (DSS) tests were conducted on dry loose to dense sand under constant normal stresses of 12.5 kPa–400 kPa to investigate the effects of confining pressure on stress–strain behaviour. The monotonic test results show an increased shear to normal stress ratio, and thereby the mobilized friction angle, at the low-stress level, compared to high normal stresses. The strain-controlled (constant strain amplitude) cyclic test results show that the stress–strain behaviour and cyclic compaction are governed by the normal stress and shear strain amplitude.

The sand becomes densified when the applied shear strain amplitude is greater than a threshold value. DSS tests were also conducted with stress-controlled loading conditions by applying a constant stress amplitude cyclic loading. In strain-controlled tests, the lower the normal stress, the higher the compaction is; however, an opposite trend exists in stress-controlled (constant stress amplitude) cyclic tests.

Multistage cyclic tests under a wide range of constant normal stresses were conducted on dry sand by applying stress- and strain-controlled cyclic loads. Test results show that the volumetric compaction depends on normal stress and shear strain amplitude. The cyclic shear modulus and damping ratio are not affected by the low-amplitude cyclic loading history. The cyclic stress–dilatancy relationship depends on stress level, number of cycles, and shear strain amplitude. After a few cycles, the stress–dilatancy can be expressed by two parallel lines for loading and unloading, except for the initial part of the loading and unloading paths. The DSS test results show a good agreement with the results of hollow cylinder torsional shear tests.

The effects of confining pressure and reconstituted sand sample preparation method on the behaviour of sand in the direct simple shear and triaxial compression modes are also investigated. The DSS tests were conducted on sand samples prepared by four methods: funnel raining, multiple-sieve raining, dry tamping, and table tapping. In addition to the monotonic DSS tests under constant vertical stress, a set of undrained DSS tests was conducted by maintaining a constant height of the sample during shearing, using the advanced computer-controlled system. Based on stress–strain response, it is inferred that the table tapping could give a stronger fabric than that of dry tamping and multiple-sieve raining methods. In the undrained tests, the phase transformation and steady-state lines in the stress space change by 3° – 4° due to specimen preparation method, relative density and the initial consolidation pressure.

This thesis is dedicated to my late father, late mother and late sister,
who inspired me to continually reach for knowledge and wisdom
wherever I may find it.

ACKNOWLEDGMENTS

I would like to acknowledge and express my utmost gratitude to my supervisor, Dr. Bipul Hawlader, Professor and Research Chair in Seafloor Mechanics, Memorial University of Newfoundland, Canada, for his continuing support, guidance and encouragement throughout my Ph.D. program. Without his timely advice and generous help, this endeavor would not have been successful. I would also like to thank my co-supervisor and supervisory committee member, Dr. Ashutosh Dhar and Dr. Amgad Hussein, for their invaluable suggestions and comments. My sincere thanks go to Mr. Anup Fouzder, a Research Assistant, for his help with some of the experiments in my research.

Also, I would like to thank the Civil Engineering staff of Memorial University of Newfoundland, Canada, for having enriched my knowledge with their excellent courses, along with expressing great appreciation for the staff of GDS Instruments Ltd, for help and continuing support with the Combined Advanced Dynamic Cyclic Simple Shear (ADVDCSS).

I would like to express my sincere admiration to the Geological Engineering Department at the University of Tripoli, Libya, for giving me an opportunity to do my Ph.D. abroad. Also, I want to praise and express my sincerest thanks to the state of Libya for giving me a scholarship. Without the financial support, I would not have been able to conduct this research. I am thankful for supports from NSERC, RDC, and CFI, Canada for funding the ADVDCSS.

I would like to thank all of my family in Libya, especially my brothers, sisters, my father-in-law and his family for encouraging me during my studies. Finally, I owe my loving thanks to my wife, Reima Sharif, for her patience, and for taking care of our children, Yakean, Mohamed, Ayesha and Noor, throughout our years in Canada. Without her encouragement and understanding, it would have been impossible for me to finish this work.

Table of Contents

ABSTRACT..... **i**

ACKNOWLEDGMENTS..... **iv**

Table of Contents..... **v**

List of Figures..... **xii**

List of Tables..... **xvii**

List of Symbols..... **xviii**

CHAPTER 1..... **1**

Introduction..... **1**

 1.1 Background and Motivation..... 1

 1.2 Rationale 7

 1.3 Objectives..... 7

 1.4 Thesis Organization..... 9

 1.5 Significant Contributions 10

CHAPTER 2..... **11**

Literature Review..... **11**

 2.1 Introduction..... 11

 2.2 Sand Behaviour under Drained Monotonic Loading 11

 2.3 Sand Behaviour under Undrained Monotonic Loading 14

2.4 Sand Behaviour under Constant Stress Cyclic Loading	17
2.4.1 Stress–strain and Volume Change Behaviour.....	17
2.4.2 Factors Affecting Volumetric Strain.....	18
2.4.3 Stress–dilatancy Relationship under Cyclic Loading	21
2.5 Effects of Sample Preparation on Sand Behaviour	27
2.6 Influence of Loading Mode on Sand Behaviour	29
2.7 Dynamic Properties of Sand.....	32
2.8 An Overview of Direct Simple Shear Apparatus	35
2.9 Stresses and Strains in Triaxial Compression and Direct Simple Shear	39
2.10 Summary	42
CHAPTER 3.....	43
Monotonic and Cyclic Behaviour of Sand in Direct Simple Shear Test Conditions	
Considering Low-Stresses	43
Abstract:	43
3.1. Introduction.....	44
3.2. Direct Simple Shear Apparatus	47
3.2.1. Apparatus Capabilities	49
3.2.2. Load and Displacement.....	50
3.2.3. Data Acquisition and Control	51
3.2.4. Interpretation of Stress State in DSS Specimen.....	51

3.3. Method	53
3.3.1. Materials	53
3.3.2. Specimen Preparation	53
3.3.3. Repeatability	54
3.4. Test program	55
3.5. Monotonic DSS Test Results	55
3.5.1. Stress–strain Behaviour	55
3.5.2. Mobilized Dilation Angle	57
3.5.3. Critical State and Peak Friction Angles	58
3.5.4. Practical Implications.....	60
3.6. Strain-controlled (constant strain amplitude) Cyclic DSS Test Results	62
3.6.1. Stress–strain Behaviour	62
3.6.2 Influence of Normal Stress and Strain Amplitude on Cyclic Behaviour.....	62
3.7. Stress-controlled (constant stress amplitude) Cyclic DSS Test Results	64
3.7.1. Stress–strain Behaviour	65
3.7.2. Effect of Normal Stress on Volumetric Strain.....	65
3.8. Conclusions	66
Acknowledgments.....	68
Notation.....	68
References	70

CHAPTER 4.....	96
Drained Cyclic Behaviour and Stress–Dilatancy Relationship of Sand in Direct Simple Shear Tests.....	96
Abstract	96
4.1. Introduction	97
4.2. Experimental Works.....	100
4.2.1 Direct Simple Shear Apparatus.....	100
4.2.2 Material Tested	101
4.2.3 Cyclic Tests.....	101
4.3. Observed Stress–strain Behaviour	103
4.3.1 Single-stage Test.....	103
4.3.2 Typical Response of Multistage Cyclic Test	104
4.3.3 Effects of Vertical Stress and Strain Amplitude in Multistage Tests	106
4.3.4 Volumetric Strain without Cyclic Loading History.....	107
4.3.5 Effects of Vertical Stress on Volumetric Strain in Multistage Tests.....	107
4.4. Dynamic Properties	109
4.4.1 Shear Modulus	109
4.4.2 Effects of Number of Cycles on Shear Modulus	109
4.4.3 Effects of Strain History on Shear Modulus	110
4.4.4 Empirical Correlation of Shear Modulus.....	111

4.4.5 Damping Ratio	111
4.5. Stress-dilatancy in DSS Tests	112
4.5.1 Stress–dilatancy in Strain-controlled (constant strain amplitude) Cyclic DSS Tests	113
4.5.2 Effect of Normal Stress on Stress–dilatancy	114
4.5.3 Stress–dilatancy in Multistage Tests.....	115
4.5.4 Stress–dilatancy in Stress-controlled (constant stress amplitude) Tests.....	117
4.6. Conclusions	118
Acknowledgments.....	120
Notation.....	120
References	121
CHAPTER 5.....	150
Effects of Confining Stress and Sample Preparation Methods on Behaviour of Sand in Direct Simple Shear and Triaxial Tests.....	150
Abstract	150
5.1 Introduction.....	151
5.2 Materials.....	153
5.3 Apparatus for Shear Testing.....	153
5.3.1 Direct Simple Shear	153
5.3.2 Triaxial.....	154
5.4 Direct Simple Shear Sample Preparation	155

5.4.1 Funnel Raining (FR)	155
5.4.2 Multiple-sieve Raining (MSR)	156
5.4.3 Dry Tamping (DT).....	157
5.4.4 Table Tapping (TT)	157
5.5 Summary of the Conducted DSS Tests.....	157
5.6 Constant Stress DSS Test Results	158
5.6.1 Multiple-sieve Raining (MSR) Method.....	158
5.6.2 Funnel Rain (FR) Method.....	159
5.6.3 Dry Tamping (DT) Method	160
5.6.4 Table Tapping (TT) Method	160
5.7 Discussion on Constant Stress DSS tests	162
5.7.1 Dense Sand.....	162
5.7.2 Loose Sand.....	165
5.8 Constant Height DSS Tests Results	166
5.8.1 Sample preparation	167
5.8.2 Test Results.....	168
5.9 Drained Triaxial Compression Tests.....	171
5.9.1 Specimen Preparation and Testing.....	171
5.9.2 Drained Triaxial Compression Test results.....	172
5.9.3 Comparison of DSS and TXC Test Results.....	173

5.10 Conclusions	174
Acknowledgments	176
Notation.....	176
References	177
CHAPTER 6.....	200
Conclusions and Recommendations for Future Research	200
6.1 Conclusions	200
6.2 Recommendations for Future Studies	204
REFERENCES.....	205

List of Figures

Fig. 1.1 Increase in density of seabed sand due to wave loading (Clukey et al. 1989)	2
Fig. 1.2 Cyclic loading on offshore foundations (Arshad and O’Kelly 2013)	4
Fig. 1.3 Simple shear loading conditions in the field	5
Fig. 1.4. Effect of friction and dilation angle on uplift resistance of pipe: (a) simplified limit equilibrium method (modified from White et al. 2008); (b) finite element analysis based on mobilized friction and dilation angles (Roy et al. 2018)	6
Fig. 2.1 Dilation of dense sand in a simple shear test (Houlsby 1991).....	12
Fig. 2.2. Undrained behaviour of sand at different relative densities in monotonic triaxial compression tests: (a) stress–strain response, (b) stress path, (Vaid and Chern 1985)	16
Fig. 2.3. Stress–strain and volume change in a cyclic drained direct simple shear test (Finn et al. 1982)	17
Fig. 2.4. Compaction of a DSS sample under 48 kPa vertical stress due to cycling loading (Youd 1972)	19
Fig. 2.5. Effect of vertical stress on vertical strain in DSS tests (Duku et al. 2008)	19
Fig. 2.6. Effect of cyclic shear strain amplitude on volumetric strain of dense sand (Kang et al. 2016)	20
Fig. 2.7. Effect of confining pressure on volumetric strain of dense sand (Kang et al. 2016)	20
Fig. 2.8. Shear stress ratio–dilatancy rate in constant load cyclic drained simple shear tests (Ueng and Lee 1990)	22
Fig. 2.9. Stress–dilatancy relationship for medium dense sand under torsional simple shear loading (Shahnazari and Towhata 2002)	23

Fig. 2.10. Effect of sample preparation methods on the stress–strain response of Syncrude sand under undrained simple shear loading (Vaid et al. 1995)	28
Fig. 2.11. Accumulated axial strain variation with initial relative density for different methods of sample preparation in drained triaxial tests (Wichtmann and Knittel 2020)	29
Fig. 2.12. Influence of loading mode on the monotonic behaviour of sand (Yoshimine et al. 1999)	31
Fig. 2.13. Influence of shearing mode on behaviour of medium and dense sand (Yang et al. 2016)	32
Fig. 2.14. Definitions of the shear modulus and damping ratio.....	33
Fig. 2.15. Dynamic properties: (a) Shear modulus; (b) damping ratio (Kramer 1996)	34
Fig. 2.16. Damping ratio of very dense sand in large shear strains (Blaker and Andersen 2019)	35
Fig. 2.17. Two types of direct simple shear apparatus.....	36
Fig. 2.18. Different sample confinements configuration of simple shear apparatuses	37
Fig. 2.19. Stress non-uniformity in DSS specimen based on elastic theory (Roscoe 1953).....	38
Fig. 2.20. Stresses and strains in triaxial and direct simple shear specimens	41
Fig. 3.1. Apparatus used: (a) Combined Advanced Dynamic Cyclic Simple Shear apparatus; (b) Schematic of DSS apparatus	76
Fig. 3.2. Stresses and strains in triaxial and direct simple shear specimens	78
Fig. 3.3. Grain size distribution of silica sand used in this study	79
Fig. 3.4. Repeatability in cyclic direct simple shear test	80
Fig. 3.5. Effects of normal stress on monotonic test results: (a) Stress–strain behaviour; (b) Stress ratio; (c) Volume change; (d) Mobilized dilation angle	81

Fig. 3.6. Effects of normal stress on friction angles: (a) critical state friction angle; (b) peak friction angle.....	85
Fig. 3.7. Stress–strain response in first cycle of loading for varying normal stresses	87
Fig. 3.8. Stress–strain response for varying normal stresses at low-strain amplitudes.....	88
Fig. 3.9. Axial strain for varying normal stresses and shear strain amplitudes in constant strain amplitude cyclic tests	89
Fig. 3.10. Effects of normal stress on axial strain at 15 cycles in strain-controlled tests	90
Fig. 3.11. Stress–strain response in stress-controlled cyclic tests at low stress for 100 cycles	91
Fig. 3.12. Effects of normal stress on axial strain in constant stress amplitude cyclic loading....	92
Fig. 3.13. Normalized axial strain in stress- and strain-controlled tests	93
Fig. 4.1. Typical response: (a) shear stress–strain behaviour; (b) axial strain in 1000 cycles; (c) axial strain in 15 cycles; (d) stress ratio and axial strain variation	126
Fig. 4.2. Development of axial strain in multistage test T3.....	129
Fig. 4.3. Effect of normal stress and shear strain amplitude on cyclic behaviour (Test T8 and T13)	130
Fig. 4.4. Axial strain generation in first stage of cyclic loading in dense (T14–T18) and loose (T23–T25) specimens for shear strain amplitude of 1%	131
Fig. 4.5. Accumulated axial strain at 15 cycles of each stage in multistage tests on dense (T14–T18) and loose (T23–T25) specimens	132
Fig. 4.6. Relative density at the end of each stage in multistage tests on dense (T14–T18) and loose (T23–T25) specimens	133
Fig. 4.7. Effects of the small-strain amplitude loading on axial strain in large-amplitude loading for dense sand	134

Fig. 4.8. Typical hysteresis loops at different cycles	135
Fig. 4.9. Effects of shear strain amplitude and number of cycles on shear modulus.....	136
Fig. 4.10. Effects of shear strain amplitude on shear modulus at 15 th cycle for varying cyclic loading histories and normal stresses.....	137
Fig. 4.11. Shear modulus: (a) effects of normal stress and shear strain amplitude; (b) effects of shear strain amplitude on K and m parameters	138
Fig. 4.12. Effects of shear strain amplitude and normal stress on damping ratio.....	140
Fig. 4.13. Cyclic stress–dilatancy response in test T1 ($\sigma'_z = 100$ kPa, $\gamma_a = 1\%$): (a) initial loading and subsequent five cycles; (b) at large number of cycles.....	141
Fig. 4.14. Effects of normal stress on stress ratio–dilatancy in 1 st cycle for strain amplitude of 1%, (Tests T14–T18).....	143
Fig. 4.15. Stress–dilatancy in multi-stage cyclic test: (a) normal stress 12.5 kPa; (b) normal stress 400 kPa.....	144
Fig. 4.16. Stress ratio–dilatancy in stress-controlled tests: (a) effects of number of cycles; (b) effects of normal stress	146
Fig. 5.1. Grain size distribution of silica sand	185
Fig. 5.2. Sample preparation methods	186
Fig. 5.3. Constant stress tests on loose and dense repeatable samples: (a) stress-strain behaviour; (b) volume change behaviour.....	187
Fig. 5.4. Effects of sample preparation: (a) stress–strain behaviour; (b) volume change behaviour	189

Fig. 5.5. Constant height tests: (a) Stress–strain behaviour; (b) Normalized stress–strain behaviour;
(c) Variation of stress ratio of very dense specimens prepared by dry tamping and table tapping;
(d) Stress path 191

Fig. 5.6. Drained triaxial test results: (a) Stress–strain behaviour; (b) Stress ratio; (c) volume
change 195

List of Tables

Table 2.1 Stress–dilatancy relationship in cyclic simple shear loading.....	24
Table 3.1. Summary of direct simple shear test conditions	94
Table 4.1 Summary of test conditions	148
Table 5.1 Summary of direct simple shear and triaxial test conditions	198

List of Symbols

As the thesis is written in manuscript format, the symbols used in this study are listed and defined in each chapter (Chapters 3–5).

CHAPTER 1

Introduction

1.1 Background and Motivation

Sand might be subjected to various types of loading—from monotonic to cyclic loading, at a wide range of amplitudes, frequencies and durations in drained and undrained conditions. In many practical geotechnical engineering problems, such as soil under shallow foundations, backfills and typical slopes, the soil might simply experience a monotonic loading. On the other hand, a cyclic loading might be resulted from waves, wind, traffic, machine vibrations and earthquakes.

Two key parameters of sand that govern the geotechnical design for drained condition are the angles of internal friction (ϕ') and dilation (ψ). Laboratory and field tests are conducted to determine these parameters. Among the laboratory tests, direct shear (DS) and triaxial compression (TXC) are the most popular. In these tests, the soil sample is consolidated by applying normal stress in DS and confining pressure in TXC in the range of 100–500 kPa and then sheared. Tests outside this pressure range have also been performed but have been limited. However, in many geotechnical problems, monotonic and cyclic behaviour of sand at a low-stress level is required. Some examples are given below.

Buried pipelines are widely used to transport oil, natural gas and water, in both onshore and offshore environments. Typically, it is buried within 1 m to 2 m from the ground surface. Therefore, pipeline–soil interaction is governed by the low effective stress of the soil around the pipe. In most of the cases, the backfill materials are placed in loose to medium dense conditions. However, natural events, such as wave loading in offshore, and traffic loading in onshore, might densify the soil. As an example, Figure 1.1 shows the density of the soil near the seabed where a test pipe section was installed at 9.1-m water depth at Mobile Bay, Alabama, in the Gulf of Mexico (Clukey

et al. 1989). The sand seabed was loose during installation—after one week, the relative density was 57%, which increased to about 70% within two weeks. The soil became very dense (relative density ~90%) after five months. Two key points in this example are: (i) low frequency drained cyclic loading can densify the soil significantly; (ii) the response of a pipeline should be investigated for loose to dense conditions, with special attention to the low-stress level.

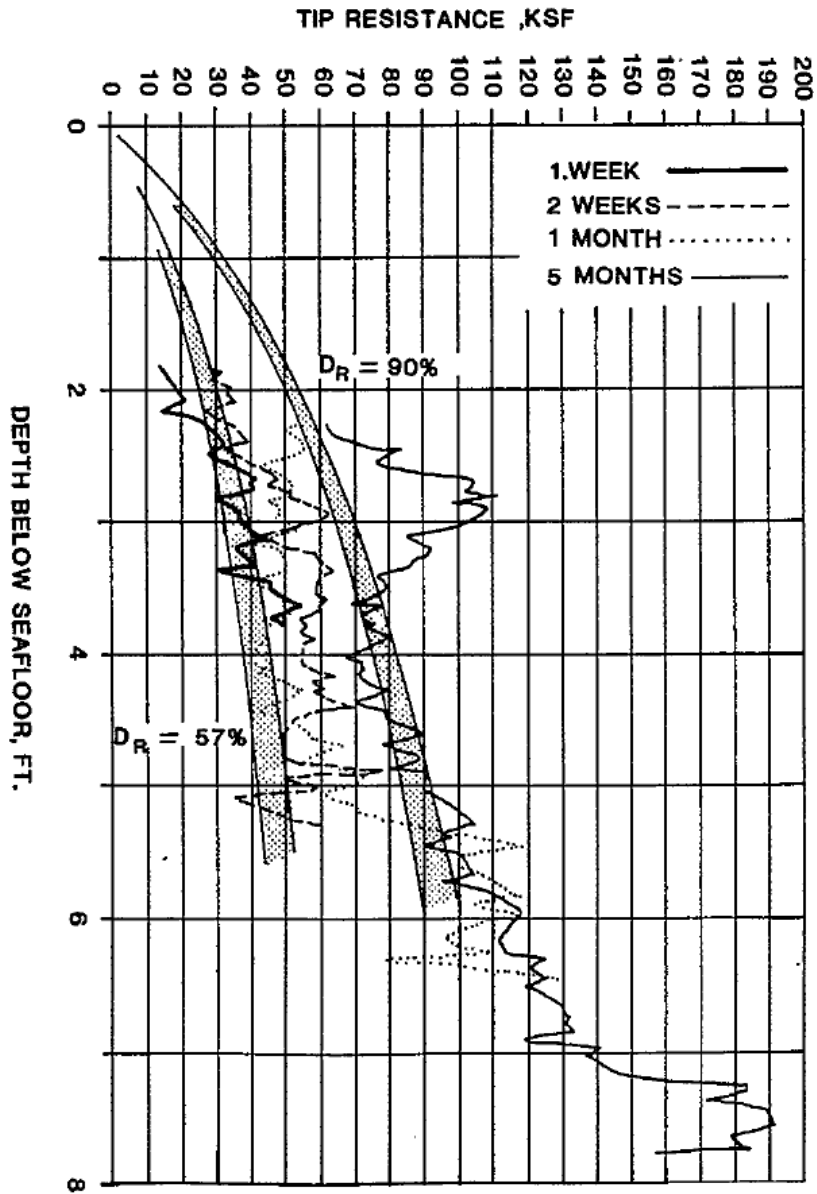


Fig. 1.1. Increase in density of seabed sand due to wave loading (Clukey et al. 1989)

Cyclic compaction not only occurs in the offshore environment due to wave loading, but also in onshore cohesionless soils due to earthquakes, machine vibration and traffic loading. For example, traffic-load-induced dynamic stress can cause a permanent (plastic axial strain) compaction settlement of the road laying on loose sand. Also, the excessive settlement due to cyclic loading might cause damage to structures. Therefore, the volume change of sand due to cyclic loading became a subject of research several decades ago (e.g., Silver and Seed 1971; Youd 1972).

Cyclic loading due to wind and waves also affects the soil behaviour around the foundation. For example, different types of innovative foundations have been used for offshore wind turbines, as shown in Fig. 1.2. These foundations are subjected to cyclic loading due to waves, currents, and wind. In the design of these foundations, not only for low-stress level, but also for sufficiently large stress level, cyclic behaviour is needed.

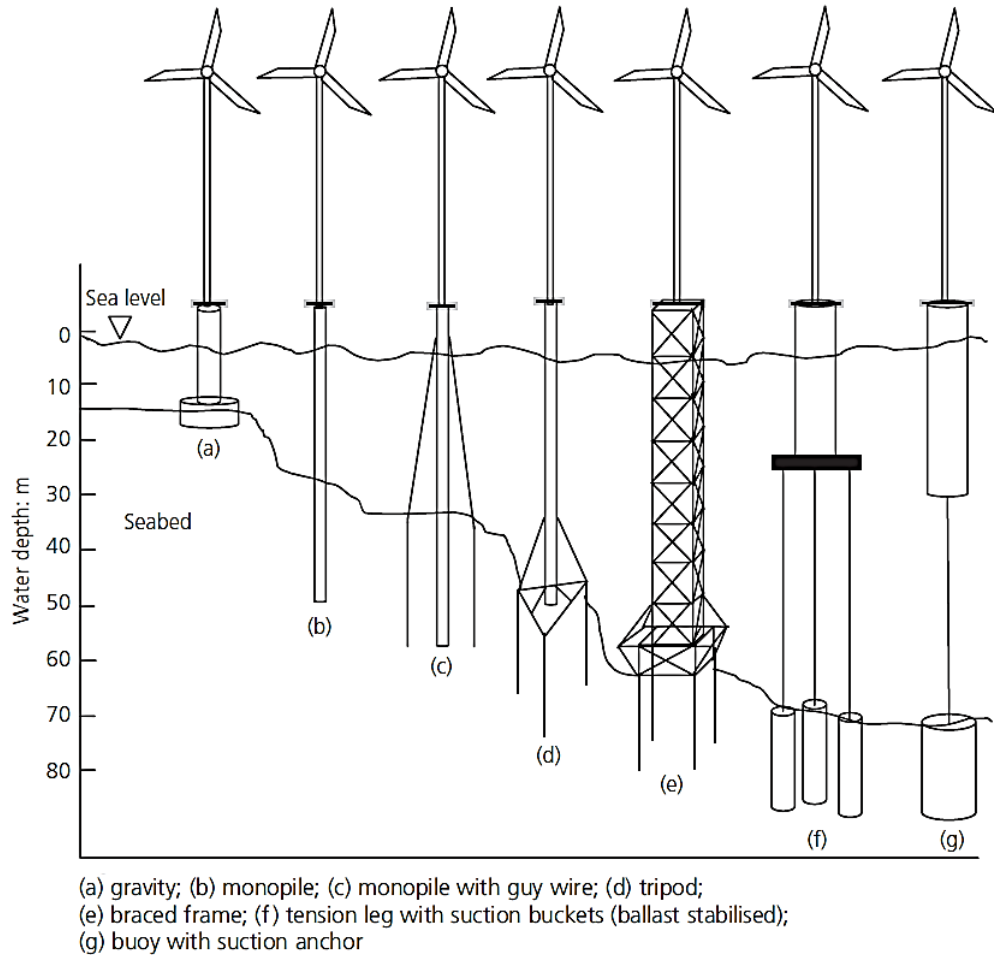
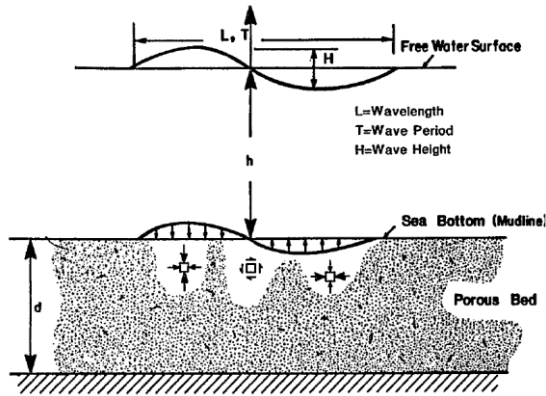


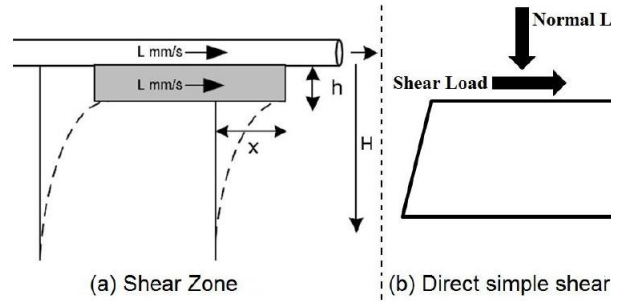
Fig. 1.2. Cyclic loading on offshore foundations (Arshad and O’Kelly 2013)

The direct shear and triaxial (TX) test apparatuses are readily available in most geotechnical laboratories. However, the loading in many geotechnical problems is similar to the simple shear loading condition, as shown in Fig. 1.3. It has been widely accepted that the response of soil in simple shear is different from the triaxial condition. Therefore, to obtain appropriate estimation of soil parameters, direct simple shear (DSS) or hollow cylinder torsional (HCT) shear tests could be performed. DSS and HCT allow the rotation of the principal stresses, similar to that which occurs in the field, which is the main advantage over triaxial tests. Laboratory testing using DSS is relatively easy, compared to HCT. The DSS apparatus is available in some advanced

geotechnical testing laboratories; however, in most cases, it not designed for low-stress level testing.

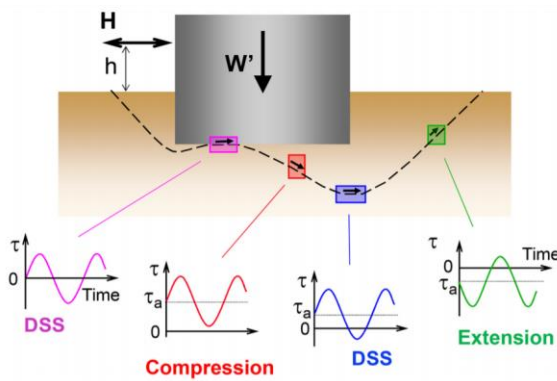


(a) Wave-induced loading



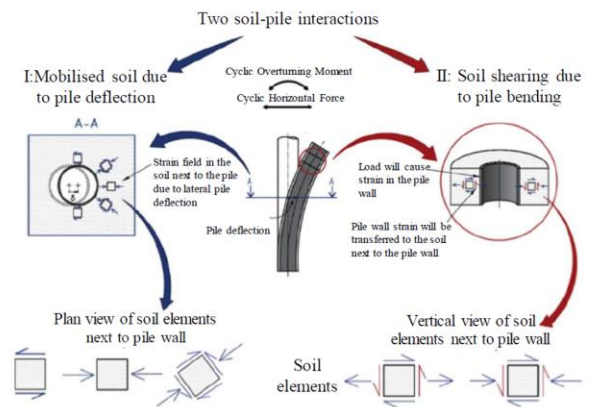
(b) Offshore pipeline axial walking

(Ao et al. 2014)



(c) Offshore gravity foundation

(Andersen 2009)



(d) Offshore wind foundation

(Nikitas et al. 2017)

Fig. 1.3. Simple shear loading conditions in the field

Low-stress shear strength behaviour could be significantly different from that of a high-stress level. Bolton (1986) showed that the peak friction angle and maximum dilation angle decrease linearly with the logarithm of mean stress. Not only the friction angle, but also the dilation angle, could affect the response. For example, the maximum uplift resistance of a pipe, which is required for upheaval buckling analysis, can be calculated using the peak friction angle (ϕ'_p) and maximum dilation angles (ψ_p), as shown in Fig. 1.4(a). The mobilized friction and dilation angles also depend on plastic shear strain. Considering the mobilized values, Roy et al. (2018) showed that the uplift resistance also changes with the displacement of the pipe (Fig. 1.4b).

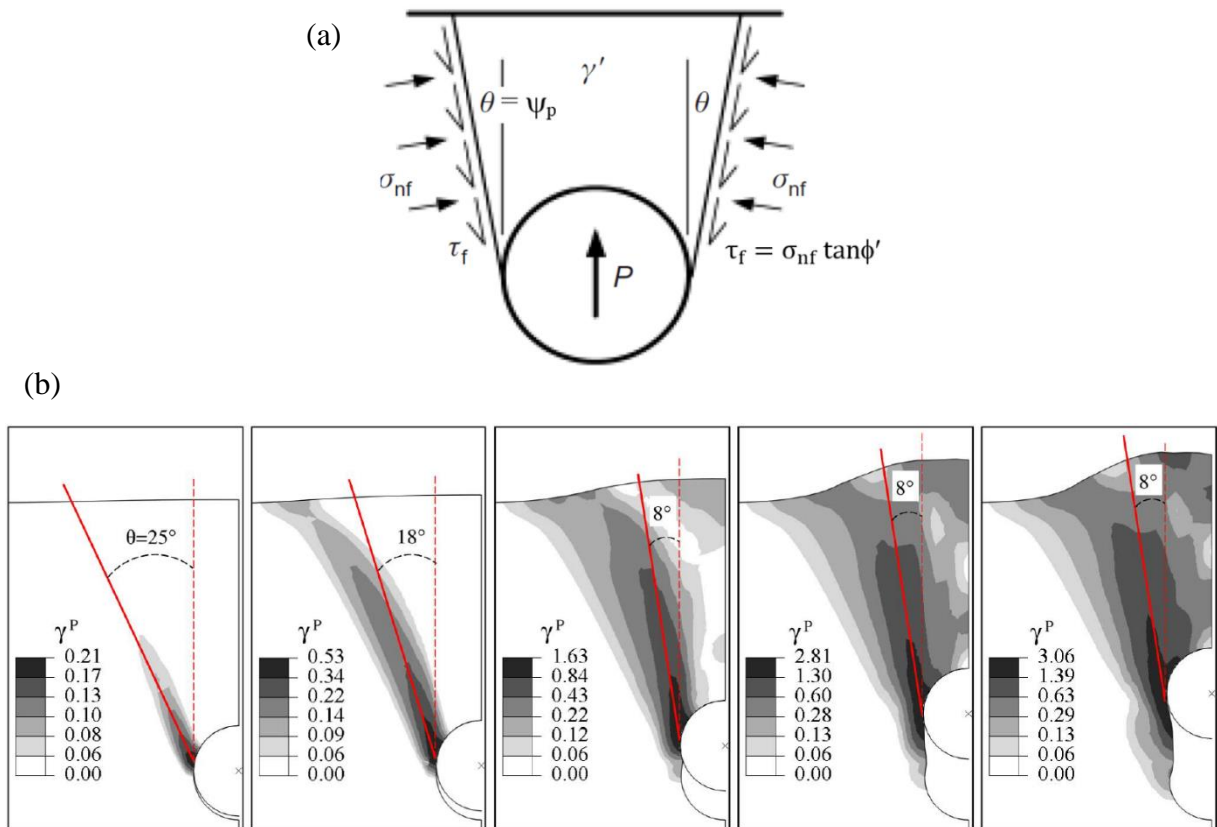


Fig. 1.4. Effect of friction and dilation angle on uplift resistance of pipe: (a) simplified limit equilibrium method (modified from White et al. 2008); (b) finite element analysis based on mobilized friction and dilation angles (Roy et al. 2018)

The above discussion shows that the monotonic and cyclic behaviour of sand at a wide range of confining stresses is required for geotechnical design.

1.2 Rationale

Many studies in the literature have investigated sand behaviour at medium- to high-stress levels. Studies on the behaviour at low-stress levels are limited. Therefore, the proposed models in the literature—for example, stress ratio and dilatancy relationship—might only be valid above a limiting stress (e.g., Bolton 1986). Most of the low-stress level tests were conducted under triaxial conditions. Also, while several stress–dilatancy relationships for monotonic loading are available, the relationships for cyclic (reverse) loading are limited. Most of these relationships were developed based on triaxial and hollow cylinder cyclic torsional shear tests; again from tests at medium to high-stress levels. Therefore, a key question is whether the soil behaviour obtained from medium- to high-stress levels is applicable to the problems at the low-stress level. This can be clarified by conducting tests at a wide range of stresses using an apparatus with advanced technologies, including data acquisition and control.

1.3 Objectives

The main objective of this study is to investigate the stress–strain behaviour of sand under monotonic and cyclic simple shear loading at a low-stress level. A new direct simple shear apparatus called the Combined Advanced Dynamic Cyclic Simple Shear (ADVDCSS), which was supplied by GDS Instruments Ltd. and developed for Memorial University of Newfoundland, is used in this research study. Given the first use of this apparatus, necessary preliminary tests have

been made to check its capabilities, including different types of testing for varying loading conditions, data acquisition and controls, and improvements where necessary, such as testing at low-stress. Techniques have been developed for accurate measurement of forces and displacements by conducting different types of simple shear tests. Also, a suction mould and different sample preparation techniques in dry conditions have been developed. This research has the following objectives:

- Investigate the monotonic behaviour of sand under constant stress simple shear loading. The effects of low stress on the peak and critical state are examined.
- Investigate the cyclic behaviour of sand under constant stress simple shear loading at a wide range of stress levels and shear strain amplitudes. The dependency of the accumulative axial strain on the stress level, shear strain amplitude and type of loading (i.e., stress- or strain-controlled) is examined.
- Identify the effects of strain history, shear strain amplitude, stress level and number of cycles on the cyclic behaviour of sand for a better understanding of the stress ratio–dilatancy relation and dynamic properties at a low-stress level. The effects of strain history are investigated by applying a wide range of multi-stage shear strain amplitudes.
- Investigate the factors that influence the monotonic behaviour of sand, such as sample preparation and loading mode. Four different sample preparation methods are used to investigate the effects of fabric resulting from sample preparations on constant stress simple shear loading. A set of constant height simple shear and drained triaxial tests are performed for comparison of responses between different loading modes.

1.4 Thesis Organization

This thesis is prepared in manuscript style and contains six chapters.

Chapter 1 describes the background, motivation, rationale and objectives of this study.

Chapter 2 presents a review of the literature. It highlights the current understanding of sand behaviour under monotonic and cyclic loading conditions. This chapter also provides an overview of the direct simple shear apparatus. The problem-specific literature review is provided in Chapters 3–5.

Chapter 3 illustrates the details of the new simple shear apparatus that is used for experiments in the present study. The monotonic and cyclic test results under constant stress levels ranging from 12.5 to 400 kPa are presented. For the monotonic loading, the peak stress ratio, critical stress ratio and dilation are described. The cumulative axial strain under constant stress simple shear loading and its relation with the stress level, shear strain amplitude and stress control type tests are investigated.

Chapter 4 presents the cyclic behaviour, and dynamic properties of the tested sand. Based on test results, the stress–dilatancy relationship at a low-stress level is developed. The cyclic behaviour is also investigated by conducting multi-stage and single-stage tests under a wide range of shear strain amplitudes. The influence of the loading mode, stress level, shear strain amplitude, and strain history is examined.

Chapter 5 investigates the effects of confining stress and reconstituted sand specimen preparation on the monotonic behaviour of sand. A series of constant height and constant stress simple shear tests, as well as triaxial compression (TXC) tests, are conducted. The DSS tests are conducted on reconstituted dry sand specimens prepared through four methods of specimen preparation: funnel raining, multiple-sieve raining, dry tamping, and table tapping. The response in direct simple shear

and the triaxial compression is compared. DSS and TXC in terms of the peak and post-peak softening are examined.

Chapter 6 presents the general conclusions and recommendations of the thesis. The problem-specific conclusions are presented in Chapters 3–5.

The references cited in Chapters 1 and 2 are listed in the reference section at the end of the thesis.

1.5 Significant Contributions

One of the major contributions is the development of the new direct simple shear testing equipment at Memorial University of Newfoundland. Although the apparatus was supplied by GDS, the author was involved in its installation and prepared additional accessories (e.g., suction mould, multiple sieve raining technique) and documents for future testing. He also conducted many trial tests, in addition to the tests shown in this thesis, to evaluate the capabilities of the apparatus.

This research has generated three journal manuscripts (Chapters 3–5) and two conference papers.

Co-Authorship Statement

I, Mahmud Amer Al Tarhouni, hold principal author status for all the manuscripts (Chapters 3–5), and the two conference papers coming from this thesis. Most of the research presented in this thesis, including the experimental work, data analyses and preparation for the draft manuscripts, has been performed by Mr. Al Tarhouni under the supervision of Dr. Bipul Hawlader. Mr. Anup Fouzder, as a research assistant, helped me perform some of the experiments and develop sample preparation methods. Drs. Ashutosh Dhar and Amgad Hussein co-supervised the research and reviewed the manuscripts.

CHAPTER 2

Literature Review

2.1 Introduction

The thesis is presented in a manuscript format. However, a literature review is presented in this chapter to provide further information on available studies related to this research. A detailed research-focused literature review of each manuscript is presented in Chapters 3–5. This chapter provides a review of the behaviour of sand under monotonic and cyclic loading. The factors affecting sand behaviour under monotonic and cyclic loading are described. Finally, as the experiments were conducted primarily using a direct simple shear (DSS) apparatus, the key concept of the development of the DSS apparatus and interpretation of the results are discussed. The references for the studies cited in this chapter are provided in the reference list at the end of the thesis.

2.2 Sand Behaviour under Drained Monotonic Loading

Many studies have investigated the drained behaviour of sand for monotonic loading (e.g., Roscoe et al. 1963; Castro 1969; Houlsby 1991). The typical behaviour of dense sand under drained simple shear loading condition is shown in Fig. 2.1. A dense sand specimen shows a contractive response up to a certain shear strain (γ) level and then changes to dilative behaviour; the sample expands and becomes looser. The volume change behaviour due to shearing is generally expressed using the dilation rate ($d\varepsilon_v/d\gamma$), or simply dilation, where $d\varepsilon_v$ is the volumetric strain increment (positive for compression and negative for expansion) due to the shear strain increment of $d\gamma$. As the plastic component mainly causes the volume change, the dilation (D) is generally

related to strain increments as $D = d\varepsilon_v^p/d\gamma^p$, where the superscript p represents the plastic component of the corresponding strain. The stress ratio reaches the peak value when the peak friction angle (ϕ'_p) mobilizes. The stress ratio then decreases with an increase in shear strain, and at one stage it might come to the critical state where the critical state friction angle (ϕ'_c) would be mobilized. During the post-peak deformation, localized failure planes might develop in the form of shear bands, and stress and strain non-uniformity might occur in the sample (Budhu 1985 & 1988).

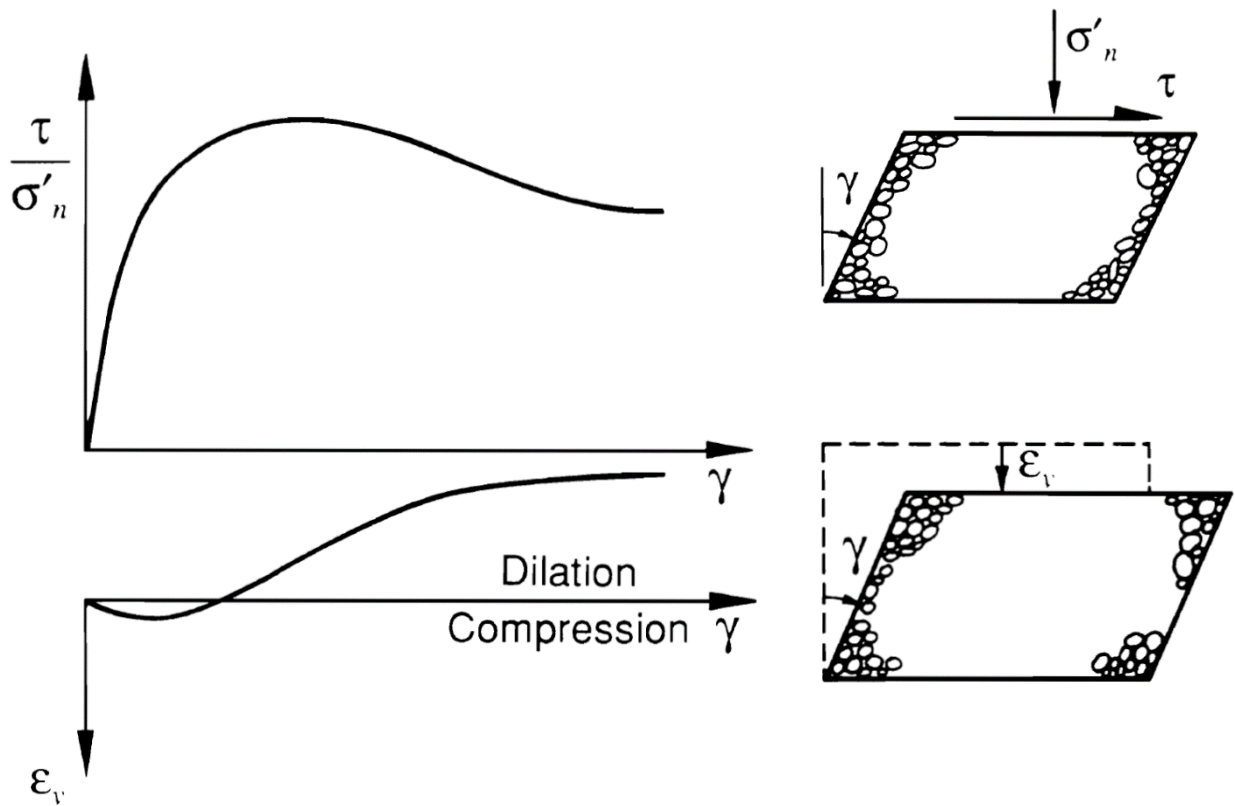


Fig. 2.1. Dilation of dense sand in a simple shear test (Houlsby 1991)

Various attempts have been made to identify the relationship between the mobilized angles of internal friction (ϕ') and of dilation ($\psi = \tan^{-1}(d\varepsilon_v/d\gamma)$). The early attempts used a theoretical

approach. If one considers the sawtooth analogy, where the teeth are inclined at an angle ψ to the horizontal, ϕ' can be calculated as:

$$\phi' = \phi'_c + \psi \quad (2.1)$$

Based on the concept of dissipation of work, Taylor (1948) developed the following equation:

$$\tan \phi' = \tan \phi'_c + \tan \psi \quad (2.2)$$

Rowe (1962) used a different approach and analyzed the response of different assemblies of particles. It is shown that the mobilized friction angle depends on sliding resistance at the contact and dilation, and that the stress ratio is proportional to the dilatancy ratio.

Bolton (1986) examined the stress–dilatancy relation from experimental results. Analyzing a large volume of experimental results on 17 sands, he showed that Eq. (2.1) overestimates the friction angle, and proposed Eqs. (2.3) and (2.4) for plane strain (PS) and triaxial compression (TXC), respectively.

$$\phi'_p = \phi'_c + 0.8\psi_{\max} \quad (2.3)$$

$$\phi'_p = \phi'_c + 0.5\psi_{\max} \quad (2.4)$$

where ψ_{\max} is the maximum dilation angle. The data considered by Bolton (1986) covered the behaviour of sand for mean effective stress (p') mostly greater than 100 kPa. For the tests at a low-stress level, he identified two issues: (i) the effect of stress and strain non-uniformities, and (ii) reduced accuracy of the apparatus in measurements. Therefore, for the low-stress level, a limiting value of $\phi'_p - \phi'_c$ of 20° for plane strain and 12° for the triaxial condition were recommended. Triaxial and plane strain compression tests on clean Toyoura sand show that the peak friction and dilation angles are not significantly dependent on effective consolidation pressure less than 50 kPa (Fukushima and Tatsuoka 1984; Tatsuoka et al. 1986). Bolton (1987) then

suggested that, for a given relative density, the peak friction angle and dilation angle increase with a decrease in mean stress until 150 kPa and then remain constant for low mean stresses. He also recommended further studies to understand the response of sand in drained conditions at low stresses. Chakraborty and Salgado (2010) reanalyzed the above-mentioned test results on Toyoura sand and found that a modification of the Bolton (1986) constant Q , as a function of confining pressure, can define the relationships among ϕ' , ϕ'_c and ψ from very low to high stresses (196 kPa).

While many studies focused on the peak friction angle and maximum dilation angle, the relationship between the mobilized friction angle and the current value dilation angle with the progress of the test can provide further insights. In the field, the progressive formation of failure planes (shear bands)—for example, under a shallow foundation on dense sand (Loukidis and Salgado 2011) or pipe–soil interaction (Roy et al. 2018), can be better modelled using the mobilized friction and dilation angles. Several relationships have been proposed to model the mobilized ϕ' and ψ as a function of plastic shear strain, which have also been compared with laboratory tests data and implemented in numerical programs to simulate different geotechnical problems (Hsu and Liao 1998; Guo and Stolle 2005; Roy et al. 2016;).

2.3 Sand Behaviour under Undrained Monotonic Loading

The monotonic behaviour of sand has been widely studied for undrained loading to investigate liquefaction phenomena (Castro 1969; Seed 1979; Chern 1985; Vaid and Chern 1985). Figure 2.2 shows the typical responses of sand for undrained monotonic triaxial loading for varying relative densities (Vaid and Chern, 1985). The stress–strain plot (Fig. 2.2(a)) shows that the response changes from strain-softening to strain-hardening with an increase in initial relative

density. In a very loose state, sand has a low shear strength and shows post-peak strain-softening (contractive) behaviour (curve 1 in Fig. 2.2(a & b)). This behaviour is referred to as liquefaction, flow liquefaction and true liquefaction by Castro (1969), Casagrande (1975) and Chern (1985), respectively. At a medium density (curve 2), the response of sand is initially strain-softening (contractive behaviour); then the response changes to strain-hardening. This behaviour has been referred to as partial liquefaction and limited liquefaction by Lee and Seed (1967) and Castro (1969), respectively. Sand in a dense state (curve 3) has a strain-hardening response, and the behaviour is always dilative.

In undrained loading conditions, two different lines are commonly used to describe two key locations on the stress path, namely the phase transformation and the ultimate steady-state lines. As shown in Fig 2.2, the phase transformation (PT) is the temporary state when the rate of excess pore pressure generation becomes zero (e.g. symbol n in Figure 2.2). At this condition, the behaviour of the sand transforms from contractive to dilative (Ishihara et al. 1975). Several studies reported that the mobilized friction angle at the PT line is independent of the relative density, confining stress and the mode of shearing (Vaid and Chern 1985; Vaid et al. 1990). The ultimate failure is the state at which the effective stress path approaches a straight line in the stress space, typically above the PT line, and reaches the maximum stress obliquity (Ishihara et al. 1975). Some researchers found that the angle of maximum obliquity is unique and is independent of the initial state prior to undrained shear loading (Vaid and Chern 1985).

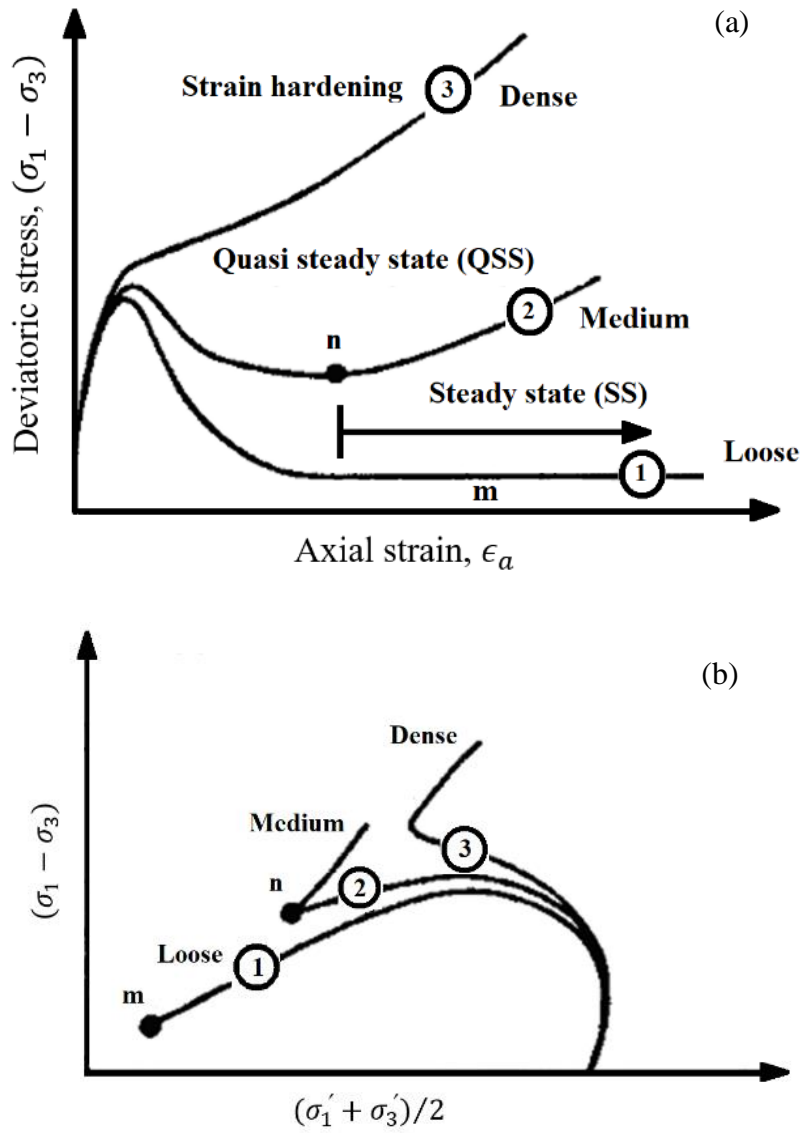


Fig. 2.2. Undrained behaviour of sand at different relative densities in monotonic triaxial compression tests: (a) stress–strain response, (b) stress path, (Vaid and Chern 1985)

2.4 Sand Behaviour under Constant Stress Cyclic Loading

2.4.1 Stress–strain and Volume Change Behaviour

Figure 2.3(a) shows the stress–strain behaviour of Ottawa sand in simple shear loading for a constant strain amplitude cyclic loading (Finn et al. 1982). The test was conducted using a direct cyclic simple shear apparatus at the University of British Columbia (UBC), which was similar to the Cambridge University type (CU-type) apparatus. The sand was placed in a rigid-wall sample container and then sheared. As shown in Fig. 2.3(a), the shear stress increases in each loading cycle, which represents the strain-hardening behaviour of sand. The increase in shear sand strength is associated with decreases in the volumetric strain (compaction) (Fig 2.3(b)). The volumetric strain per cycle is higher initially (e.g. the first cycle), and the rate decreases with the number of cycles.

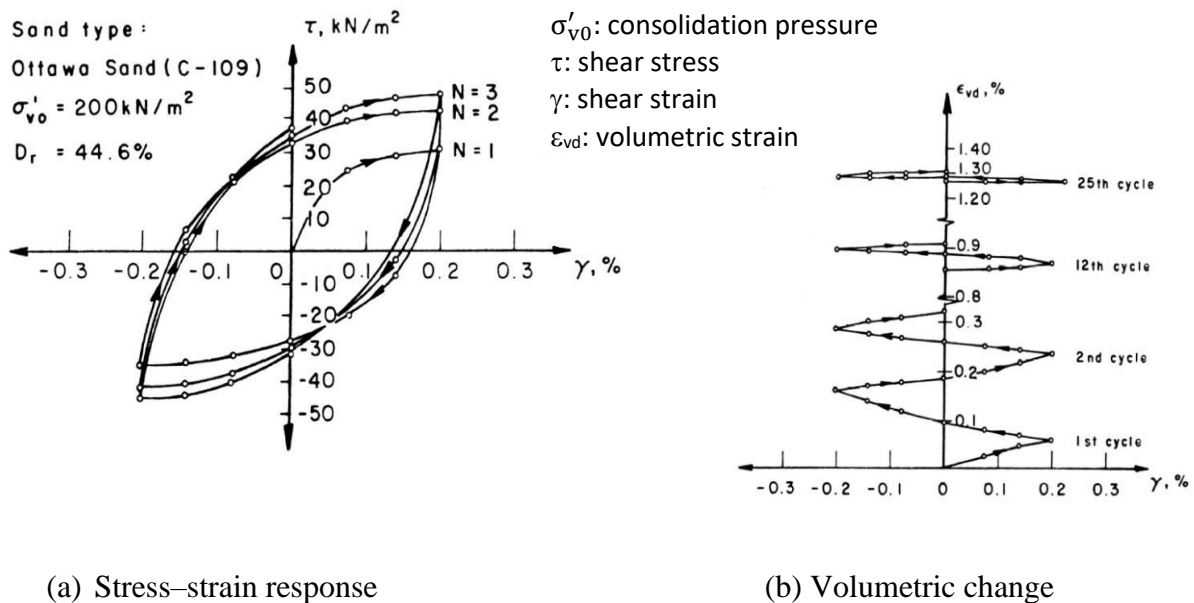


Fig. 2.3. Stress–strain and volume change in a cyclic drained direct simple shear test (Finn et al.

1982)

2.4.2 Factors Affecting Volumetric Strain

Youd (1972) used a direct simple shear apparatus (NGI-type) to investigate the volume change response of Ottawa sand due to strain-controlled cyclic loading at shear strain amplitudes of 0.1% to 9% in drained conditions (Fig. 2.4). It was reported that the volume change increases with the shear strain amplitude. The influence of vertical stress on volume change was not observed for shear strain amplitudes exceeding 0.05% (Silver and Seed 1971; Youd 1972). It was mentioned that the absence of the influence of vertical stress on volume change could be due to the limitations of the experimental measurements. Duku et al. (2008) showed that the vertical axial strain increases with a decrease in normal stress and an increase in the shear strain amplitude (Fig. 2.5). Kang et al. (2016) modified a direct simple shear apparatus by applying confining pressure together with radial strain measurements, instead of using radial constraints in a typical DSS apparatus. They found that the volumetric strain increases with an increase in shear strain amplitude (Fig 2.6). Also, less volumetric strain was observed when relative density and confining pressure were increased (Fig 2.7). The above-mentioned recent findings contradict the studies conducted by Silver and Seed (1971) and Youd (1972) on the influence of stress level on the volumetric strain. Also, the behaviour at a low-stress level < 50 kPa and the effects of large shear strain amplitude $> 1\%$ were not investigated in recent studies.

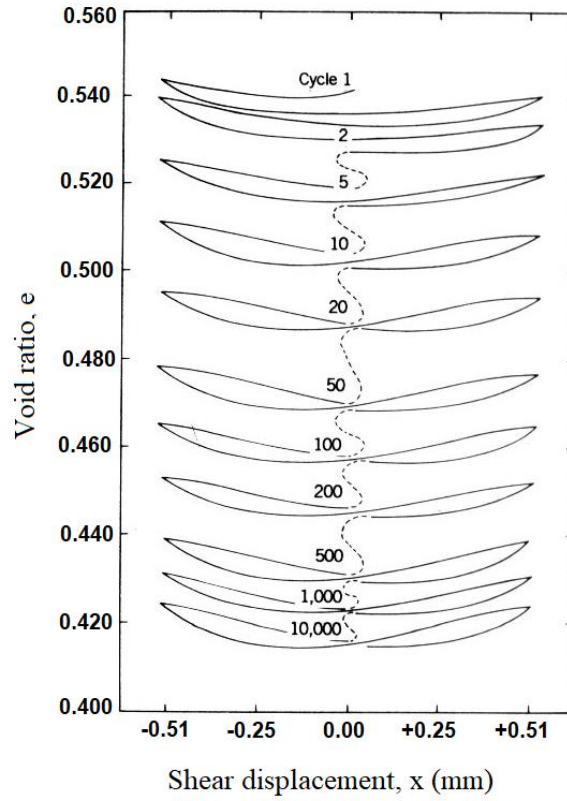


Fig. 2.4. Compaction of a DSS sample under 48 kPa vertical stress due to cycling loading (Youd 1972)

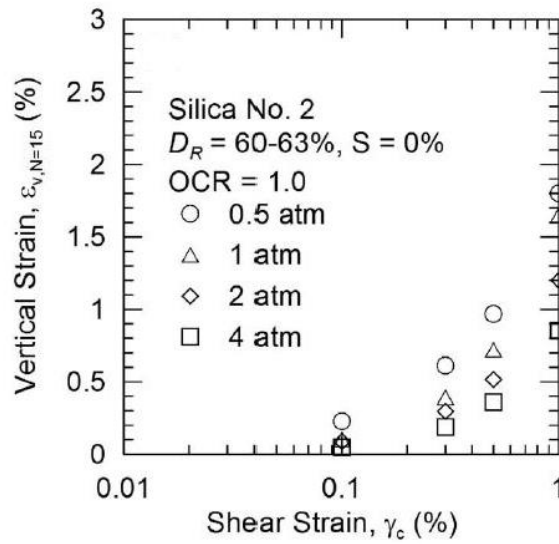


Fig. 2.5. Effect of vertical stress on vertical strain in DSS tests (Duku et al. 2008)

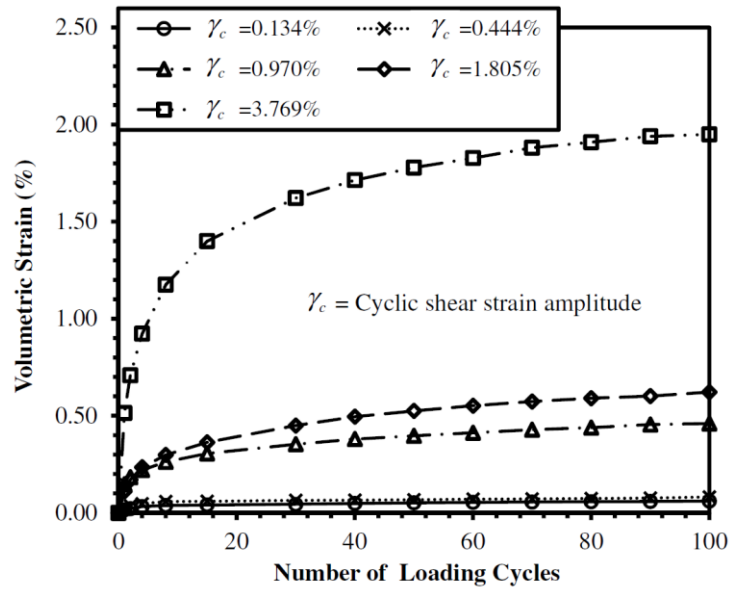


Fig. 2.6. Effect of cyclic shear strain amplitude on volumetric strain of dense sand (Kang et al. 2016)

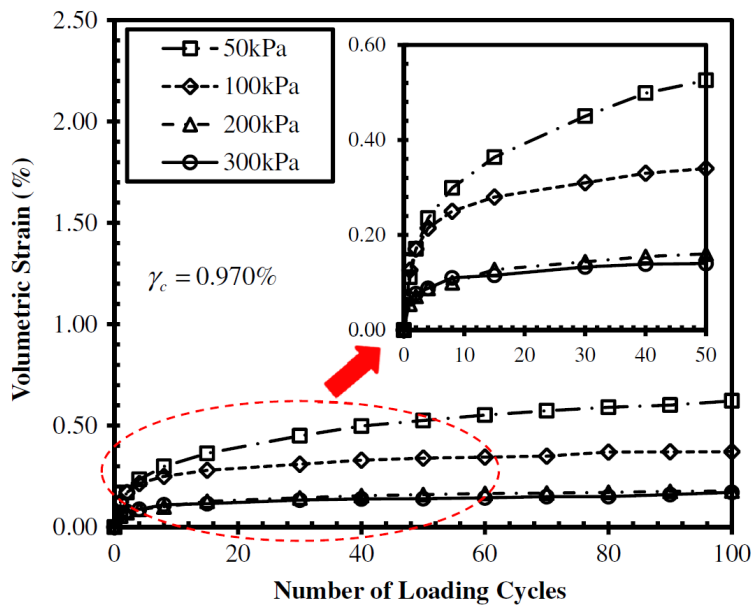


Fig. 2.7. Effect of confining pressure on volumetric strain of dense sand (Kang et al. 2016)

2.4.3 Stress–dilatancy Relationship under Cyclic Loading

The stress–strain and cyclic stress–dilatancy ratio relationships are required to model the volumetric response under cyclic loading (De Silva et al. 2014). The cyclic stress–dilatancy relationship presents the changes between the stress ratio (τ_{zx}/σ'_z) and dilatancy ($d\varepsilon_z^p/d\gamma^p$). The relationships were developed initially for monotonic loading conditions (Taylor 1948; Rowe 1962; Roscoe et al. 1963), as described in previous sections. Since then, more experimental investigations have been conducted to examine the cyclic stress–dilatancy relationship for different loading conditions. For instance, drained cyclic triaxial tests were conducted by Pradhan and Tatsuoka (1989) and López-Querol and Coop (2012). Based on a series of cyclic drained simple shear tests on Ottawa sand and Fulung sand, Lee (1991) found a linear stress–dilatancy relationship, which is independent of relative density and stress level (Fig 2.8). The cyclic stress–dilatancy relationship under drained simple shear conditions was also investigated using a torsional shear testing apparatus (Pradhan and Tatsuoka, 1989; Shahnazari and Towhata 2002; Gerorgiannou et al. 2008; Wahyudi et al. 2010; Wahyudi and Koseki 2012; De Silva et al. 2014). Table 2.1 shows a summary of stress ratio–dilatancy relationship investigations under simple shear loading, including the parameters of interest and key findings. Figure 2.9 shows a typical stress-dilatancy relationship for dense sand under cyclic torsional loading (Shahnazari and Towhata 2002). The dilatancy ratio changes as the number of cycles increases. Also, the stress ratio increases due to sample densification. It should be noted that the first loading path has a different response than the following cycle.

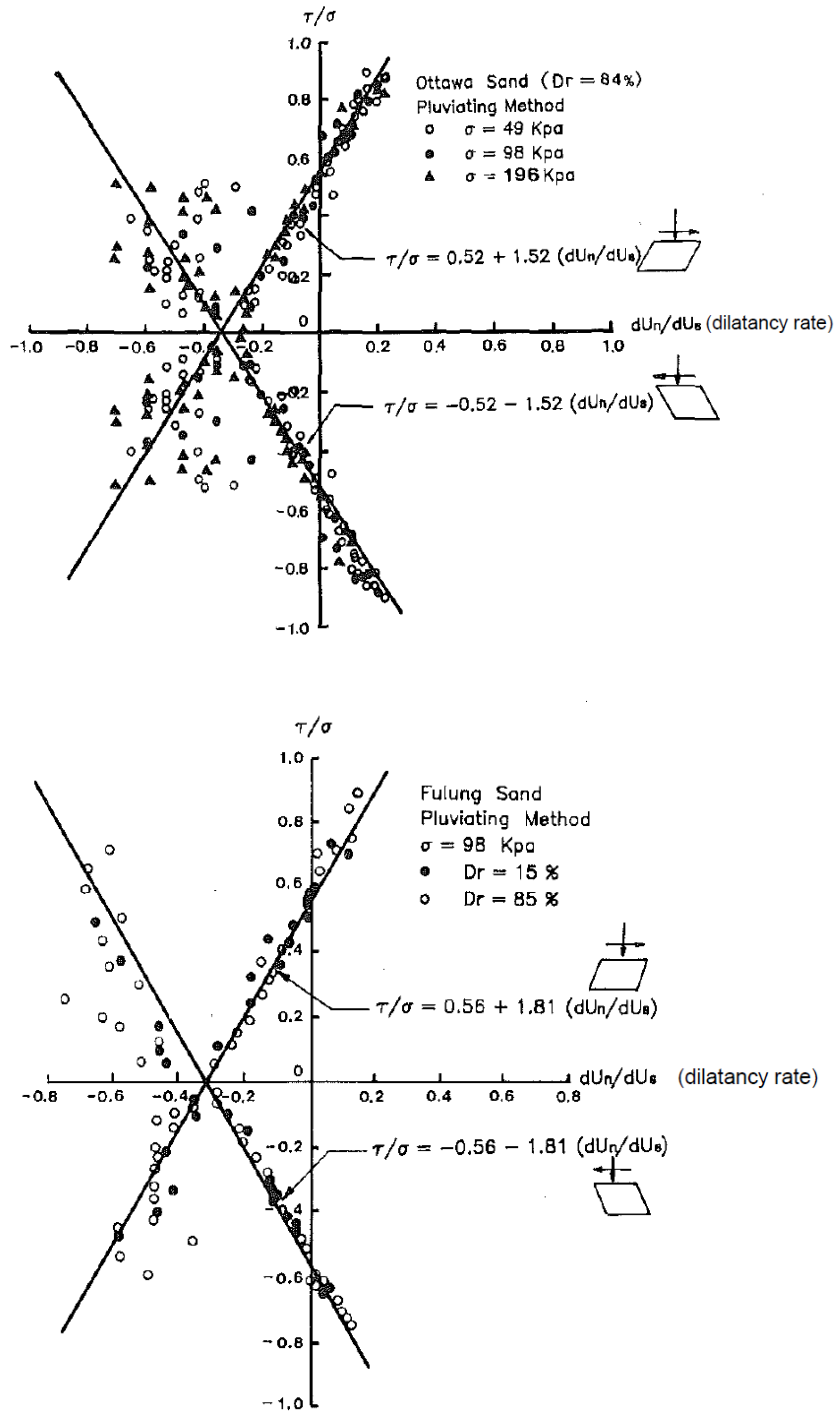


Fig. 2.8. Shear stress ratio–dilatancy rate in constant load cyclic drained simple shear tests (Ueng and Lee 1990)

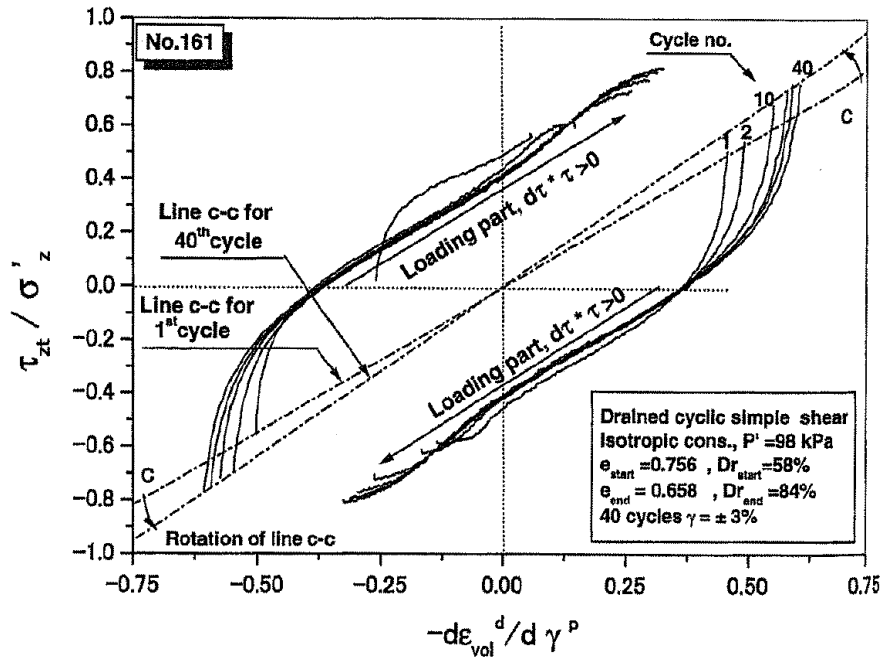


Fig. 2.9. Stress–dilatancy relationship for medium dense sand under torsional simple shear loading (Shahnazari and Towhata 2002)

Table 2.1 Stress–dilatancy relationship in cyclic simple shear loading

Reference Apparatus	Tests conditions	Remarks
Ueng & Lee (1990); Lee (1991)	<ul style="list-style-type: none"> • DSS • Dry Ottawa & Fulung sands • Constant vertical stress • $\sigma'_z = \sim 50\text{--}200$ kPa • $D_r = 7\%\text{--}88\%$ 	<ul style="list-style-type: none"> • Stress–dilatancy can be represented by two straight lines, independent of vertical stress level and density. • Some limitations in measurements of the displacement.
Nemat-Nasser and Takahashi (1984)	<ul style="list-style-type: none"> • HCT • Monterey No. 0 sands • Constant cyclic strain • $D_r = 43\%\text{--}85\%$ • $\sigma'_z = 40\text{--}160$ kPa • $K (= \sigma_h / \sigma_v) = 0.4\text{--}2$ • $\gamma_{amp} = 0.5\%\text{--}10\%$ 	<ul style="list-style-type: none"> • Stress–dilatancy curve consists of two parallel segment lines that have apposite slopes connected with two nearly vertical segments lines. • It depends on relative density, shear history and shear strain amplitude. • The initial anisotropic consolidation is important only at the initial stage of loading.
Pradhan and Tatsuoka (1989)	<ul style="list-style-type: none"> • HCT, TX • Toyoura sand • $D_r = 24\text{--}76\%$ • $\sigma'_z \sim 53\text{--}184$ kPa 	<ul style="list-style-type: none"> • Four models: sliding block theory, Rowe's theory, Roscoe's theory and Taylor's theory modified to fit stress–dilatancy obtained from experiments.

	<ul style="list-style-type: none"> • $\gamma_{amp} = 0.5\%–3\%$ 	<ul style="list-style-type: none"> • Stress–dilatancy consists of two parallel segment lines connected with two nearly vertical segments. • It is dependent on relative density, shear history and shear strain amplitude.
Shahnazari and Towhata (2002)	<ul style="list-style-type: none"> • HCT, TX • Toyoura sand • $D_r = 24–76\%$ • $\sigma'_z \sim 53–184$ kPa • $\gamma_{amp} = 0.5\%–3\%$ 	<ul style="list-style-type: none"> • Confirmed the findings by Nemat-Nasser and Takahashi (1984), the relative density, shear history and shear strain amplitude influence the stress–dilatancy relationship. • The effect of the initial anisotropic consolidation is important only at the initial stage of loading. • The response of the first loading cycle is different than for the subsequent cycles.
Georgiannou et al. (2008)	<ul style="list-style-type: none"> • HCT • Fontainebleau sand • Constant stress cyclic • $D_r \sim 46\%$ • $p'_i = 130$ kPa • $\Delta\tau_{\theta z} \sim \pm 73$ kPa 	<ul style="list-style-type: none"> • Confirmed the previous works that the stress–dilatancy relationship of the first loading cycle is different than in the following cycles. • For large number of cycles, the form of the stress–dilatancy relationship is independent of the number of cycles.

<p>Wahyudi and Koski (2012)</p>	<ul style="list-style-type: none"> • HCT • Toyoura sand • $D_r = 56 - 82\%$ • $p'_i = 35$ kPa, • $\tau_{\theta z} = \pm 50$ & ± 60 kPa • $\gamma_{amp} = \pm 2.5$ & $\pm 5\%$ • OCR = 1 & 4 	<ul style="list-style-type: none"> • Confirmed the previous work that showed the stress–dilatancy relationship of the first loading cycle is different than in the following cycles. • Confirmed that the stress–dilatancy curve consists of two parallel segment lines connected with two nearly vertical segment lines. • The OCR and initial density have less effect than the shear strain amplitude on the stress–dilatancy relationship.
<p>De Silva (2014)</p>	<ul style="list-style-type: none"> • HCT • Toyoura sand • $D_r \sim 57 - 79\%$ • $\sigma'_z = \sigma'_r = \sigma'_{\theta} = 100$ kPa, • OCR = 1 & 4 	<ul style="list-style-type: none"> • Confirmed that the stress ratio–dilatancy during virgin loading and subsequent cycling loading is different • Modeling of the stress–dilatancy as a bilinear relationship

DSS: Direct simple shear; HCT: Hollow cylinder torsional shear; TX: triaxial; D_r : Relative density;

γ_{amp} : Shear strain amplitude; $\tau_{\theta z}$ = shear stress, p'_i = mean effective stress; $\sigma'_z = \sigma'_r$ & σ'_{θ} = axial, radial and circumferential stresses; OCR = over-consolidation ratio.

2.5 Effects of Sample Preparation on Sand Behaviour

The influence of the induced fabric by sample preparation methods on the behaviour of sand has been demonstrated in the literature using a simple shear apparatus, mainly for the assessment of liquefaction resistance, monotonic and cyclic loading conditions (Silver et al. 1980; Vaid et al. 1999; Vaid and Sivathayalan 2000; Li et al. 2018). However, most of the experiments have been conducted for the axisymmetric loading condition using a triaxial apparatus (Oda 1972a; Mulilis et al. 1977; Miura and Toki 1982; Tatsuoka et al. 1986; Yamashita and Toki 1993; Sze and Yang 2014). Figure 2.10 shows three different responses of Fraser River sand in constant height direct simple shear tests, simply because of different sample preparation methods (Vaid et al. 1995). The sand response changes from strain-hardening to strain-softening for samples prepared by water pluviation/sedimentation (WP) and moist tamping (MT), respectively. The specimen prepared by air/dry pluviation (AP) exhibits less strain-softening than the MT sample. A more recent study by Li et al. (2018) found that the liquefaction resistance of sand is the greatest when using the dried wet tamping method, followed by the dry funnel method and, lastly, the air pluviation method. They reported that the sample preparation method has an insignificant impact on the constant height response tests at $\sigma'_z = 200$ kPa, and relative density of 27–68%.

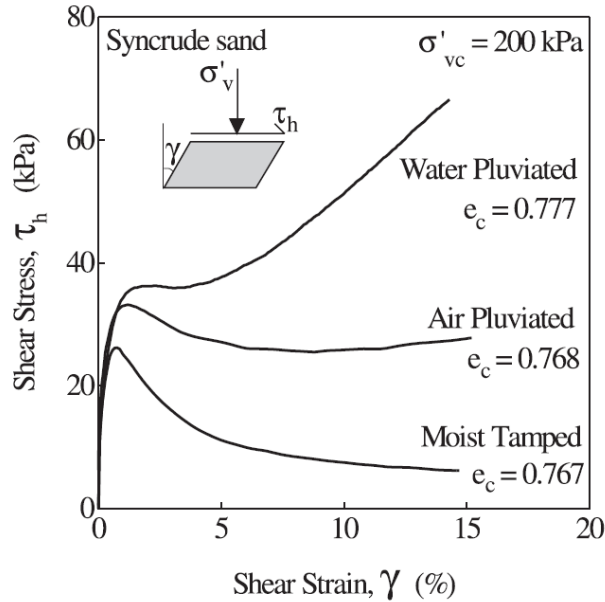


Fig. 2.10. Effect of sample preparation methods on the stress–strain response of Syncrude sand under undrained simple shear loading (Vaid et al. 1995)

The induced fabric due to sample preparation influences the cyclic behaviour and dynamic properties of sands under different modes of shearing (Mulilis et al. 1977; Nemat-Nasser and Takahashi 1984; Miura and Toki 1982; Tatsuoka et al. 1986; Sze and Yang 2014; Li et al. 2018; Wichmann and Knittel 2020). Tatsuoka et al. (1986) demonstrated that the impact of sample preparation methods is not consistent under cyclic undrained condition between the triaxial and torsional shear tests. This indicates that the sand behaviour is effected by the changes in the principal stresses during cyclic loading and the sample preparation methods. Wichtmann and Knittel (2020) showed that the accumulated axial strain after 10^5 cycles is dependent on induced energy during the sample preparation process (Fig. 2.11). The accumulated strain for the samples prepared with no vibrations has a closer trend than the samples prepared with a vibration technique. As shown in Fig. 2.11, the accumulated strains of the samples prepared in dry conditions are in a close trend, especially for the initial relative density of 40–80%. This indicates that the influence

of the dry sample preparation method has less impact on the accumulative axial strain under cyclic loading.

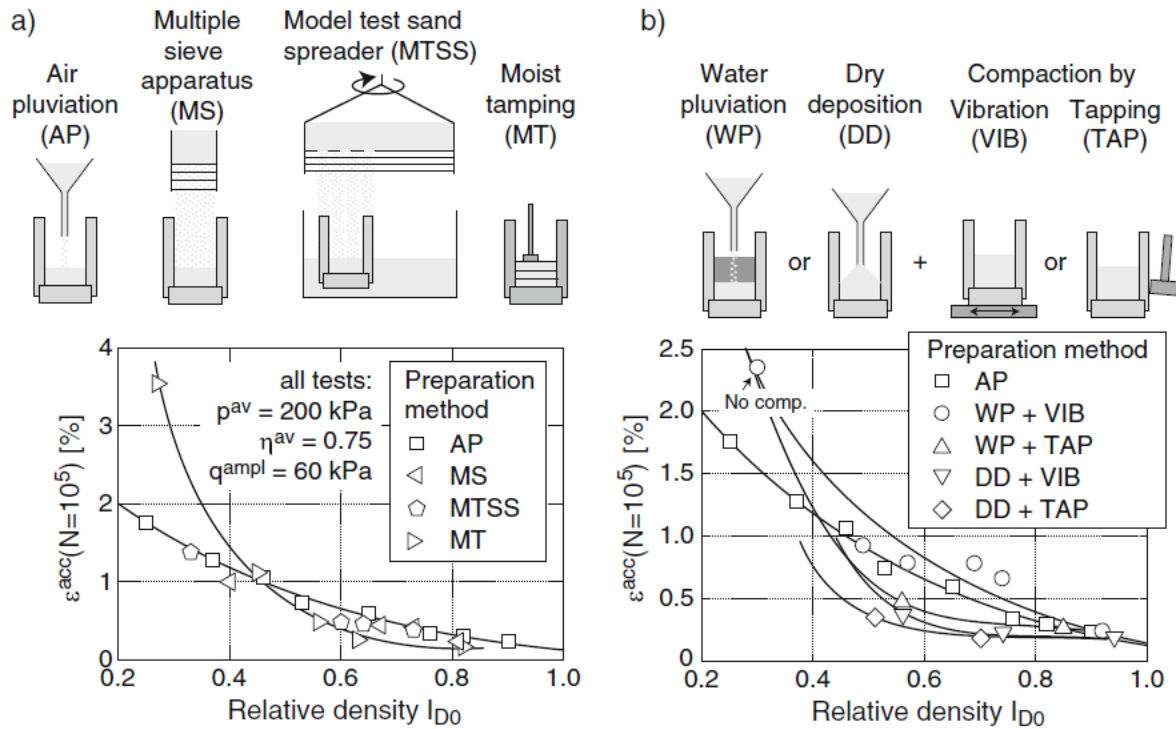


Fig. 2.11. Accumulated axial strain variation with initial relative density for different methods of sample preparation in drained triaxial tests (Wichtmann and Knittel 2020)

2.6 Influence of Loading Mode on Sand Behaviour

Experimental results show that the loading mode has a significant influence on the behaviour of sand. Figure 2.12 shows the comparison of the undrained behaviour of sand among simple shear, triaxial compression and triaxial extension conditions (Yoshimine et al. 1999). The triaxial test shows strain hardening while a significant strain-softening occurs in the triaxial extension test. The response in simple shear loading condition is in between the responses of the triaxial compression

and triaxial extension (Vaid and Sivathyalan 1996; Yoshimine et al. 1999). The simple shear, triaxial compression and triaxial extension loading modes have different principal stress directions (α) and dimensionless parameters, b ($= (\sigma'_2 - \sigma'_3)/(\sigma'_1 - \sigma'_3)$). The major principal stress during shearing is inclined at an angle $\alpha = 0^\circ$ to the bedding planes in triaxial compression, $\alpha \approx 45^\circ$ in simple shear, and $\alpha = 90^\circ$ in triaxial extension tests. Also, the dimensionless parameters (b) for triaxial compression, simple shear and triaxial tension are 0, 0.3–0.4 and 1.0, respectively. Experimental results of hollow cylinder torsional shear under undrained conditions have shown that two variables, α and b , influence the behaviour of sand (Uthayakumar and Vaid; 1998; Yoshimine et al.; 1998; Vaid and Sivathyalan 2000). Generally, the behaviour of sand becomes more contractive as α increases, and an α of 45° (simple shear) produces an intermediate stress–strain response between the triaxial compression and extension.

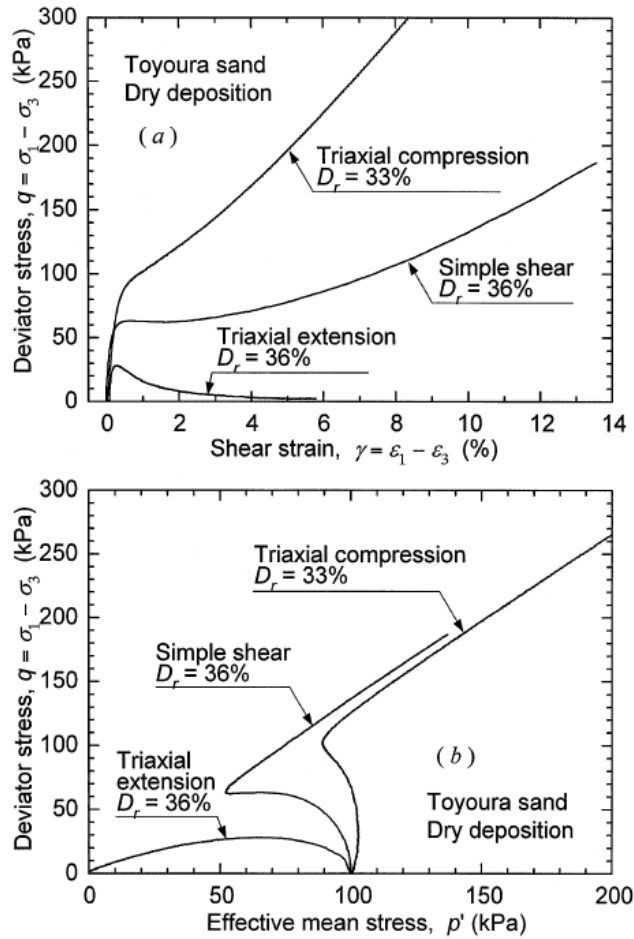


Fig. 2.12. Influence of loading mode on the monotonic behaviour of sand (Yoshimine et al. 1999)

Limited studies in the literature have investigated the influence of the loading direction using a hollow cylinder apparatus in drained conditions (Razeghi et al. 2015; Yang et al. 2016). Figure 2.13 shows the behaviour of medium and dense sand at different loading conditions. The highest peak shear strength was found when $\alpha = 0^\circ$, and it reduces with an increase in α . The samples are highly dilative when $\alpha = 0^\circ$ (TXC) but remain compressive for the whole range of shear strain when sheared at $\alpha = 0^\circ$ (TXE), even though the other conditions are the same.

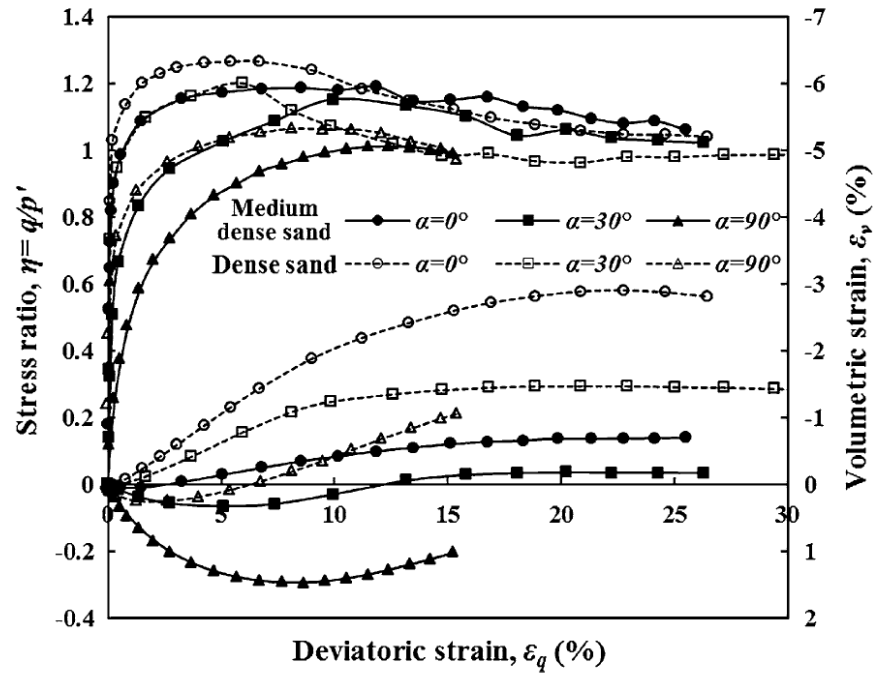


Fig. 2.13. Influence of shearing mode on behaviour of medium and dense sand (Yang et al. 2016)

2.7 Dynamic Properties of Sand

The shear modulus and damping ratio are commonly used to characterize and model sand under cyclic loading. The definitions of the shear modulus and damping ratio are shown in Fig. 2.14. A wide range of experimental investigations, including small-strain and large-strain levels, have been conducted to understand the factors that influence the dynamic properties. These factors include loading mode, drainage conditions, relative density, stress level, shear strain amplitude, strain history, and number of cycles (Iwasaki et al. 1978; Tatsuoka et al. 1978; Hardin and Drnevich 1972; Uthayakumar 1992; Kang et al. 2016). It is established that the damping ratio of sand and shear modulus are strain dependent.

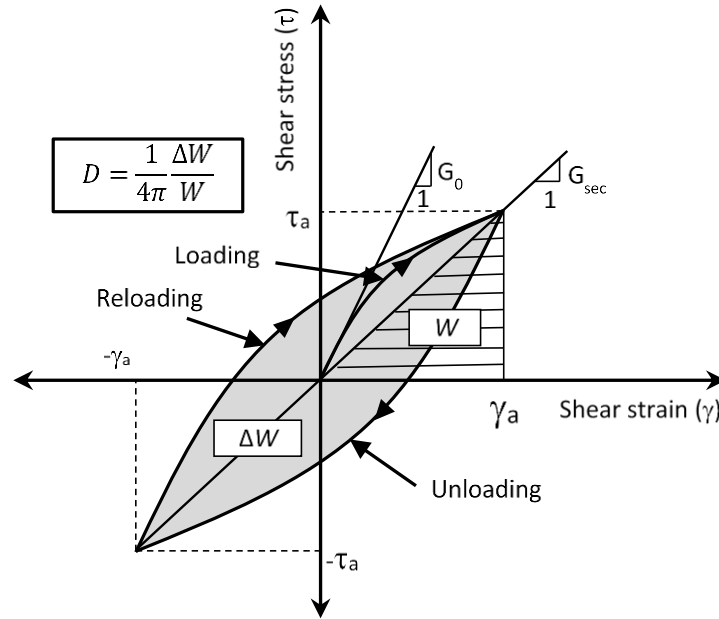


Fig. 2.14. Definitions of the shear modulus and damping ratio

Figure 2.15(a) shows that the shear modulus reduces with cyclic shear strain amplitude, and is highly dependent on stress level (i.e., increases with confining stress). The damping ratio increases with the shear strain amplitude (Fig. 2.14b). However, a recent study by Blaker and Andersen (2019) on very dense sand under undrained cyclic simple shear and triaxial loading shows that the damping ratio decreased after reaching a peak value at large shear strain amplitudes (Fig 2.16).

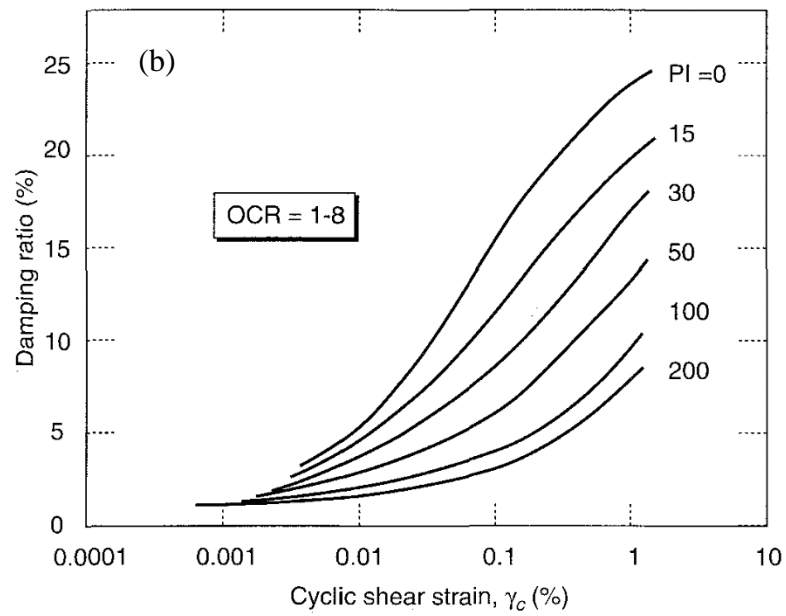
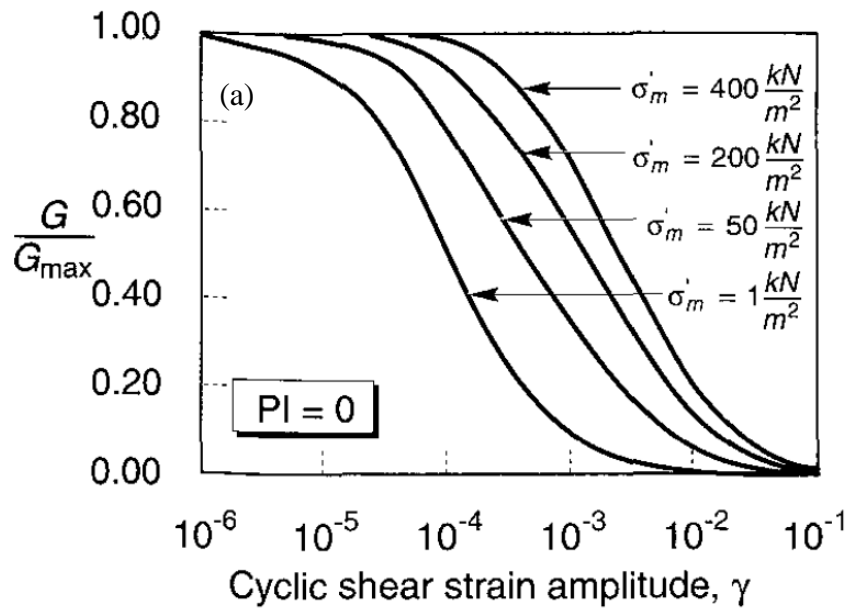


Fig. 2.15. Dynamic properties: (a) Shear modulus; (b) damping ratio (Kramer 1996)

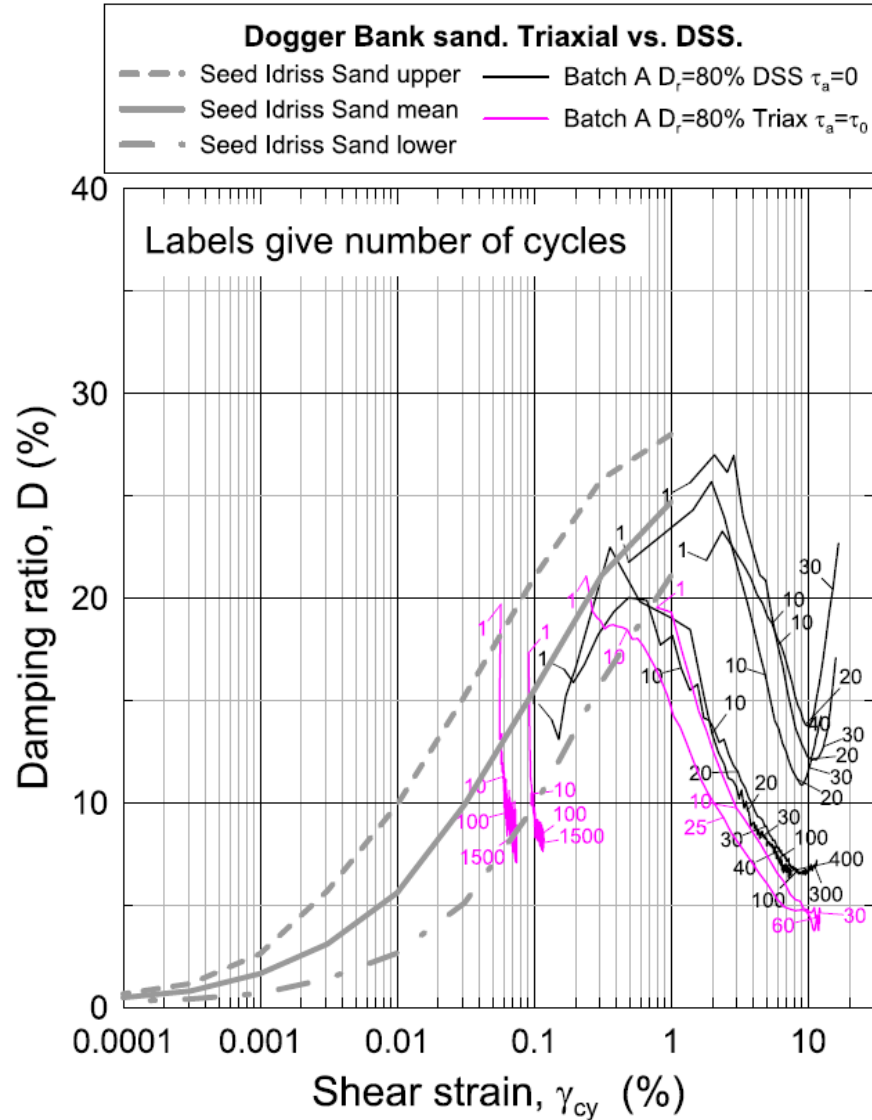
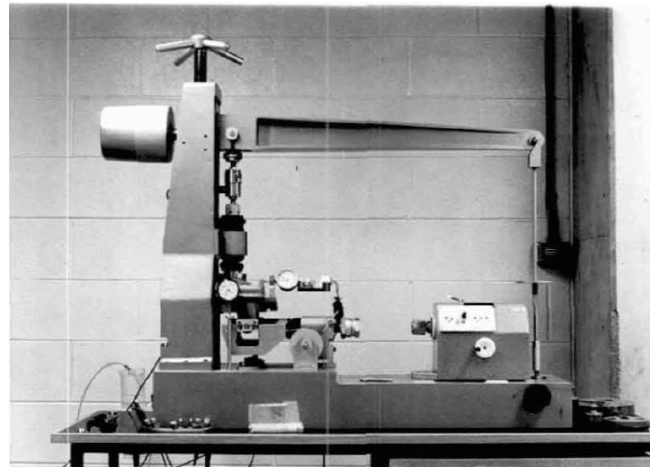
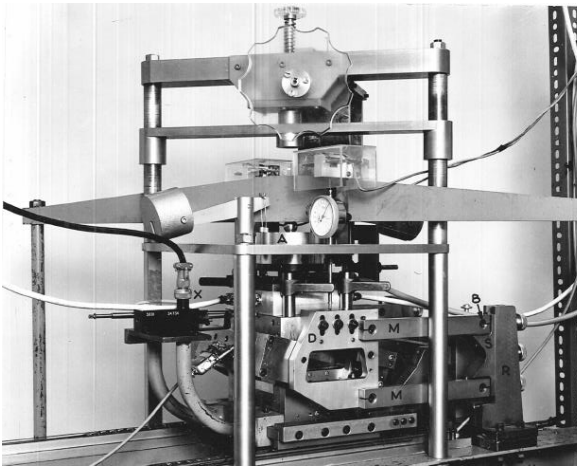


Fig. 2.16. Damping ratio of very dense sand in large shear strains (Blaker and Andersen 2019)

2.8 An Overview of Direct Simple Shear Apparatus

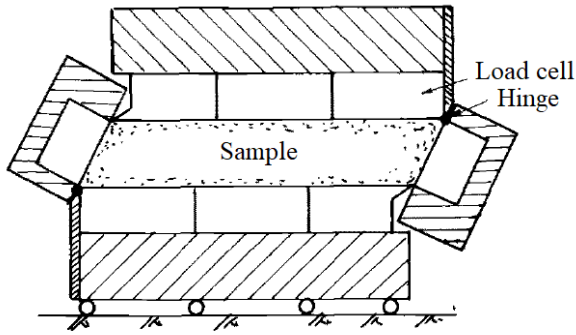
Two types of direct simple shear apparatus (DSS)—the Cambridge University simple shear apparatus (CU-type) and Norwegian Geotechnical Institute simple shear apparatus (NGI-type) — have been widely used to investigate monotonic and cyclic behaviour of soils (Fig. 2.17(a–b)). The CU-type apparatus was originally developed by Roscoe (1953) and was then upgraded by several

researchers at Cambridge University. In the CU-type apparatus, the soil specimen is placed in rigid cubical boundaries in which the vertical and horizontal load cells can be easily mounted (Fig. 2.18(a)). The NGI-type apparatus was developed by Bjerrum and Landva (1966) has become more widely used than the CU-type because of its simplicity. A cylindrical soil sample is enclosed in a wire-reinforced rubber membrane that keeps the lateral strain at zero to achieve the simple shear condition (Fig 2.18(b)).

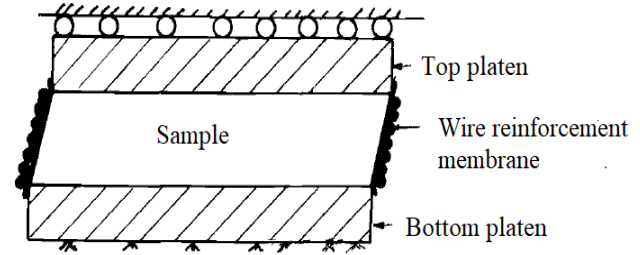


a) CU-type apparatus (Mk 7) (Stroud 1971) b) NGI-type apparatus (Zimmie and Floess 1979)

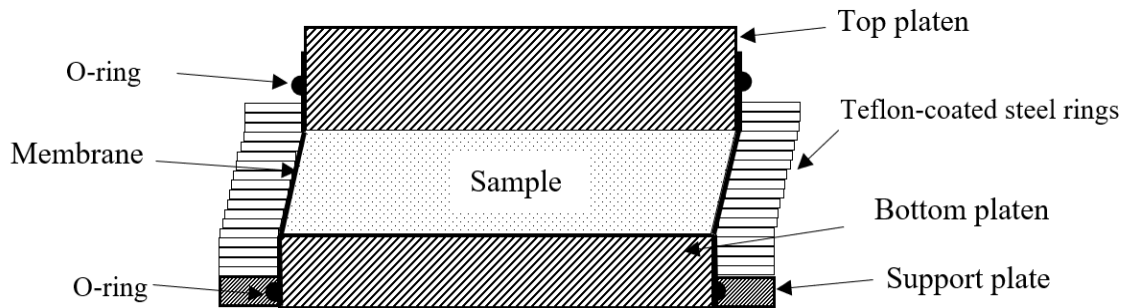
Fig. 2.17. Two types of direct simple shear apparatus



(a) Sample confinement in CU-type apparatus



(b) Sample confinement in NGI-type apparatus



(c) Sample confinement using Teflon-coated steel rings

Fig. 2.18. Different sample confinements configuration of simple shear apparatuses

The sample confinement configuration of the NGI-type apparatus has been criticized, as the wire-reinforced rubber membrane is not stiff enough to keep the radial strain at zero at large shear strains. Ishihara and Yamazaki (1980) used a new confinement configuration; the sample is placed in a rubber membrane confined with a stack of rigid Teflon-coated steel rings to test sand in saturated and multi-direction loading conditions (Fig. 2.18(c)). In the direct simple shear apparatuses, no

shear stress is applied at the lateral sides of the specimen. Therefore, there is a lack of complementary shear stresses acting on the lateral boundaries and an inability to apply uniform stresses and strains, particularly near the lateral boundaries. Several studies investigated the effect of this non-uniformity on overall response. Figure 2.19 shows the normal stress and shear stress distributions based on the elastic analysis by Roscoe (1953). The study indicated that stress distribution in the middle third of the specimen could be considered as uniform, that and the stress non-uniformities are high only at the lateral boundaries. Stroud (1971) showed that the middle third of the sample is in a state of uniform strain until the loading to the maximum shear stress ratio. Budhu (1984) showed that the sample is uniform up to a 5% shear strain. Upon recognizing some of the limitations of the simple shear apparatus, modifications have been made, mostly in the area of lateral stress measurement/control, to better interpret the test results (Youd and Craven 1975; Dyvik et al. 1981; Budhu 1985).

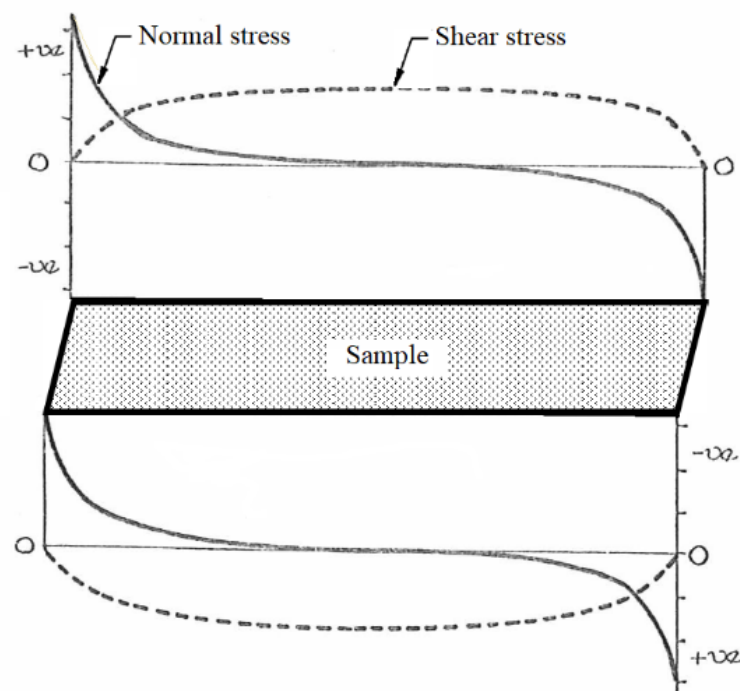


Fig. 2.19. Stress non-uniformity in DSS specimen based on elastic theory (Roscoe 1953)

2.9 Stresses and Strains in Triaxial Compression and Direct Simple Shear

Figure 2.20 shows the stresses and strains in TXC and DSS tests. Further details on the similarities and differences between these two tests can be found in previous studies (Atkinson et al. 1991; Wijewickreme et al. 2013). Soil specimens are cylindrical in shape in both the TXC and DSS tests used in this thesis. Figures 2.20(a & b) show the dimensions of the specimens. Figure 2.20(c) shows the axial (σ'_a) and radial (σ'_r) effective stresses on the triaxial soil specimen, which are the major (σ'_1) and minor (σ'_3) principal stresses, respectively, in a triaxial compression test. By drawing a Mohr's circle with these two stresses (σ'_1 and σ'_3), and then a tangent on this circle from the origin, the angle of internal friction of sand for triaxial compression (ϕ'_T) can be obtained (Fig. 2.20(e)). The stress ratio is related to the angle of internal friction in the triaxial condition as $\phi'_T = \sin^{-1}[(\sigma'_1/\sigma'_3 - 1)/(\sigma'_1/\sigma'_3 + 1)]$. However, in a constant stress DSS test, the vertical stress (σ'_z) is applied and then sheared horizontally, which creates a shear stress (τ_{zx}) on the top and bottom horizontal surface (Fig. 2.20(d)). As the sample remains in a set of stacked rigid rings in the apparatus used in this research thesis, the radial stress (σ'_r) prior to shearing can be calculated as $\sigma'_r = K_0\sigma'_z$, where K_0 is the coefficient of earth pressure at-rest. During shearing, the radial stress is not measured. Moreover, the vertical frictional resistance between the soil and membrane is not known. In other words, in a DSS test, only two stresses $A(\sigma'_z, \tau_{zx})$ are known (Fig. 2.20(f)). Therefore, to construct Mohr's circles and to find shear strength parameters, some assumptions are required. Two common assumptions are used for calculating the friction angle for the DSS condition (ϕ'_{SS}):

- (i) If the horizontal plane is the plane of the maximum shear stress obliquity, the angle of internal friction can be approximately calculated as $\phi'_{SS} = \tan^{-1}(\tau_{zx}/\sigma'_z)$ (Roscoe et al. 1967; Stroud 1971);

- (ii) If the maximum shear stress, τ_{\max} , is acting on the horizontal plane, the angle of internal friction can be approximately calculated as $\phi'_{\text{ss}} = \sin^{-1}(\tau_{\text{zx}}/\sigma'_z)$.

Figures 2.20(g) and 2.20(h) show the deformed shape of TXC and DSS specimens, respectively. The lateral strain increment $d\varepsilon_r \neq 0$ in TXC; however, $d\varepsilon_r = 0$ in the DSS test. As $d\varepsilon_r = 0$ in DSS tests, the vertical strain increment ($d\varepsilon_z$) represents the volumetric strain increment ($d\varepsilon_v$). Mohr's circles for strain state could be drawn for both TXC and DSS, as shown in Figs. 2.20(i) and 2.20(j), respectively.

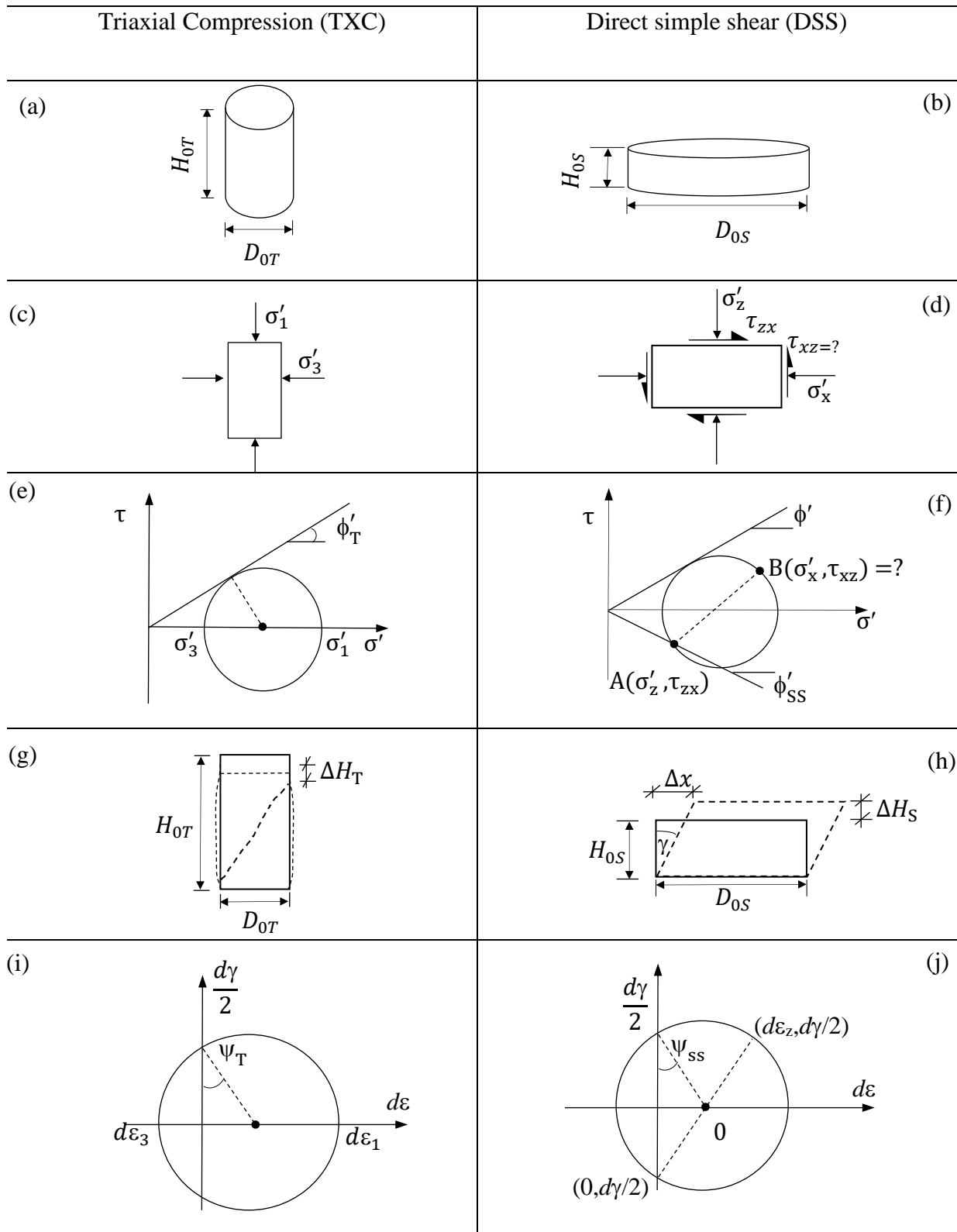


Fig. 2.20. Stresses and strains in triaxial and direct simple shear specimens

2.10 Summary

The behaviour of sand in monotonic and cyclic loading is influenced by several factors. In geotechnical engineering practice, direct shear (DS) and triaxial compression (TXC) tests are commonly performed to obtain soil parameters. However, stresses and strains in many geotechnical problems are similar to the simple shear condition. Compared to DS and TXC tests, a limited number of studies is available for simple shear loading conditions, especially at low normal stress levels. Laboratory tests at a low-stress level are challenging. Moreover, the sample preparation methods could have a significant influence on sand behaviour. In the present study, the monotonic and cyclic behaviour of sand is investigated using an advanced direct simple shear apparatus. Tests cover a wide range of normal stresses, including low stresses. DSS sample preparation effects on the response of sand are also investigated.

CHAPTER 3

Monotonic and Cyclic Behaviour of Sand in Direct Simple Shear Test Conditions Considering Low-Stresses

Abstract:

Many geotechnical problems, such as buried pipeline–soil interaction and wave loading on sand seabeds, require the soil behaviour at relatively low effective stresses as compared to that in typical geotechnical practice. Monotonic and cyclic direct simple shear (DSS) tests were conducted on dry sand under constant normal stress, ranging from 12.5 kPa to 400 kPa, to investigate the effects of confining pressure on stress–strain behaviour. The tests were conducted using a combined advanced dynamic cyclic simple shear apparatus, which has a high-precision feedback system for controlling and measuring the forces and displacements while maintaining a high level of accuracy, which is essential, especially for tests at low normal stresses. The monotonic test results show an increased shear to normal stress ratio, thereby the mobilized friction angle, at the low-stress level compared to that of high normal stresses. The strain-controlled (constant strain amplitude) cyclic test results show that the load–displacement behaviour and cyclic compaction are governed by the normal stress and shear strain amplitude. The sand becomes densified when the applied shear strain amplitude is greater than its threshold value. In strain-controlled tests, the lower normal stresses result in higher compaction; however, an opposite trend exists in stress-controlled (constant stress amplitude) cyclic tests.

3.1. Introduction

Soil behaviour depends on effective stress. In some geotechnical problems, the mean effective stress is small compared to that encountered in typical geotechnical engineering practice. For example, the soil–structure interaction of a pipeline buried at typical burial depths (1–2 m) and densification of sand or slope failure near the seabed due to wave loading involves soils at low effective stresses. The shear strength parameters of soils are generally obtained from laboratory tests at medium to relatively high effective stress. Some attempts have also been made to capture the low-stress (confining pressure or normal stress) behaviour; however, the reliability of the test results has been questioned (Stroud 1971; Fukushima and Tatsuoka 1984; Alshibli et al. 2003; Lings and Dietz 2004; Adams 2017; Rousé 2018; Wu et al. 2020).

Direct shear (DS) and triaxial tests (TX) are widely used to obtain shear strength parameters. However, many geotechnical problems in the field resemble the simple shear condition. Hollow cylinder torsional (HCT) and direct simple shear (DSS) apparatuses are used to obtain soil parameters for simple shear (SS) conditions; however, a DSS test is relatively easier than a HCT shear tests. The rotation of the principal stresses is allowed in the DSS test, which is the main advantage of this apparatus over triaxial tests; however, it has been criticized for non-uniformity of stresses and strains in the specimen during shearing, and difficulties in interpreting test results, because the normal (lateral) and shear stresses on the vertical faces are not measured in typical DSS tests. However, for practical engineering, the DSS apparatus has been more widely used than HCT tests.

Fukushima and Tatsuoka (1984) conducted drained triaxial compression (TXC) tests on Toyora sand under confining pressure (σ'_c) of 2–392 kPa and showed that the peak friction angle (ϕ'_p) and peak dilation angle (ψ_p) do not increase significantly over the range of low-stress level up to ≤ 50

kPa. Analyzing extensive TXC and plane strain compression (PSC) test data of 17 sands, Bolton (1986) showed that both ϕ'_p and ψ_p decrease linearly with the logarithm of mean effective stress (p'), assuming a pressure-independent critical state friction angle (ϕ'_c). However, he recognized severe difficulties in the accurate measurement of stresses below 15 kPa and recommended a limiting mean effective stress, in terms of relative dilatancy (< 4), above which his proposed relationships are valid. Conducting TXC tests on Ottawa sand in the laboratory and in a microgravity environment, where the tests could be done at a very low-stress level, Alshibli et al. (2003) showed a continued increase of ϕ'_p and ψ_p with a decrease in σ'_c , and, at $\sigma'_c = 2$ kPa, ϕ'_p could be as high as $\sim 56^\circ$ and $\psi_p \sim 26^\circ$. Using a modified direct shear apparatus to accommodate large deformation, Lings and Dietz (2004) found an increase of both ϕ'_p and ϕ'_c of dry Leighton Buzzard sand up to the minimum normal stress (σ'_z) of 25 kPa considered in their study. Rousé (2018) conducted DS tests on seven sands, including low-stress range ($\sigma'_z = 4\text{--}150$ kPa), and showed that ϕ'_c decreases with σ'_z , and that the rate of decrease is higher when $\sigma'_z < 50$ kPa.

Low-stress level direct simple shear tests are limited. Stroud (1971) conducted constant stress DSS tests on Leighton Buzzard sand and showed a decrease in shear to vertical stress ratio (τ_{zx}/σ'_z , where τ_{zx} is the shear stress on the horizontal plane) with σ'_z for a range of $\sigma'_z = 13.8\text{--}172$ kPa. Adams (2017) conducted constant stress DSS tests on a beach sand with $\sigma'_z = 6\text{--}300$ kPa and showed that both ϕ'_p and ϕ'_c increase significantly at low-stress level, although the author mentioned some difficulties in the tests at very low stresses. These studies suggest that the response of sand at low stress could be different from higher-stress level behaviour, and this needs to be investigated further using advanced test facilities.

Sand might also be subjected to cyclic loading of varying intensities and frequencies. The cyclic stress–strain behaviour of sand under drained condition has received less interest compared to the undrained condition. This is mainly due to the focus on the liquefaction phenomenon of sand, which could cause catastrophic failures during an earthquake. Drained cyclic loading could induce settlement (cyclic compaction), which could cause significant damage to structures. Cyclic compaction was investigated by conducting DSS tests on dry sands under constant normal stress (Silver and Seed 1971; Seed and Silver 1972; Tokimatsu and Seed 1987; Vucetic 1994; Vucetic et al. 1998; Hsu and Vucetic 2004; Ramadan 2007; Duku et al. 2008; Yee et al. 2012). Compaction occurs only when the cyclic shear strain amplitude (γ_a) is greater than a threshold value (γ_{tv}) (Hsu and Vucetic 2004). The accumulated volumetric strain (ε_v) due to cyclic loading increases with γ_a ($\geq \gamma_{tv}$), and the number of loading cycles (Silver and Seed 1971; Hsu and Vucetic 2004). Yee et al. (2012) showed the cyclic compaction is also related to initial relative density, fine content and degree of saturation. Contradictory or inconclusive results have been presented on the effect of normal stress on ε_v and γ_{tv} . DSS tests on dry Ottawa sand under $\sigma'_z = 24\text{--}191$ kPa (Silver and Seed 1971) and saturated Ottawa sand under $\sigma'_z = 5\text{--}192$ kPa (Youd 1972) show that the volumetric compression is not significantly influenced by the vertical stress and it occurs when $\gamma_a > 0.05\%$. Dobry et al. (1982) found that γ_{tv} for sand to build up cyclic pore water pressure in sand is independent of confining stress. However, recent DSS tests on several sands of varying fine contents and saturation levels show that cyclic compaction decreases significantly with normal stress (Hsu and Vucetic 2004; Duku et al. 2008; Yee et al. 2012). They conducted the tests under $\sigma'_z = 50\text{--}400$ kPa, and showed that the volumetric compaction for $\sigma'_z = 50$ kPa could be double of that for $\sigma'_z = 400$ kPa. For the sand they tested, $\gamma_{tv} = 0.01\text{--}0.02\%$.

Compared to strain-controlled tests, fewer studies are available on volume change due to cyclic loading, based on stress-controlled tests (Oh-oka 1976; Georgiannou et al. 2008; Wu et al. 2020). The stress-controlled ring torsional shear tests on Toyoura sand (Oh-oka 1976) and HCT shear tests on Fontainebleau sand (Georgiannou et al. 2008) show unsymmetrical hysteresis loops with the shear stress axis. Wu et al. (2020) investigated the effect of normal stress of Fontainebleau sand and found that, for a given critical stress ratio, the accumulated volumetric strain increases with the increase of the normal stress ranging from 52 kPa to 416 kPa and $D_r = 68\text{--}70\%$, which contradicts the behaviour observed in strain-controlled tests, as discussed above.

In summary, stress-dependent response of sand is expected not only in the intermediate (e.g., peak) and large shear strains (critical state) but also at the low shear strain level, such as in cyclic loading. Limited studies are available on sand behaviour at the low-stress level. The objective of this paper is to present monotonic and cyclic DSS test results on a silica sand using a Combined Advanced Dynamic Cyclic Simple Shear apparatus. The paper has been organized in the following way. First, the capability of the apparatus is discussed, because one of the aims of this study is to investigate the behaviour at low stresses, which requires better accuracy in stress and strain measurements and control. Second, a series of monotonic DSS test results for a wide range of normal stresses are presented. Finally, stress- and strain-controlled cyclic DSS test results for varying normal stresses and shear strain amplitudes are presented.

3.2. Direct Simple Shear Apparatus

Two types of DSS apparatus are mainly used for soil testing. In the Cambridge University type (CU-type) apparatus, a cubical specimen is placed in rigid vertical boundaries, while in the Norwegian Geotechnical Institute-type (NGI-type), a cylindrical soil specimen is enclosed in a

wire-reinforced rubber membrane. The non-uniformity in the specimen during shearing has been investigated both experimentally and numerically. Stroud (1971) showed that the middle third of the specimen is in a state of uniform strain up to maximum shear stress ratio, $(\tau_{zx}/\sigma'_z)_{\max}$. Budhu (1984) found that the specimen is uniform up to 5% shear strain (γ). The stress and strain distributions in a DSS specimen have also been investigated through numerical simulations using the discrete element method (DEM) and finite element method (FEM) (Budhu and Britto 1987; Dabeet 2014; Bernhardt et al. 2016), and it has been found that the stresses and strains are non-uniform near the boundaries and uniform in the central part. The DEM of Dabeet (2014) shows a significant stress non-uniformity only in a narrow zone (\sim two particles) near the lateral boundaries of the specimen. Bernhardt et al. (2016) showed that a sufficiently large number of particles should be used in DEM to simulate the stress–strain response, and that an increased diameter to height ratio reduces the non-uniformity of the DSS specimen.

Several studies have attempted to measure radial stress in the NGI-type DSS apparatus (Youd and Craven 1975; Dyvik et al. 1981). The modification of DSS apparatus was mainly in the lateral stress measurement/control, for a better interpretation of the test results. Budhu (1985) presented some test results in which lateral stresses were measured using the modified NGI- and CU-types of DSS apparatuses. Some researchers replaced the wired reinforcement of the NGI-type DSS apparatus with cell pressure, which led them to control the lateral stress during consolidation and the shearing stages (Franke et al. 1979; Kang and Kang 2015). Moreover, simple shear apparatus configurations have been proposed for different purposes, such as small-strain measurements (Doroudian and Vucetic 1995; Mortezaie and Vucetic 2012) and multidirectional loading types (Ishihara and Yamazaki 1980; Boulanger et al. 1993; DeGroot et al. 1993; Rutherford and

Biscontin 2013; Duku et al. 2007). However, few experimental studies at a low-stress level are available in the literature, as discussed in the introduction.

3.2.1. Apparatus Capabilities

Figure 3.1(a) shows the DSS apparatus built by GDS Instruments Ltd. for Memorial University of Newfoundland, Canada. Figure 3.1(b) shows some of the key components of this apparatus. The apparatus can be used to conduct monotonic and cyclic tests for simple shear and triaxial modes on a wide range of soil types (fine to coarse-grained) at drained, undrained, constant stress, and constant height conditions. A brief description of the capabilities of the apparatus is provided in this section, although only drained monotonic and cyclic test results are presented in this paper.

For DSS testing, the soil in a latex membrane is confined laterally with a stack of 1-mm-thick rigid Teflon-coated steel rings. No volume change occurs if the specimen height is kept constant during shearing, which represents an undrained test (also known as constant height or constant volume DSS test). The effective normal stress is kept constant in a drained (constant stress) DSS test.

The present DSS apparatus can be used to conduct tests in saturated conditions, a feature that is not available in many conventional CU-type or NGI-type DSS apparatuses. For the simple shear mode, a soil specimen can be saturated under K_0 conditions by applying back pressure, cell pressure and/or normal stress. For triaxial tests, Linear Variable Displacement Transducers (LVTD) are available to measure the local axial and lateral strains.

The data acquisition and control software allows the creation of different stages in the same test, such as consolidation, followed by drained or undrained monotonic or cyclic shearing at sinusoidal, square, and triangle waveforms or user-defined waveforms for earthquake loading. The apparatus

is mounted with a bender element system for the measurement of soil moduli at small strains in triaxial and DSS modes.

3.2.2. Load and Displacement

A dual-axis 5-kN load cell controls and measures the axial and lateral loads with an accuracy better than 0.1% and a resolution of 0.2 N. A 1-kN load cell is also available for more accurate measurements at lower shear stress levels. Moreover, a 10-kN axial pancake load cell is mounted on the machine for higher-stress level tests. An LVDT of ± 2.5 mm range is mounted close to the DSS specimen to measure the axial displacement with an accuracy better than 0.1% and a resolution of 0.1 micron. In addition, an axial displacement transducer and motor encoder are used to crosscheck the measured vertical displacements. A shear displacement transducer of ± 10 mm range with an accuracy better than 0.1% and a resolution of 0.1 micron is located under the specimen base. The shear displacement is also measured using an encoder.

For tests in saturated conditions, a digital pressure/volume controller of 3 MPa range with an accuracy of 0.15% and volumetric capacity of 200 cc with an accuracy of 0.25% is available. A pore water pressure transducer located close to the specimen drainage line provides a good measurement of the pore water pressure in the specimen, with a maximum capacity of 1 MPa and an accuracy of 0.15%. In addition, for the measurement and control of the pore water pressure at a low-stress level, a Digital Remote Feedback Module (Digi RFM), is available. The Digi RFM is an external transducer that has a maximum working pressure of 200 kPa and an accuracy of 0.15%. A pneumatic pressure controller is used to regulate an external air pressure source and apply cell pressure. The maximum air pressure that can be applied to the cell chamber is 1 MPa, and the maximum air pressure supply should be 1,300 kPa. For accurate cell pressure measurement and

control, a pressure transducer located inside the cell chamber is available with a maximum capacity of 1 MPa and an accuracy of 0.15%.

3.2.3. Data Acquisition and Control

A high-precision feedback system controls forces and displacements while maintaining a high level of accuracy. Two electrical-mechanical brushless DC servo motors are used as axial and horizontal actuator units. The axial and horizontal motor platens are mounted on high-precision linear guides. The axial platen is attached to the specimen top-cap and only moved in the axial direction, whereas the horizontal platen is attached to the specimen base pedestal and is free to move on the horizontal axis. The servo motors work within a closed loop to control the force and displacement by a digital control system (DCS) via optical encoders. The DCS unit consists of a combination of the dynamic control processor and signal conditioning. The dynamic processor runs a very fast control loop frequency of 5 kHz (5000 loops/sec). The apparatus is controlled by sharing data between the control firmware and software.

During cyclic loading, the density and stiffness of the soil specimen change with the number of cycles (N). The adaptive control system in the present apparatus uses the updated stiffness, which allows better control than the systems using conventional proportional-integral-derivative (PID) control algorithms based on initial stiffness.

3.2.4. Interpretation of Stress State in DSS Specimen

Figure 3.2 shows a comparison between the stresses in a DSS and triaxial compression (TXC) specimen. A detailed discussion on the similarities and differences between these two types of test can be found in Atkinson et al. (1991), Wijewickreme et al. (2013), Al Tarhouni et al. (2017). In

a TXC test, the axial (σ'_a) and radial (σ'_r) effective stresses represent the major (σ'_1) and minor (σ'_3) principal stresses, respectively. By drawing a Mohr's circle with these two stresses (σ'_1 and σ'_3), and then a tangent on this circle from the origin, the angle of internal friction of sand for triaxial compression (ϕ'_T) can be obtained (Fig. 3.2 (c)), which is related to the stress ratio (σ'_1/σ'_3) as $\phi'_T = \sin^{-1}[(\sigma'_1/\sigma'_3 - 1)/(\sigma'_1/\sigma'_3 + 1)]$.

However, in a constant stress DSS test, the vertical stress (σ'_z) is applied and then sheared horizontally, creating a shear stress (τ_{zx}) on the horizontal plane (Fig. 3.2 (b)). As the specimen remains in a set of stacked rigid rings, the radial stress (σ'_r) prior to shearing can be calculated as $\sigma'_r = K_0\sigma'_z$, where K_0 is the coefficient of earth pressure at rest. However, the radial stress is not measured during shearing. Moreover, the frictional resistance on the vertical face between the soil and membrane is not known. In other words, in a DSS test, only two stresses A (σ'_z, τ_{zx}) are known (Fig. 3.2(d)). Therefore, to construct Mohr's circles and to find shear strength parameters, some assumptions are required. The following two assumptions are commonly used for calculating the friction angle for the DSS condition (ϕ'_{SS}):

- i) If the horizontal plane is the plane of the maximum shear stress obliquity, the angle of internal friction can be approximately calculated as $\phi'_{SS} = \tan^{-1}(\tau_{zx}/\sigma'_z)$, Roscoe et al. 1967; Stroud 1971)
- ii) If the maximum shear stress, τ_{max} is acting on the horizontal plane, the angle of internal friction can be approximately calculated as $\phi'_{SS} = \sin^{-1}(\tau_{zx}/\sigma'_z)$.

At the low-stress level, the peak stress ratio (τ_{zx}/σ'_z) could be close to 1 for dense sand, as shown later in this study. The estimated friction angle, according to Assumption-ii, would lead to an overestimation of the friction angle for sand tested at low-stress levels. The interpretation of the friction angle for the DSS condition (ϕ'_{SS}) depends on the assumption of the stress state during

shearing. Atkinson et al. (1991) reported that the friction angle calculated as $\phi'_{ss} = \tan^{-1}(\tau_{zx}/\sigma'_z)$ is less than the triaxial ϕ' , and the difference depends on the ratio between horizontal to vertical stresses. In this study, ϕ'_{ss} is calculated based on the assumption-i.

3.3. Method

3.3.1. Materials

The grain size distribution of the fine-grained silica sand used in this study is shown in Fig.3.3. The sand is classified as poorly graded, according to the Unified Soil Classification System (USCS). The grain shape of the sand is sub-rounded to sub-angular. The mean diameter (D_{50}), uniformity coefficient (C_u), and coefficient of gradation (C_c) are 0.18 mm, 1.12, and 2.23, respectively. The specific gravity of sand grains (G_s) is 2.65. The maximum (e_{max}) and minimum (e_{min}) void ratios are 1.048 and 0.606, respectively. The testing of the physical properties of sand was conducted according to ASTM standards.

3.3.2. Specimen Preparation

Sand specimens were prepared using the dry tamping method. To prepare a DSS specimen, a latex membrane was placed and secured to the bottom pedestal using O-rings. Teflon-coated steel rings were then placed around the membrane. A suction mould, developed in-house, was placed around the steel rings. The advantage of using the suction mould is that the latex membrane becomes lined inside the steel rings such that the specimen has less disturbance, and the void ratio can be measured more precisely. After folding the flank of the membrane over the mould, a vacuum was applied. For dense sand specimens, dry sand was poured through a 2-mm-diameter funnel with

zero drop height. A tamping rod was used to compact the sand in three layers. For loose specimens, sand was poured through a 5-mm diameter funnel without any compaction. The height of the specimen was recorded using a digital dial indicator to achieve the targeted relative density. The sand specimen with the mould was then placed on the base of the DSS apparatus. A normal stress of 2.5 kPa was applied to ensure proper seating of the top platen on the specimen. The upper part of the membrane was then fixed with the top cap using O-rings. The vacuum mould was removed, and the bottom pedestal was attached to the base of the DSS apparatus. The height of the specimen was verified from the encoder displacement measurement, and the axial LVTD was mounted. Further details on the effects of various sample preparation methods on sand behaviour are presented in Chapter 5.

3.3.3. Repeatability

To show the repeatability, two cyclic DSS tests under constant normal stress are considered, because maintaining the constant vertical stress, especially at a low stress and high frequency, requires better control and measurements. Two identical silica sand specimens were prepared at the same relative density ($D_{rc} = 82\%$) and under a consolidation pressure (i.e., normal stress σ'_z) of 12.5 kPa. The term consolidation is used in this study for the compression of the dry DSS sand specimen under vertical stress σ'_z . Both specimens were sheared under drained cyclic loading at a constant shear strain amplitude of 1% and a frequency (f) of 0.1 Hz. Figure 3.4 shows that the cyclic stress–strain curves for both specimens match very well, which demonstrates an excellent performance of the apparatus. Also, the inset of Fig. 3.4 shows that the shear stress (τ_{zx}) in both tests follows the same line with number of cycle (N). In this figure, the response in only the first 10 cycles is shown to maintain clarity.

3.4. Test program

A total of 29 DSS tests under constant (normal) stress was conducted: 11 monotonic (7 on dense and 4 on loose sand), 14 strain-controlled (constant strain amplitude) cyclic, and 4 stress-controlled (constant stress amplitude) cyclic loading conditions (Table 3.1). The discussion in this study is primarily focused on these test results. Moreover, constant height DSS and monotonic drained triaxial compression (TXC) tests were conducted to compare the peak and critical state friction angles for these two modes of shearing. Further details about the constant height DSS and TXC tests are available in Chapter 5. The cyclic tests were conducted to fill the gap in the literature on the dependency of drained cyclic compaction on the stress level and type of loading.

3.5. Monotonic DSS Test Results

3.5.1. Stress–strain Behaviour

Figure 3.5(a) shows the stress–strain behaviour of six dense sand specimens ($D_{rc} = 87\%$) consolidated at a wide range of normal stresses ($\sigma'_z = 12.5\text{--}400$ kPa). The shearing was conducted under constant σ'_z and at a strain rate of 0.16%/min. For $\sigma'_z = 12.5\text{--}100$ kPa, the shear stress (τ_{zx}) increases with the shear strain (γ), reaches the maximum value at $\gamma = 6\text{--}10\%$, and then decreases slightly at large γ . For $\sigma'_z = 200\text{--}400$ kPa, the percentage of decrease of τ_{zx} at large γ is smaller than that of the tests at low stresses, which can be better shown by plotting the stress ratio (Fig. 3.5(b)). The lower the normal stress, the higher the maximum stress ratio is. The maximum stress ratio of ~ 1.4 is obtained for the test at the lowest $\sigma'_z (= 12.5$ kPa). The maximum stress ratio decreases from ~ 1.4 for $\sigma'_z = 12.5$ kPa to ~ 0.67 for 400 kPa. It is noted here that a decreasing trend in the stress ratio with σ'_z has also been reported in previous studies. For example, Stroud (1971) showed

a decrease in the stress ratio from ~ 1.0 at $\sigma'_z = 13.8$ kPa to ~ 0.9 at $\sigma'_z = 172$ kPa for a dense sand. However, compared to Stroud (1971) test results, the present study shows a higher decrease in the stress ratio with normal stress. The decrease in stress ratio after the peak is not significant for the high-stress level. Moreover, the stress ratio at large shear strains for the range of σ'_z considered in this study is very different (~ 0.67 to 1.25). This indicates that the unique critical state friction angle (ϕ'_c), which is considered a fundamental soil property, could not be obtained from these constant stress DSS tests, especially at the low-stress level, or ϕ'_c is higher at low normal stresses. The significant difference in stress ratios at large shear strains can be attributed to two different sources. Firstly, ϕ'_c increases with a decrease in σ'_z , and the increase of ϕ'_c is significant at a low σ'_z . A similar trend has been reported by Lings and Dietz (2004) based on their tests on coarse Leighton Buzzard sand using an improved direct shear test apparatus. Rousé (2018) showed that ϕ'_c decreases with increases in normal stress at the low-stress level in direct shear tests. Also, ring shear tests show that the critical state friction angle of sand decreases slightly with stress level and becomes essentially constant at normal stresses higher than about 200 kPa (Sadrekarimi and Olson 2011). The abovementioned findings agree with the result shown in Fig. 3.5(b) (i.e., τ_{zx}/σ'_z is ~ 0.67 for $\sigma'_z = 200\text{--}400$ kPa). The second source for increase in stress ratio at large strains could be because of the increase in lateral stress from the stacked rings and rotation of principal stresses. Atkinson et al. (1991) showed that the simple shear critical state stress ratio depends on the ratio between lateral and vertical stresses (K). However, the lateral stress is not measured in a typical DSS test, like the one used in the present study, although attempts have been made to measure the lateral stresses. Budhu (1985) measured horizontal stresses on the vertical faces in his tests using Cambridge- and NGI-type simple shear apparatuses and showed that the lateral stress at the start of the test is less than the vertical stress ($K = K_0 < 1$). During shearing, the increase in lateral stresses

continued over large strains (up to $\gamma \sim 40\%$), while the maximum stress ratio (τ_{zx}/σ'_z) mobilized at $\gamma \sim 12\%$ and then remained almost constant. This implies that K in DSS changes even after mobilization of the peak stress ratio. Kang and Kang (2015) modified the NGI-type DSS apparatus by replacing the wire reinforcement with cell pressure. In their test setup, the lateral stress could be controlled by cell pressure, and the tests could be performed by maintaining the K_0 condition during the whole shearing period. They showed that the stress ratio is almost the same at a large γ ($\sim 17\%$) for tests on dense sand, for a range of σ'_z between 50 and 400 kPa.

Figure 3.5(c) shows the variation in axial strain (ϵ_z) with the shear strain (γ) in the DSS tests. As the cross-sectional area of the specimen (i.e. the area between the stacked rings) remains constant during shearing, the axial strain (ϵ_z) represents the volumetric strain (ϵ_v). All the specimens show some initial compression (positive ϵ_v) followed by dilation. The rate of dilation is higher for lower σ'_z . The dilation continues until ~ 10 to $\sim 12\%$ of shear strain, and then the rate of dilation decreases. The rate of dilation is very small at a large strain.

3.5.2. Mobilized Dilation Angle

In the Mohr-Coulomb model, which is generally used for the modelling of sand, constant values of friction and dilation angles are defined. Recognizing the limitation of this modelling technique, some authors have modified the Mohr-Coulomb models, defining the mobilization of friction and dilation angles as functions of plastic shear strain (Guo and Stolle 2005; Jung et al. 2013; Roy et al. 2016).

In the DSS tests shown in Fig. 3.5(a), the shearing was done under a constant vertical stress without radial deformation. Fitting ϵ_z versus γ ($= \int d\gamma$) curves as a polynomial function and then differentiating it, the mobilized dilation angle (ψ) is calculated. Figure 3.5(d) shows that, for low

normal stresses, ψ increases to the maximum value (ψ_{\max}) at $\gamma = 5\text{--}8\%$ and then decreases to $\psi \sim 0$ again at large shear strain. The maximum dilation angle decreases with σ'_z , which is similar to the trend observed in previous studies. For example, Bolton (1986) showed that the maximum dilation angle decreases linearly with the logarithm of mean effective stress for triaxial and plane strain compression tests. The present study shows that this trend is also valid for low-stress levels.

3.5.3. Critical State and Peak Friction Angles

As discussed above, the peak and critical state friction angles are calculated from the stress ratio at these conditions as $\tan^{-1}(\tau_{zx}/\sigma'_z)$. Determining the critical state condition from drained tests on dense sand for low stress level is difficult because a large shear strain, in the order of 40%–50%, is required (Been et al. 1991; Adams 2017). However, at such a strain level, a significant non-uniformity in stresses and strains might develop in the specimen. Figures 3.5(c & d) show that the constant volume condition (zero dilation angle) did not occur in the tests at low normal stresses (=12.5 & 25 kPa) even after $\gamma = 20\%$, which is potentially due to the non-uniformity in the specimen, rather than real behaviour, that could slightly increase the shear stress (Fig. 3.5b). However, the dilation angle is very small ($< 2^\circ$) at $\gamma \sim 16\%$. Therefore, the critical state friction angle in DSS ($\phi'_{c_{SS}}$) is calculated using the stress ratio at $\gamma \sim 16\%$ (Fig. 3.5(b)) which could give a slightly higher value than the actual critical state friction angle. Figure 3.6(a) shows that $\phi'_{c_{SS}}$ does not vary significantly above $\sigma'_z > 100$ kPa; however, $\phi'_{c_{SS}}$ increases at a faster rate with decrease in σ'_z at low stresses, especially for $\sigma'_z < 50$ kPa. Figure 3.6(a) also shows the critical state friction angle of different sands for a wide range of normal stresses from different types of tests, including direct shear (DS), ring shear (RS) and improved direct shear (IDS) (Lings and Dietz

2004; Sadrekarimi & Olson 2011; Adams 2017). The calculation of $\phi'_{c_{ss}}$ is also slightly different; for example, Adams (2017) used the stress ratio at $\gamma = 30\text{--}50\%$ to calculate $\phi'_{c_{ss}}$. However, the trend of increasing $\phi'_{c_{ss}}$ at low stress is very similar.

Generally, the non-uniformity increases with the increase in density because of post-peak strain localization during shearing. Therefore, four tests were conducted on loose sand ($D_{rc} = 20\text{--}40\%$) at $\sigma'_z = 12.5\text{ kPa--}80\text{ kPa}$. The $\phi'_{c_{ss}}$ obtained from these tests are shown (solid triangles) in Fig. 3.6(a), which is smaller than the values obtained from DSS tests on dense sand, especially at low normal stresses.

The shear strain required to reach the critical state is less in an undrained test than that in a drained test. Eight constant height (undrained) tests were conducted on the same sand for varying initial normal stresses and densities. Further details of these tests are available in Chapter 5. The critical state friction angle (i.e., slope of the steady-state line) obtained from these tests are also plotted in this figure for comparison. Note however that conflicting evidence exists in the literature, whether the critical state and steady state conditions are the same or not (Been et al. 1991; Yoshimine et al. 1999).

The solid circles in Fig. 3.6(b) show that the peak friction angle of dense sand ($\phi'_{p_{ss}}$), calculated as $\tan^{-1}(\tau_{zx}/\sigma'_z)_{\max}$, decreases rapidly with normal stress for $\sigma'_z < 50\text{ kPa}$. After that, the rate of decrease of $\phi'_{p_{ss}}$ with σ'_z is small.

To compare the peak friction angles measured in DSS and triaxial compression tests, a series of monotonic drained triaxial tests, including tests at a low stress level, were conducted (Al Tarhouni et al. 2017). Tests were conducted on saturated sand with a relative density of 85%. The peak friction angle in TXC decreases from 49.5° to 40.3° for an increase in confining pressure from

12.5 kPa to 400 kPa, which implies that the interpreted $\phi'_{p_{ss}}$ (solid dots) is smaller than $\phi'_{p_{TC}}$. Note that Atkinson et al. (1991) also reported that the peak friction angle in DSS tests is less than that in triaxial tests. Note that the stress–strain behaviour of saturated sand is somewhat different from that of dry sand (as used in DSS tests); however, this issue has not been addressed in this study.

The peak friction angle depends several factors, including the interpretation of DSS tests results (Oda 1972; de Josselin de Jong 1988; Atkinson et al. 1991; Wijewickreme et al. 2013). Based on discrete element simulations, Wijewickreme et al. (2013) suggested that $\phi'_{p_{ss}} = \sin^{-1}(\tau_{zx}/\sigma'_z)_{\max}$ for the peak and that a large strain friction angle (e.g., $\phi'_{c_{ss}}$) equal to $\tan^{-1}(\tau_{zx}/\sigma'_z)$ is more appropriate to capture the rotation of the principal stresses. However, for dense sand, the high value of τ_{zx}/σ'_z , especially for low stress (Fig. 3.5), gives an unrealistically high friction angle. The open circles in 3.6(b) show the calculated peak friction angle as $\phi'_{p_{ss}} = \sin^{-1}(\tau_{zx}/\sigma'_z)_{\max}$ for $\sigma'_z \geq 50$ kPa, which indicates a considerable difference in interpreted $\phi'_{p_{ss}}$ between these two approaches. Although the trend of increasing $\phi'_{p_{ss}}$ with a decrease in σ'_z is clear, further studies are required for a better approach to estimate $\phi'_{p_{ss}}$ from DSS tests on dense sand at low stresses.

3.5.4. Practical Implications

Bolton (1986) suggested that the peak friction angle (ϕ'_p) is related to the critical state friction angle (ϕ'_c) and maximum dilation angle (ψ_p) as: $\phi'_p = \phi'_c + k\psi_p$, where $k = 0.5$ and 0.8 for triaxial and plane strain conditions, respectively. This empirical approach has been widely used for many geotechnical problems. It is also suggested that ϕ'_c depends on soil type and mode of shearing but

is independent of confining pressure (Bolton 1986; Randolph et al. 2004; Chakraborty and Salgado 2010). If ϕ'_c remains constant, even at the low-stress level, the increase in ϕ'_p at low confining stress can be captured by increased ψ_p . Bolton (1986) recognized that, at low-stress level, the ψ_p increase in proportion to $-\ln(p')$, where p' is the mean effective stress, was not reliable because of experimental limitations, and suggested a limiting value of $\phi'_p - \phi'_c$ of 20° and 12° for plane strain and triaxial compression, respectively.

The increase in peak friction angle (Fig. 3.6(b)) with a decrease in normal stress can also be described by an increase in ϕ'_c (Fig. 3.6a), instead of only high ψ_p . Note that a high value of ψ_p could give very different results in some low-stress geotechnical problems—for example, uplift and lateral resistance of pipelines and anchors in sand (White et al. 2008; Roy et al. 2018).

Bolton (1986) also suggested that $\phi'_p = \phi'_c + k\psi_p$ is applicable for $I_R (= I_D(10 - \ln p') - 1)$ less than 4, which implies that this equation represents the behaviour of dense sand at a relatively high p' . For example, for the sand tested in this study ($D_{rc} = 87\%$, i.e. $I_D = 0.87$), the above equation is applicable for $p' \geq 70$ kPa, and, below this stress, ϕ'_p and ψ_p remain the same. The experimental setup used in the present study gives reliable results for $\sigma'_z \geq 25$ kPa, although tests have been done for $\sigma'_z = 12.5$ kPa (also, Adams (2017) conducted DSS tests under $\sigma'_z = 6.0$ kPa), which might give less reliable results. Therefore, for practical applications, limiting values of friction and dilation angles at $\sigma'_z = 25$ kPa are recommended. The increased ϕ'_p and ψ_p below $\sigma'_z = 25$ kPa will not have a significant effect in many low-stress geotechnical problems, such as shallow pipeline–soil interaction, because there will be a small change in the calculated strength for such a change in strength parameters.

3.6. Strain-controlled (constant strain amplitude) Cyclic DSS Test Results

A series of strain-controlled cyclic DSS tests was performed under a constant normal stress of 12.5 kPa to 400 kPa. The shear strain amplitude (γ_a) varied from 0.005–0.1% and the tests were conducted for 100 loading cycles. Table 3.1 shows the details of the test conditions.

3.6.1. Stress–strain Behaviour

Figure 3.7 shows the stress–strain behaviour of the first cycle of each test. The shear stress at the end of the first quarter cycle increases with an increase in normal stress. The maximum shear stress at the end of the first quarter cycle for $\sigma'_z = 400$ kPa is ~ 5.85 times of that for $\sigma'_z = 12.5$ kPa. Another observation is the difference in the shape of the stress–strain curve. For the test at low normal stress, the slope of the stress–strain curve reduces significantly, with an increase in shear strain, compared to that at a low strain, while such a change is not observed in the test at high normal stresses. This implies that the normal stress influences the dynamic behaviour of soil.

3.6.2 Influence of Normal Stress and Strain Amplitude on Cyclic Behaviour

To study the influence of normal stress on the threshold shear strain amplitude (γ_{tv}), the strain amplitude above which plastic deformation occurs, strain-controlled cyclic DSS tests were conducted for the following conditions: (i) $\gamma_a = 0.005\%$ under $\sigma'_z = 12.5$ kPa, (ii) $\gamma_a = 0.01\%$ under $\sigma'_z = 100$ and 400 kPa, and (iii) $\gamma_a = 0.1\%$ under $\sigma'_z = 12.5, 100$ and 400 kPa. Figures 3.8(a–c) show the response for low strain amplitude loading cases: $\gamma_a = 0.005\%$ under $\sigma'_z = 12.5$ kPa and $\gamma_a = 0.01\%$ under $\sigma'_z = 100$ and 400 kPa. In these tests, the loading-unloading curves follow almost a single line, which represents only elastic deformation with a negligible cumulative volumetric strain (i.e., $\gamma_a < \gamma_{tv}$ in these tests). The effects of normal stress on cyclic behaviour are noticeable

in the tests with $\gamma_a = 0.1\%$ (Figs. 3.8(d)–(f)). For $\sigma'_z = 12.5$ kPa, considerable inelastic response starts from the first cycle (i.e., $\gamma_a \geq \gamma_{tv}$). The accumulated axial strain (ε_z) rapidly increases with the number of cycles (Fig. 3.9). However, for $\sigma'_z = 400$ kPa, the inelastic strain is very small, even after 100 cycle loading (Fig. 3.9). The loading-unloading curves again follow almost a single line for $\sigma'_z = 400$ kPa with slight variations in the early cycles (Fig. 3.8(f)). For $\sigma'_z = 100$ kPa, the specimen exhibits some inelastic deformation in the early cycles, which causes some densification, and then follows almost the same hysteresis loop (Fig. 3.8(e)).

Figure 3.9 shows the accumulated axial strain with the number of cycles (N) for the tests with $\gamma_a \geq \gamma_{tv}$, as presented in Fig. 3.8, and additional tests with $\gamma_a = 1\%$ under $\sigma'_z = 12.5$ – 400 kPa. At a given stress level and γ_a , the axial strain increases rapidly in the first few cycles, and then the rate of increase in ε_z decreases with N . For the given γ_a , the lower the stress level, the higher the accumulative axial strain is. Moreover, at a given number of cycles and normal stress, the ε_z increases with shear strain amplitude when $\gamma_a > 0.1\%$.

A major part of the axial strain accumulation occurs within the first few cycles, which is similar to previous studies (Duku et al. 2008; Tong et al. 2010). Figure 3.10 shows that the accumulated axial strain after 15 cycles ($\varepsilon_{z,15}$) increases with shear strain amplitude. Also, $\varepsilon_{z,15}$ increases with a decrease in normal stress, and the effect of stress on ε_z is very significant for a large strain amplitude loading (e.g., $\gamma_a = 1\%$). This finding is in contrast with the test results of Silver and Seed (1971) and Youd (1972), who conducted cyclic DSS tests on Ottawa sand using an NGI-type DSS apparatus, and found no dependency of the accumulative axial strain on the stress level. However, our results are consistent with more recent studies conducted by Duku et al. (2008) and Yee et al. (2012), who used a digitally controlled DSS apparatus to test different sands under $\sigma'_z = 50$ – 400

kPa, and that found that ε_z depends on the stress level. The present study shows the dependency of accumulative axial strain on stress levels, including low stresses ($\sigma'_z = 12.5\text{--}400$ kPa).

Figure 3.10 shows that the threshold shear strain amplitude (γ_{tv}) decreases with applied normal stress—for example, γ_{tv} is $\sim 0.01\%$ and $\sim 0.03\%$ for σ'_z of 12.5 kPa and 400 kPa, respectively.

Additional tests with $\gamma_a = 0.01\text{--}0.1\%$ might give the exact value of γ_{tv} for $\sigma'_z = 25\text{--}400$ kPa. Hsu and Vucetic (2004) reported $\gamma_{tv} = 0.01\text{--}0.02\%$ for sand; however, they could not find any trend of dependency of γ_{tv} on normal stress. A higher value of γ_{tv} ($= 0.05\%$) was reported by Silver and Seed (1971) and Youd (1972). In summary, the present study shows that threshold shear strain amplitude and accumulated axial strain depend on stress level.

Duku et al. (2008) proposed the following power function: $\varepsilon_{z,15} = a(\gamma_a - \gamma_{tv})^b$, where a and b are the material parameters. As the value of γ_{tv} is very small, $\varepsilon_{z,15} = a\gamma_a^b$ can be used for simplicity. Yee et al. (2012) showed that the parameter a depends on relative density and normal stress, in addition to fine content and degree of saturation. For the soil with varying fine contents and relative density, the material constant a decreases with normal stress. Based on regression analysis, $b = 1.2$ was suggested (Duku et al. 2008). The calculated values using this power function are shown by the thick solid lines in Fig. 3.10 for $\sigma'_z = 12.5$ kPa ($a = 3.58$ & $b = 1.0$) and 400 kPa ($a = 1.62$ & $b = 1.70$). These values of a and b are within the range reported by Duku et al. (2008) and Yee et al. (2012) for sand.

3.7. Stress-controlled (constant stress amplitude) Cyclic DSS Test Results

Generally, stress-controlled cyclic DSS tests are conducted in undrained (constant height) conditions to investigate liquefaction behaviour. However, cyclic DSS tests for the constant stress condition are challenging, especially at the low-stress level and for high frequency, because the

control system needs to maintain the normal stress constant. The present DSS apparatus has a better control system for this type of test, as discussed above.

A series of stress-controlled cyclic DSS tests was conducted under constant normal stress for a cyclic stress ratio ($CSR = \tau_a/\sigma'_z$, where τ_a is the shear stress amplitude) of 0.4. It was found that $CSR = 0.4$ is sufficiently large to generate inelastic strain during shearing. The cyclic stress was applied at a frequency of 0.1 Hz, and the test was continued to 100 loading cycles. Table 3.1 shows the further details of the tests.

3.7.1. Stress–strain Behaviour

Figure 3.11 shows the stress ratio (τ/σ'_z) versus shear strain (γ) curves for four tests with a normal stress ranging between 12.5 and 100 kPa. The shear stress increases with shear strain up to $CSR (= 0.4)$, reverses direction (unloading), and changes the direction again at $\tau/\sigma'_z = -0.4$. The shear strain required to reach a certain stress ratio decreases with the number of loading cycles; for example, in the test with $\sigma'_z = 100$ kPa (Fig. 3.11(d)), $\tau/\sigma'_z = 0.4$ is at $\gamma = 2.5\%$ for the first loading, while the required γ is 1% for the same stress ratio in the third loading cycle. Moreover, for a given number of cycles, γ required to reach a τ/σ'_z is smaller in the test with low normal stress. For example, to reach $\tau/\sigma'_z = 0.4$ at the end of the first loading, the specimen with $\sigma'_z = 12.5$ kPa required $\gamma = 0.74\%$ while the required γ is 2.5% for $\sigma'_z = 100$ kPa. The hysteresis loop is also larger in the test with higher normal stress (e.g., compare Figs. 3.11(a & d)).

3.7.2. Effect of Normal Stress on Volumetric Strain

Figure 3.12 shows the accumulated volumetric strain (axial strain) with the number of cycles (N), for varying normal stresses. Similar to strain-controlled tests (Fig. 3.9), the volumetric strain

increases with N , and a major part of the ε_v develops within the first few cycles. The accumulated volumetric strain is highly dependent on normal stress, especially at the low-stress level; for example, ε_v after 15 cycles in the tests with $\sigma'_z = 12.5$ kPa is about two-thirds of that with $\sigma'_z = 25$ kPa. Also, in terms of the effect of σ'_z on ε_v , an opposite trend exists in stress-controlled tests as compared to strain-controlled tests. In the former, ε_v increases with an increase in σ'_z (Fig. 3.9) while it decreases with σ'_z in the latter (Fig. 3.12), which is due to an increase in shear strain amplitude with σ'_z in the stress-controlled tests while it remains the same in the strain-controlled tests.

Figure 3.13 shows the variation of normalized vertical strain, $C_N (= \varepsilon_z/\varepsilon_{z,15})$ with the logarithm of the number of cycles. For comparison, the results of both stress-controlled and strain-controlled ($\gamma_a > \gamma_{tv}$) tests are plotted in this figure. For a given γ_a or SCR , no significant effects of σ'_z on C_N are found before $N = 15$; however, a considerable effect is found for large cycles (e.g., $N = 100$), especially for low $\gamma_a (= 0.1\%)$. At a large N , the higher the σ'_z , the higher the C_N is. Duku et al. (2008) found an approximate loglinear relation between C_N and N within 25 cycles from strain-controlled tests with $\gamma_a = 0.12\text{--}0.77\%$. The present study shows that a loglinear relationship is valid around $N = 15$; however, the slope of the line depends on shear strain amplitude.

3.8. Conclusions

The behaviour of sand under relatively low to higher confining stresses at low strains (e.g., low amplitude cyclic loading), intermediate strains (e.g., strain at the peak shear strength) and large strains (e.g., critical state) is necessary for various geotechnical problems. Limited experimental studies at the low-stress level are available in the literature. The present study investigates the low-stress behaviour of sand using an advanced DSS apparatus. Monotonic and cyclic DSS tests were

conducted for a wide range of normal stresses and the response at low-stress level is compared with that at the typical stress level used in laboratory tests. The following conclusions can be drawn from this study.

- a) The peak and critical state friction angle increase with a decrease in normal stress, especially when the normal stress is less than 50 kPa. Less significant effects of normal stress on the critical state friction angle in the tests on loose sand and the steady-state friction angle in constant height tests are found.
- b) In monotonic DSS tests on dense sand, the dilation angle decreases with an increase in normal stress. The dilation angle also decreases with shear strain (γ) after the peak; however, ψ is not always zero at the typical large strain generally applied in laboratory tests (e.g., $\gamma = 20\%$), although it is small ($\psi < 2^\circ$).
- c) Cyclic compaction occurs when the applied shear strain amplitude is greater than the threshold value, γ_{tv} . Although a clear relation was not found from the limited number of tests, γ_{tv} at high normal stress is larger.
- d) Magnitude of cyclic compaction is significantly influenced by normal stress, especially at the low-stress level. In strain-controlled (constant strain amplitude) tests, cyclic compaction decreases with an increase in normal stress. However, the opposite trend is found for stress-controlled (constant stress amplitude) tests.
- e) Axial strain at 15 cycles can be expressed as a power function of shear strain amplitude.
- f) An approximate loglinear relation exists between the accumulated axial strain and number of cycles. However, it is nonlinear at low and high cycles, depending upon normal stress and shear strain amplitudes.

Finally, although careful attempts have been taken during testing and the present apparatus was developed using advanced technologies for better control and data acquisition, the tests at very low-stress levels (< 10 kPa) are still challenging. Also, further studies are required to investigate the effects of other factors, such as soil type, sample preparation technique, saturation and comparison with field data.

Acknowledgments

The works presented in this paper have been supported by the Natural Sciences and Engineering Research Council of Canada (NSERC), InnovateNL, the former Research and Development Corporation of Newfoundland and Labrador (RDC), the Canadian Foundation for Innovation (CFI) and the state of Libya.

Notation

The following abbreviations and symbols are used in this paper:

C_N = normalized strain, $\varepsilon_z/\varepsilon_{z,15}$

CSR = critical stress ratio, τ_a/σ'_z

D_{rc} = relative density after consolidation

DSS = direct simple shear

DT = dry tamping

$\varepsilon_{z,15}$ = accumulated axial strain after 15 cycles

ε_z = axial strain

ϕ'_{DSS} = friction angle in DSS, $\tan^{-1}(\tau_{zx}/\sigma'_z)$

- ϕ'_p = peak friction angle
- ϕ'_{PT} = phase transformation friction angle
- ϕ'_{ss} = steady state friction angle
- ϕ'_T = friction angle in TXC
- ϕ'_c = critical state friction angle
- γ = shear strain in DSS
- γ_a = cyclic shear strain amplitude
- γ_{tv} = threshold shear strain amplitude
- I_R = relative density index
- K_0 = at-rest earth pressure coefficient
- N = number of cycles
- ψ_p = peak dilation angle
- σ_c = consolidation pressure in TXC
- σ'_1 = major principal effective stress in TXC
- σ'_3 = minor principal effective stress in TXC
- σ'_a = axial effective stress in TXC
- σ'_r = radial effective stress in TXC
- σ'_z = effective axial stress in DSS
- τ_a = shear stress amplitude
- τ_{zx} = shear stress in DSS
- τ_{zx}/σ'_z = stress ratio in DSS
- TXC = triaxial compression

References

- Adams, R.K., 2017. *Near-surface response of beach sand: An experimental investigation*. Master's Thesis, Oregon State University, Oregon, USA.
- Al Tarhouni, M., Fouzder, A., Hawlader, B., and Dhar, A., 2017. Direct simple shear and triaxial compression tests on dense silica sand at low effective stress. *GeoOttawa 70th Canadian Geotechnical Conference*, Ottawa, Canada, Oct. 1–4, 7p.
- Alshibli, K.A., Batiste, S.N., and Sture, S., 2003. Strain localization in sand: plane strain versus triaxial compression. *Journal of Geotechnical and Geoenvironmental Engineering*, 129(6): 483–494.
- Atkinson, J.H., Lau, W.H.W., and Powell, J.J.M., 1991. Measurement of soil strength in simple shear tests. *Canadian Geotechnical Journal*, 28(2): 255–262.
- Been, K., Jefferies, M.G., and Hachey, J., 1991. The critical state of sands. *Géotechnique*, 41(3): 365–381.
- Bernhardt, M.L., Biscontin, G., and O'Sullivan, C., 2016. Experimental validation study of 3D direct simple shear DEM simulations. *Soils and Foundations*, 56(3): 336–347.
- Bolton, M.D., 1986. The strength and dilatancy of sands. *Géotechnique*, 36(1): 65–78.
- Boulanger, R.W., Chan, C.K., Seed, H.B., Seed, R.B., and Sousa, J.B., 1993. A low-compliance bi-directional cyclic simple shear apparatus. *Geotechnical Testing Journal*, 16(1): 36–45.
- Budhu, M., 1984. Nonuniformities imposed by simple shear apparatus. *Canadian Geotechnical Journal*, 21(1): 125–137.
- Budhu, M., 1985. Lateral stresses observed in two simple shear apparatus. *Journal of Geotechnical Engineering*, 111(6): 698–711.

- Budhu, M., and Britto, A., 1987. Numerical analysis of soils in simple shear devices. *Soils and Foundations*, 27(2): 31–41.
- Chakraborty, T., and Salgado, R., 2010. Dilatancy and shear strength of sand at low confining pressures. *Journal of Geotechnical and Geoenvironmental Engineering*, 136(3): 527–532.
- Dabeet, A., 2014. *Discrete element modeling of direct simple shear response of granular soils and model validation using laboratory tests*. Ph.D. Thesis, University of British Columbia. Canada.
- de Josselin de Jong, G., 1988. Elasto–plastic version of the double sliding model in undrained simple shear tests. *Géotechnique*, 38(4): 533–555.
- DeGroot, D.J., Germaine, J.T., and Ladd, C.C., 1993. The multidirectional direct simple shear apparatus. *Geotechnical Testing Journal*, 16(3): 283–295.
- Dobry, R., Ladd, R. S., Yokel, F. Y., Chung, R. M., and Powell, D., 1982. Prediction of pore water pressure buildup and liquefaction of sands during earthquakes by the cyclic strain method. *National Bureau of Standards Building Science Series 138*, Washington, D.C.
- Doroudian, M., and Vucetic, M., 1995. A direct simple shear device for measuring small-strain behavior. *Geotechnical Testing Journal*, 18(1): 69–85.
- Duku, P.M., Stewart, J.P., Whang, D.H., and Venugopal, R., 2007. Digitally controlled simple shear apparatus for dynamic soil testing. *Geotechnical Testing Journal*, 30(5): 368–377.
- Duku, P.M., Stewart, J.P., Whang, D.H., and Yee, E., 2008. Volumetric strains of clean sands subject to cyclic loads. *Journal of Geotechnical and Geoenvironmental Engineering*, 134(8): 1073–1085.

- Dyvik, R., Zimmie, T.F., and Floess, C.H.L., 1981. Lateral stress measurements in direct simple shear device. In *Laboratory shear strength of Soil. ASTM International*. ASTM STP 740: 191–206.
- Franke, E., Kiekbusch, M., and Schuppener, B., 1979. A new direct simple shear device. *Geotechnical Testing Journal*, 2(4): 190–199.
- Fukushima, S. and Tatsuoka, F., 1984. Strength and deformation characteristics of saturated sand at extremely low pressures. *Soils and Foundations*, 24(4): 30–48.
- Georgiannou, V.N., Tsomokos, A., and Stavrou, K., 2008. Monotonic and cyclic behaviour of sand under torsional loading. *Géotechnique*, 58(2): 113–124.
- Guo, P.J., and Stolle, D.F., 2005. On the failure of granular materials with fabric effects. *Soils and Foundations*, 45(4): 1–12.
- Hsu, C.-C., and Vucetic, M., 2004. Volumetric threshold shear strain for cyclic settlement. *Journal of Geotechnical and Geoenvironmental Engineering*, 130(1): 58–70.
- Ishihara, K., and Yamazaki, F., 1980. Cyclic simple shear tests on saturated sand in multi-directional loading. *Soils and Foundations*, 20(1): 45–59.
- Jung, J.K., O'Rourke, T.D., and Olson, N.A., 2013. Uplift soil–pipe interaction in granular soil. *Canadian Geotechnical Journal*, 50(7): 744–753.
- Kang, X., and Kang, G.-G., 2015. Modified monotonic simple shear tests on silica sand. *Journal of Marine Georesources and Geotechnology*, 33(2): 122–126.
- Lings, M.L., and Dietz, M.S., 2004. An improved direct shear apparatus for sand. *Géotechnique*, 54(4): 245–256.
- Mortezaie, A.R., and Vucetic, M., 2012. Small-strain cyclic testing with standard NGI simple shear device. *Geotechnical Testing Journal*, 35(6): 935–948.

- Oda, M., 1972. Initial fabrics and their relations to mechanical properties of granular material. *Soils and Foundations*, 12(1): 17–36.
- Oh-oka, H., 1976. Drained and undrained stress-strain behavior of sands subjected to cyclic shear stress under nearly plane strain condition. *Soils and Foundations*, 16(3): 19–31.
- Ramadan, J.I., 2007. *Settlement of dry cohesionless soil deposits under earthquake induced loading*. Ph.D. Thesis, University of Southern California, California, USA.
- Randolph, M.F., Jamiolkowski, M.B., and Zdravkovic, L., 2004. Load carrying capacity of foundations. *Proc. Skempton Memorial Conf.*, London 1, 207–240.
- Roscoe, K.H., Bassett, R.H., and Cole, E.R.L., 1967. Principal Axes Observed During Simple Shear of a Sand. *In Proceedings of the Geotechnical Conference on Shear Strength Properties of Natural Soils and Rocks*, Oslo, Norway, 19–22 September. 213–237.
- Rousé, P.C., 2018. Relation between the critical state friction angle of sands and low vertical stresses in the direct shear test. *Soils and Foundations*, 58(5): 1282–1287.
- Roy, K., Hawlader, B., Kenny, S., and Moore, I., 2016. Finite element modeling of lateral pipeline–soil interactions in dense sand. *Canadian Geotechnical Journal*, 53(3): 490–504.
- Roy, K., Hawlader, B., Kenny, S., and Moore, I., 2018. Upward Pipe–Soil interaction for shallowly buried pipelines in dense sand. *Journal of Geotechnical and Geoenvironmental Engineering*, 144(11): DOI: 10.1061/(ASCE)GT.1943-5606.0001957.
- Rutherford, C.J., and Biscontin, G., 2013. Development of a multidirectional simple shear testing device. *Geotechnical Testing Journal*, 36(6): 858–866.
- Sadrekarami, A., and Olson, S.M., 2011. Critical state friction angle of sands. *Géotechnique*, 61(9): 771–783.

- Seed, H.B. and Silver M.L., 1972. Settlement of Dry Sands during Earthquakes. *Journal of the Soil Mechanics & Foundations Div., ASCE*, 98(4): 381–397.
- Silver, M.L. and Seed, H.B., 1971. Volume changes in sands during cyclic loading. *Journal of Soil Mechanics & Foundations Div.*, 97(9): 1171–1182.
- Stroud, M.A., 1971. *The behaviour of sand at low stress levels in simple shear apparatus*. Ph.D. Thesis, University of Cambridge, Cambridge, England.
- Tokimatsu, K., and Seed, H.B., 1987. Evaluation of settlements in sands due to earthquake shaking. *Journal of Geotechnical Engineering*, 113(8): 861–878.
- Tong, Z.-X., Zhang, J.-M., Yu, Y.-L., and Zhang, G., 2010. Drained deformation behavior of anisotropic sands during cyclic rotation of principal stress axes. *Journal of Geotechnical and Geoenvironmental Engineering*, 136(11): 1509–1518.
- Vucetic, M., 1994. Cyclic threshold shear strains in soils. *Journal of Geotechnical engineering*, 120(12): 2208–2228.
- Vucetic, M., Lanzo, G., and Doroudian, M., 1998. Damping at small strains in cyclic simple shear test. *Journal of Geotechnical and Geoenvironmental Engineering*, ASCE, 124(7): 585–594.
- White, D.J., Cheuk, C.Y., and Bolton, M.D., 2008. The uplift resistance of pipes and plate anchors buried in sand. *Géotechnique*, 58(10): 771–779.
- Wijewickreme, D., Dabeet, A., and Byrne, P., 2013. Some observations on the state of stress in the direct simple shear test using 3D discrete element analysis. *Geotechnical Testing Journal*, 36(52): 1–8.
- Yee, E., Stewart, J.P., and Duku, P.M., 2012. Seismic compression behavior of sands with fines of low plasticity. In *GeoCongress 2012: State of the Art and Practice in Geotechnical Engineering*, ASCE, 839–848.

- Yoshimine, M., Robertson, P.K., and Wride, C.E., 1999. Undrained shear strength of clean sands to trigger flow liquefaction. *Canadian Geotechnical Journal*, 36(5):891–906.
- Youd, L.T., and Craven, T.N., 1975. Lateral stress in sands during cyclic loading. *Journal of Geotechnical Engineering Division*, ASCE, 101(2): 217–221.
- Youd, T.L., 1972. Compaction of sands by repeated shear straining. *Journal of Soil Mechanics & Foundations Div*, 98(SM7): 709–725.
- Wu, Z.-X., Yin Z.-Y., Dano C., and Hicher P.-Y., 2020. Cyclic volumetric strain accumulation for sand under drained simple shear condition. *Applied Ocean Research*, 101(2020): 102200. <https://doi.org/10.1016/j.apor.2020.102200>.

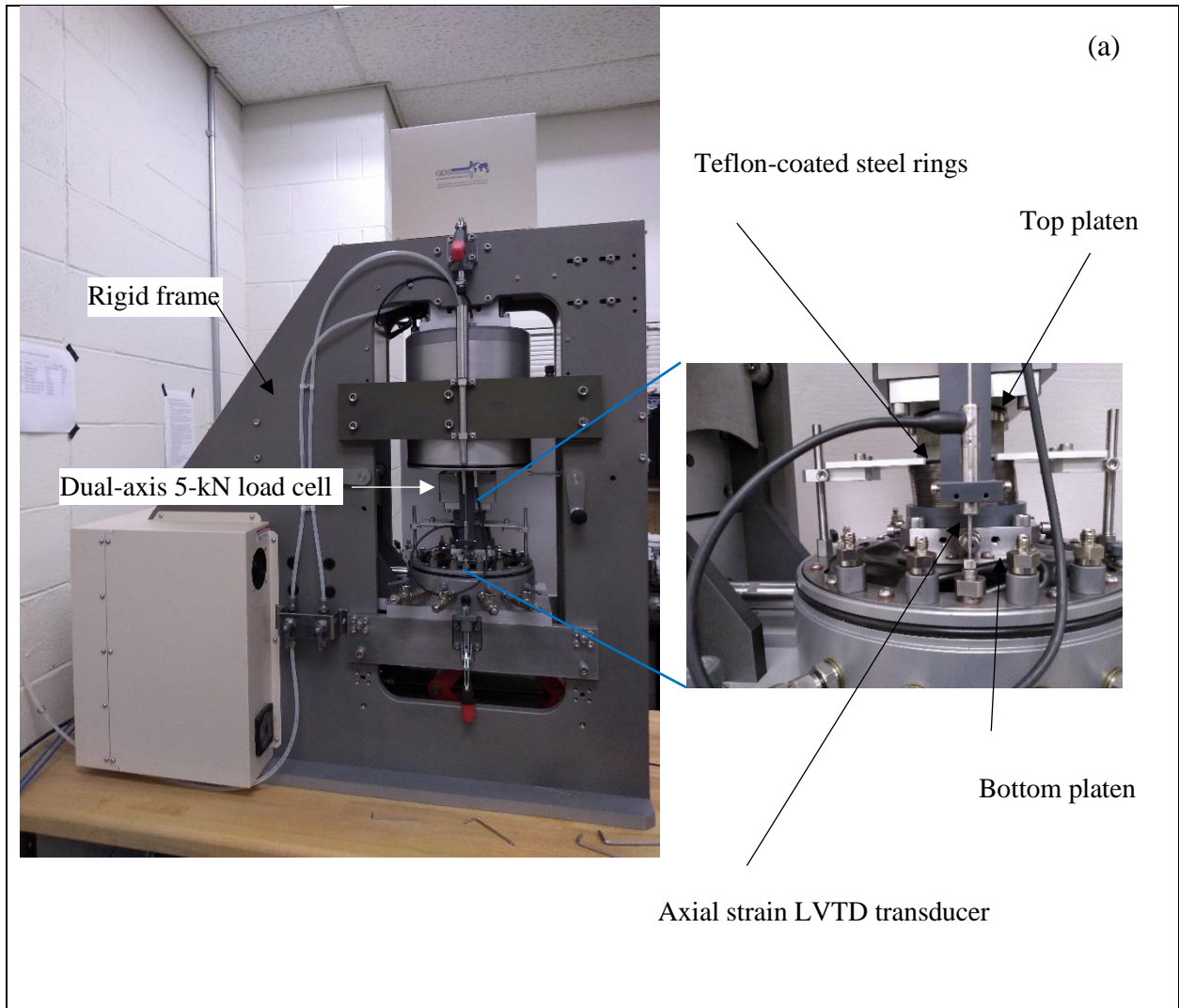


Fig. 3.1. Apparatus used: (a) Combined Advanced Dynamic Cyclic Simple Shear apparatus; (b) Schematic of DSS apparatus

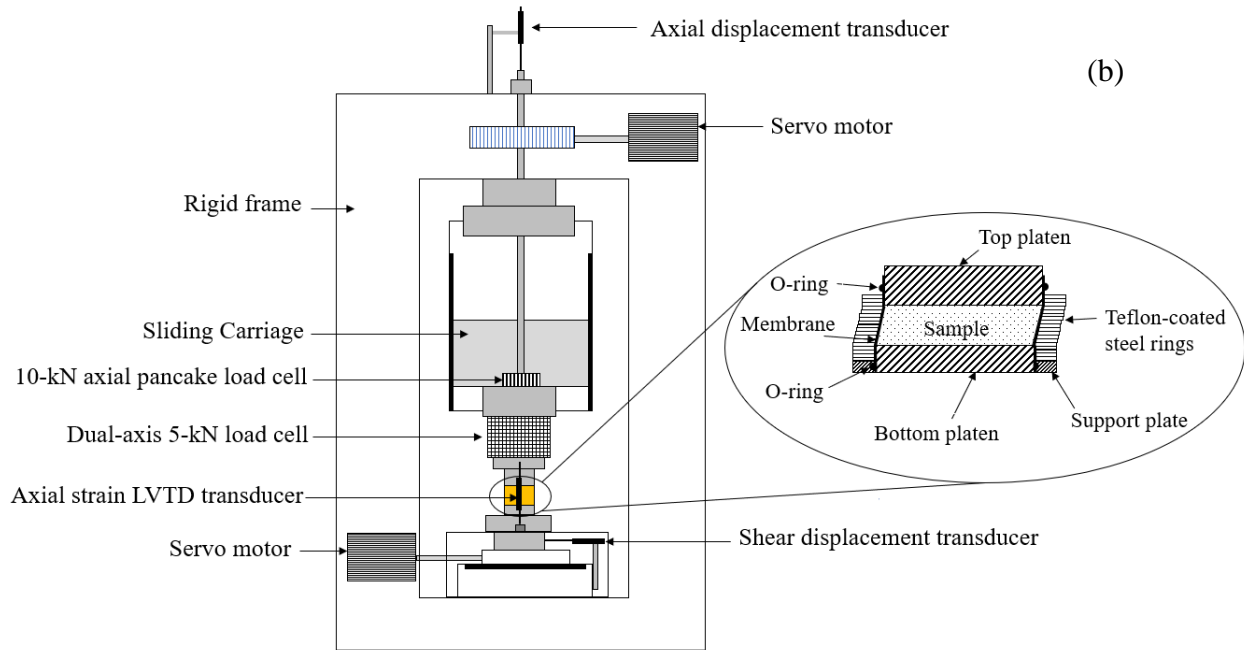


Fig. 3.1. Apparatus used: (a) Combined Advanced Dynamic Cyclic Simple Shear apparatus; (b) Schematic of DSS apparatus

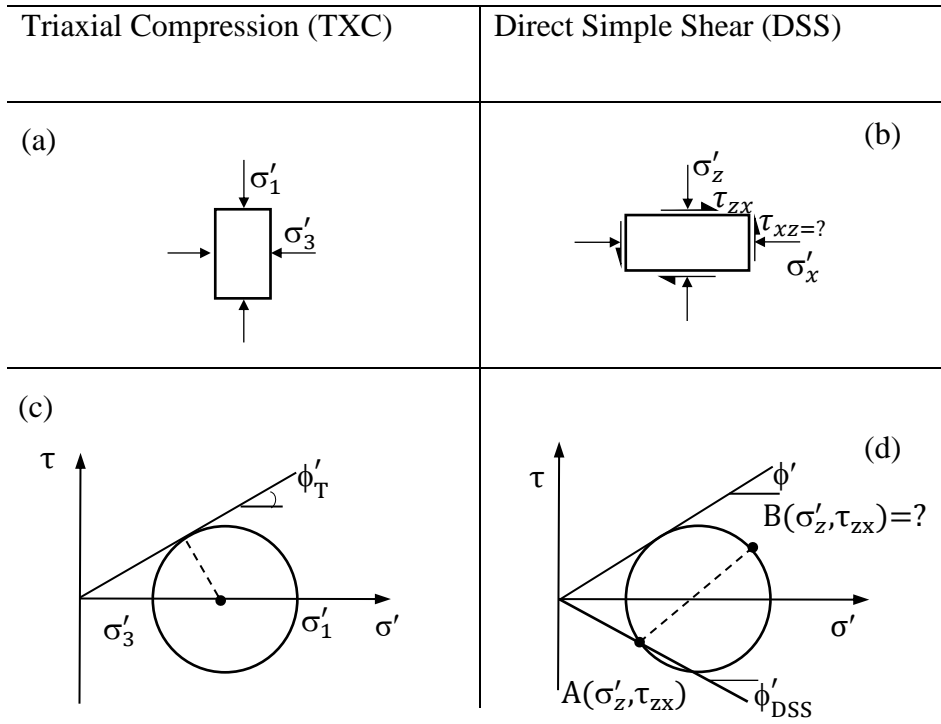


Fig. 3.2. Stresses and strains in triaxial and direct simple shear specimens

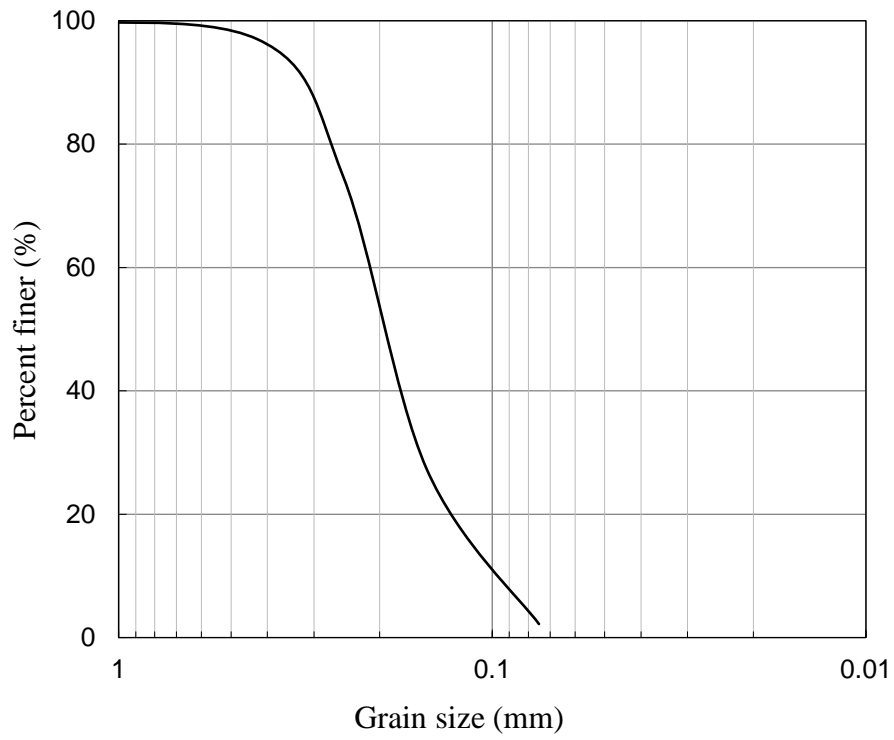


Fig. 3.3. Grain size distribution of silica sand used in this study

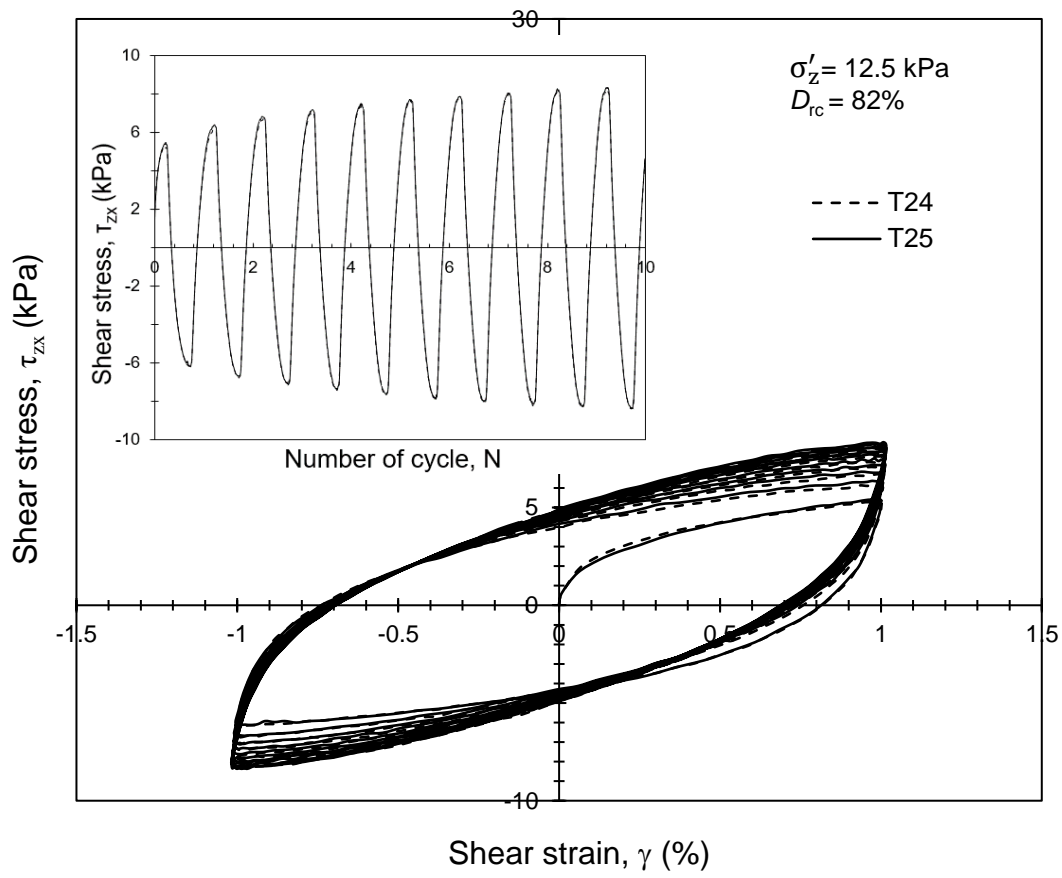


Fig. 3.4. Repeatability in cyclic direct simple shear test

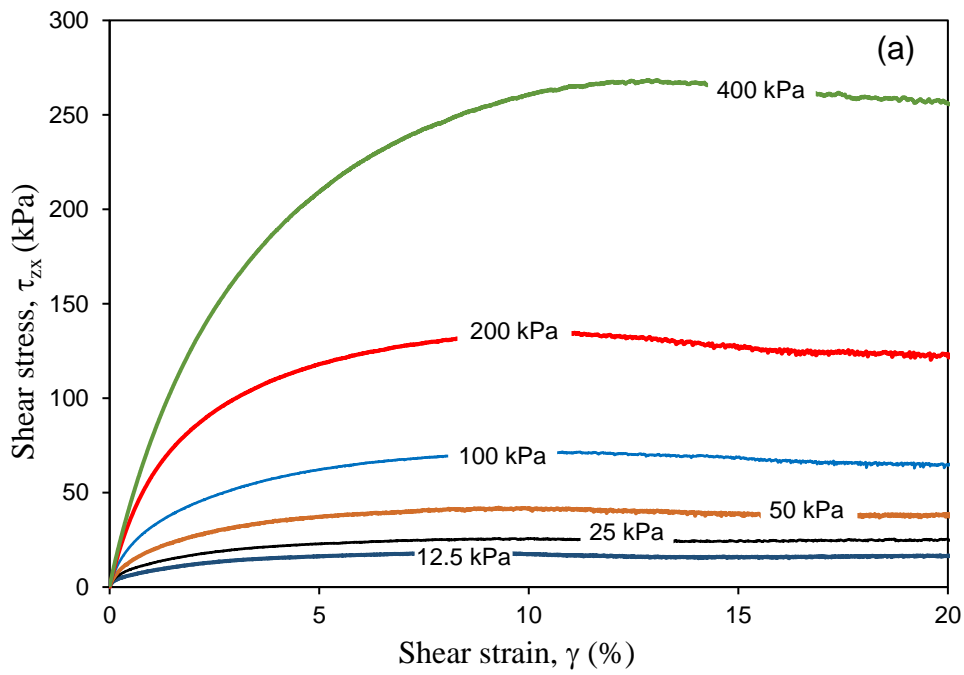


Fig. 3.5. Effects of normal stress on monotonic test results: (a) Stress–strain behaviour; (b) Stress ratio; (c) Volume change; (d) Mobilized dilation angle

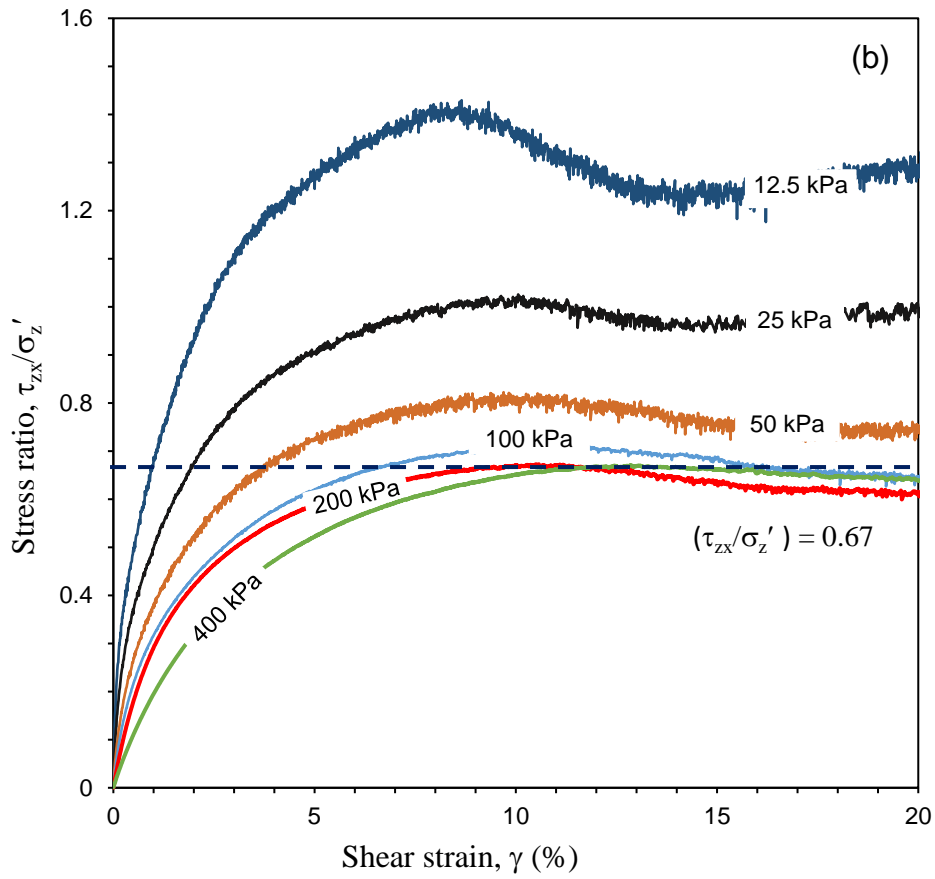


Fig. 3.5. Effects of normal stress on monotonic test results: (a) Stress–strain behaviour; (b) Stress ratio; (c) Volume change; (d) Mobilized dilation angle

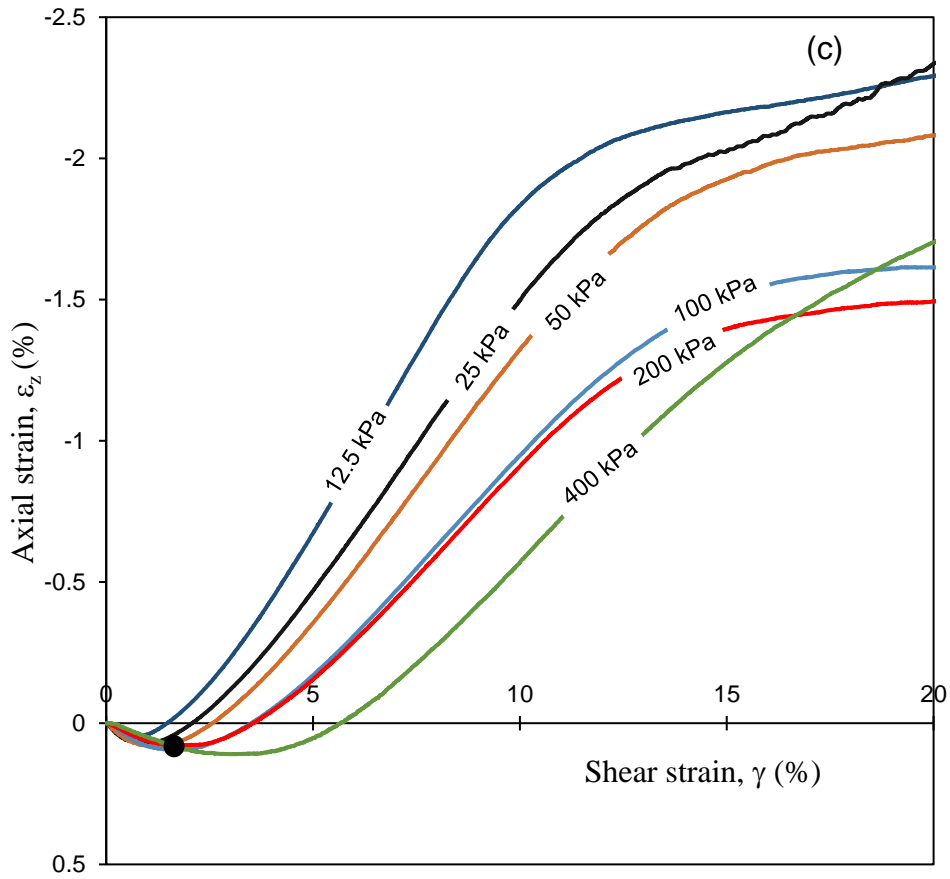


Fig. 3.5. Effects of normal stress on monotonic test results: (a) Stress–strain behaviour; (b) Stress ratio; (c) Volume change; (d) Mobilized dilation angle

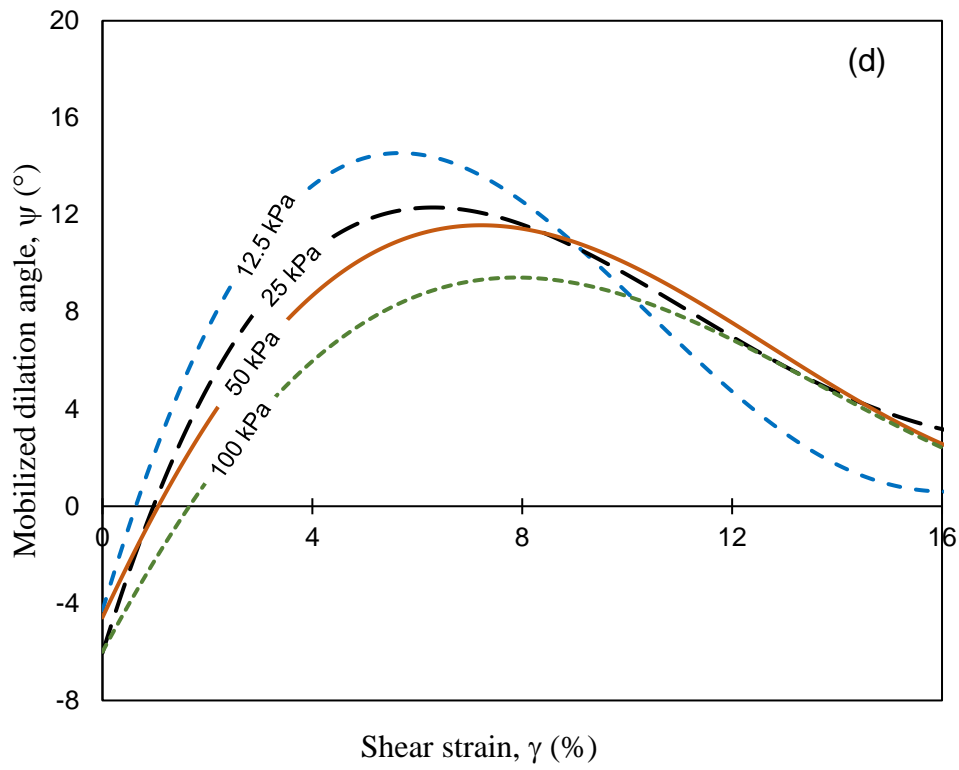


Fig. 3.5. Effects of normal stress on monotonic test results: (a) Stress–strain behaviour; (b) Stress ratio; (c) Volume change; (d) Mobilized dilation angle

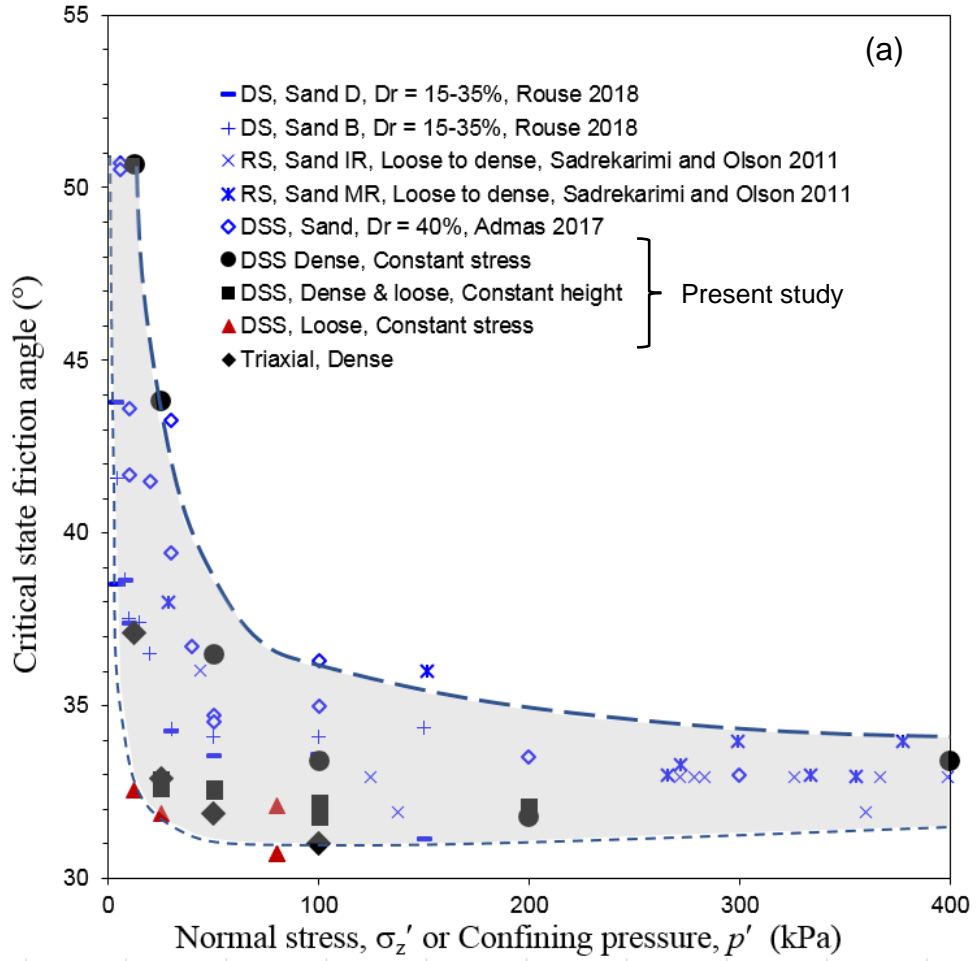


Fig. 3.6. Effects of normal stress on friction angles: (a) critical state friction angle; (b) peak friction angle

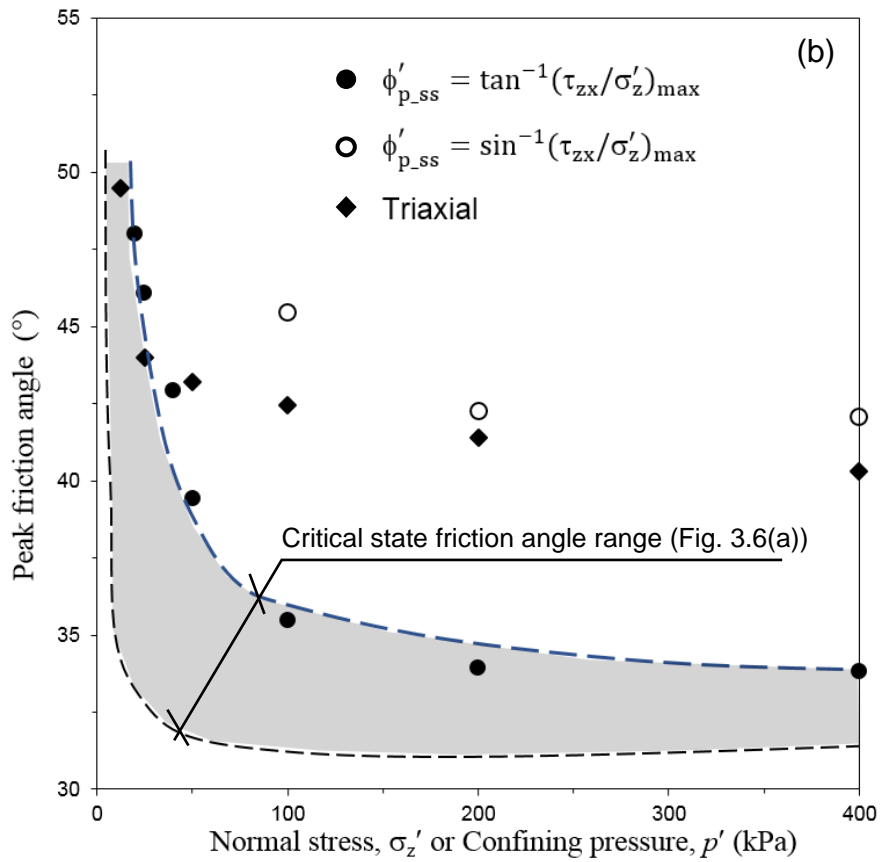


Fig. 3.6. Effects of normal stress on friction angles: (a) critical state friction angle; (b) peak friction angle

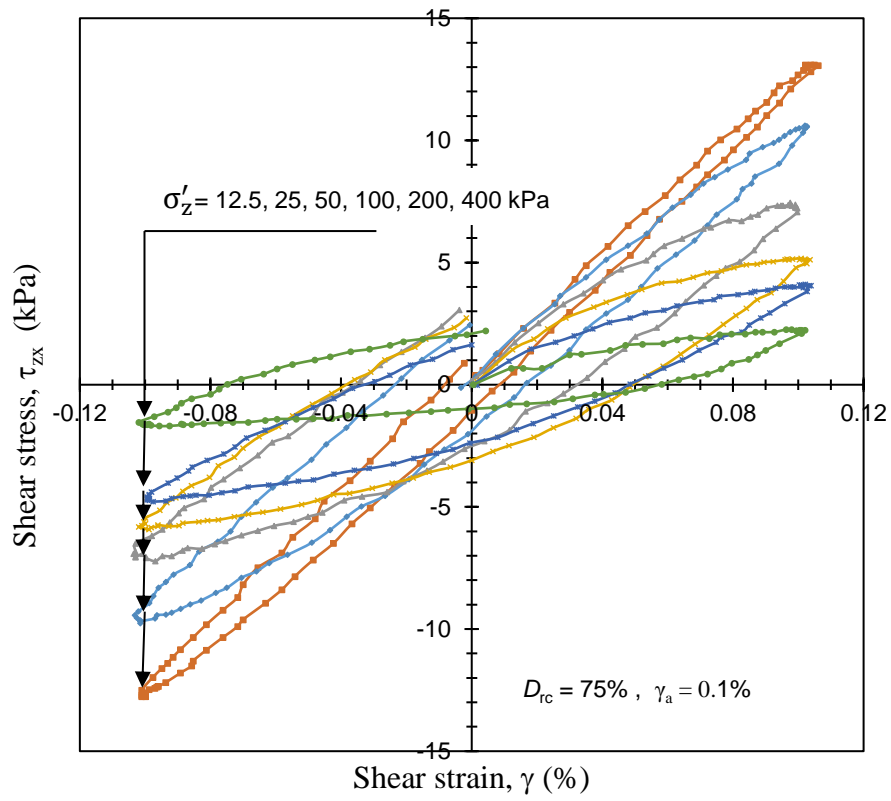


Fig. 3.7. Stress–strain response in first cycle of loading for varying normal stresses

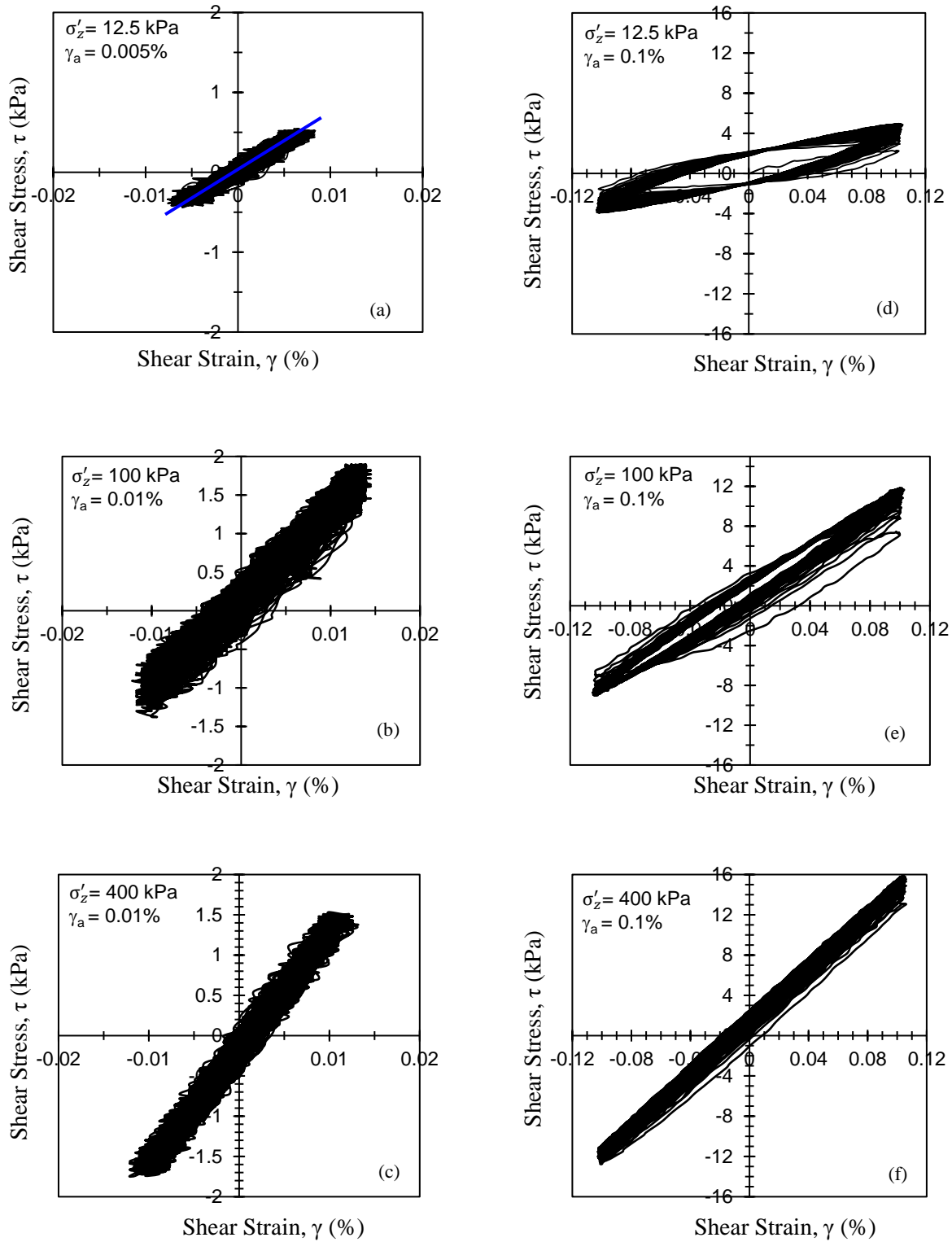


Fig. 3.8. Stress–strain response for varying normal stresses at low-strain amplitudes

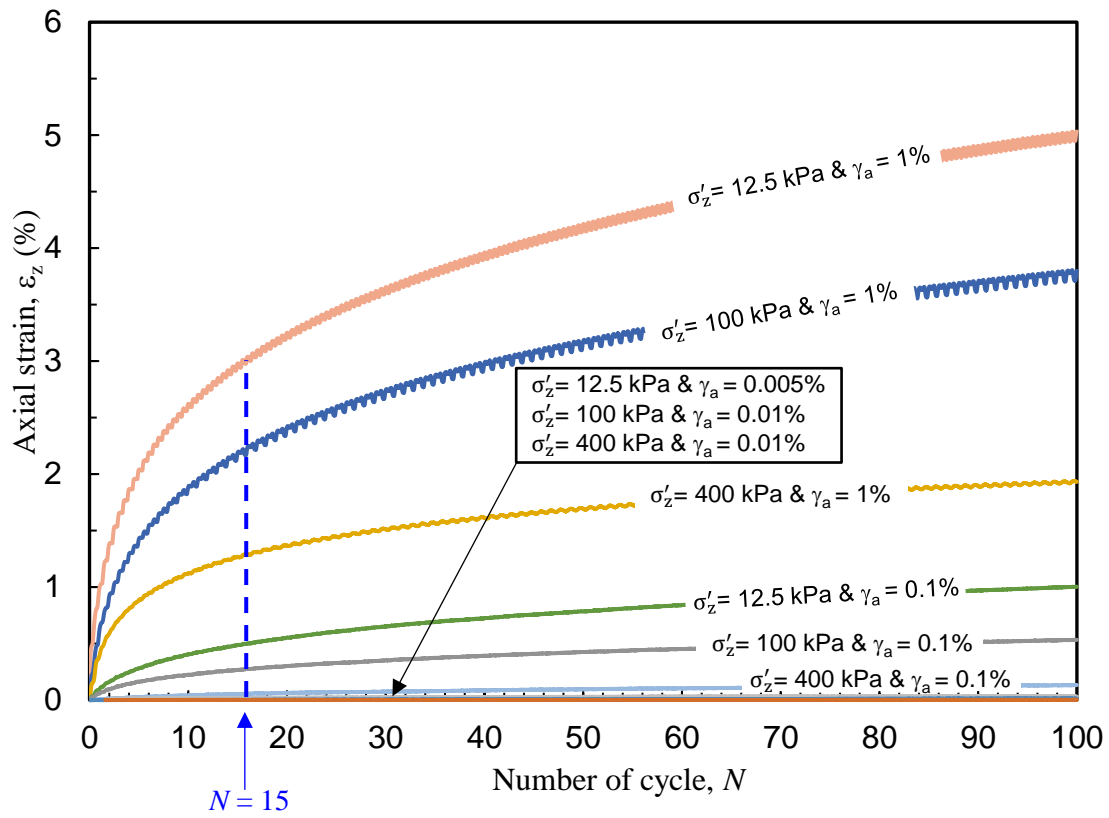


Fig. 3.9. Axial strain for varying normal stresses and shear strain amplitudes in constant strain amplitude cyclic tests

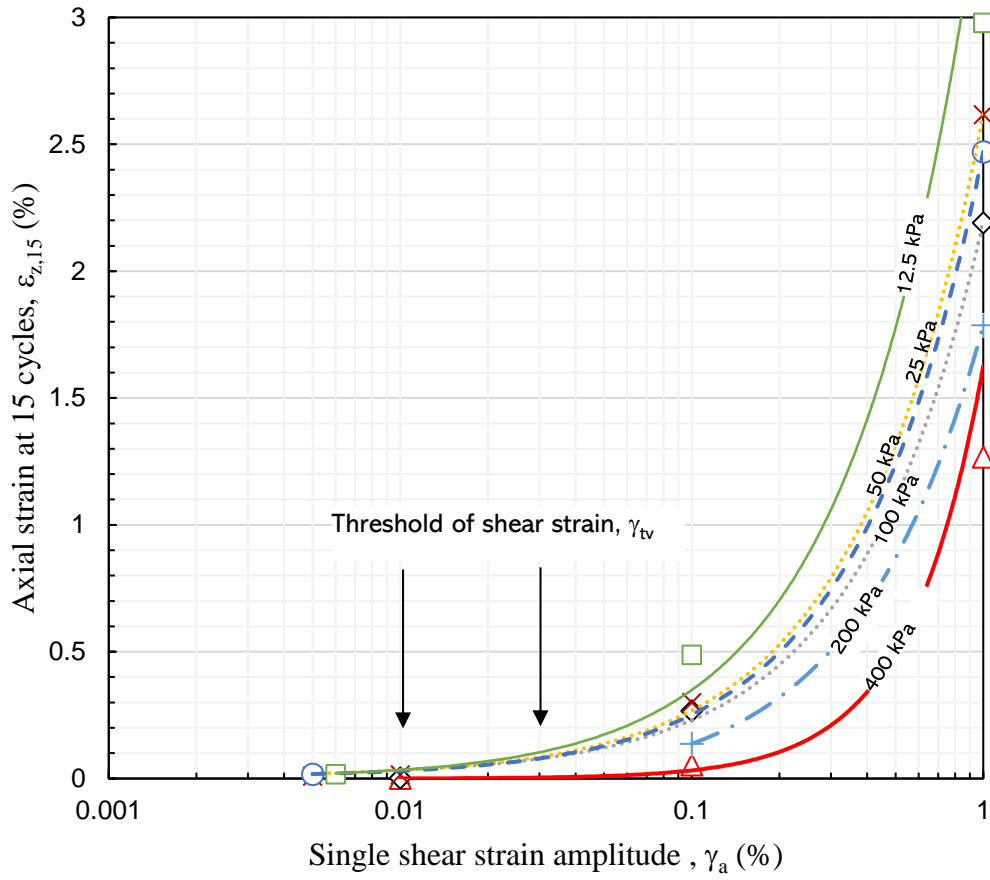


Fig. 3.10. Effects of normal stress on axial strain at 15 cycles in strain-controlled tests

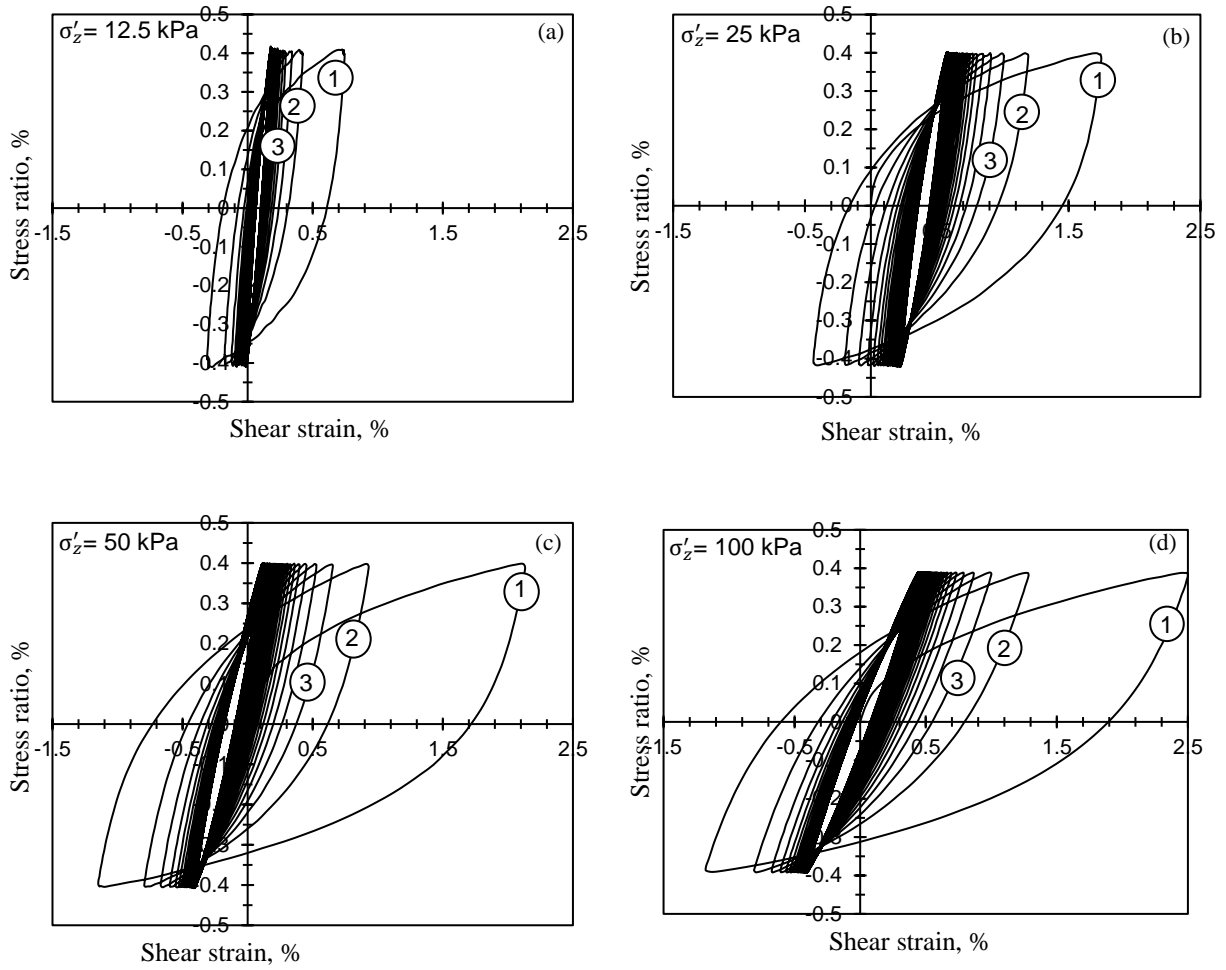


Fig. 3.11. Stress–strain response in stress-controlled cyclic tests at low stress for 100 cycles

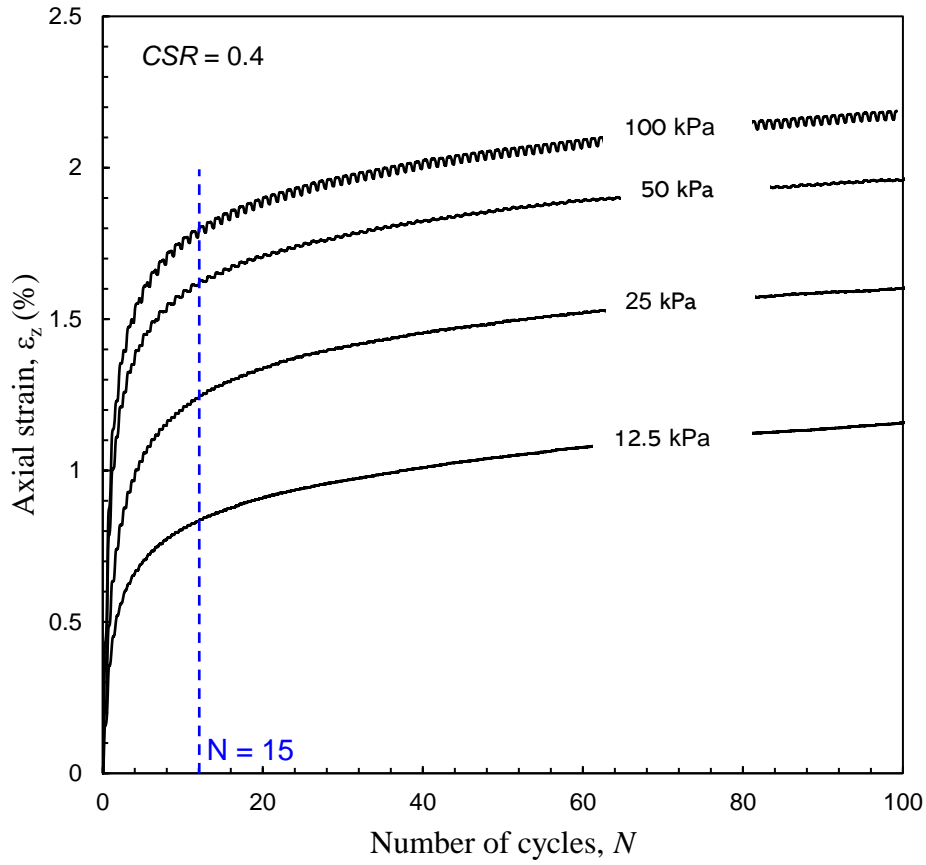


Fig. 3.12. Effects of normal stress on axial strain in constant stress amplitude cyclic loading

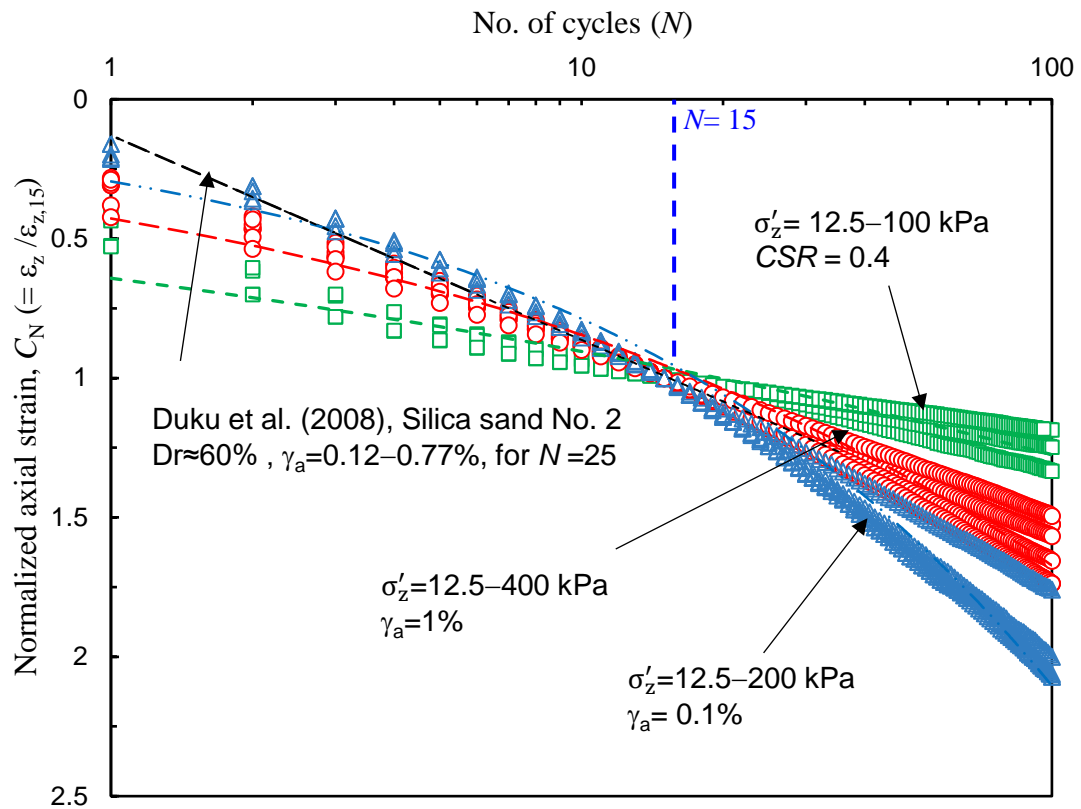


Fig. 3.13. Normalized axial strain in stress- and strain-controlled tests

Table 3.1. Summary of direct simple shear test conditions

Test no.	Normal stress (kPa)	D_{rc} (%)	Strain rate (%/min)	Shear strain amplitude, γ_a (%)	Cyclic stress ratio (CSR)
a) Monotonic					
T1	12.5			-	-
T2	20			-	-
T3	40			-	-
T4	50	87	0.16	-	-
T5	100			-	-
T6	200			-	-
T7	400			-	-
<hr/>					
T8	12.5	20		-	-
T9	25	28	0.16	-	-
T10	80	40		-	-
T11	80	40		-	-
<hr/>					
b) Cyclic, strain-controlled (constant strain amplitude)					
T12	12.5	75	-	0.005%	-

T13	100		-		-
		75		0.01%	
T14	400		-		-
T15	12.5		-		-
T16	25		-		-
T17	50		-		-
		75		0.1%	
T18	100		-		-
T19	200		-		-
T20	400		-		-
T21	12.5		-		-
T22	100	75	-	1%	-
T23	400		-		-
T24	12.5		-		-
		82		1%	
T25	12.5		-		-

c) Cyclic, stress-controlled (constant stress amplitude)

T26	12.5		-	-	
T27	25		-	-	
		75			0.4
T28	50		-	-	
T29	100		-	-	

CHAPTER 4

Drained Cyclic Behaviour and Stress–Dilatancy Relationship of Sand in Direct Simple Shear Tests

Abstract

A series of direct simple shear tests were conducted to investigate the cyclic behaviour, dynamic properties, and stress–dilatancy relationship of sand for a wide range of constant vertical stresses, including low stresses. Multistage strain-controlled tests were conducted by applying low to high amplitudes of cyclic loading. Test results show that volumetric strain is related to the vertical stress and shear strain amplitude. The cyclic shear modulus decreases and damping ratio increases with shear strain amplitude; however, they are influenced by the low-amplitude cyclic loading history. The cyclic stress–dilatancy relationship depends on the vertical stress, shear strain amplitude, and the number of cycles. In some tests, the stress–dilatancy relationship can be represented by two parallel lines for unloading and reloading, except for the initial parts. The increase in density with cyclic loading reduces the contractive behaviour and increases the dilative response in the large-amplitude loading cases, which reduces the rate of volumetric compaction with the number of cycles.

Keywords: direct simple shear; constant stress; cyclic stress–dilatancy; multistage loading; cyclic compaction sand.

4.1. Introduction

Sand in the field might be subjected to cyclic loading for a wide range of frequencies, durations, and shear stress/strain amplitudes. When drainage is permitted, the generated volumetric strain causes settlement, which might exceed the serviceability limit state. On the other hand, pore water pressure might build up and liquefy the sand in undrained conditions. The undrained cyclic behaviour of sand has received much more attention than the drained one because the liquefaction could cause catastrophic failures. However, the drained cyclic behaviour is essential for the safe design of many structures where the volume change due to cyclic loading is a critical parameter. As well as for loose and medium dense sands, laboratory tests show that cyclic loading could further densify dense sand, and, in some cases, cause even more than 100% relative density (denser than the maximum density achieved by ASTM 4253) (Youd 1972).

For monotonic loading, the volume change in a drained condition can be related to the pore water pressure build up in an undrained condition. The volume change due to drained cyclic loading is more complex. Youd (1972) conducted drained direct simple shear (DSS) tests on dense Ottawa sand ($D_r = 75\% - 79\%$) for cyclic loads of different shear strain amplitudes (γ_a) (0.1%–9%). It was found that the volumetric strain (ε_z) increases with shear strain amplitude ($> 0.05\%$), and ε_z is not influenced by the vertical stress (σ'_z), which is in line with the experimental results of Silver and Seed (1971). Kang et al. (2016) modified a DSS apparatus to apply the confining pressure and measure the radial strain, instead of radial constraints, as in the typical DSS apparatus. They found that ε_z increases with an increase in γ_a but decreases with an increase in initial relative density and confining pressure. Generally, a sand layer in the field does not experience uniform cyclic loading. Conducting multistage drained cyclic triaxial tests for the initial consolidation pressures of 200–500 kPa, López-Querol and Coop (2012) showed that the sand might have a memory of previously

occurring volumetric strain, which could influence the behaviour in the subsequent loading cycles. Hsu and Vucetic (2004) conducted multistage drained DSS tests under vertical stresses of 95–666 kPa to evaluate the threshold shear strain amplitude (γ_{tv}), above which a considerable volumetric strain occurs.

The volumetric response can be evaluated using the cyclic stress–dilatancy relationship—a relation between the stress ratio, (τ_{zx}/σ'_z) and dilatancy ($-d\varepsilon_v^p/d\gamma^p$), where τ_{zx} is the shear stress on the horizontal plane, and $d\varepsilon_v^p$ and $d\gamma^p$ are the plastic components of the volumetric and shear strain increments, respectively. Several stress–dilatancy relationships have been developed for monotonic loading (Taylor 1948; Rowe 1962; Roscoe et al. 1963). Some studies also developed a cyclic stress–dilatancy relationship by conducting drained cyclic triaxial tests (Pradhan and Tatsuoka 1989; López-querol and Coop 2012) and hollow cylinder torsional shear tests (Pradhan and Tatsuoka 1989; Shahnazari and Towhata 2002; Georgiannou et al. 2008; Wahyudi et al. 2010; Wahyudi and Koseki 2012; De Silva et al. 2014).

Attempts have also been made to evaluate stress–dilatancy from DSS test results. Based on a particulate mechanics concept and using slip and nonslip conditions between the grains, Ueng and Lee (1990) and Lee (1991) developed a simple stress–dilatancy relation, which consists of two straight lines for unloading and reloading paths. Ueng and Lee (1990) showed a reasonable agreement between their proposed linear stress–dilatancy relation and cyclic DSS and triaxial test results on Ottawa and Fulung sands. Tests were conducted under vertical stresses (confining pressure in triaxial) of 98 kPa and 196 kPa and two tests under 49 kPa. Park et al. (2005) presented a ‘swing plane model,’ where the stress–dilatancy for unloading and reloading was defined by two linear lines, which is similar to the Lee (1991) model. Implementing this model in a computer

program, they compared the numerical prediction and undrained cyclic simple shear test results for the vertical effective stress of 100 kPa.

Pradhan and Tatsuoka (1989) conducted drained cyclic triaxial and cyclic simple shear tests and found a unique stress–dilatancy relationship—independent of initial density, shearing mode, cyclic loading history and confining pressure—that can be modelled by modifying the sliding block theory, Rowe’s theory and Taylor’s energy dissipation theory. Shahnazari and Towhata (2002) conducted drained cyclic torsional simple shear tests on Toyoura sand and found that the stress–dilatancy relationship after the virgin loading was influenced by the initial density and shear history but was independent of the initial confining pressures (53–184 kPa) and methods of consolidation (isotropic/anisotropic). De Silva et al. (2014) conducted stress-controlled cyclic tests on normally and overconsolidated sand and found a stress–dilatancy relationship similar to that of Shahnazari and Towhata (2002). They also modified the linear stress–dilatancy relationship proposed by Nishimura (2002), using a bilinear relation to capture the response near the stress reversal.

These studies show contradictory or inconclusive results for the factors affecting the stress–dilatancy relationship. Most of the studies developed stress–dilatancy relationships based on experimental results on loose to medium dense sands under sufficiently large confining stresses. However, the sand might be compacted to a sufficiently dense condition (e.g., compacted soil around foundations, compacted seabed sediments by wave and wind loadings) prior to large-amplitude cyclic loading. Moreover, the confining stress might be small in many cases, compared to the stress level considered in many previous studies (e.g., soil around buried pipelines).

The objective of this study is to present the drained behaviour of sand from multistage cyclic loading tests for a wide range of vertical stresses, including low stresses. The paper begins with a

brief description of the capabilities of the DSS apparatus used in this study, which are critical, especially for the low-stress level tests. A series of multistage cyclic loading tests are then discussed. Finally, the stress–dilatancy relationship for cyclic loading is evaluated.

4.2. Experimental Works

The DSS tests have been extensively used to investigate undrained response for soil. Many DSS apparatuses have been designed primarily for undrained testing (constant height), which can be done relatively easily, simply by maintaining zero displacement (locking) during shearing. However, maintaining constant stress during cyclic loading requires an advanced control system. In fact, constant stress cyclic simple shear behaviour for a large number of cycles and the interpretation of stress–dilatancy behaviour are not well studied. The DSS apparatus used in this study has the advantage of measuring and controlling stresses and strains with high precision. Also, the tests can be done at a low-stress level.

4.2.1 Direct Simple Shear Apparatus

A Combined Advanced Dynamic Cyclic Simple Shear apparatus at Memorial University of Newfoundland, supplied by GDS Instruments Ltd., was used. A wide range of soil types (fine- to coarse-grained) can be tested for constant stress and undrained conditions. The soil specimen is confined laterally within a stack of 1-mm thick rigid Teflon-coated steel rings. This apparatus can be used to conduct tests in a saturated condition, which is not available in many DSS apparatuses.

One of the main advantages of this apparatus is that the test can be performed for a wide range of vertical stresses, including at low-stress levels, with sufficient confidence in the measurements. This system is equipped with dual-axis 5-kN load cells to control and measure axial

and lateral loads with an accuracy better than 0.1% and a resolution of 0.2 N. The high precision feedback system controls the stresses and displacements while maintaining a high level of accuracy. Further details of the apparatus specifications and capabilities are available in Chapter 3. Tests can be performed for different consolidation and shearing stage scenarios without any time lag between the stages, such as during multistage cyclic loading, as presented in this study.

4.2.2 Material Tested

DSS tests were conducted on a poorly graded fine-grained silica sand. The sand grains were sub-rounded to sub-angular. The mean diameter, uniformity coefficient, and coefficient of gradation were 0.18 mm, 1.12, and 2.23, respectively. The specific gravity of sand grains was 2.65. The maximum and minimum void ratios were 1.048 and 0.606, respectively. All these tests were conducted according to ASTM standards.

4.2.3 Cyclic Tests

Soil specimens were prepared using a dry tamping method, as described in Al Tarhouni et al. (2017). The specimen was consolidated first by applying a vertical stress, and then, keeping the vertical stress constant, the cyclic load was applied at the bottom of the specimen, either in strain-controlled condition with varying shear strain amplitudes (γ_a), or stress-controlled condition with a cyclic stress ratio, $CSR (= \tau_a / \sigma'_z$, where τ_a is the shear stress amplitude). For dense specimens, the relative density after consolidation (D_{rc}) was $\sim 75\%$, except for test T1 where $D_{rc} = 80\%$; however, $D_{rc} = 43\%$ for the loose specimens (T23–T25) (Table 4.1). Similar to previous studies (e.g, Hsu and Vucetic 2004), the cyclic load was applied at a frequency (f) of 0.1 Hz, except for the last stage with $\gamma_a = 8\%$, where $f = 0.01$ Hz.

Table 4.1 shows the 25 cyclic DSS test conducted for varying vertical stresses. Among them, 18 strain-controlled (T1–T18) and four stress-controlled (T19–T22) tests were on dense and 3 strain-control (T23–T25) tests were on loose sand specimens. The first test (T1) was conducted at $\sigma'_z = 100$ kPa, and a single-stage shear strain amplitude of 1% was applied for 1000 cycles. It was found that after 100 cycles, the volume change of the specimen was small. A similar response has been observed in previous studies (Silver and Seed 1971; Kang et al. 2016). Therefore, in the multistage tests (T2–T18 & T23–T25), 100 cycles of load were applied in each stage. The stress-controlled (T19–T22) cyclic tests were conducted with $CSR = 0.4$ and $f = 0.1$ Hz.

The multi-stage tests started with $\gamma_a = 0.005\%$ in T2–T4, $\gamma_a = 0.01\%$ in T5–T7, $\gamma_a = 0.1\%$ in T8–T13, and $\gamma_a = 1\%$ in T14–T18 & T23–T25 (Table 4.1). The first stage of each test represents a cyclic test without any experience of cyclic loading history. The purpose of applying a multistage shear strain amplitude is to investigate the strain history effects on cyclic behaviour, dynamic properties and stress–dilatancy relationship. Note that some previous studies have also investigated the effects of the strain history on cyclic behaviour and dynamic properties, using hollow cylinder torsional and resonant column torsional devices (Tatsuoka et al. 1979; Alarcon-Guzman et al. 1989; Stephenson et al. 1991; Uthayakumar 1992).

The multistage tests were conducted for shear strain amplitudes ranging between 0.005% and 8% to investigate the response of sand both in small strains and nonlinear plastic zones, which are required for modelling cyclic behaviour. For example, for a liquefaction assessment, it is recommended to consider a 2.5% axial strain amplitude in triaxial tests, which is equivalent to $\sim 3.75\%$ shear strain amplitude (National Research Council (NRC) 1985; Ishihara 1993). The first author of this paper adopted this recommendation to investigate the cyclic behaviour of non-plastic silts in undrained simple shear loading conditions (Al Tarhouni et al. 2011). The Japanese

Geotechnical Society Standards (JGS 0541-2009) suggested a 5% double amplitude axial strain in cyclic triaxial tests, which represents $\sim 7.5\%$ of the shear strain amplitude in DSS. Most of the studies available in the literature conducted DSS tests with $\gamma_a \leq 2\%$ (Youd 1972; Hsu and Vucetic 2004; Duku et al. 2008) while some considered a higher γ_a (2%–5%) (Shahnazari and Towhata 2002; Wahyudi and Koseki 2012).

4.3. Observed Stress–strain Behaviour

4.3.1 Single-stage Test

The stress–strain response of the specimen in test T1 ($D_{rc} = 80\%$, $\sigma'_z = 100$ kPa & $\gamma_a = 1\%$) is shown in Fig. 4.1(a). The shear stress (τ) increases with the shear strain (γ) up to the shear stress amplitude (τ_a) at $\gamma = \gamma_a$ where the shear stress and strain reverse direction (unloading). The shear stress and shear strain increments ($d\tau$ & $d\gamma$) are positive in the virgin loading (backbone curve) and reloading while they are negative in unloading paths. A cycle represents the loop starting from unloading to the end of reloading, and N represents the number of cycles.

Figure 4.1(b) shows the axial strain (ε_z , positive for compaction) generated incrementally in each cycle. The axial strain generated quickly in the first few cycles ($N \sim 15$), although 1,000 cycles were applied. The axial strain increment per cycle is small after 100 cycles. In the earlier cycles (e.g., $N = 1-6$ in Fig. 4.1(c)), the plastic shear strain resulted only in a decrease in volume of the specimen (positive ε_z), which increased the density. However, at a large number of cycles, the dense soil sample exhibits both compaction at the start and dilation (expansion) at the end of each unloading and reloading path, which results in small net compaction of the specimen per cycle.

Figure 4.1(d) shows that the maximum stress ratio in a cycle increases rapidly in the first few cycles, which is because of the quick compaction of the soil in these cycles. The axial strain in these cycles is primarily (or completely) contractive. However, at a large number of cycles, it changes from contractive to dilatative twice within the same cycle, which makes a shadow similar to a palm shape (Fig. 4.1(d)). A similar shape of stress–strain behaviour was also reported by Shahnazari and Towhata (2001) from cyclic hollow cylinder tests.

4.3.2 Typical Response of Multistage Cyclic Test

Volumetric strain generation in a typical multistage test (T3) ($\sigma'_z = 25$ kPa) is shown in Fig. 4.2. In this test, the shearing was started with a low amplitude cyclic loading of $\gamma_a = 0.005\%$, which was then increased to $\gamma_a = 0.01, 0.1, 1.0, 2.0, 4.0$ and 8.0% without a time lag. In each stage, 100 cycles of load were applied; however, only 10 cycles were applied in the last stage. Figure 4.2 shows that ϵ_z was almost zero in the first 100 cycles with $\gamma_a = 0.005\%$ (Stage 1). The axial strain started to increase with N when $\gamma_a = 0.01\%$ (Stage 2), which indicates that the threshold shear strain amplitude (γ_{tv}) is between 0.005% and 0.01% . In Stage 3 ($\gamma_a = 0.1\%$), the accumulated axial strain was $\sim 1\%$. The maximum axial strain of $\sim 3.3\%$ generated in Stage 4 with $\gamma_a = 1\%$. However, in the latter three stages with higher γ_a ($= 2\%–8\%$ in Stages 5–7), the total accumulated axial strain was smaller than those of the previous stage.

This observation can be explained considering the volume change behaviour in a cycle at different stages. Inset I of Fig. 4.2 shows the volumetric strain in the 5th cycle ($N = 3.75–4.75$) in Stages 4 and 6. The lower part of this inset for Stage 4 shows that the shearing starts with almost zero volume change, and then dilates later when it reaches close to the maximum shear strain. During unloading, the sample first contracts and then dilates at the end. Finally, for reloading, it again

contracts. The whole process causes considerable compaction (compare the points at $\gamma = 0$). However, in Stage 6 (upper part of Inset I), large shear strains cause more dilation of the dense sand specimen, which compensates for the compaction component, and gives small net compaction in this cycle.

The dilative response increased with the number of cycles as the soil was densified. Therefore, a thick band of ε_z was found in the last three stages (Fig. 4.2). For a given cycle, the maximum value of ε_z in that band represents the most compacted condition (point A in Inset I), and the minimum value is the state where the maximum dilation occurred (point B in inset-I).

At the point of increase in shear strain amplitude—for example, point P in Fig. 4.2, where γ_a was increased from 0.1% to 1.0%—the axial strain generation per cycle increased rapidly once γ_a was increased. However, with such an increase at a large shear strain amplitude—for example, point Q in Fig. 4.2, where γ_a was increased from 2.0% to 4.0%—a significant dilation occurred in the first reloading period (path XY in Inset II) because the soil is very dense at this stage (as discussed later) and dilates considerably due to such a large shear strain. Although subsequent unloading and reloading resulted in overall densification, there was a decrease in density in the first cycle of this stage (i.e., ε_z at point Z is smaller than that at X).

In summary, the volumetric strain generation due to cyclic loading could involve both compaction and dilation in the same cycle, depending upon the shear strain amplitude and cyclic loading history of the soil element, which makes the process more complex, compared to monotonic loading cases. Therefore, the cyclic stress ratio–dilatancy relation needs to be developed, which is discussed later.

4.3.3 Effects of Vertical Stress and Strain Amplitude in Multistage Tests

Figures 4.3(a–f) show the variation of the stress ratio (τ_{zx}/σ'_z) for tests T8 and T13, which were carried out at $\sigma'_z = 12.5$ kPa and $\sigma'_z = 400$ kPa, respectively. In these tests, all other conditions, including the shear strain amplitudes and density, were the same. The hysteresis loops for only the first 15 cycles in each stage of loading are shown in this figure, although 100 cycles of load were applied before moving to the next stage.

The following are the key observations. Firstly, at the low strain amplitudes (e.g., $\gamma_a = 0.1\%$), the maximum stress ratio for $\sigma'_z = 12.5$ kPa is 4.6–8.1 times that of $\sigma'_z = 400$ kPa (Fig. 4.3(a)). The stress ratio for $\sigma'_z = 12.5$ kPa increases with the number of cycles, while it remains almost constant for $\sigma'_z = 400$ kPa. Secondly, the hysteresis loop for a low γ_a is significantly larger in $\sigma'_z = 12.5$ kPa than that of $\sigma'_z = 400$ kPa. The hysteresis loops for $\sigma'_z = 400$ kPa are almost a single line; however, for $\sigma'_z = 12.5$ kPa, the stress–strain curves follow different paths for loading and unloading. Note, however, that the shear stress is normalized by σ'_z in Fig. 4.3. That is why the size of the loop is smaller in Fig. 4.3 for a large σ'_z . Thirdly, the shapes of the hysteresis loop for these specimens are different. The shape for a high-stress level is like a lens. However, for a low-stress level, it is an oval shape with four segments, two almost vertical and two inclined parallel lines. Fourthly, the size of the loop increases with an increase in shear strain amplitude (e.g., Fig. 4.3(f)), which implies the generation of plastic shear strain for a large γ_a . Finally, the maximum stress ratio at the end of each loading stage increases with an increase in shear strain amplitude. However, for $\sigma'_z = 12.5$ kPa, the maximum stress ratio decreases in $\gamma_a = 4\%$ and 8% loading stages. The maximum stress ratio is almost the same (~ 0.85) for both $\sigma'_z = 12.5$ kPa and $\sigma'_z = 400$ kPa for $\gamma_a = 8\%$.

It is observed that the size and shape of the hysteresis loop depend on the shear strain amplitude, the number of cycles, and vertical stress, which affect the shear modulus and damping ratio that

are commonly used for modelling soil behaviour. These two parameters are further examined in the following sections based on the results of all the tests listed in Table 4.1.

4.3.4 Volumetric Strain without Cyclic Loading History

Figure 4.4 shows the accumulated axial strain for eight DSS tests on loose and dense specimens under constant vertical stresses of 12.5–400 kPa. These specimens were sheared by a cyclic loading of $\gamma_a = 1\%$, and did not have any experience of previous cyclic loading (i.e., 1st stage of multistage tests). Figure 4.4 clearly shows that, for a given number of cycles, the lower the stress level, the higher the axial strain. For instance, at $N = 15$, the axial strain for $\sigma'_z = 12.5$ kPa is approximately twice that of $\sigma'_z = 400$ kPa. This finding contradicts some of the previous studies (Silver and Seed 1971; Youd 1972), which found no dependency of the axial strain on the stress level in DSS tests. However, more recent studies have reported that the axial strain depends on the stress level (Duku et al. 2008; Yee et al. 2012; Kang et al. 2016). While the exact cause of stress-independent behaviour found by Silver and Seed (1971) and Youd (1972) are not known, this might be due to the limitations of their strain and stress measurement and control.

4.3.5 Effects of Vertical Stress on Volumetric Strain in Multistage Tests

Figure 4.4 shows the axial strain (ϵ_z) in 8 tests on loose and dense sand specimens. The axial strain decreases with increase in normal stress. Also, for a given normal stress, ϵ_z is significantly higher for looser specimens. Figure 4.4 shows that the major part of the axial strain is generated within the first few cycles. Following Duku et al. (2008), the strain at 15 cycles ($\epsilon_{z,15}$) is considered for the purpose of comparison of the response. Figure 4.5 shows the axial strain at 15 cycles for dense (T14–T18) and loose (T23–T25) sand specimens, where the multistage cyclic loading was started

with $\gamma_a = 1\%$ in the first cycle. As shown in this figure, $\varepsilon_{z,15}$ increases with an increase in shear strain amplitude. For the first two stages ($\gamma_a = 1\%$ & 2%), the lower the vertical stress, the higher the $\varepsilon_{z,15}$. However, for large γ_a , the influence of vertical stress on $\varepsilon_{z,15}$ reduces. For the low-stress cases ($\sigma'_z = 12.5$ & 25 kPa), the sand densifies quickly (Fig. 4.5) that increases the dilative response at larger γ_a , which reduces the overall compaction in each cycle, thereby the rate of increase in $\varepsilon_{z,15}$ with γ_a .

To understand better the effects of γ_a and σ'_z on axial strain, the relative density (D_r) at the end of each stage of cyclic loading is shown in Fig. 4.6. Recall that the initial relative density of the dense specimens was 75%. At the end of the first loading stage, the relative density increased to 81% and 96% for $\sigma'_z = 400$ and 12.5 kPa, respectively. This trend is similar to the observation by Duku et al. (2008), who conducted tests at $\sigma'_z = 50$ – 400 kPa. The relative density increases further in the subsequent stages at higher amplitude loading; however, the rate of increase is smaller at larger shear strain amplitudes, except for the test with $\sigma'_z = 400$ kPa. At the end of the last stage, the relative density is slightly above 100%, which implies that cyclic loading could decrease the void ratio to a value lower than the ASTM Standard minimum void ratio. Youd (1972) also found a relative density greater than 100% after cyclic loading. For loose sand, the relative density increases rapidly in early stages. For example, at the end of the first stage of loading with $\gamma_a = 1\%$, D_r increases from 43% to 60%–82%, depending upon normal stress.

Figure 4.7 shows the change in relative density in two sets of multistage tests which were started with different shear strain amplitudes. Tests T8 and T13 started with $\gamma_a = 0.1\%$, while tests T14 and T18 started with $\gamma_a = 1\%$. However, all these tests finished with $\gamma_a = 8\%$ loading in the final stage. These tests were conducted under $\sigma'_z = 12.5$ & 400 kPa to cover a wide range of stress. The differences among the relative densities for given vertical stress are small, especially at high σ'_z .

This implies that, for this stress range and initial density, the low amplitude loading stages ($\gamma_a = 0.1\%$ & 0.5%) did not significantly affect the compaction of the soil in the subsequent stages with higher amplitude loading.

4.4. Dynamic Properties

Shear modulus and damping ratio are the two commonly used parameters for modelling sand under cyclic loading. This section presents the influence of the following factors on shear modulus and damping ratio: stress level, shear strain amplitude, strain history, and the number of cycles.

4.4.1 Shear Modulus

Figure 4.8 shows the stress–strain response of test T1. For clarity, only four loading cycles ($N = 1, 10, 100,$ and 1000) are shown in this figure. The shear stress amplitude (τ_a) increases with the number of cycles because of the densification of the specimen, which also increases the secant shear modulus, $G_s (= \tau_a/\gamma_a)$. The shear modulus G_s is ~ 2.5 MPa in the 1st cycle, while it increases to ~ 6.0 MPa after 100 cycles. However, G_s increases only by ~ 0.7 MPa in the following 900 cycles, and G_s is 6.7 MPa after 1000 cycles. A similar increase in shear modulus was found in previous experimental studies (e.g., Kang et al. 2016), where the tests were conducted using a modified DSS apparatus with radial strain measurements. Kang et al. (2016) also reported a G_s increase within the first ten cycles.

4.4.2 Effects of Number of Cycles on Shear Modulus

Fig. 4.9 shows the variation of the shear modulus (G_s) with the shear strain amplitude (γ_a) in Test T3 ($\sigma'_z = 25$ kPa) for four loading cycles ($N = 1, 5, 10,$ and 100). For a given number of

cycles, the shear modulus decreases with an increase in the shear strain amplitude. The reduction of the shear modulus with increase in the shear strain amplitude was also reported in previous studies based on drained simple shear tests on sand (Seed and Silver 1972; Kang et al. 2016). For a given shear strain amplitude, the shear modulus increases with N . As an example, for $\gamma_a = 0.01\%$, $G_s = 6.4$ MPa for $N = 1$, while it is 8.77 MPa for $N = 100$. This increase is primarily due to the densification of sand with N . However, once γ_a is increased to a higher amplitude in the subsequent stage, G_s decreases. For example, when γ_a was increased from 0.01% to 0.1%, G_s reduced to 2.9 MPa for the first cycle (i.e., $N = 1$). Then, the densification process continues with the loading cycles. However, for a large shear strain amplitude ($\gamma_a = 2\%$, 4% and 8%) no such increase in G_s with the number of cycles was found, which is potentially due to the volume change mechanisms—both contraction and dilation occur in a single loading cycle for such a large shear strain amplitude, as discussed in the previous sections.

4.4.3 Effects of Strain History on Shear Modulus

Table 4.1 shows that tests T2–T18 were conducted with different shear strain amplitudes at the first stage (0.005, 0.01, 0.1 and 1%). All the tests have similar loading stages except for T5–T7, which have an additional loading stage of $\gamma_a = 0.05\%$. Therefore, four sets of tests are compared to investigate the effects of strain history (i.e., previous loading stage) for a given stress level. The solid symbols in Fig. 4.10 show the test results where two loading stages were completed prior to the stage of $\gamma_a = 0.1\%$. The open symbols represent the tests, which started with $\gamma_a = 0.1$ and 1%. Figure 4.10 shows that the secant shear modulus at 15 cycles ($G_{s,15}$) is almost independent of the strain history. Uthayakumar (1992) also found insignificant effects of small-strain history on dynamic properties from cyclic hollow cylinder torsional shear tests.

4.4.4 Empirical Correlation of Shear Modulus

Figure 4.11(a) shows that $G_{s,15}$ increases almost linearly with the logarithm of vertical stress, with higher $G_{s,15}$ for lower shear strain amplitudes (γ_a). The slope of $G_{s,15}-\log\sigma'_z$ lines increases with γ_a . Therefore, similar to the empirical equation for small strain shear modulus (Hardin and Black 1966), $G_{s,15}$ can be related to vertical stress as: $G_{s,15} = K(\gamma_a)\sigma'_z{}^{m(\gamma_a)}$, where the parameters K and m are functions of shear strain amplitude. Note that these factors could also be related to the initial void ratio, as reported by Kokusho (1980) for cyclic triaxial tests. In this study, the tests result of dense sand ($D_{rc}=75\%$) was considered to obtain the parameters for shear modulus.

The values of K and m of the fitted lines in Fig. 4.11(a) are obtained, which are then plotted against shear strain amplitude in Fig. 4.11(b). K decreases more than an order of magnitude and m increases from 0.25 to 0.92 when γ_a is increased from 0.005% to 8%. Iwasaki et al. (1978) showed that the exponent m (~ 0.5) does not vary significantly for small strains ($\gamma_a < 10^{-4}$) but increases rapidly for $\gamma_a > 10^{-4}$ and $m \sim 1.0$ in some cases at large γ_a .

4.4.5 Damping Ratio

The damping ratio represents the energy absorption in the specimen (Ishihara 1996; Kramer 1996), which is equal to $\Delta W/4\pi W$, where ΔW is the area of the hysteresis loop and W is the maximum stored energy (inset of Fig. 4.12).

Figure 4.12 shows the effects of the strain history and vertical stress on the damping ratio at the 15th cycle for the same multistage tests presented in Fig. 4.10, to discuss shear modulus. The damping ratio increases with shear strain amplitude and decreases with vertical stress. The rate of increase of damping ratio is high at large shear strain amplitudes. At low amplitudes ($\gamma_a < 1\%$), the

damping ratio for low stresses is significantly higher than that of high stresses. The increase in damping ratio at low stress and high amplitude is due to the increase in the size of the hysteresis loop, as compared to the stored energy.

Similar to shear modulus (Fig. 4.10), the damping ratio is almost independent of the strain history for high vertical stresses (e.g., $\sigma'_z = 400$ kPa) (compare solid and open circles in Fig. 4.12). However, the tests under low vertical stresses show that the damping ratio is somehow influenced by the strain history (i.e., having prior cyclic loading stages with lower shear strain amplitudes), although, the trend is not very clear (e.g., compare solid and open squares in Fig. 4.12). Conducting drained cyclic hollow cylinder torsional shear tests, Uthayakumar (1992) reported that the damping ratio is insensitive to the multistage loading history for a mean effective stress of 100 kPa and shear strain amplitude of 0.015%–0.2%.

4.5. Stress-dilatancy in DSS Tests

To develop the relationship between stress ratio (τ_{zx}/σ'_z) and dilatancy, $D (= -d\varepsilon_z^p/d\gamma^p)$, the plastic components of axial and shear strains are needed. In the present study, the DSS tests were conducted under constant vertical stress. The advanced control system in this apparatus ensures the negligible change in the vertical stress during shearing, which represents a negligible elastic component of axial strain. Also, assuming that the ratio between lateral and vertical stresses remains the same during cyclic loading, the change in mean stress is neglected, which implies $d\varepsilon_z^p = d\varepsilon_z$. Following the work of Shahnazari and Towhata (2002), the plastic shear increment is calculated as $d\gamma^p = d\gamma - d\gamma^e$. Here, $d\gamma^e$ is the elastic component of shear strain increment, which is calculated by dividing the shear stress increment by the initial shear modulus of the loading or unloading path of that cycle. After that, $d\varepsilon_z^p$ is plotted against $d\gamma^p$ and then fitted with a six-degree

polynomial for each loading and unloading paths. The derivative of the fitted curves gives $d\varepsilon_z^p/d\gamma^p$. Two- and four-degree polynomials were used in previous studies to fit the experimental data (Shahnazari and Towhata 2002; Georgiannou et al. 2008). However, reducing the degree might give misleading results in some cases.

4.5.1 Stress–dilatancy in Strain-controlled (constant strain amplitude) Cyclic DSS Tests

Fig. 4.13(a) shows the variation of stress ratio and dilatancy for the first five cycles of a strain-controlled test (T1), where $\sigma'_z = 100$ kPa and $D_{rc} = 80\%$. During the virgin loading ($d\gamma > 0$), shearing starts from point 1 with $-d\varepsilon_z^p/d\gamma^p \sim -0.45$ and reaches point 2 at the end of the shear strain amplitude (γ_a). At this stage, the shear strain reverses direction ($d\gamma < 0$); therefore, the dilatancy changes from a negative to a positive value (point 2'), although the specimen continued to decrease in volume, due to contraction ($d\varepsilon_z^p > 0$) (Fig. 4.1b). The contraction and dilation of the specimen during unloading and loading are shown in Fig. 4.13(b). Figure 4.13(a) also shows that the dilatancy changes from a positive (point 3') to a negative value (point 3) when reloading ($d\gamma > 0$) occurs. When $\gamma = 0$ during reloading (point 4), the stress ratio is ~ 0.2 , which is not zero because a hysteresis loop forms due to plastic deformation (cf. inset of Fig. 4.8). In the first cycle, the only compaction occurs during the whole unloading-reloading process. The process is continued in the following cycles. However, starting from the third cycle, both positive and negative dilatancy occurs for a given shear direction (i.e., $-d\varepsilon_z^p/d\gamma^p > 0$ and $-d\varepsilon_z^p/d\gamma^p < 0$ at the end of reloading and unloading, respectively). This implies that some dilation of the specimen occurred during the last part of unloading and reloading (Fig. 4.1(b)). However, the contraction of the specimen is more than the dilation; therefore, the net volume change represents overall compaction in each cycle (Fig. 4.1(b)). The dilation in the reloading and unloading phases increases with the number

of loading cycles because of the increase in density. The location where the dilation changes from positive to negative value for reloading and vice versa for unloading (i.e. $-d\varepsilon_z^p/d\gamma^p = 0$, points A & B in Fig. 4.13(b)) is equivalent to the “phase transformation” in undrained tests. As the soil became denser and dilated more at the end of unloading and reloading (i.e., the length of the τ_{zx}/σ'_z vs. $-d\varepsilon_z^p/d\gamma^p$ line after the phase transformation increases), more contractive response was observed at the initial part of the subsequent loading and unloading stages. Therefore, the initial part of the stress ratio–dilatancy curve shifts to the left in reloading, and to the right in unloading, with an increase in the number of cycles (Fig. 4.13b).

Figure 4.13(b) shows that, except for the initial part of unloading and reloading, the stress dilatancy relation can be expressed by two parallel linear lines (thick dashed lines), as in the work of De Silva et al. (2014).

$$\tau_{zx}/\sigma'_z = R_k(-d\varepsilon_z^p/d\gamma^p) \pm C \quad (4.1)$$

where $R_k = 1.55$ and $C = 0.31$. Drained hollow cylinder torsional shear tests, primarily on loose to medium dense Toyoura sands for initial consolidation pressures of 49–184 kPa, show a similar response, where $R_k = 1.2$ – 1.7 and $C = 0.3$ – 0.5 (Shahnazari and Towhata 2002; De Silva et al. 2014).

4.5.2 Effect of Normal Stress on Stress–dilatancy

Figure 4.14 shows the stress–dilatancy of the first cycle for varying vertical stresses. The unloading and reloading start with a higher dilatancy in the low-stress level tests, as shown in the first and third quadrants of Fig. 4.14. However, the vertical stress effects on stress–dilatancy relation decrease with shearing, and the lines become closer to each other in the second and fourth quadrants of Fig. 4.14. The change in dilatancy in each shearing path is larger in the low-stress

level tests because the shear strain required to change from contractive to dilative response is less for low vertical stresses. For example, the reloading in the test with $\sigma'_z = 50$ kPa starts with a dilatancy of -0.4, which gradually changes to 0; however, a small change in dilatancy occurs for $\sigma'_z = 400$ kPa.

4.5.3 Stress–dilatancy in Multistage Tests

Figures 4.15(a) and (b) show the stress–dilatancy at the first cycle of multistage tests under $\sigma'_z = 12.5$ kPa and $\sigma'_z = 400$ kPa, respectively. Figure 4.15(a) shows that the unloading starts at $\tau_{zx}/\sigma'_z = 0.26$ for $\gamma_a = 1\%$; however, in the next loading stage ($\gamma_a = 2\%$), the unloading starts at $\tau_{zx}/\sigma'_z = 0.87$. In the following two stages ($\gamma_a = 4\%$ & 8%), the maximum and minimum stress ratio do not change significantly because the volumetric strain (compaction) is not significant in the second and third stages as compared to the first stage (similar to Fig. 4.2). The unloading and reloading start with a higher dilatancy ratio in the low-stress level tests, as shown in the first and third quadrants of Fig. 4.15(a). However, with the progress of shearing, the vertical stress effects on stress–dilatancy decrease, and the lines become closer to each other, as shown by the shaded zone Fig. 4.15(a). The largest dilatancy is found for $\gamma_a = 4\%$.

A very different stress–dilatancy relation is found for a larger stress level ($\sigma'_z = 400$ kPa) (Fig. 4.15b), as compared to Fig. 4.15(a). The sample is contractive for $\gamma_a = 1\%$ (i.e., $-d\varepsilon_z^p/d\gamma^p$ is positive and negative for unloading and loading, respectively, as described in Fig. 4.13(b)). The sample densified in the first 100 cycles with $\gamma_a = 1\%$, and the contractive behaviour reduces in the second stage for $\gamma_a = 2\%$. In the next loading stage with $\gamma_a = 4\%$, the sample passes the phase transformation point (i.e., dilates at the end of unloading and reloading paths). Therefore,

unloading and reloading start with higher $|d\varepsilon_z^p/d\gamma^p|$ values. At the same time, the stress ratio increases because of increasing shear strain amplitude. The increase in τ_{zx}/σ'_z and $|d\varepsilon_z^p/d\gamma^p|$ increase the size of the loop formed by the unloading and reloading processes. Finally, for $\gamma_a = 8\%$, the loop becomes bigger for the same reason as in the $\gamma_a = 4\%$ loading stage. The stress–dilatancy relationship at this stage is similar to Fig. 4.13(b), having two approximate straight line segments. To understand better the normal stress dependent stress–dilatancy relationship, monotonic DSS tests were conducted on dense samples ($D_{rc} = 87\%$). The inset of Fig. 4.15(a) shows that the sample becomes dilative quickly at a low shear strain for a low normal stress, which implies dominating effects of plastic deformation at low strains. Therefore, the trend of two parallel lines (shaded zone in Fig. 4.15(a) is found in $\gamma_a \geq 1\%$ for $\sigma'_z = 12.5$ kPa while a similar trend is found in higher $\gamma_a (\geq 4\%)$ for $\sigma'_z = 400$ kPa (Fig. 4.15(b)).

Figures 4.14 and 4.15(a & b) clearly show that the stress–dilatancy relation depends on stress level, cyclic loading history, and shear strain amplitude. Shahnazari and Towhata (2002) showed that the stress–dilatancy relationship can essentially be represented by two parallel lines, similar to Fig. 4.13(b), from HCT shear tests on loose ($D_r = 22\text{--}24\%$), medium ($D_r = 57\text{--}58\%$), and some on dense Toyoura sand ($D_r = 74\text{--}75\%$) for the shear strain amplitudes of 1% and 3%. De Silva et al. (2014) showed that the stress–dilatancy lines shift with the number of cycles, although they remain almost parallel for unloading and reloading. The present DSS test results show a similar response to the studies mentioned above for single amplitude loading under a similar range of confining stress and shear strain amplitudes. However, the cyclic loading history with $\gamma_a \geq \gamma_{tv}$ in the multistage tests could change the density of the soil sample, and thereby the phase transformation stress and strain, depending upon the vertical stress. Therefore, the subsequent cyclic loading with

a larger shear strain amplitude might shift the stress–dilatancy lines first towards and then outward from the origin, as shown in Fig. 4.15(b).

4.5.4 Stress–dilatancy in Stress-controlled (constant stress amplitude) Tests

Figure 4.16(a) shows the stress–dilatancy in test T20 where a stress-controlled cyclic load ($CSR = 0.4$) was applied. At the end of virgin loading, this sample experienced 1.75% shear strain, which is larger than the threshold shear strain. Therefore, plastic deformation causes cyclic compaction. In the first and second cycles, the unloading and reloading start with an almost vertical line and then follow an inclined straight line, which is similar to the response observed in strain-controlled tests (Fig. 4.13). With an increase in the number of cycles, the sample becomes denser and $|d\varepsilon_z^p/d\gamma^p|$ smaller, which represents less compaction per cycle. After a large number of cycles (e.g., $N = 100$), $|d\varepsilon_z^p/d\gamma^p|$ is almost zero during shearing and a small volume change occurs.

Figure 4.16(b) shows the stress–dilatancy response in the stress-controlled tests for varying vertical stresses. In the first cycle, the unloading starts with a higher dilatancy in a low-stress level test; however, the stress–dilatancy relation becomes almost independent of vertical stress with the progress of loading in this cycle. The stress–dilatancy response becomes stress-dependent after a number of cycles, as shown for 10 cycles (Fig. 4.16(b)). The inset of Fig. 4.16(b) shows the stress–strain response in the first cycle for two vertical stresses. For a given stress ratio, the sample under higher vertical stress experienced a higher shear strain; for example, γ is 0.72% and 2.5% at the end of virgin loading for the vertical stresses of 12.5 kPa and 100 kPa, respectively. Therefore, the compaction of the sample and dilatancy change with the number of cycles, depending on the vertical stress. In summary, the stress–dilatancy relationship depends on vertical

stress, shear strain amplitude and the number of cycles, which influence the relative density change due to cyclic loading.

Finally, both strain- and stress-controlled tests show that the volumetric strain (compaction) per cycle decreases with the number of cycles. Two factors should be considered to explain the mechanisms. Firstly, as observed in some strain-controlled tests (Fig. 4.13(b)), the specimens become densified with cyclic loading, which results in an increase of the dilation segment of the stress–dilatancy line, as compared to the contraction segment. Therefore, the net volumetric compaction per cycle decreases at large N , although the stress–dilatancy data follow the same line. Secondly, the densification due to cyclic loading could reduce $|d\varepsilon_z^p/d\gamma^p|$ for a given stress ratio. For example, as shown in Fig. 4.15(b), the cyclic loading with $\gamma_a = 1\%$ reduces the magnitude of dilation and therefore, the compaction in the second stage is less than in the first stage. The reduction of $|d\varepsilon_z^p/d\gamma^p|$ is also the cause of reduced volumetric compaction per cycle with N in the stress-controlled tests (Fig. 4.16(a)).

4.6. Conclusions

Drained cyclic direct simple shear (DSS) tests were conducted to investigate the volume change behaviour of sand. A series of multistage DSS tests were conducted with increasing shear strain amplitude (γ_a) in the subsequent stage of the strain-controlled (constant strain amplitude) cyclic tests. To investigate the effects of cyclic loading history on sand behaviour, the multistage tests were started with different shear strain amplitudes. The tests cover a wide range of shear strain amplitudes (0.005%–8.0%) and vertical stresses prior to shearing. A series of DSS tests were also conducted by stress-controlled (constant stress amplitude) cyclic loading. To understand the

volume change mechanisms, the stress–dilatancy relationship in cyclic loading is examined. The following conclusions can be drawn for the experimental conditions considered in this study.

- a) Although the number of cycles is the same in each stage of the multistage tests ($N = 100$), the maximum volumetric compaction occurs in the loading stage of $\gamma_a = 1\%$.
- b) For both loose and dense sands, the accumulated volumetric strain depends on applied vertical stress and shear strain amplitude. For the lower shear strain amplitudes (1%–2%), the volumetric strain generated in 100 cycles of each stage is more in the low-stress level tests than those of the higher stress level. An opposite trend is found in the higher shear strain amplitude (4%–8%) tests.
- c) A low amplitude ($\gamma_a \leq 0.5\%$) cyclic loading history does not have a significant influence on the volumetric compaction (or relative density) and the secant shear modulus at 15 cycles in the higher amplitudes loading ($\gamma_a = 1\%$ –8%).
- d) The secant shear modulus at 15 cycles of each stage can be expressed by a power function of vertical stress, $G_{s,15} = K\sigma'_z{}^m$, where K increases and m decreases with shear strain amplitude. The damping ratio at 15 cycles also increases with shear strain amplitude.
- e) The stress–dilatancy relationship in strain-controlled tests with constant shear strain amplitude can be represented by two parallel lines with a curved segment at the beginning of unloading and reloading. However, the stress–dilatancy depends on vertical stress, shear strain amplitude, the number of cycles and cyclic loading history with a shear amplitude greater than a threshold value.
- f) For a given shear stress and shear strain amplitude, the decrease in compaction per cycle with an increase in the number of cycles can be explained by two factors: (i) increase in the

dilation segment of the stress–dilatancy relation, and (ii) reduction of the magnitude of dilatancy ratio.

Acknowledgments

The works presented in this paper have been supported by the Natural Sciences and Engineering Research Council of Canada (NSERC), InnovateNL, the former Research and Development Corporation of Newfoundland and Labrador (RDC), the Canadian Foundation for Innovation (CFI) and the state of Libya.

Notation

The following abbreviations and symbols are used in this paper:

CSR = cyclic stress ratio (τ_a/σ'_z)

D = dilatancy ($-d\varepsilon_v^p/d\gamma^p$)

$d\varepsilon_v^p$ = plastic component of volumetric strain increment

$d\gamma$ = shear strain increment

$d\gamma^e$ = elastic component of shear strain increment

$d\gamma^p$ = plastic component of shear strain increment

D_r = relative density

D_{rc} = relative density after consolidation

DSS = direct simple shear

ε_z = axial strain

- $\varepsilon_{z,15}$ = axial strain at 15 cycles
- f = frequency
- γ = shear strain
- γ_a = cyclic shear strain amplitude
- γ_{tv} = threshold shear strain amplitude
- G_s = secant shear modulus (τ_a/γ_a)
- K & m = parameters for shear modulus
- N = number of cycles
- σ'_z = effective axial stress
- τ_a = shear stress amplitude
- τ_{zx} = shear stress
- τ_{zx}/σ'_z = stress ratio

References

- Al Tarhouni, M., Fouzder, A., Hawlader, B., and Dhar, A., 2017. Direct simple shear and triaxial compression tests on dense silica sand at low effective stress. *GeoOttawa, 70th Canadian Geotechnical Conference*, Ottawa, Canada, Oct. 1–4, 7p.
- Al-Tarhouni, M., Simms, P., and Sivathayalan, S., 2011. Cyclic behaviour of reconstituted and desiccated–rewet thickened gold tailings in simple shear. *Canadian Geotechnical Journal*, 48(7): 1044–1060.

- De Silva, L.I.N., Koseki, J., Wahyudi, S., and Sato, T., 2014. Stress–dilatancy relationships of sand in the simulation of volumetric behavior during cyclic torsional shear loadings. *Soils and Foundations*, 54(4): 845–858.
- Duku, P.M., Stewart, J.P., Whang, D.H., and Yee, E., 2008. Volumetric strains of clean sands subject to cyclic loads. *Journal of Geotechnical and Geoenvironmental Engineering*, 134(8): 1073–1085.
- Georgiannou, V.N., Tsomokos, A., and Stavrou, K., 2008. Monotonic and cyclic behaviour of sand under torsional loading. *Géotechnique*, 58(2): 113–124.
- Alarcon-Guzman, A., Chameau, J.L. Leonards, G.A., and Frost, J.D., 1989. Shear modulus and cyclic undrained behavior of sands. *Soils and Foundations*, 29(4): 105–119.
- Hardin, B.O., and Black, W.L., 1966. Sand stiffness under various triaxial stresses. *Journal of Soil Mechanics & Foundations Div, ASCE*, 92(2): 27–42.
- Hsu, C.-C., and Vucetic, M., 2004. Volumetric threshold shear strain for cyclic settlement. *Journal of Geotechnical and Geoenvironmental Engineering*, 130(1): 58–70.
- Ishihara, K., 1996. *Soil Behaviour in Earthquake Geotechnics*, Clarendon Press, Oxford, UK.
- Ishihara, K., 1993. Liquefaction and flow failure during earthquakes. *Géotechnique*, 43(3): 351–451.
- Iwasaki, T., Tatsuoka, F., and Takagi, Y., 1978. Shear moduli of sands under cyclic torsional shear loading. *Soils and Foundations*, 18(1): 39–56.
- Japanese Geotechnical Society (JGS), 2009. Method for cyclic undrained triaxial test on soils, JGS0541-2009. Japan

- Kang, X., Ge, L., Chang, K.-T., and Kwok, A.O.-L., 2016. Strain-controlled cyclic simple shear tests on sand with radial strain measurements. *Journal of Materials in Civil Engineering*, 28(4): 04015169.
- Kokusho, T., 1980. Cyclic triaxial test of dynamic soil properties for wide strain range. *Soils and Foundations*, 20(2): 45–60.
- Kramer, S.L., 1996. *Geotechnical Earthquake Engineering*. Prentice-Hall, New Jersey, USA.
- Lee, C.-J., 1991. Deformation of sand under cyclic simple shear loading. *Second International Conferences on Recent Advances in Geotechnical Earthquake Engineering and Soil Dynamics*. 13. St. Louis, Missouri. 33–36.
- López-Querol, S., and Coop, M.R., 2012. Drained cyclic behaviour of loose Dogs Bay sand. *Géotechnique*, 62(4): 281–289.
- National Research Council (NRC), 1985. *Liquefaction of soils during earthquakes*. National Academy Press, Washington, D.C., <https://doi.org/10.17226/19275>.
- Nishimura, S., 2002. *Development of three dimensional stress–strain model of sand undergoing cyclic undrained loading and stress-axes rotation*. M. Eng. thesis. Dept. of Civil Engineering, University of Tokyo, Japan.
- Park, S.-S., Byrne, P.M., and Wijewickreme, D., 2005. A swinging plane model for soil liquefaction analysis. *Proceedings of the 16th International Conference on Soil Mechanics and Geotechnical Engineering*, 845–850.
- Pradhan, T.B., and Tatsuoka, F., 1989. On stress-dilatancy equations of sand subjected to cyclic loading. *Soils and Foundations*, 29(1): 65–81.
- Roscoe, K.H., Schofield, A., and Thurairajah, A., 1963. Yielding of clays in states wetter than critical, *Géotechnique*, 13(3): 211–240.

- Rowe, P.W., 1962. The stress-dilatancy relation for static equilibrium of an assembly of particles in contact. *Proceedings of the Royal Society of London. Series A. Mathematical and Physical Sciences*, London, 269(1339): 500–527.
- Seed, H. B., and Silver M. L., 1972. Settlement of dry sands during earthquakes. *Journal of the Soil Mechanics & Foundations Div., ASCE*, 98(4): 381–397.
- Shahnazari, H., and Towhata, I., 2002. Torsion shear tests on cyclic stress-dilatancy relationship of sand. *Soils and Foundations*, 42(1): 105–119.
- Shahnazari, H., and Towhata, I., 2001. Prediction of volumetric strain for sand under cyclic loading. *4th International Conference on Recent Advances in Geotechnical Earthquake Engineering and Soil Dynamics*, Missouri University of Science and Technology, December. 13. Paper no. 1.16, 8p.
- Silver, M.L., and Seed, H.B., 1971. Volume changes in sands during cyclic loading. *Journal of Soil Mechanics & Foundations Div., ASCE*, 97(9): 1171–1182.
- Stephenson, R.W., Stringer, S.K., and Sutterer, K., 1991. The influence of large prestrains on dynamic properties of sand. *Second International Conferences on Recent Advances in Geotechnical Earthquake Engineering and Soil Dynamics*. Louis, Missouri, 1921–1926.
- Tatsuoka, F., Iwasaki, T., Fukushima, S., and Sudo, H., 1979. Stress conditions and stress histories affecting shear modulus and damping of sand under cyclic loading. *Soils and Foundations*, 19(2): 29–43.
- Taylor, D., 1948. *Fundamentals of soil mechanics*. Chapman and Hall, Limited., New York.
- Ueng, T.-S., and Lee, C.-J., 1990. Deformation behavior of sand under shear—particulate approach. *Journal of Geotechnical Engineering*, 116(11): 1625–1640.

- Uthayakumar, M., 1992. *Dynamic properties of sands under cyclic torsional shear*. Ph.D. Thesis, University of British Columbia, Canada.
- Wahyudi, S., and Koseki, J., 2012. Stress-dilatancy characteristics of sand in drained cyclic torsional shear tests, *Institute of Industrial Science, University of Tokyo Japan, Bulletin of ERS*, No. 40. 131–140.
- Wahyudi, S., Chiaro, G., De Silva, L.I.N, and Koseki, J., 2010. Stress-dilatancy behavior of loose sand during drained cyclic torsional shear loading, *12th International Summer Symposium of JSCE*, Tokyo, Japan. 183–186.
- Yee, E., Stewart, J.P., and Duku, P.M., 2012. Seismic compression behavior of sands with fines of low plasticity. *In GeoCongress 2012: State of the Art and Practice in Geotechnical Engineering*, ASCE, 839–848.
- Youd, T.L., 1972. Compaction of sands by repeated shear straining. *Journal of Soil Mechanics & Foundations Div.*, 98(SM7): 709–725.

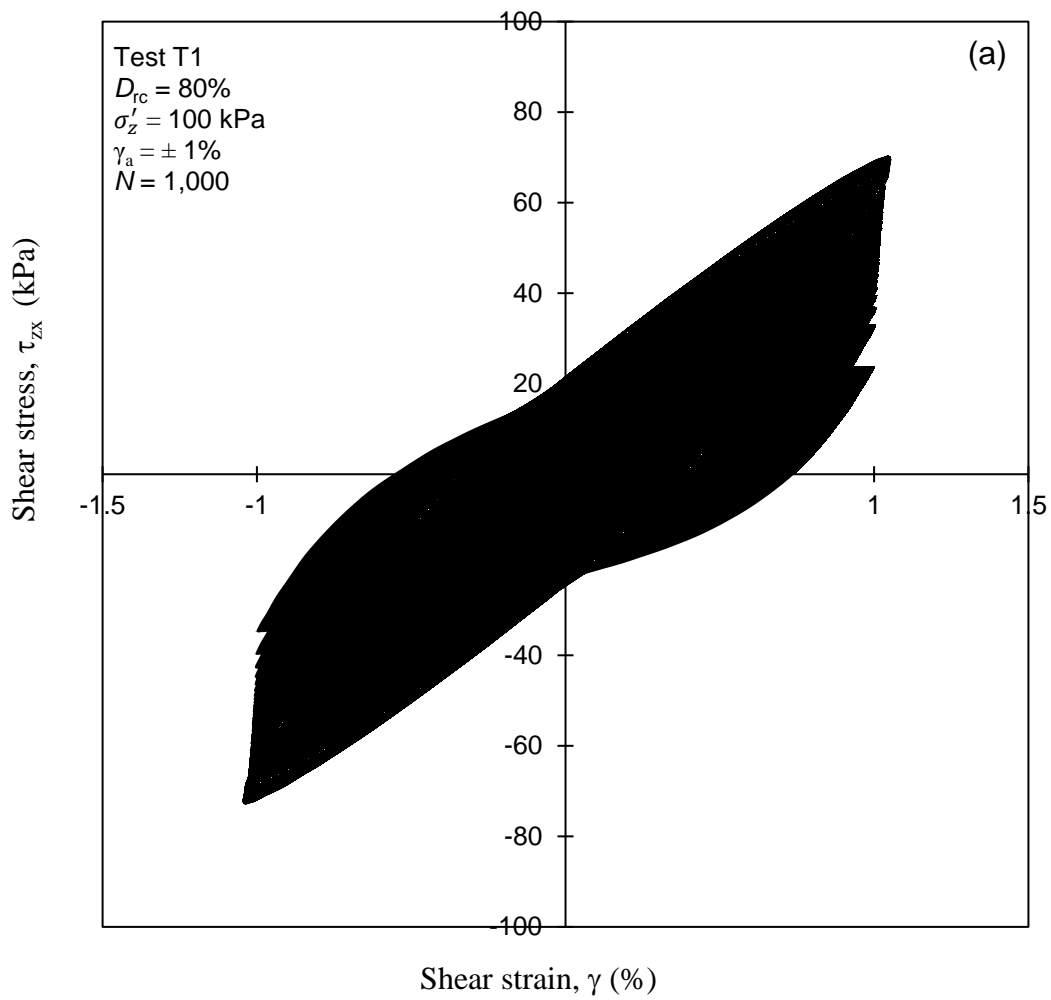


Fig. 4.1. Typical response: (a) shear stress–strain behaviour; (b) axial strain in 1000 cycles; (c) axial strain in 15 cycles; (d) stress ratio and axial strain variation

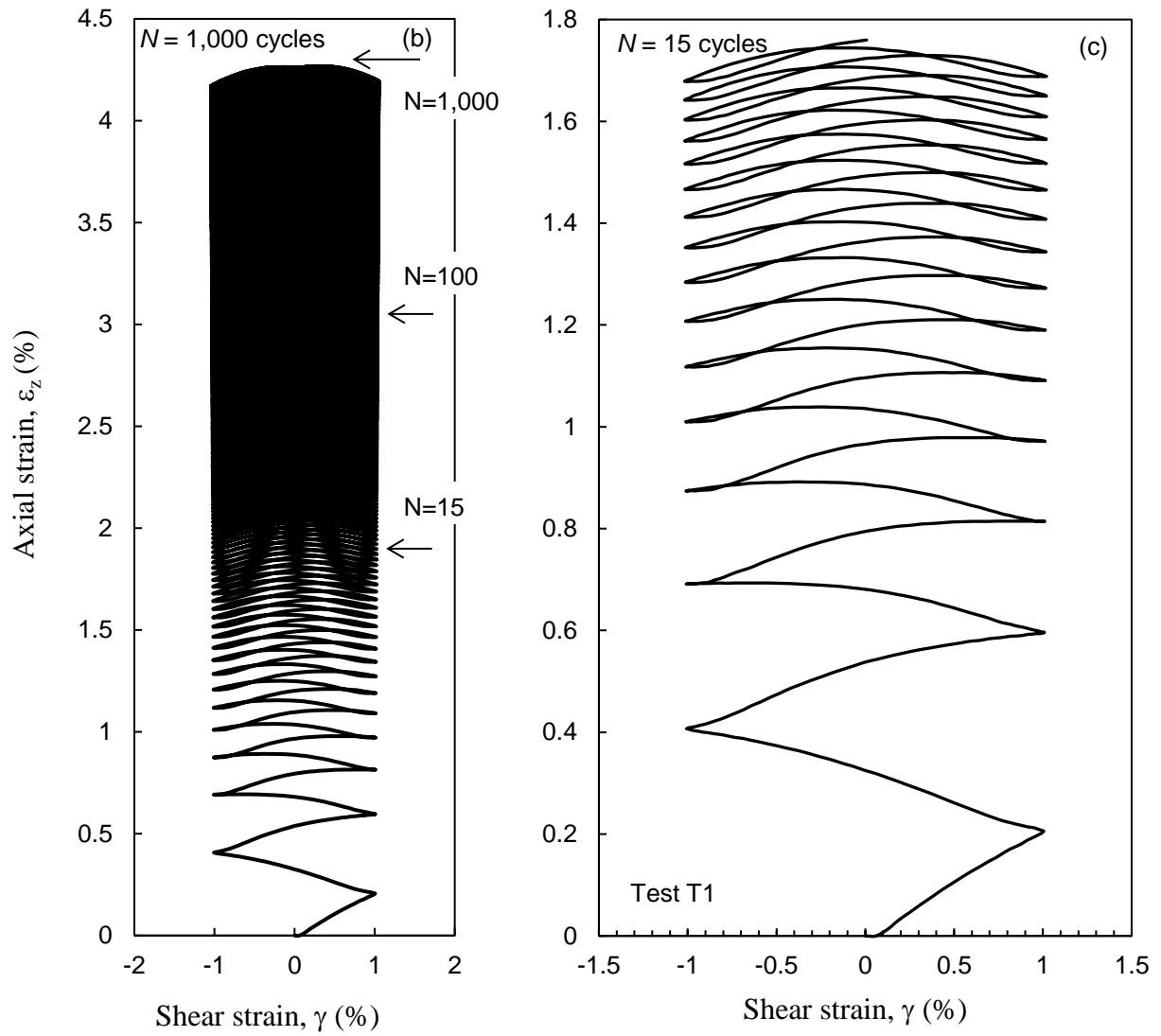


Fig. 4.1. Typical response: (a) shear stress–strain behaviour; (b) axial strain in 1000 cycles; (c) axial strain in 15 cycles; (d) stress ratio and axial strain variation

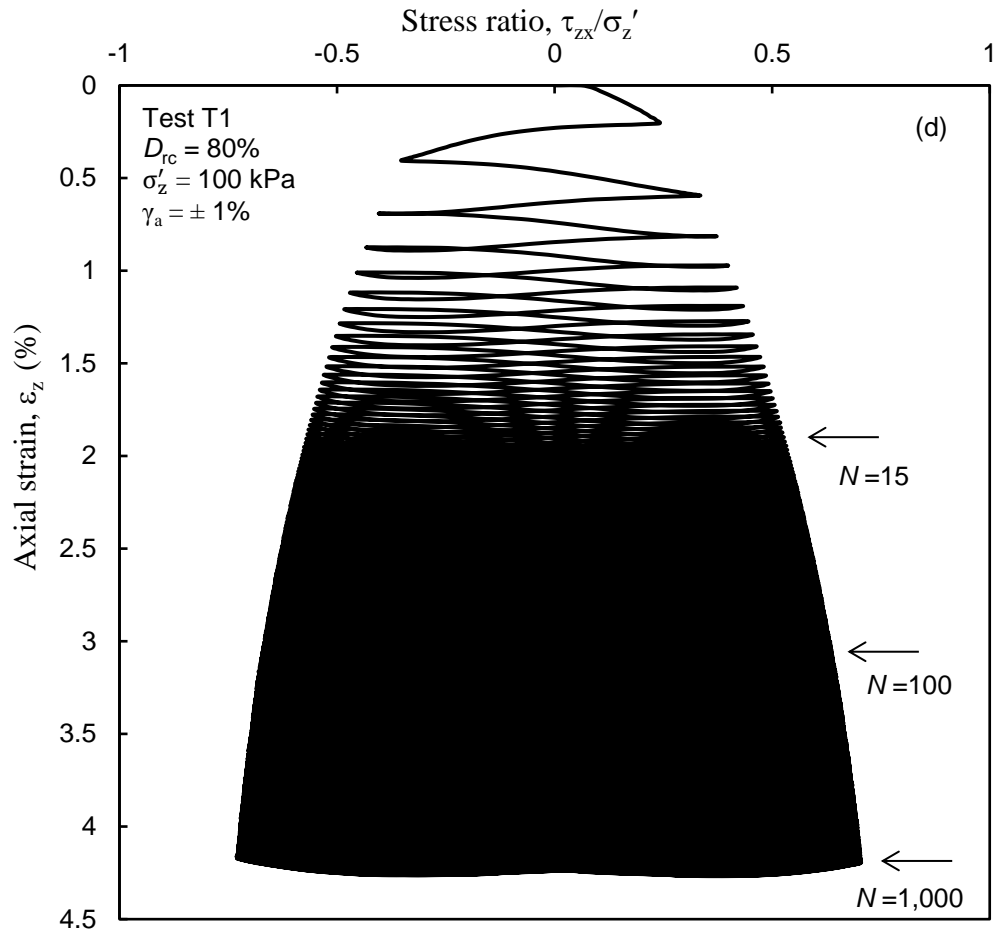


Fig. 4.1. Typical response: (a) shear stress–strain behaviour; (b) axial strain in 1000 cycles; (c) axial strain in 15 cycles; (d) stress ratio and axial strain variation

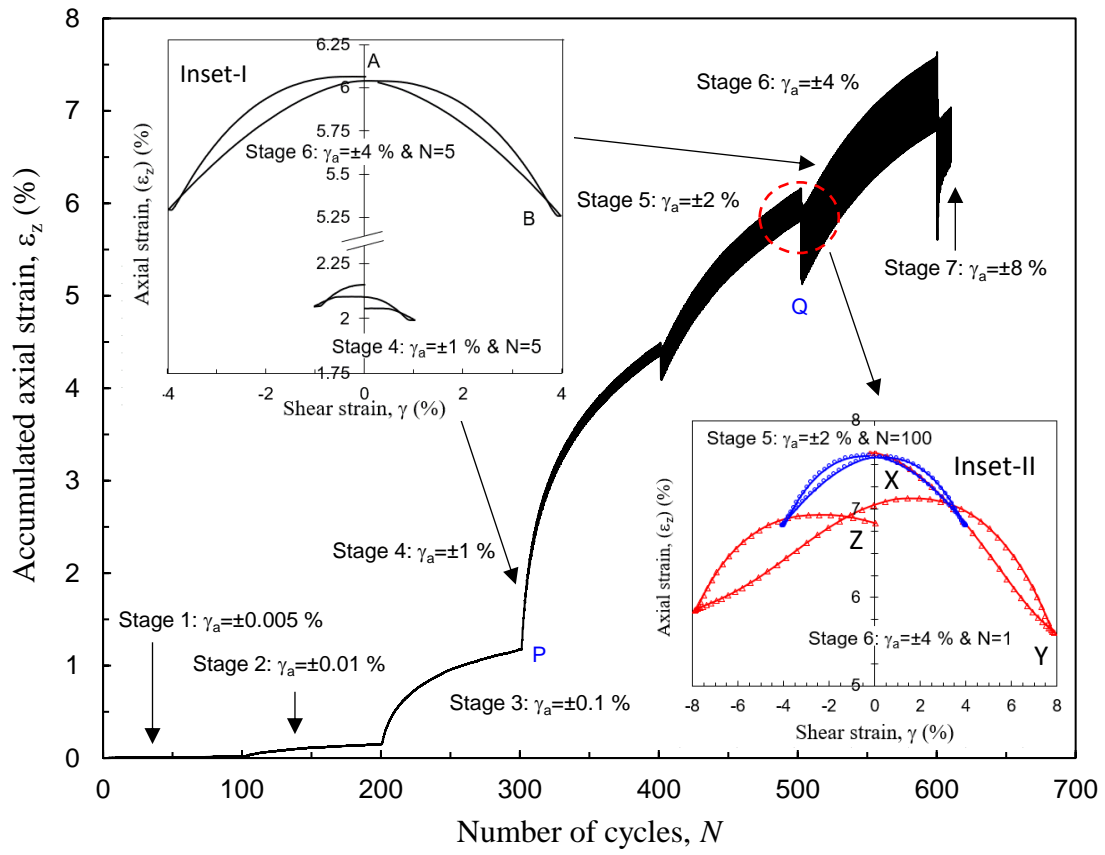


Fig. 4.2. Development of axial strain in multistage test T3

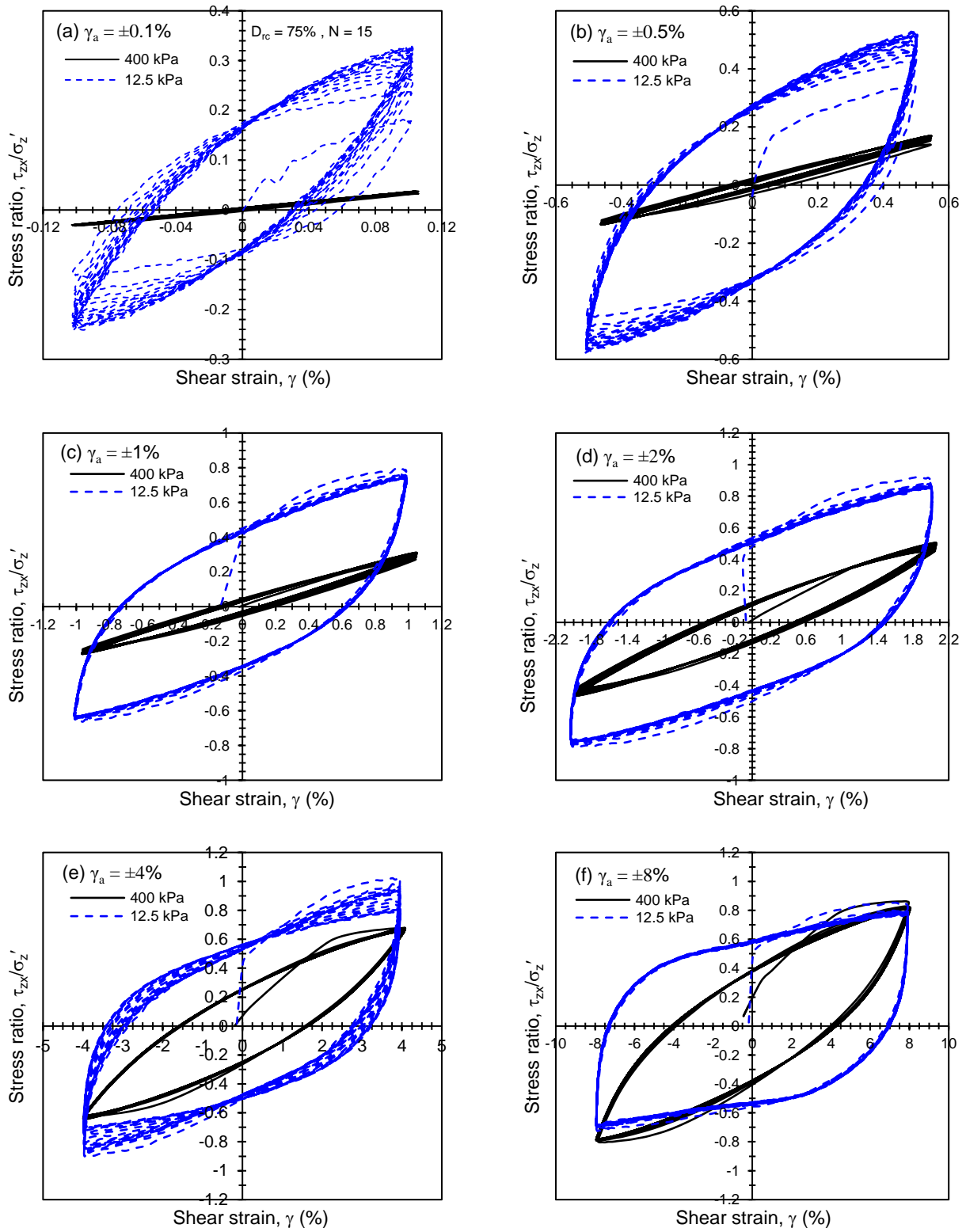


Fig. 4.3. Effect of normal stress and shear strain amplitude on cyclic behaviour (Test T8 and T13)

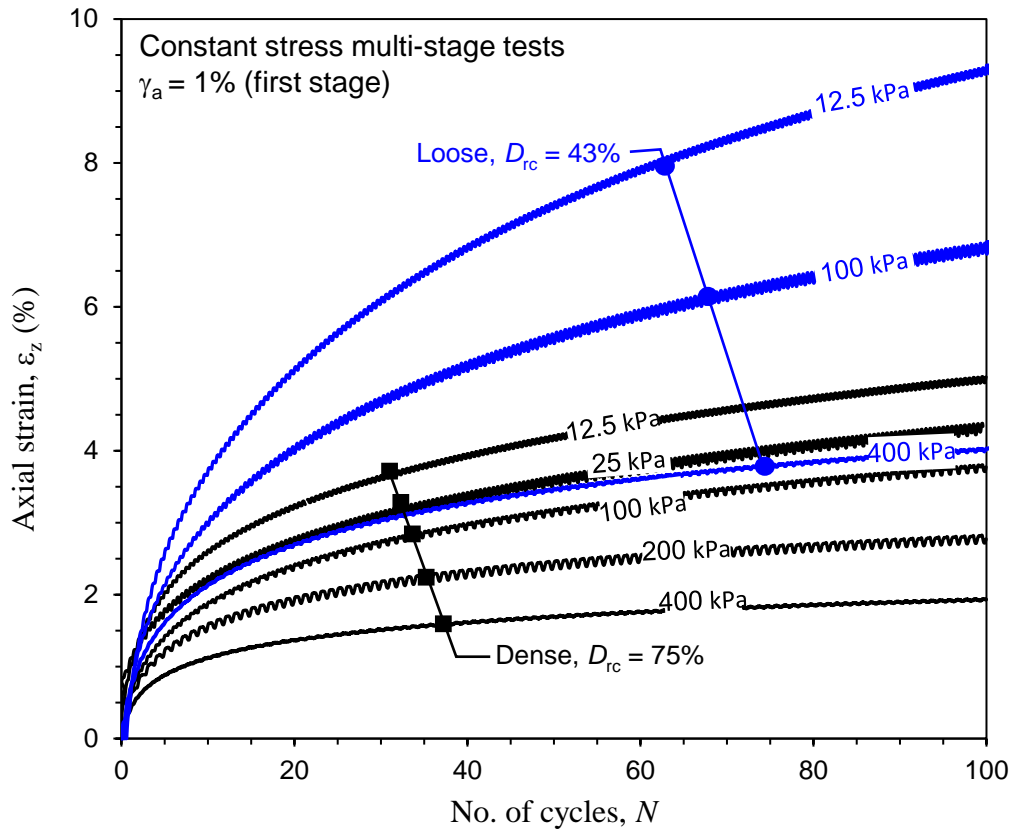


Fig. 4.4. Axial strain generation in first stage of cyclic loading in dense (T14–T18) and loose (T23–T25) specimens for shear strain amplitude of 1%

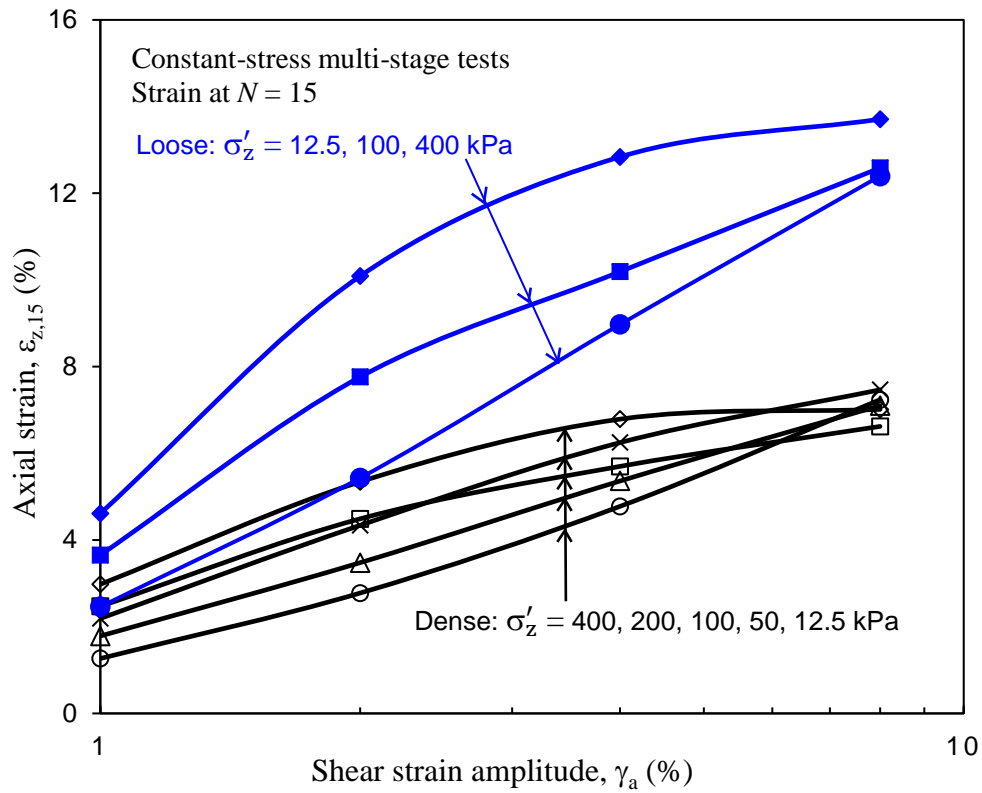


Fig. 4.5. Accumulated axial strain at 15 cycles of each stage in multistage tests on dense (T14–T18) and loose (T23–T25) specimens

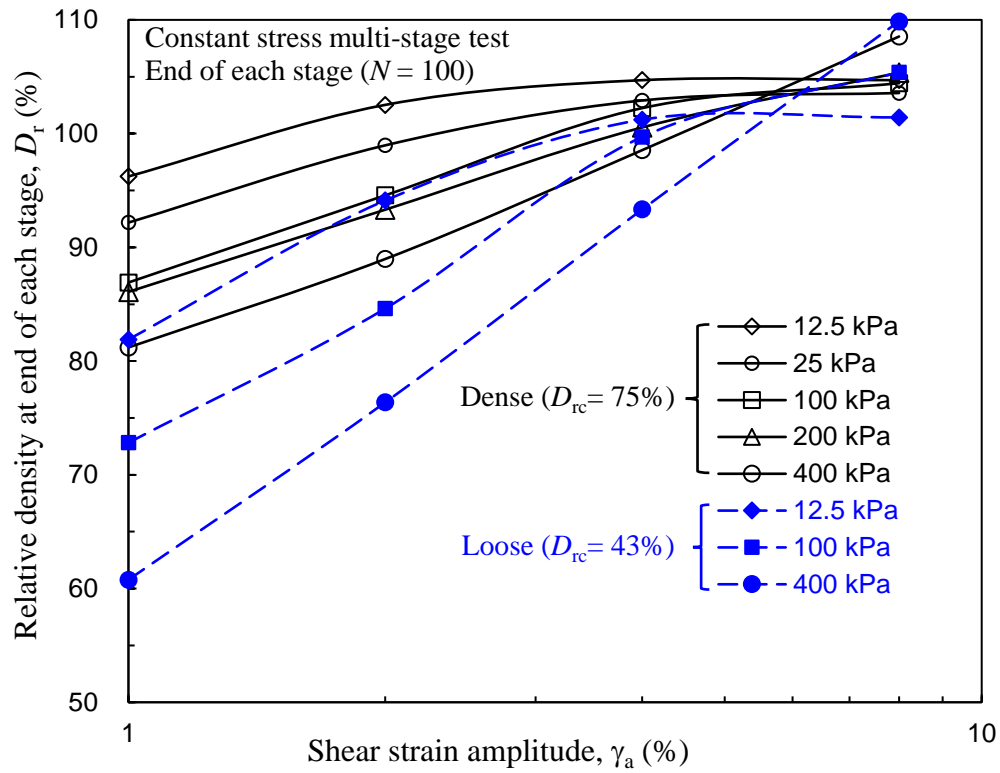


Fig. 4.6. Relative density at the end of each stage in multistage tests on dense (T14–T18) and loose (T23–T25) specimens

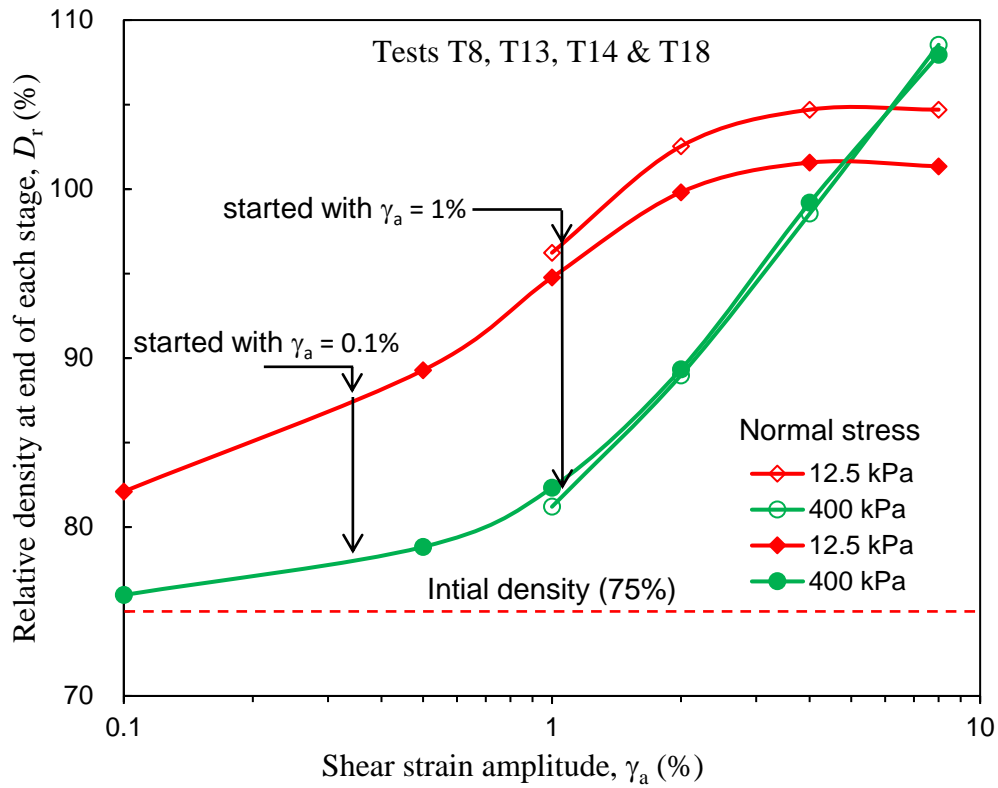


Fig. 4.7. Effects of the small-strain amplitude loading on axial strain in large-amplitude loading for dense sand

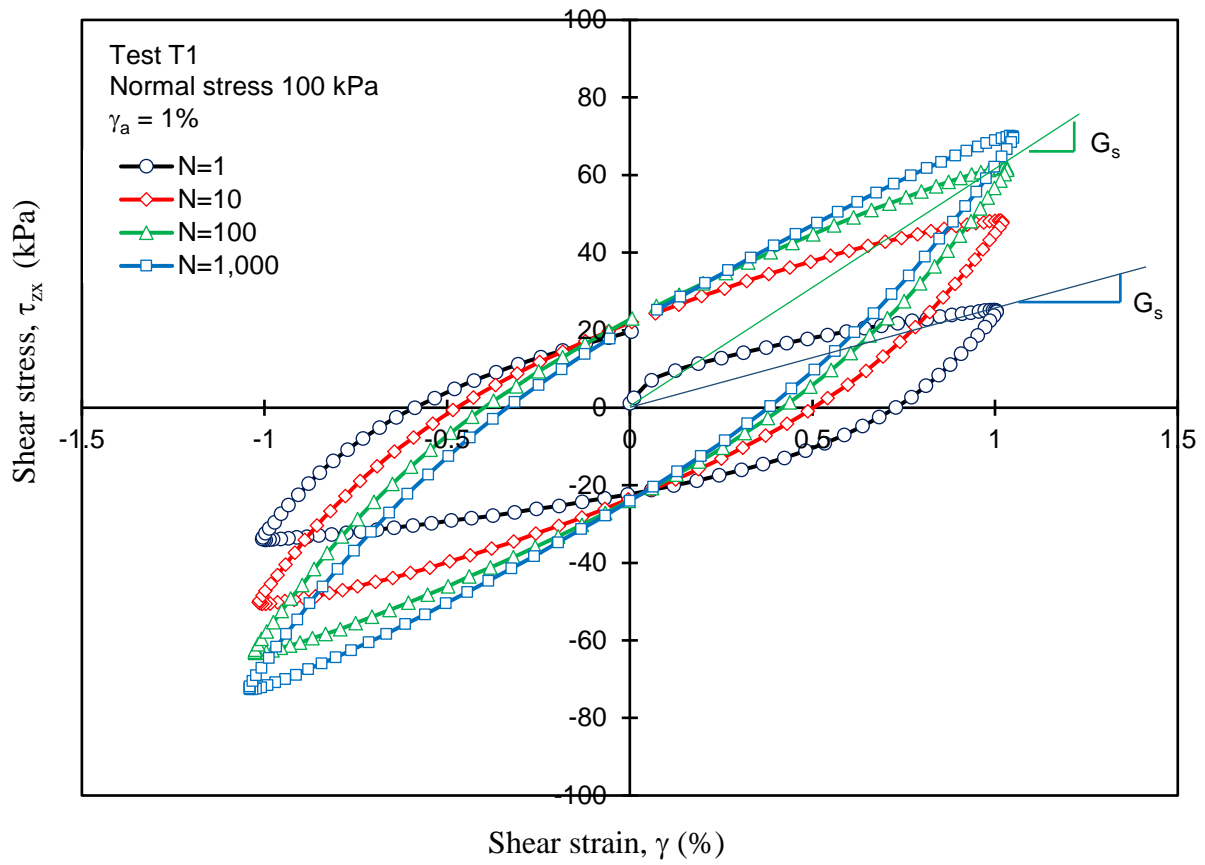


Fig. 4.8. Typical hysteresis loops at different cycles

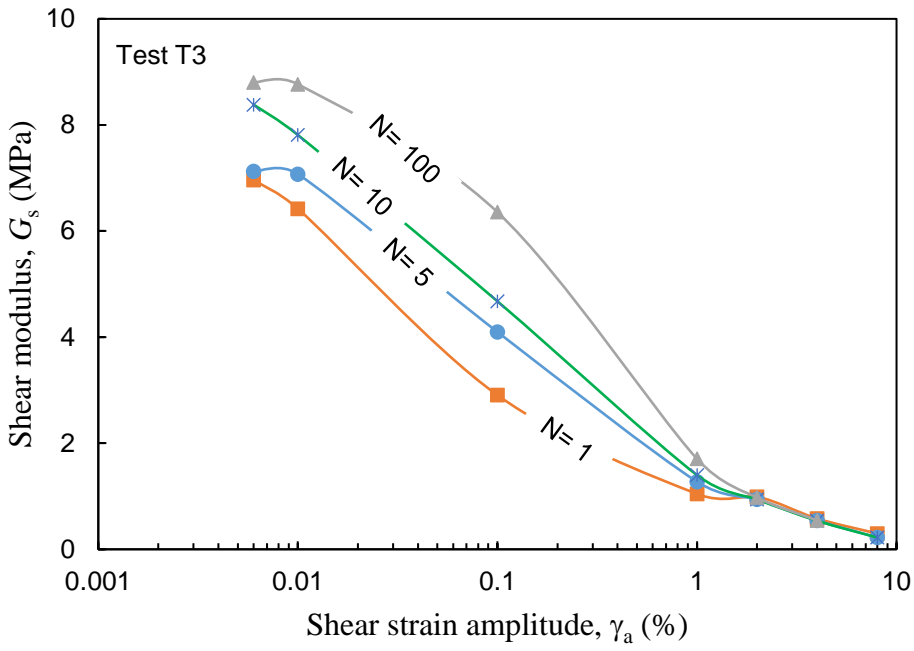


Fig. 4.9. Effects of shear strain amplitude and number of cycles on shear modulus

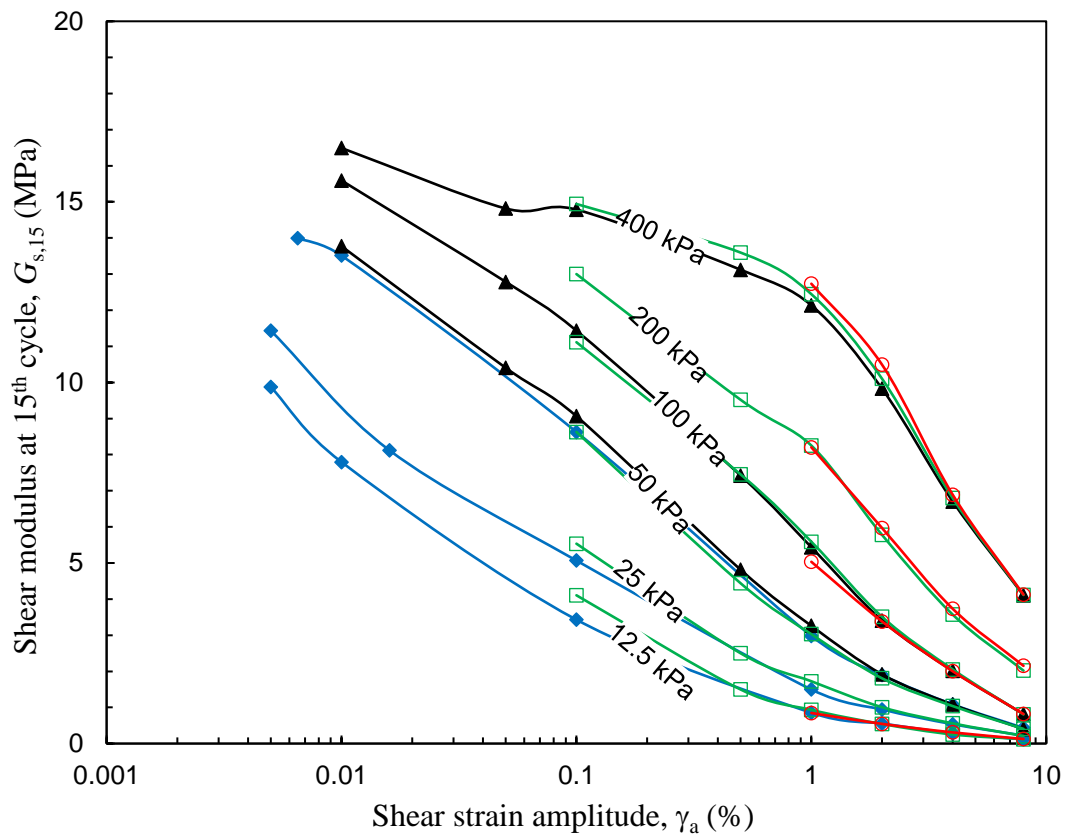


Fig. 4.10. Effects of shear strain amplitude on shear modulus at 15th cycle for varying cyclic loading histories and normal stresses

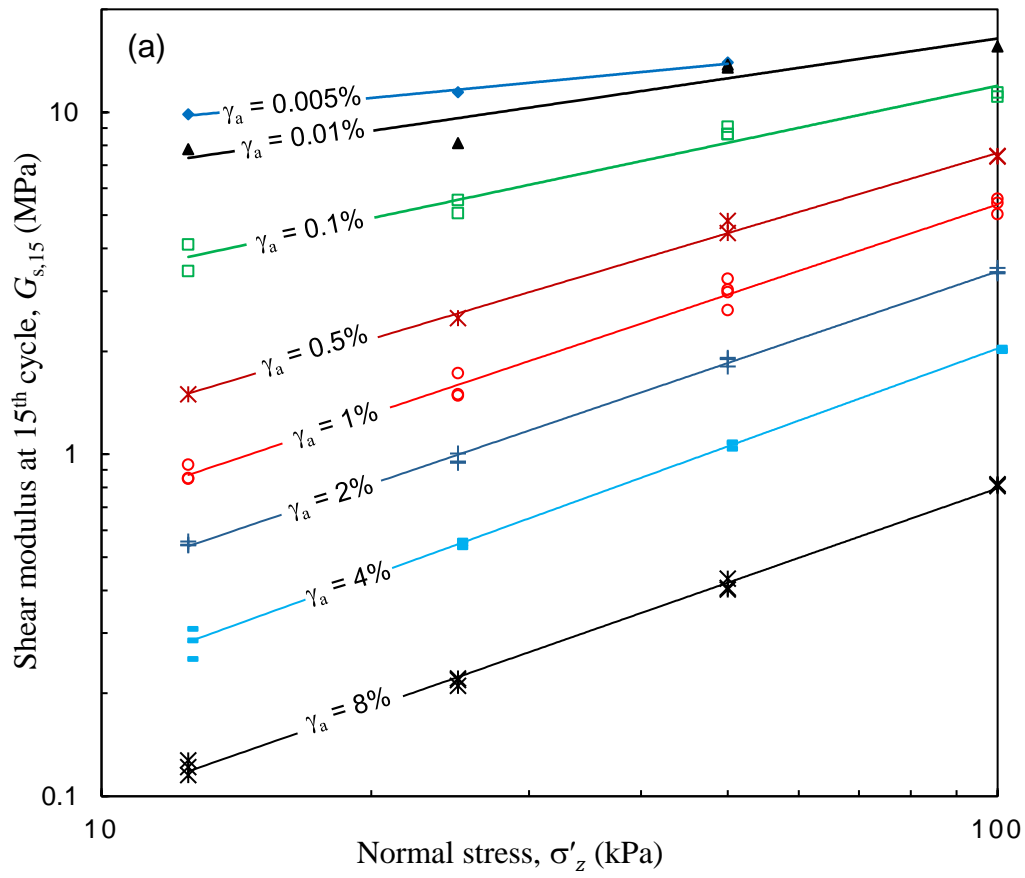


Fig. 4.11. Shear modulus: (a) effects of normal stress and shear strain amplitude; (b) effects of shear strain amplitude on K and m parameters

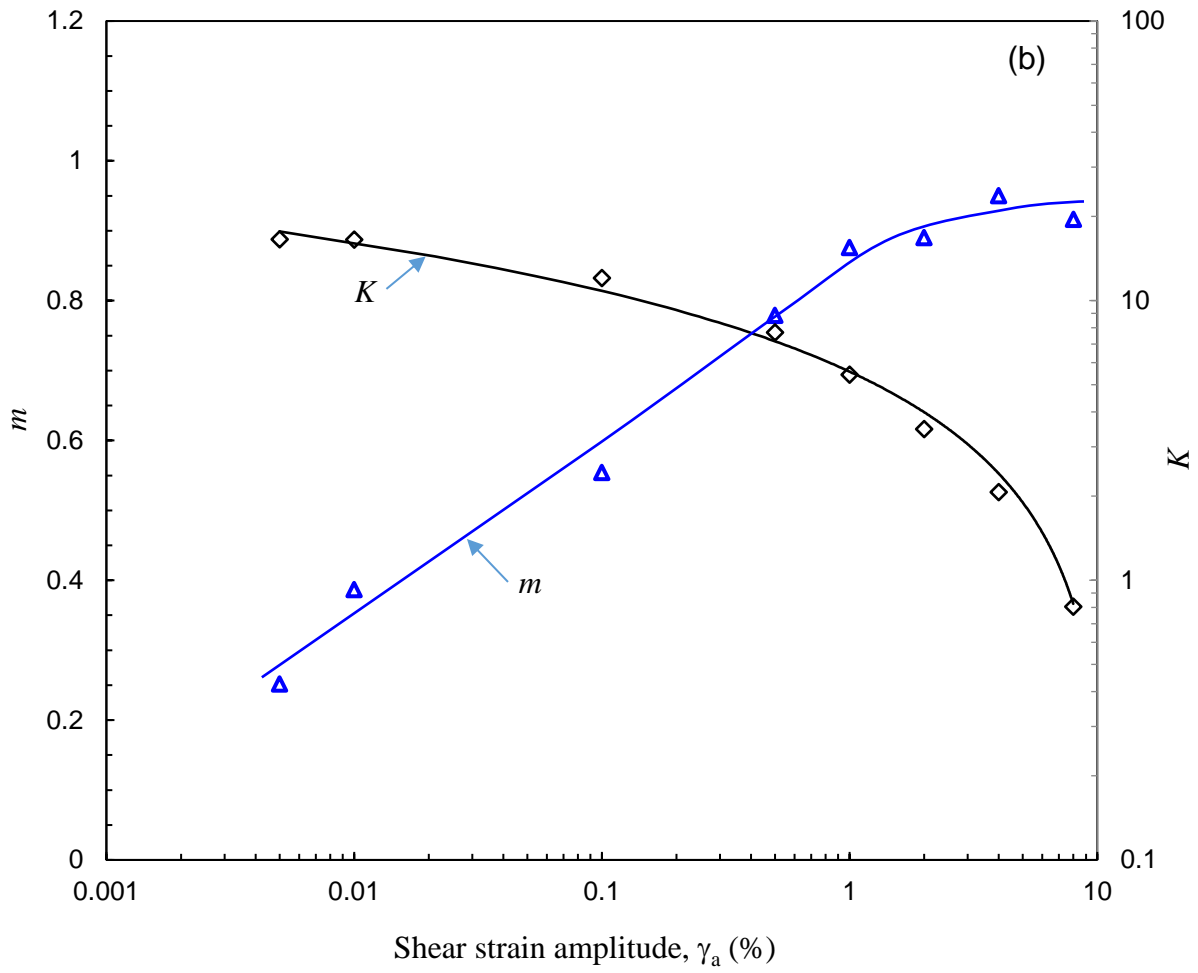


Fig. 4.11. Shear modulus: (a) effects of normal stress and shear strain amplitude; (b) effects of shear strain amplitude on K and m parameters

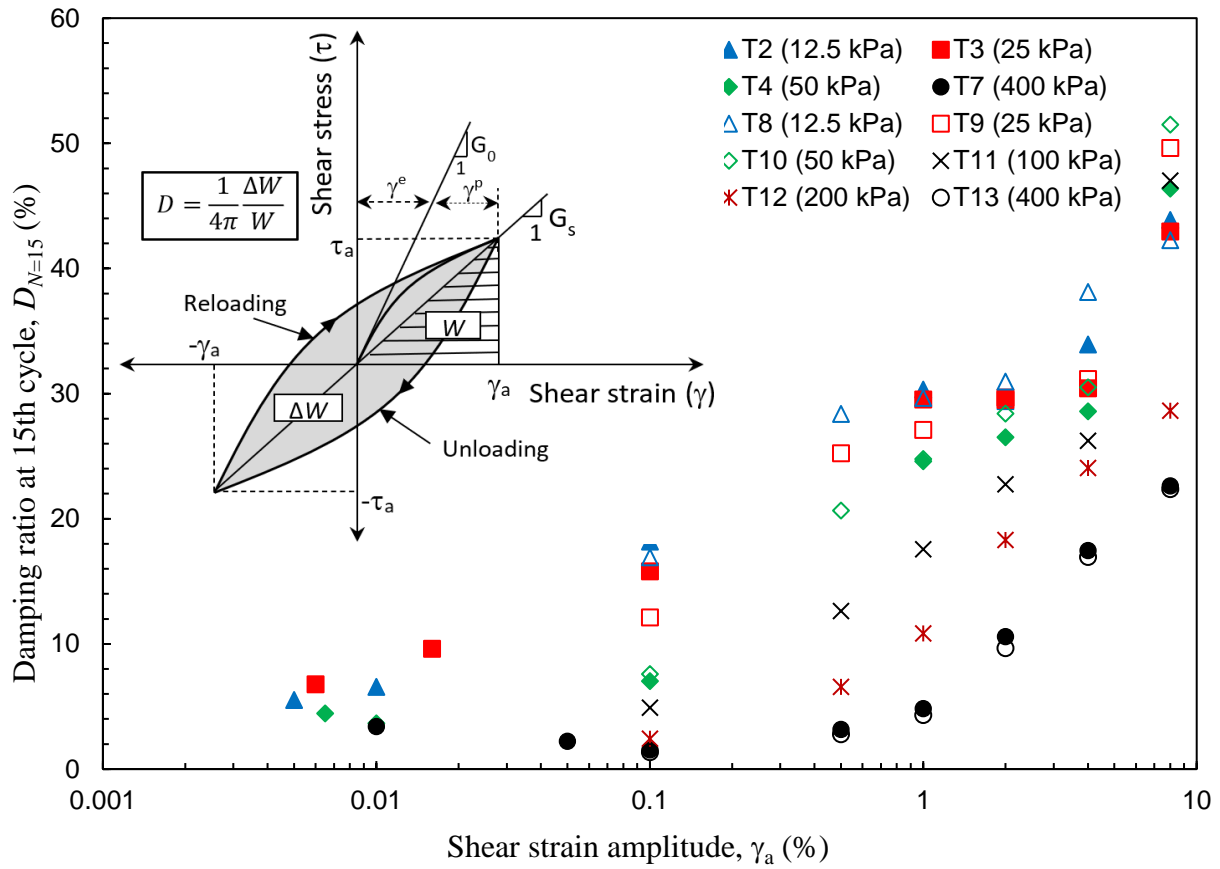


Fig. 4.12. Effects of shear strain amplitude and normal stress on damping ratio

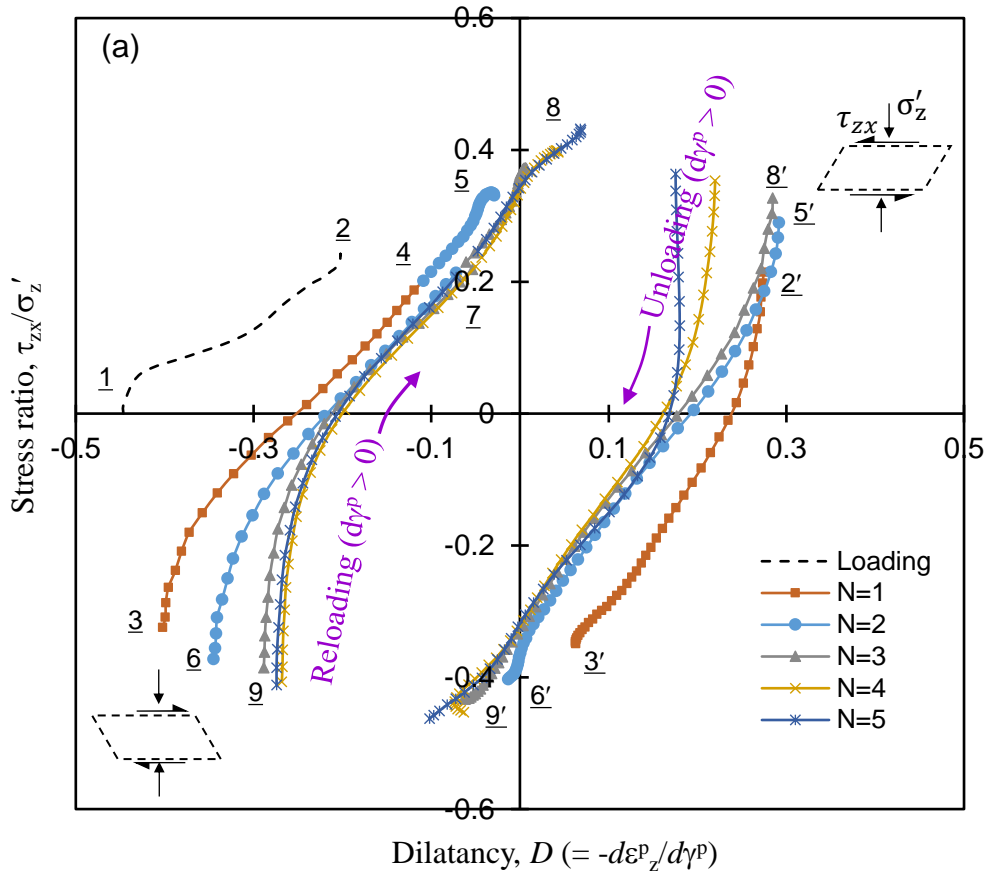


Fig. 4.13. Cyclic stress–dilatancy response in test T1 ($\sigma_z' = 100$ kPa, $\gamma_a = 1\%$): (a) initial loading and subsequent five cycles; (b) at large number of cycles

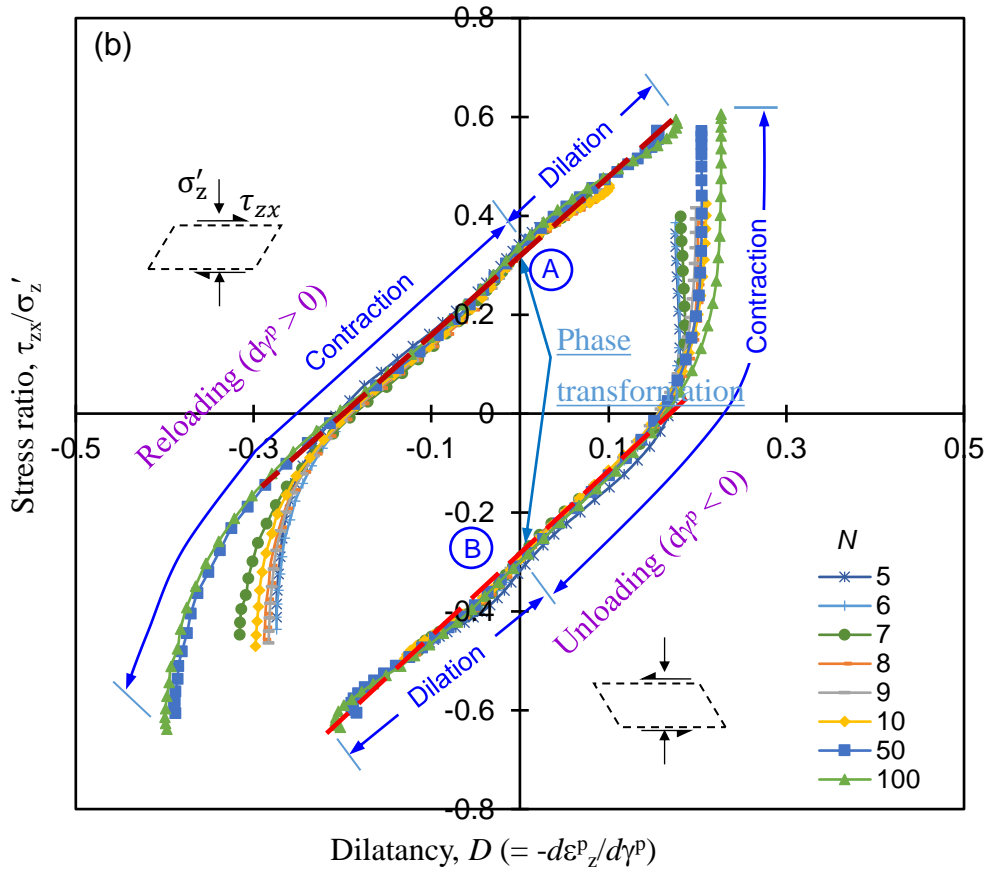


Fig. 4.13. Cyclic stress–dilatancy response in test T1 ($\sigma'_z = 100$ kPa, $\gamma_a = 1\%$): (a) initial loading and subsequent five cycles; (b) at large number of cycles

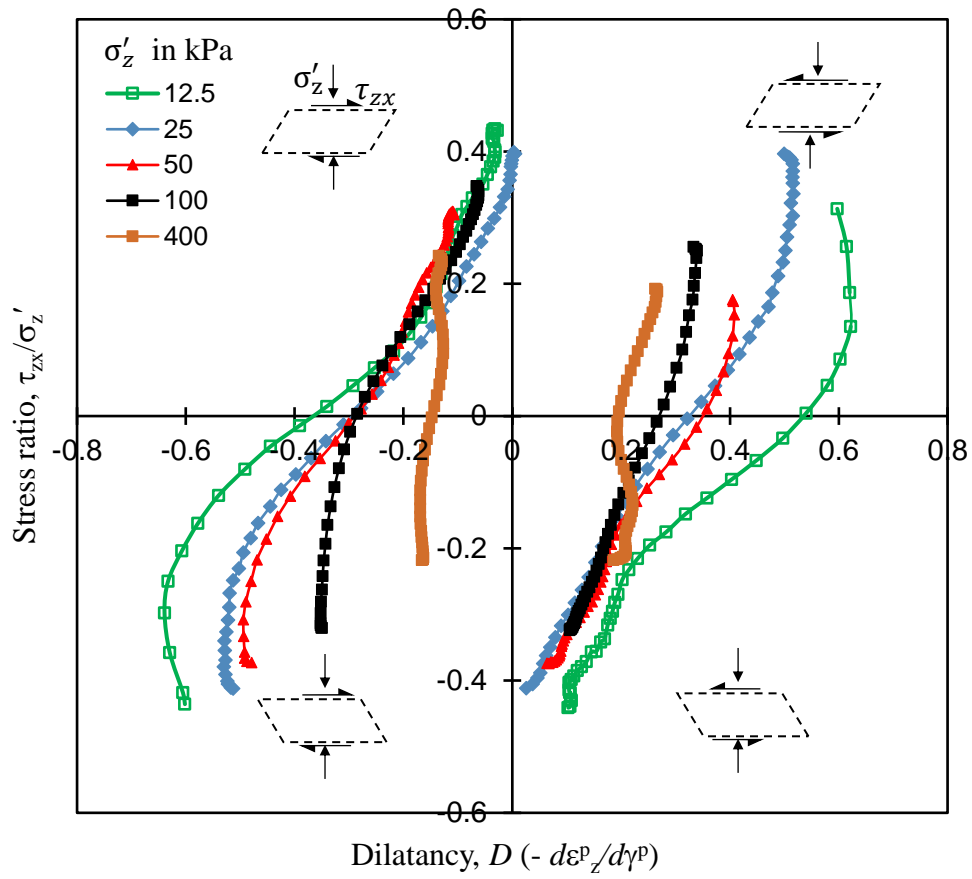


Fig. 4.14. Effects of normal stress on stress ratio–dilatancy in 1st cycle for strain amplitude of 1%, (Tests T14–T18)

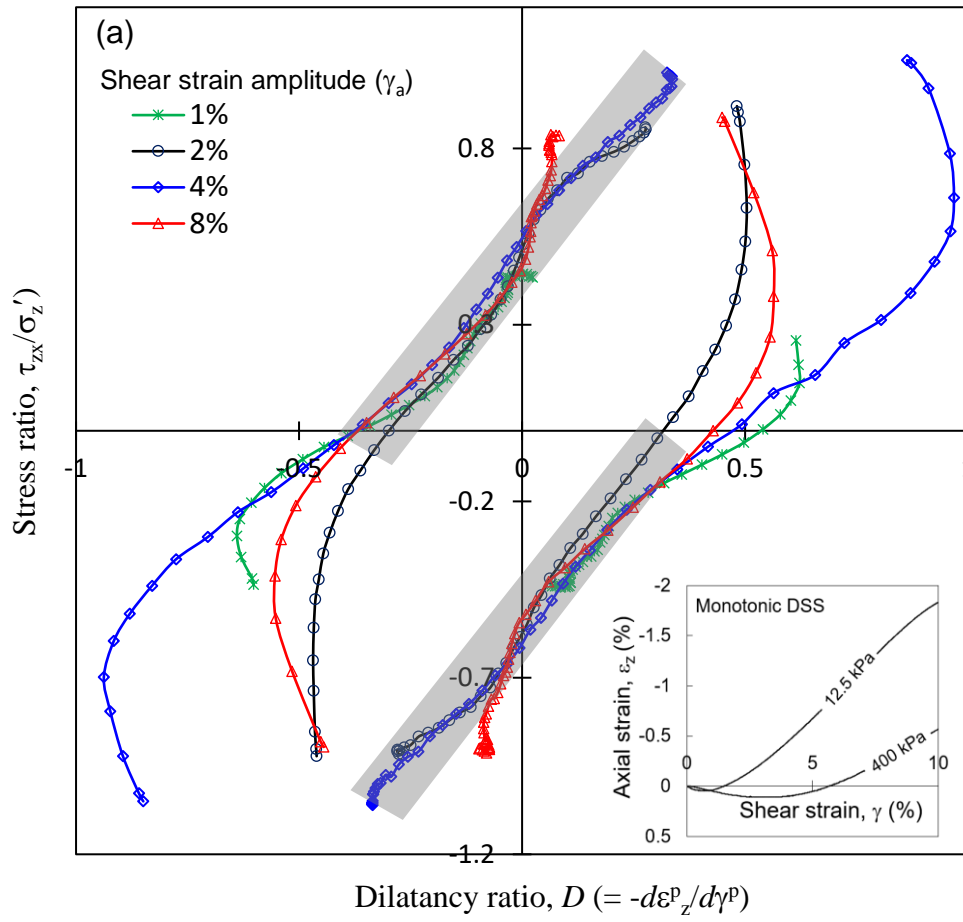


Fig. 4.15. Stress–dilatancy in multi-stage cyclic test: (a) normal stress 12.5 kPa; (b) normal stress 400 kPa

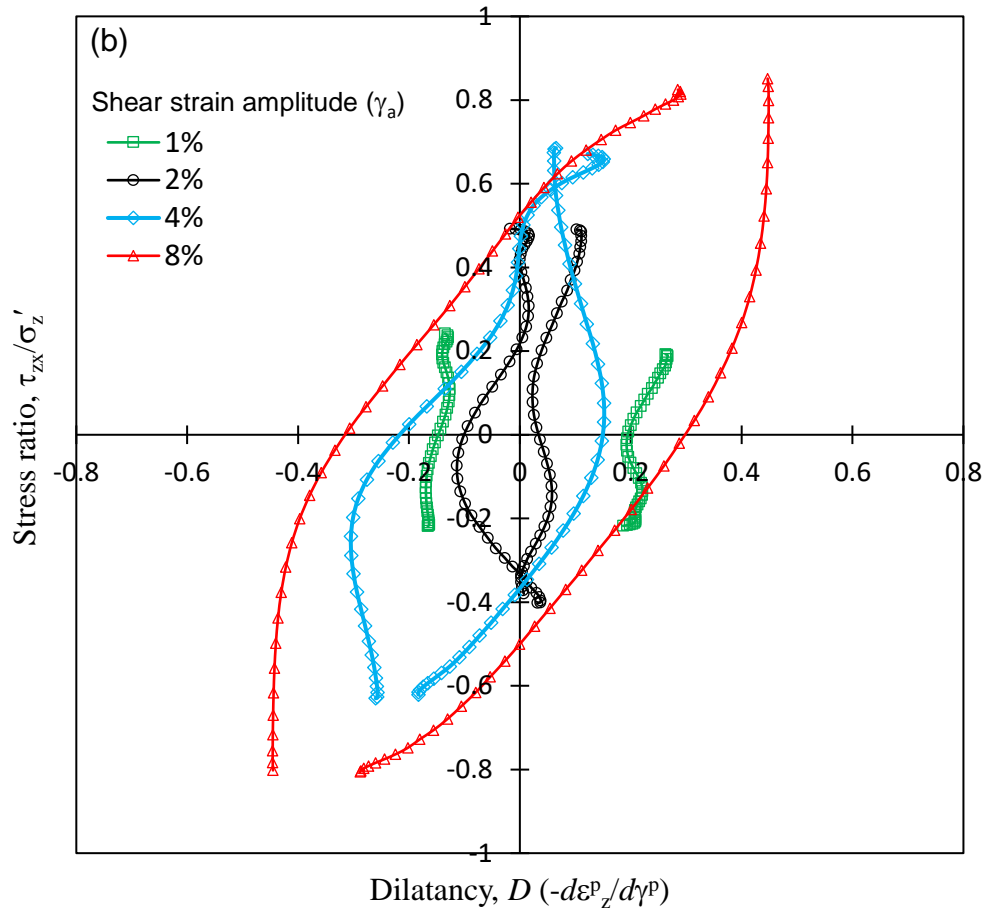


Fig. 4.15. Stress–dilatancy in multi-stage cyclic test: (a) normal stress 12.5 kPa; (b) normal stress 400 kPa

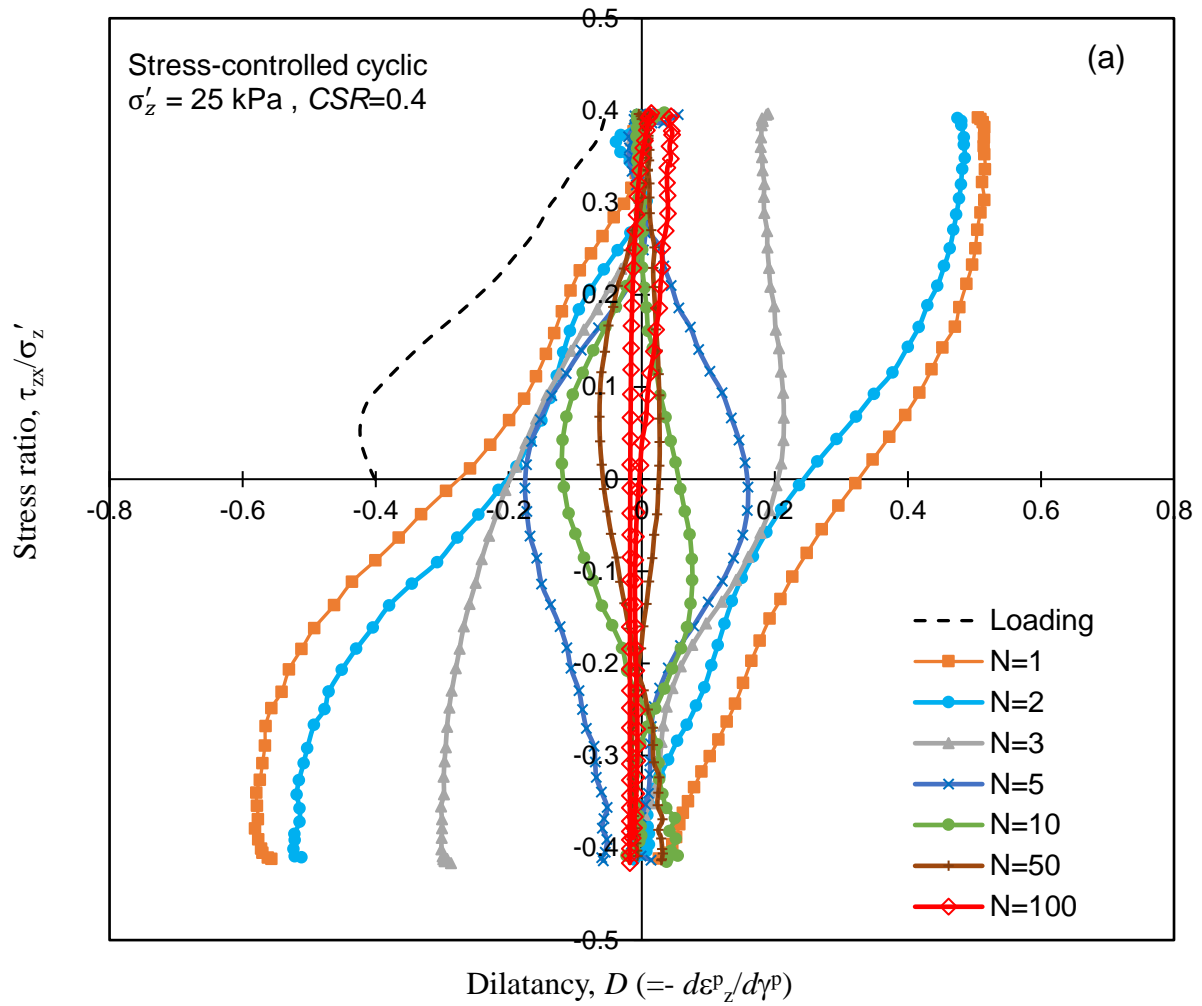


Fig. 4.16. Stress ratio–dilatancy in stress-controlled tests: (a) effects of number of cycles; (b) effects of normal stress

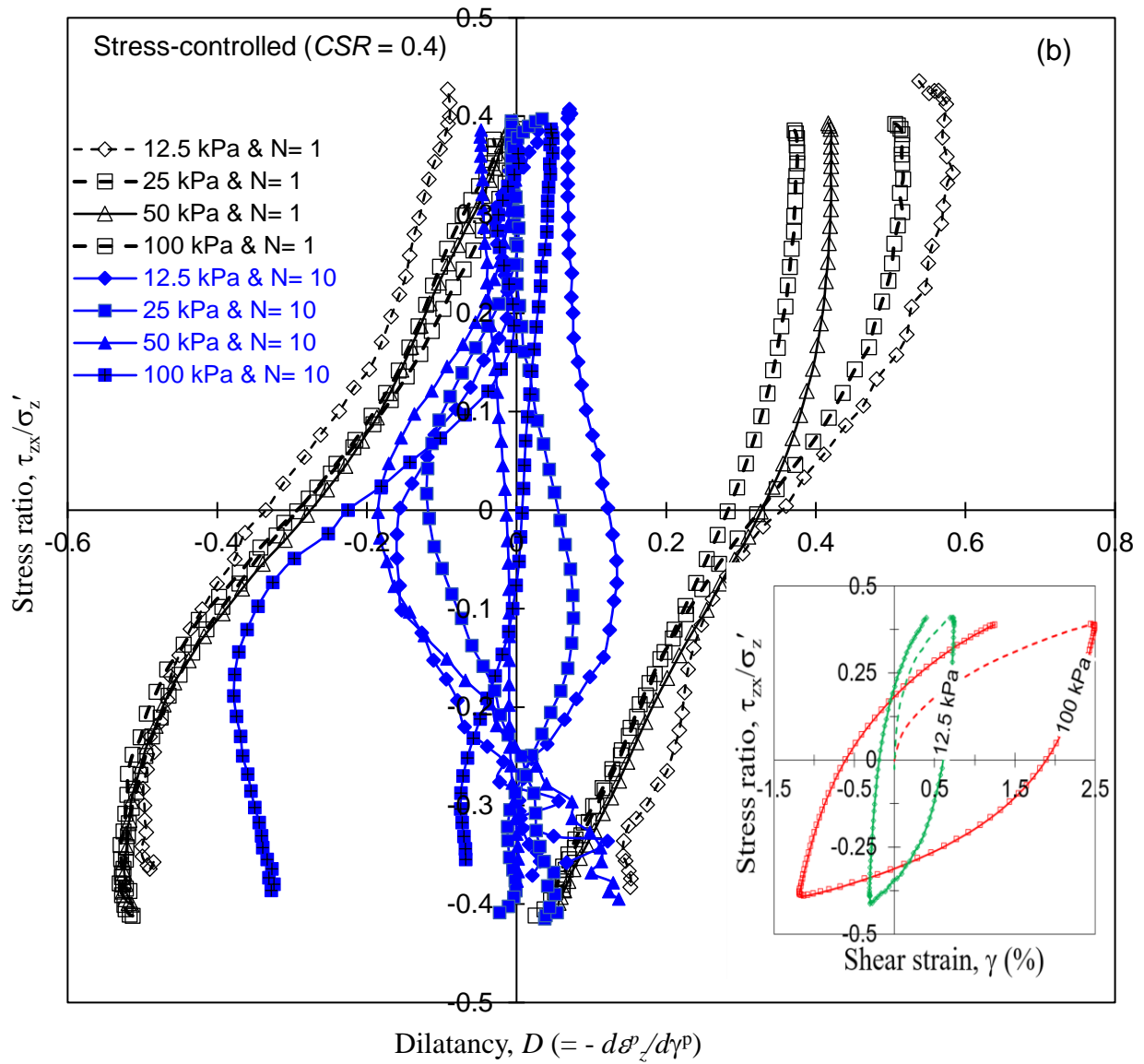


Fig. 4.16. Stress ratio–dilatancy in stress-controlled tests: (a) effects of number of cycles; (b) effects of normal stress

Table 4.1 Summary of test conditions

Test #	Normal stress (kPa)	Shear strain amplitude, γ_a (%) or Cyclic stress ratio (<i>CSR</i>)								
Dense specimens										
T1	100	-	-	-	-	-	1.0	-	-	-
T2	12.5	0.005	0.01	-	0.1	0.5	1.0	2.0	4.0	8.0
T3	25	0.005	0.01	-	0.1	0.5	1.0	2.0	4.0	8.0
T4	50	0.005	0.01	-	0.1	0.5	1.0	2.0	4.0	8.0
T5	50	-	0.01	0.05	0.1	0.5	1.0	2.0	4.0	8.0
T6	100	-	0.01	0.05	0.1	0.5	1.0	2.0	4.0	8.0
T7	400	-	0.01	0.05	0.1	0.5	1.0	2.0	4.0	8.0
T8	12.5	-	-	-	0.1	0.5	1.0	2.0	4.0	8.0
T9	25	-	-	-	0.1	0.5	1.0	2.0	4.0	8.0
T10	50	-	-	-	0.1	0.5	1.0	2.0	4.0	8.0
T11	100	-	-	-	0.1	0.5	1.0	2.0	4.0	8.0
T12	200	-	-	-	0.1	0.5	1.0	2.0	4.0	8.0
T13	400	-	-	-	0.1	0.5	1.0	2.0	4.0	8.0
T14	12.5	-	-	-	-	-	1.0	2.0	4.0	8.0
T15	25	-	-	-	-	-	1.0	2.0	4.0	8.0
T16	100	-	-	-	-	-	1.0	2.0	4.0	8.0
T17	200	-	-	-	-	-	1.0	2.0	4.0	8.0
T18	400	-	-	-	-	-	1.0	2.0	4.0	8.0

T19	12.5	CSR=0.4									
T20	25	CSR=0.4									
T21	50	CSR=0.4									
T22	100	CSR=0.4									
Loose specimens											
T23	12.5	-	-	-	-	-	1.0	2.0	4.0	8.0	
T24	100	-	-	-	-	-	1.0	2.0	4.0	8.0	
T25	400	-	-	-	-	-	1.0	2.0	4.0	8.0	

Notes: i) T1 is a strain-controlled single-stage test of 1,000 cycles

ii) T2–T18 & T23–T25 are strain-controlled multi-stage tests of 100 cycles per stage

iii) T19–T22 are stress-controlled single-stage tests of 100 cycles

CHAPTER 5

Effects of Confining Stress and Sample Preparation Methods on Behaviour of Sand in Direct Simple Shear and Triaxial Tests

Abstract

The stress–strain behaviour of silica sand in direct simple shear (DSS) and triaxial compression (TXC) tests is investigated. The DSS tests were conducted on reconstituted dry sand specimens prepared through four methods of specimen preparation: funnel raining (FR), multiple-sieve raining (MSR), dry tamping (DT), and table tapping (TT). Monotonic drained simple shear tests were conducted under constant vertical stress (σ'_z), while in undrained (constant height) tests, σ'_z prior to shearing varied from 25 kPa to 200 kPa. Air pluviation, especially multiple-sieving, was a better controlled method of sample preparation as compared to DT and TT, including in the response at relatively large strains. The very dense specimens prepared by DT and TT methods show a clear trend of expected behaviour at lower strains. However, potential effects of non-uniform compaction of the specimen and localized shear band formation influence the stress–strain behaviour at larger strains in the post-peak softening stage in the constant stress tests and after the phase transformation in the constant height tests. Consolidated-drained triaxial compression tests show a continued increase of maximum dilation angle and peak friction angle with a decrease in confining pressure.

KEYWORDS: dry sand sample preparation, drain and undrained behaviour, low stress, monotonic loading, direct simple shear and triaxial tests

5.1 Introduction

The collection of undisturbed sand specimens by maintaining in-situ arrangement of the particles is an extremely challenging task, although there are some methods available (e.g., in-situ ground freezing). Most of the time, sand properties are determined through the element test on reconstituted sands. Different methods have been used to prepare soil specimens for laboratory element tests and physical modelling (e.g., centrifuge tests). Laboratory test results show that the specimen preparation technique could significantly influence the stress–strain behaviour (Oda 1972a–c; Oda et al. 1985; Ishihara 1993; DeGregorio 1990; Vaid et al. 1999).

Moist tamping (MT), water pluviation (WP), and air pluviation are the common methods of sand specimen reconstitution. Generally, MT specimens have a more non-uniform void ratio than the specimens prepared by air or water pluviation (Castro 1969; Mulilis et al. 1978; Ladd 1978; Vaid and Negussey 1988; Vaid and Sivathayalan 2000). The fabric of WP specimens is similar to the fabric of fluvial and hydraulic fills (Vaid and Sivathayalan 2000). The dry air pluviated specimen represents the natural deposition process (Vaid and Negussey 1984; Yang et al. 2008).

Several experimental studies explained the effects of sample preparation on the behaviour of sand (Oda 1972a–c; Ladd 1978; Mulilis et al. 1977; Silver et al. 1980; Miura and Toki 1982; Ishihara 1993; Kuo and Frost 1996; Frost and Park 2003; Yamamuro and Wood 2004). Most of these studies focused on liquefaction potential due to cyclic loading (Mulilis et al. 1978; Yamashita and Toki 1993). Also, the majority of the experiments were conducted for the axisymmetric loading condition, using a triaxial apparatus (Mulilis et al. 1977; Sze and Yang 2014). However, soil failure in many field situations resembles simple shear conditions. Experimental studies show that sand might behave differently in triaxial compression (TXC), triaxial extension (TXE) and simple shear (SS) loadings, even if the specimens are prepared using the same sample preparation technique

and have the same initial void ratio (or relative density) and confining stress (Vaid and Chern 1985; Riemer and Seed 1997; Yoshimine et al. 1998; Vaid and Sivathayalan 2000). For example, in monotonic loading, loose Fraser Delta sand shows strain hardening in triaxial compression, softening in triaxial extension and in between in simple shear loading (Vaid and Sivathayalan 2000). For cyclic loading, a correction factor is recommended while using cyclic triaxial test results for cyclic simple shear loading scenarios (Finn et al. 1971; Peacock and Seed 1968). Dry specimen preparation methods are commonly used in many DSS tests (Silver and Seed 1971; Seed and Silver 1972; Amer et al. 1986; Duku et al. 2008; Sivathayalan and Ha 2011; Monkul et al. 2015; Li et al. 2018). In addition to ease of preparation, the prepared dry specimens can be used for both drained and undrained testing. The tests are conducted by applying a constant vertical confining stress (σ'_z) first and then sheared under the same σ'_z in drained tests, and maintaining constant height for undrained loading. The change in vertical stress during shearing of a dry specimen in a constant height DSS test is equivalent to the change in pore water pressure in a saturated specimen in an undrained DSS test for a similar condition (Vaid and Finn 1979; Dyvik et al. 1987). It has also been considered that undrained static and cyclic liquefaction can be assessed based on constant height DSS tests on dry sand (Wijewickreme et al. 2005; Sivathayalan and Ha 2011; Monkul et al. 2015). As DSS testing is the primary focus of the present study, the effects of only dry sand specimen preparation are considered.

The present study aims to investigate the influence of dry dense sand specimen preparation techniques and confining stress on stress–strain behaviour. The paper has been organized as follows. First, the results of a series of monotonic drained DSS tests are presented to explain the variation of shear resistance and dilation of the specimens prepared by four specimen preparation methods. Loosely poured sand could be compacted in different ways. The effects of compaction

techniques on sand behaviour are examined. Second, a series of undrained (constant height) DSS tests were conducted to understand whether the compaction methods during specimen preparation affect the phase transformation and steady-state friction angles for varying normal stresses, including at low stresses. Finally, the behaviour of sand in DSS condition is compared with drained triaxial compression test results.

5.2 Materials

Figure 5.1 shows the particle size distribution of the poorly-graded fine-grained silica sand used in this study. The sand particles are sub-rounded to sub-angular. The mean diameter, uniformity coefficient, and coefficient of gradation are 0.18 mm, 1.12, and 2.23, respectively. The specific gravity (G_s) of the sand is 2.65. The maximum (e_{max}) and minimum (e_{min}) void ratios are 1.048 and 0.606, respectively, which correspond to the minimum (γ_{min}) and maximum (γ_{max}) density of 1,294 kg/m³ and 1,650 kg/m³, respectively. All the index tests have been conducted according to ASTM standards.

5.3 Apparatus for Shear Testing

5.3.1 Direct Simple Shear

Simple shear tests are conducted using the Combined Advanced Dynamic Cyclic Simple Shear (ADVDCSS) apparatus at Memorial University of Newfoundland. It can accommodate a 70-mm diameter and 20-mm height specimen. This specimen is confined laterally with a stack of 1-mm-thick rigid Teflon coated low friction steel rings that allow K_0 consolidation and ensure constant volume during undrained testing by maintaining constant height. The ADVDCSS has a 16 bit high-precision feedback system for controlling stresses and displacements while maintaining a high

level of accuracy. Although the system has recently been upgraded by installing a dual-axis 5-kN load cell, the test results presented in this paper are conducted using a system with two separate 5-kN load cells for axial and lateral loads with an accuracy and resolution better than 0.1% and 0.2 N, respectively. A ± 2.5 -mm LVDT is mounted close to the sample to measure the axial displacement. In addition, an axial displacement transducer (stroke) and the motor encoder are used to crosscheck the measured vertical displacements. A ± 10 -mm displacement transducer under the sample base measures the shear displacement, which is also crosschecked with shear displacement measurement using the encoder. The displacement transducers have an accuracy better than 0.1% of the full range and resolution of 0.1 microns. Further details on this apparatus are available in the work of Al Tarhouni et al. (2017 and 2019). A wide range of soil (fine to coarse-grained) can be tested for drained and undrained conditions. This apparatus can also be used to conduct tests in a saturated condition, which is not available in many typical NGI-type or CU-type DSS apparatuses (Kjellman 1951 and Roscoe 1953).

5.3.2 Triaxial

The triaxial apparatus used in this test program contains three main components: an electro-mechanical digital load frame (50 kN), a triaxial cell, and two GDS pressure/volume controllers for cell pressure and backpressure. The axial displacement is measured using a ± 10 -mm transducer with an accuracy better than 0.25% of the full range. A pore water pressure transducer, located close to the sample drainage line, provides the pore water pressure inside the sample. The control of the test and data acquisition are performed using GDSLab software. The apparatus can be used to conduct monotonic triaxial compression and extension under drained and undrained conditions

for isotropic and K_0 consolidations. In the present study, only isotropically consolidated TXC tests were performed.

5.4 Direct Simple Shear Sample Preparation

The basic requirements for a reconstituted sand specimen preparation are to make the sample homogeneous, with a uniform distribution of void ratio, and the preparation technique should be able to create specimens of a wide range of density (Ishihara 1993). Also, it is preferred that the researcher's skill and ability should not significantly influence the quality and repeatability of producing a similar sample. For DSS specimen preparation, a latex membrane was placed on and secured to the bottom pedestal by O-rings. Teflon coated steel rings were then placed around the membrane. A suction mould, made in-house, was placed around the steel rings. After folding the flank of the membrane over the mould, a vacuum was applied to tauten the membrane against the rings. In this experimental program, the cylindrical specimens were 70-mm diameter and 18- to 19-mm high. Figure 5.2 shows the dry sand specimen preparation schematically using the following four methods: (i) Funnel raining (FR), (ii) multiple-sieve raining (MSR), (iii) dry tamping (DT), and (iv) table tapping (TT).

5.4.1 Funnel Raining (FR)

Funnel raining is a dry pluviation method; where no energy is used to densify the sand except for gravity. Air-dry sand particles were deposited in the cavity inside the taut membrane with the rings using a funnel with a nozzle diameter of 5 mm, at a drop height of ~420 mm, to prepare loose sand specimens T4–T6 in Table 5.1. Once it was completely filled, a siphon was used to remove the

extra sand above the level of the topmost ring and the top sand surface was evened (inset of Fig. 5.1). The mould was then placed and attached to the DSS machine.

5.4.2 Multiple-sieve Raining (MSR)

A multiple-sieve air pluviation method, similar to that proposed by Miura and Toki (1982), was built with four sieves; the top two had 2-mm and the bottom two had 1.18-mm openings. The sieves were set such a way that the center of a square opening of a sieve was at 45° to the vertical from that of the sieve above and/or below, which facilitates dispersion of the sand particles during their movement through the sieves and results in uniform raining from the bottom sieve (Rad and Tumay 1987). A funnel was placed at 540 mm (nozzle distance) above the top sieve, in which sand was poured. The sample mould was placed under the lower sieve at a constant distance (raining height) of 217 mm. A 5-mm and 50.8-mm funnel size were used to prepare dense (T1 & T2 in Table 5.1) and loose (T3) specimens, respectively. When the mould was full, similar to in the FR method, the top sand surface was made flat, and the specimen was attached to the DSS machine for testing.

The particle arrangements in the specimens prepared by the MSR method are similar to those in FR specimens. Bowman and Soga (2003) showed that, in dry pluviation methods, the longest axis of sand particles is parallel to the horizontal axis. Yang et al. (2008) found a similar particle arrangement in specimens prepared by the dry deposition (funnel rain) method. The orientation of the longest axis to the horizontal might be higher in the MSR method than for the FR method, because of the uniformity of raining in the MSR.

5.4.3 Dry Tamping (DT)

This method was used to prepare dense sand specimens (T7, T8 in Table 5.1). A predetermined amount of dry sand (~110 g) was poured in three equal layers using a 6.5-mm diameter funnel with zero drop height. The funnel was moved around to distribute the sand evenly. Each layer was compacted using a large 68-mm diameter tamping rod, with a lift height of 10–15 mm, to achieve the targeted relative density. Finally, after verifying the evenness of the top surface using a circular bubble level, the specimen was attached to the DSS apparatus.

5.4.4 Table Tapping (TT)

This method was also used to prepare dense specimens. A predetermined amount of dry sand (~110 g) was poured using a 6.5-mm diameter funnel with zero drop height. The sand surface was evened, and the top cap was placed. The seating table was tapped using a rubber hammer around the mould while the level of the top cap was checked from time to time using a circular bubble level. The height of the specimen was monitored using a digital dial gauge. The tapping was stopped when the targeted relative density (calculated based on the height of the specimen) was reached. The sample was moved and attached to the DSS machine. Note that the placement of the top cap during tapping provided a constraint to the movement of particles, which was not imposed on samples in the other methods. Therefore, the contacts between the particles were expected to be higher in TT specimens than in the specimens prepared by the other methods.

5.5 Summary of the Conducted DSS Tests

A total of 21 DSS tests was conducted (Table 5.1). Among them, 14 tests were conducted under a constant vertical stress ($\sigma'_z = 80$ kPa) on specimens prepared by the four methods of specimen

preparation, as described above. Four tests were on loose sand ($D_{rc} = 36\%–40\%$), and the remaining were on dense sand specimens ($D_{rc} = 80\%–85\%$). In the consolidation stage, the vertical stress was applied gradually. Here, consolidation represents the compression of the dry DSS specimen under vertical stress, and D_{rc} is the relative density at the end of consolidation. As the soil remained in the rigid stacked rings, the stresses in the soil specimen at the end of this loading represent the K_0 condition, where the lateral stress is $K_0\sigma'_z$. The shear displacement was then applied at the bottom of the specimen at a constant strain rate of 0.16 %/min, keeping σ'_z constant (= 80 kPa). In addition, 7 constant height DSS tests were conducted: four on very dense, one on medium and two on loose specimens (Table 5.1). Further details on these tests are provided in later sections.

5.6 Constant Stress DSS Test Results

The main focus of the following discussion is to present the successes and challenges in preparing repeatable soil specimens using different techniques. Therefore, in each case, a number of repeatable tests were conducted targeting the same initial conditions. The response of soil specimens was evaluated using the stress ratio and dilation behaviour with shear strain.

5.6.1 Multiple-sieve Raining (MSR) Method

Figure 5.3(a & b) shows the variation of the stress ratio (τ_{zx}/σ'_z) with the shear strain (γ) and axial strain (ϵ_a) for constant stress DSS tests ($\sigma'_z = 80$ kPa) of the samples prepared by the multiple-sieve raining method (MSR) (Tests T1–T3). As discussed further in the later sections, the reconstitution of dense to very dense sand is a more difficult task, and the human factor might influence the fabric of the compacted soil. Therefore, tests T1 and T2 were prepared at the same relative density (D_{rc}

= $85 \pm 1\%$) to check the repeatability. No significant difference between the stress–strain curves for tests T1 and T2 represents good repeatability. The stress ratio increases with the shear strain, and reaches the maximum at $\gamma \sim 8\%$, and becomes almost constant ($\tau_{zx}/\sigma'_z \sim 0.68$). Test T3 was conducted on loose sand $D_{rc} = 40\%$. The stress ratio in this test increases with shear strain and τ_{zx}/σ'_z reaches 0.61 at $\gamma = 20\%$.

Figure 5.3(b) shows the volume change behaviour. The loose sample (T3) exhibits a contractive response up to $\gamma = 8\%$ and then becomes slightly dilative. The dense samples (T1 & T2) initially show a small contractive response ($\gamma \leq 1.5\%$) and the response changes to dilative with an increase in γ . The difference between the rate of dilation of samples T1 and T2 is not significant, which again shows excellent repeatability in sample preparation. For verification, the vertical displacement obtained from three different sources (LVTD, axial stroke and motor encoder) are plotted in the Inset-I and -II of Fig. 5.3(b) for Test T1 and T2, respectively. All three sources give very similar ε_a , although the axial stroke gives slightly different results because it has been installed at the top of the DSS machine and this measurement involved some equipment compliance error. In summary, this set of tests showed the system performance and repeatable dense specimen preparation using the MSR method.

5.6.2 Funnel Rain (FR) Method

The funnel rain method generally gives loose specimens because the height of the nozzle from the soil is approximately zero. However, the density can be increased by tamping or tapping, as described in the following sections. Therefore, all the tests with the funnel rain method were conducted on loose specimens ($D_{rc} = 40\%$).

Three duplicated loose dry specimens were prepared by FR method (T4–T6). Vertical stress of $\sigma'_z = 80$ kPa was applied and then sheared. Figures 5.3(a & b) show the variation of stress ratio and axial strain with shear strain. All three specimens (T4–T6) show almost identical stress ratio–shear strain response. The stress ratio increases gradually with shear strain without any peak because of low density. The stress ratio (τ_{zx}/σ'_z) is equal to 0.56 at $\gamma = 20\%$, and has a trend of increasing even after this strain level, which is potentially due to an increase in radial stress with shearing, that increases the ratio between lateral and vertical stresses (Budhu 1985; Atkinson et al. 1991). All three samples exhibit a contractive response up to $\gamma = 11\%$ and then ε_a remains almost constant or increases slightly.

5.6.3 Dry Tamping (DT) Method

Depositing soil in the mould as in the funnel rain method, the soil was compacted to increase the density in tests T7 and T8 ($D_{rc} = 78\%$ & 82%). Again the samples were consolidated to $\sigma'_z = 80$ kPa and then sheared. Figure 5.4(a) shows that the stress ratio increases with shear strain, reaches the maximum at $\gamma \sim 11\%$, and then remains almost constant at 0.68–0.72, with a slightly higher stress ratio for the denser specimen. Note that although the soil is dense, DSS tests generally show less post-peak softening than in triaxial compression tests (Vaid et al. 1981). Fig. 5.4(b) shows contractive followed by dilative behaviour with an increase in strain. The dilation rate reduces to a zero or to a small value at large strains.

5.6.4 Table Tapping (TT) Method

Loosely poured sand in the mould using a funnel can also be compacted by tapping the table. Figure 5.4(a) shows the variation of stress ratio with shear strain for a series of six duplicated

specimens prepared by the table tapping method (T9–T14). The relative density and consolidation pressure of these specimens are the same as for the preceding dense specimens ($D_{rc} \sim 80\%$ and $\sigma'_z = 80$ kPa). All six specimens show a similar response of increasing stress ratio and reaching almost the same peak value at $\gamma \sim 10\%$; however, they show a different post-peak degradation response. The stress ratios decrease to 0.70 – 0.72 at large shear strains ($\gamma > 24\%$). The difference in the post-peak reduction is potentially due to the development of different initial fabrics during densification by tapping. Loose sand specimens prepared by funnel rain showed good repeatability in the stress–strain behaviour, including at large shear strains (Fig. 5.3 (a & b)); therefore, it is expected that all the specimens listed in Fig. 5.4 (a & b) had the same initial fabric. However, the densification by tapping involves human factors, such as hammer energy and location of tapping, which could generate different fabric. The soil fabric can influence the behaviour when the particles slide and roll during plastic deformation; therefore, the post-peak degradation is primarily different in these tests (Fig. 5.4 (a & b)). Note that the post-peak reduction might play a significant role in some engineering applications where the progressive formation of shear band occurs (Terzaghi et al. 1996)—for example, in the analysis of pipe–soil interaction, ultimate bearing capacity of the shallow foundation and for slope instability, where sufficiently large deformation might occur (Loukidis and Salgado 201; Roy et al. 2018).

All the specimens show a contractive response up to $\gamma = 1.5\% - 2.5\%$ and then dilative behaviour (Fig. 5.4b). Also, the rate of dilation of all the specimens is almost the same up to $\gamma = 12\%$, where the peak stress ratio is mobilized (Fig. 5.4a), and then becomes different at large strains, which is potentially due to the variation in the shear band that depends on the initial fabric developed from sample preparation, as mentioned earlier. The specimens which have a faster reduction of dilation

rate at a large strain experience a quicker post-peak reduction of stress ratio (e.g., compare the results of T9 and T13).

5.7 Discussion on Constant Stress DSS tests

5.7.1 Dense Sand

To evaluate the effects of specimen preparation, the test results of T1 and T2 (multiple-sieve raining), and T7 and T8 (dry tamping) are also plotted in Fig. 5.4(a & b). Tests T1 and T8 are the repeatable tests of T2 and T7, respectively. Note that the funnel rain method is used only for loose sand specimen preparation (Table 5.1).

Figure 5.4(a) shows that the stress ratio increases quickly for the specimen prepared by table tapping, as compared to dry tamping and multiple-sieve raining. As discussed in previous sections, the TT method might have created a fabric anisotropy with a stronger solid path and higher contact normal force between the sand grains than that with the DT and MSR methods. Therefore, during shearing, the TT method provides a high shear resistance due to the induced fabric. Moreover, the DT and MSR methods do not demonstrate a peak stress ratio. The stress ratio increases gradually up to $\gamma = 8\%–10\%$ and becomes almost constant. Also, the stress ratio–shear strain responses of the DT and MSR methods are essentially similar. Finally, the stress ratio at a high shear strain level (e.g., $\gamma \sim 28\%$) is nearly identical for all the samples, irrespective of potentially different induced fabric by sample preparation.

A similar effect of the specimen preparation technique was reported from triaxial tests on dense sand (Oda 1972a; Miura and Toki 1982). Oda (1972a) conducted triaxial compression tests on dense sand specimens prepared by two methods: (i) by plunging a hand tamper into the sand,

which is similar to the dry tamping method described above, and (ii) tapping the sidewall with a hand tamper. Analyzing microscopic views of thin sections of soil specimens, he found that the initial fabric developed with the tapping method had a strong preferred orientation of the long axis of the grain, perpendicular to the major principal stress. He also found that, for the same initial void ratio of dense sand, the deviatoric stress of tapping specimens increased quickly to a peak value, which is higher than that of dry tamping specimens. Also, the tapping specimens exhibited post-peak softening while the deviatoric stress gradually increased over a large strain for dry tamping specimens, similar to Fig. 5.4 of the present study. Similar to Oda (1972a), the particle orientation could be the main cause of stronger stress–strain behaviour in the present DSS tests on table tapping specimens than that for dry tamping and multiple-sieve raining specimens.

Li et al. (2018) conducted DSS tests on loose to medium dense Leighton Buzzard sand (relative density 27%–68%). Dry specimens were prepared by dry funnel and air pluviation methods, and the specimens were densified to the targeted level by vibrating the loosely placed sand in a mould using a small shaking table in the former method, while it was achieved by changing the drop height in the latter method. No significant effect of sample preparation was found in the stress ratio; however, slightly more dilative behaviour was found in the samples compacted by vibration. Relatively less influence of sample preparation on stress–strain behaviour in their tests than the present study might be because of lower relative density ($\leq 68\%$), higher consolidation pressure ($\sigma'_z = 200$ kPa), compaction technique, and type of sand used in that study.

Considering that the horizontal plane is the plane of the maximum shear stress obliquity, the angle of internal friction can be approximately calculated as $\phi'_{DSS} = \tan^{-1}(\tau_{zx}/\sigma'_z)$. For the stress ratio shown in Fig. 5.4, the average value of the peak friction angle ($\phi'_{p,ss}$) is 39.5° for the

table tapping specimens, and the critical state friction angle ($\phi'_{c_{SS}}$) (obtained from stresses at $\gamma = 28\%$) is 34° for all the specimens. Based on discrete element simulations, Wijewickreme et al. (2013) suggested that $\phi'_{p_{SS}} = \sin^{-1}(\tau_{zx}/\sigma'_z)_{\max}$ is a better representation of the peak friction angle, which gives $\phi'_{p_{SS}} = 55.5^\circ$. Such a considerable difference, due to the interpretation of test results, needs to be investigated further. Also, the difference in friction angles for different sample preparation methods is potentially due to different fabric development during preparation. The dependency of friction angle on particle arrangement was also recognized in previous studies (Guo 2008, Tong et al. 2014).

Fig. 5.4(b) shows that the maximum dilation rate of TT specimens is about twice of that for the specimens prepared by MSR and DT methods. This is again due to the orientation of the particles during sample preparation, as explained earlier. A similar response was observed in triaxial compression tests; for example, Oda (1972b) found a significantly higher volumetric strain increase in specimens prepared by tapping than in the specimens compacted by a tamping rod. Unlike dense sand, as used in the present study and Oda's (1972b), the difference between the dilation of medium dense specimens prepared by vibration (tapping the mould or vibrating it on a shaking table) and dry raining (MSR or funnel raining) is small in triaxial compression and DSS tests (Miura and Toki 1982; Li et al. 2018). However, Miura and Toki (1982) found that the dilation is more significant in triaxial extension (TXE) tests on medium dense sand (i.e., higher dilation in tapping than in MSR specimens). This implies that the sample preparation effect on dilation is related to stress path (TXC, TXE & DSS) and soil density before shearing.

5.7.2 Loose Sand

Without tamping or tapping, loose sand specimens ($D_{rc} \sim 40\%$) were prepared by FR and MSR methods. As discussed above, samples were consolidated at $\sigma'_z = 80$ kPa and then sheared. Figure 5.3(a) shows that the specimen T3 (prepared by MSR) is slightly stronger than the other three loose specimens (T4–T6) prepared by the FR method. Specimen T3 showed slightly dilative behaviour at large strain, while specimens T4–T6 remained contractive during the whole range of shearing (Fig. 5.3(b)). Overall, the difference in stress ratio and volume change between the specimens prepared by FR and MSR is not significant for loose sand. In triaxial compression and extension tests, Miura and Toki (1982) found a small difference between the behaviour of the specimens prepared by the MSR and the funnel raining method for the relative densities of 55% and 70%. Therefore, it can be concluded that the higher dilation and stress ratio in dense specimens prepared by tapping than in those in the MSR specimens, as discussed above, was primarily due to change in the fabric during tapping of the specimens, as compared to the MSR specimens.

In summary, dry dense sand specimens can be prepared in two different ways. Firstly, in the raining method (e.g., funnel rain, MSR) a higher density can be achieved by changing the drop height and/or the funnel diameter. Secondly, loose sand can be poured in the mould and subsequently compacted by vibration (tapping or shaking) or inside tamping. The present DSS test results show that the soil fabric with the second specimen preparation technique might be varied significantly, depending on the subsequent compaction process (tapping or tamping). The dense specimens prepared by table tapping have higher shear strength than that of tamped specimens. In terms of practical application, it is therefore recommended to use the specimen preparation techniques that resemble the field compaction and deposition processes.

5.8 Constant Height DSS Test Results

As shown above, compaction by tapping could give a stronger fabric and higher (peak) friction angle than that using the other three methods (FR, DT & MSR). In this section, the effects of specimen preparation primarily on two important soil parameters are investigated: (i) phase transformation (ϕ'_{PT}), where volumetric strain rate changes from contraction to dilation, and (ii) steady-state friction angle (ϕ'_{SS}), where the stress ratio becomes constant. Dense DSS specimens are prepared by dry tamping, and by the combination of dry tamping and table tapping for very dense condition. Note that many field compaction processes (e.g., dynamic compaction) represent densification of cohesionless soil by tamping and vibration.

Several researchers conducted triaxial (TXC and TXE), DSS, and hollow cylinder tests (HCT) on very loose to medium dense sands to study static and cyclic liquefaction (Vaid and Chern 1985; Yoshimine et al. 1999; Wan and Guo 2001; Sivathayalan and Ha 2011). Three types of undrained response of sand were observed in monotonic triaxial loading: (i) loose sands show a large deformation associated with a low shear strength after the peak strength, (ii) medium dense sand initially exhibits strain-softening followed by strain-hardening behaviour, and (iii) dense sand have strain-hardening behaviour. The undrained response also depends on the mode of shearing. For a given initial condition (void ratio and confining pressure), the soil might show strain-hardening in TXC but strain-softening in TXE, and in between in DSS tests (Yoshimine et al. 1999). However, limited studies in the literature investigated dense sand behaviour in DSS condition for undrained loading (constant height conditions), especially at low-stress level. To show the effect of dense specimen preparation, four DSS tests were conducted on very dense sand (T15–T18) (Table 5.1). For comparison, three more tests were conducted on medium (T19) and loose (T20 & T21) sands.

5.8.1 Sample preparation

The specimens were prepared following the same preparation methods for the constant stress DSS tests, as described above. The loose sand specimens (T20 & T21) were prepared by funnel rain method. The medium sand specimens (T19) were prepared by dry tamping (DT). The very dense sand specimens (T15–T18) were prepared by compacting the sand by combination of dry tamping and table tapping. Table 5.1 shows the relative density after consolidation.

Bernhardt et al. (2016) conducted three-dimensional discrete element simulations of DSS and showed that, for medium dense sand, the sidewall friction increases the strain hardening and maximum stress ratio. To investigate the sidewall friction effect, the latex membrane friction in tests on very dense sand (T15–T18) was increased as follows. After placing the membrane in the stacked rings and flipping it around, suction was applied that stuck the membrane to the rings. A resin glue was smeared over the inner surface of the membrane up to the expected specimen height. The same sand used for the tests was then poured inside the cavity, and a small dead load was placed on the top of the sand surface, such that sand particles came in close contact with the membrane. The setup was left about 24 hours, and then the sand from the mould was removed. Approximately 4 gm of sand remained glued to the membrane surface, which has been included in the later calculation of the relative density of the specimen. The glued sand also provided a frictional sidewall during shearing. Dry sand was then poured using a funnel at zero drop height in three equal layers. Each layer was compacted, first using a tamper and then by table tapping, as described before, to get a high relative density ($D_{rc} \sim 92\%$).

Placing the specimens on the DSS apparatus, the specimens were consolidated for $\sigma'_z = 25 \text{ kPa}$ – 200 kPa (Table 5.1)). The vertical displacement was very small during the consolidation phase,

especially for dense sand. The specimens were then sheared by maintaining zero vertical displacement of the Encorder and LVDT (i.e. constant specimen height).

5.8.2 Test Results

Figure 5.5(a) shows the stress–strain behaviour. As the tests were conducted for a wide range of consolidation pressure, σ'_{z0} (i.e. σ'_z prior to shearing), the normalized stress (τ_{zx}/σ'_{z0}) is plotted in Fig. 5.5(b) for clarity. All four dense sand specimens (T15–T18) exhibited strain-hardening behaviour during the entire range of shearing (Figs. 5.5(a) & 5.5(b)). Shear stress (τ_{zx}) increases rapidly at low shear strain (γ), then the rate of increase of τ_{zx} decreases approximately after $\gamma = 0.4\%–0.7\%$, and finally reaches the “ultimate steady state” (Yoshimine and Ishihara 1998) at $\gamma > 12\%$ (Fig. 5.5(a)). A “quasi-steady state” was observed in the test on medium sand (T19). However, the loose sand specimens show strain-softening behaviour after the peak at $\gamma = 0.2\%–0.4\%$.

Figure 5.5(b) shows that an increase in D_{rc} and reduction of σ'_{z0} increase the normalized shear stress prior to the peak and phase transformation. For dense sand (T15–T18), an increase in σ'_{z0} reduces the initial slope of the τ_{zx}/σ'_{z0} vs. γ curves. However, after the phase transformation ($\tau_{zx}/\sigma'_{z0} > 0.25$), the τ_{zx}/σ'_{z0} vs. γ curves do not show any clear trend with σ'_{z0} . This implies that, at this high shear stress level, localized shear bands might have formed in this dense soil specimens which affect the stress–strain behaviour when considerable plastic shear strain develops, similar to that observed during the post-peak reduction of strength in the constant stress DSS tests (Fig. 5.4). In other words, while dense sand specimens of the same relative density could be prepared by tamping and tapping, the soil fabric might be different, which could significantly affect the response at large strains.

The mobilization of shear resistance can be better understood by plotting the stress ratio (τ_{zx}/σ'_z) with γ , as shown in Fig. 5.5(c) for dense specimens. Note that, unlike constant stress tests (Fig. 5.3(a) and 5.4(a)), both τ_{zx} and σ'_z vary with shearing in constant height tests. For low strain (e.g., $\gamma \leq 4\%$), the lower the initial consolidation pressure, the higher the stress ratio, and the σ'_{z0} effect on stress ratio is more significant at low-stress level tests (Fig. 5.5(c)).

Figure 5.5(d) shows the stress paths for constant height tests, where the stresses are normalized by σ'_{z0} for clarity. Irrespective of the stress level, density, and sample preparation method, the effective normal stress during shearing initially decreases and then increases after reaching the phase transformation state for medium and dense sand. The phase transformation separates the contractive and dilative behaviour of sand (Ishihara et al. 1975). A significant initial contractive response (similar to positive pore pressure), even for medium to dense sand, was observed in previous DSS tests. Sivathayalan and Ha (2011) found an initial contractive response of the medium to dense silica sand specimens prepared by the air pluviation method. They also found a significant strain softening even for $D_{rc} = 75\%–80\%$ when the specimen was under high static shear stresses. Dyvik and Suzuki (2018) showed that a North Sea sand specimen at a high relative density (95%) experienced $\sim 45\%$ reduction of consolidation pressure to reach the phase transformation point (i.e. initially contractive behaviour). The present study shows that, although stronger fabric might be developed during table tapping, the specimens still show contractive behaviour initially.

The stronger fabric, together with increased density, results in less contractive behaviour, which also indicates less excess pore pressure (i.e., decrease in normal stress from the initial state) during shearing (compare T17 with T19 in Fig. 5.5(d)). The mobilized friction angle at the phase transformation states in dense sand and quasi-steady state in medium sand (ϕ'_{Qs}) is $24^\circ–28^\circ$,

irrespective of sample preparation methods and initial consolidation pressures considered in this study. Vaid et al. (1990) also found the same ϕ'_{PT} for varying consolidation pressure, initial void ratio and loading modes (TXC and TXE).

Shearing after the PT state moves the stress path toward the line of maximum obliquity at the ultimate steady state (Fig. 5.5(a) & 5.5(d)). The mobilized friction angle at the ultimate steady state (ϕ'_{ss}) varies from 32° to 35° for all the specimens, with a trend of higher ϕ'_{ss} for lower σ'_{z0} .

The uniqueness of the failure line of sand in stress space has been reported in several studies from triaxial compression and extension tests for initial confining pressures of 50–2500 kPa (Vaid and Chern 1985; Vaid et al. 1990; Thomas 1992; Yoshimine and Ishihara 1998). The first author of this study found unique ϕ'_{PT} and ϕ'_{ss} also for non-plastic silts in constant height DSS tests for varying densities and consolidation pressures (Al Tarhouni et al. 2011) for initial normal stresses of 100–400 kPa.

The steady state is similar to the critical state by definition, although there are disagreements among the researchers, mostly about the void ratio and fewer regarding the shear stress at these two states (Jefferies and Been 2016). Assuming $\phi'_c = \phi'_{ss}$ the effects of consolidation pressure on ϕ'_c can be explained.

All the samples in constant height tests reach the maximum stress ratio rapidly, as compared to constant stress tests (compare Fig. 5.4(a) and 5.5(b)). This implies that the critical state could be achieved at a smaller shear strain in constant height tests, while a large shear strain is required to mobilize the critical state in constant stress tests for dense sand. Test results for very large strains are less reliable because of the limitations of any typical laboratory shear apparatus. Therefore, ϕ'_{ss} is slightly smaller than the critical state friction angle (ϕ'_c) obtained from constant stress tests at a large shear strain, as discussed above. An increasing trend of ϕ'_c , with a decrease in consolidation

pressure at the low-stress level, has been reported in previous studies from triaxial compression, DSS, direct shear and ring shear tests (Alshibli et al. 2003; Lings and Dietz 2004; Adams 2017; Rouse 2018). Further details on this issue are available in Chapter 3.

5.9 Drained Triaxial Compression Tests

So far, the discussion has been focused on DSS tests. However, the DSS apparatus is not commonly available in many soil testing laboratories and, in industry practice, isotropically consolidated triaxial compression tests are commonly performed for shear strength parameters and stress–strain behaviour. In this section, the behaviour of the same silica sand as used in the DSS tests is studied with drained triaxial compression tests, with an objective to show the similarity and difference between TC and DSS test results. Similar to DSS experiments, tests were conducted on dense sands ($D_{rc} \sim 85\%$) and with a wide range of consolidation pressures, which include the low values that were not covered in many previous studies.

5.9.1 Specimen Preparation and Testing

Soil samples were prepared using the dry tamping method. A latex membrane was placed and secured to the bottom pedestal using O-rings. A split mould was placed around the membrane and secured by two clasps. Suction was applied after folding the flank of the membrane over the mould, and then other O-rings were placed around the top of the mould. Dry silica sand was poured through a 5-mm-diameter funnel with a zero-drop height in five layers. Each layer was compacted using a tamping rod to achieve the targeted relative density at the preparation stage. The top cap was then placed, and the membrane was released, which was secured by O-rings. To achieve a high level of saturation, CO₂ gas was passed through the specimens at low pressure for

about 40 minutes. After that, the specimen was flushed with de-aired water supplied from the bottom of the specimen using a GDS pressure/volume controller under 2–3 kPa. Suction was applied to keep the sample stable while completing the setup. The height and diameter of the specimen were recorded using a digital dial indicator and calliper. The triaxial cell was moved to the load frame and fixed for testing. In the saturation stage, the B-check showed a high level of saturation of the specimen ($B \geq 0.98$). The specimens were consolidated isotropically to $\sigma_c = 12.5, 25, 50, 100, 200$ and 400 kPa. The relative density of the specimens after the consolidation was $\approx 85\%$. In this study, the membrane stiffness correction was considered according to ASTM standard (D7181–20). In the shearing phase, the axial load was applied at a constant axial strain of 5% /hour to maintain the drained condition.

5.9.2 Drained Triaxial Compression Test results

The stress–strain curves plotted in Fig. 5.6(a) show that the deviatoric stress ($\sigma'_1 - \sigma'_3$) increases with the axial strain (ϵ_a) and reaches the maximum value at $\epsilon_a = 1\% - 4\%$. The higher the stress level, the higher the value of the axial strain to reach the peak strength is. The deviatoric stress remains almost constant at a large range of strains $2-7\%$, then decreases rapidly and becomes constant. For a given ϵ_a , the higher the confining pressure, the higher the deviatoric stress. To facilitate the explanation, the results are plotted in terms of the deviatoric stress ratio $(\sigma'_1 - \sigma'_3)/\sigma'_3$ (Fig. 5.6(b)). The stress ratio is related to the angle of internal friction in TC as $\phi'_T = \sin^{-1}[(\sigma'_1 - \sigma'_3)/(\sigma'_1 + \sigma'_3)]$. The deviatoric stress ratio increases with the axial strain (ϵ_a), and at $\epsilon_a \sim 2.5-4.5\%$ it reaches the peak value. The deviatoric stress ratio decreases significantly after the peak, especially for low consolidation stress. The following are the key points on the post-peak reduction of the deviatoric stress ratio: i) The post-peak degradation occurs slowly with axial strain

immediately after the peak; however, the degradation occurs quickly after some post-peak strains; and ii) the deviatoric stress and deviatoric stress ratio remain almost constant at large axial strains ($\epsilon_a > 9\%$), which represents the critical state. However, the stress ratios are not the same for all σ'_c ; the lower the σ'_c the higher the stress ratio is. This indicates that the critical state friction angle at a low confining pressure is higher than that of high confining pressures.

Figure 5.7(c) shows contractive followed by dilative behaviour in all the tests. The volumetric strain becomes constant (zero dilation rate) at large strains ($\epsilon_a > 8\%$). The maximum dilation rate increases with a decrease in consolidation pressure. The specimens at low effective stresses contract less than the samples with high effective stresses. Bolton (1986) showed that the peak dilation angle decreases linearly with a logarithmic function of mean effective stress. The present study shows that this trend is also valid for low stress levels.

5.9.3 Comparison of DSS and TXC Test Results

There are some similarities and differences between TXC and DSS tests, as explained earlier. In both tests, the specimens are of cylindrical shape. The axial (σ'_a) and radial (σ'_r) effective stresses in a TXC represent the major (σ'_1) and minor (σ'_3) principal stresses, respectively, during the whole process of shearing. However, a DSS sample remains in a set of stacked rigid rings. The radial stress (σ'_r) prior to shearing can be calculated as $\sigma'_r = K_0 \sigma'_z$, where K_0 is the coefficient of earth pressure at-rest. The lateral strain increment $d\epsilon_r \neq 0$ in TXC; however, $d\epsilon_r = 0$ in the DSS tests. Triaxial tests were conducted on saturated soil specimens. However, direct simple shear tests were conducted in dry conditions. The authors understand that the stress–strain behaviour of saturated sand is somewhat different from dry sand (as used in DSS tests); however, this issue has not been addressed in this study. However, it is worth comparing TXC and DSS tests of similar initial

conditions. For this purpose, DSS tests T7 and T8 and TXC tests T24 and T25 are considered. The former two were conducted at $\sigma'_z = 80$ kPa, and the latter two were conducted at consolidation pressures of 50 kPa and 100 kPa, respectively. All these tests had similar initial density and were prepared by dry tamping. However, the stress–strain curves in TXC tests (Fig. 5.6(a)) are very different from those of DSS tests (Fig. 5.3(a)); the TXC tests show significant post-peak softening while the shear stress gradually increases in the DSS tests, except for samples prepared by table tapping (Fig. 5.4(a)). In TXC tests, $\phi'_p = 43^\circ$ and $\phi'_c = 32^\circ$ in T24, and $\phi'_p = 42.5^\circ$ and $\phi'_c = 31^\circ$ in T25. However, the maximum mobilized friction angle at large strains in DSS tests (T7 and T8) is 35.4° . The maximum dilatancy is significantly higher in TXC (Fig. 5.6(c)) than in DSS tests (Fig. 5.3(b)). The difference in TXC and DSS tests is primarily due to the rotation of principal stresses during shear in DSS tests, calculation of the friction angle from the measured stresses in DSS tests, and the change in soil fabric during shearing, although this change is difficult to quantify from experiments. Therefore, the use of TXC test results on dense sand for a simple shear loading condition in the field would not only overestimate the friction angle, but also the stress–strain behaviour.

Both peak and critical state friction angles in TXC tests are influenced by consolidation stress, especially at low stresses, which has been discussed in detail in Chapter 3.

5.10 Conclusions

The process of deposition and methods of compaction might give sand a different fabric in the field. Although they might have similar relative density, the fabrics could influence the soil response under loading. Similarly, in the laboratory, different methods are used to prepare reconstituted sand samples. The effects of sample preparation and fabric might be investigated

microscopically based on particle arrangements; however, for practical purposes, it can be inferred from the stress–strain response. In the present study, constant stress (drained) direct simple shear (DSS) tests were conducted on silica sand samples prepared by four different methods: funnel raining (FR), multiple-sieve raining (MSR), dry tamping (DT) and table tapping (TT). In addition, constant height (undrained) DSS and triaxial compression (TXC) tests were performed to compare the soil parameters obtained from different modes of shearing. The experimental program covers a wide range of confining pressures, including low stresses. The following conclusions can be drawn from this study.

- (i) Repeatable sand samples prepared by multiple-sieve raining (dense) and funnel raining (loose) show the same stress–strain response for a wide range of strain. The repeatable dense samples prepared by table tapping give a similar response until the peak; however, the stress–strain curves are somewhat different at large strains.
- (ii) The samples prepared by table tapping show a stronger behaviour than the samples prepared by the other three methods. The former one shows a peak stress ratio, while in the latter three, the shear stress continuously increases with shear strain.
- (iii) In constant stress DSS tests, the stress ratio at a large shear strain is almost the same and independent of the sample preparation method.
- (iv) Considerable initial contractive followed by dilative behaviour was observed in the constant height DSS tests on medium to very dense sand specimens. The phase transformation and ultimate steady-state lines in the stress space change by 3° – 4° due to specimen preparation method and initial density and the initial consolidation pressure.

- (v) Post-peak softening response is clear in the drained triaxial compression tests than in DSS tests. A clear constant volume/critical state condition is achieved at a relatively small shear strain in TXC as compared to drained DSS tests.

Acknowledgments

The works presented in this paper have been supported by the Natural Sciences and Engineering Research Council of Canada (NSERC), InnovateNL, the former Research and Development Corporation of Newfoundland and Labrador (RDC), the Canadian Foundation for Innovation (CFI) and the state of Libya.

Notation

The following abbreviations and symbols are used in this paper:

CSR = cyclic stress ratio (τ_a/σ'_z)

D = dilatancy ($-d\varepsilon_v^p/d\gamma^p$)

$d\varepsilon_v^p$ = plastic component of volumetric strain increment

$d\gamma$ = shear strain increment

$d\gamma^e$ = elastic component of shear strain increment

$d\gamma^p$ = plastic component of shear strain increment

D_r = relative density

D_{rc} = relative density after consolidation

DSS = direct simple shear

ε_z = axial strain

$\varepsilon_{z,15}$ = axial strain at 15 cycles
 f = frequency
 γ = shear strain
 γ_a = cyclic shear strain amplitude
 γ_{tv} = threshold shear strain amplitude
 G_s = secant shear modulus (τ_a/γ_a)
 K & m = parameters for shear modulus
 N = number of cycles
 σ'_z = effective axial stress
 τ_a = shear stress amplitude
 τ_{zx} = shear stress
 τ_{zx}/σ'_z = stress ratio

References

- Adams, R.K., 2017. *Near-surface response of beach sand: An experimental investigation*. Master's Thesis, Oregon State University, Oregon, USA.
- Al Tarhouni, M., Fouzder, A., Hawlader, B., and Dhar, A., 2017. Direct simple shear and triaxial compression tests on dense silica sand at low effective stress. *GeoOttawa, 70th Canadian Geotechnical Conference*, Ottawa, Canada, Oct. 1–4, 7p.
- Al Tarhouni, M., Hawlader, B., Fouzder, A., and Dhar, A., 2019. Dynamic behaviour of dry sand in simple shear loading at a wide range of normal stresses. *GeoSt.John's, 72nd Canadian Geotechnical Conference*, St. John's, Canada, Sep. 29–Oct. 2, 7p.

- Alshibli, K.A., Batiste, S.N., and Sture, S., 2003. Strain localization in sand: plane strain versus triaxial compression. *Journal of Geotechnical and Geoenvironmental Engineering*, 129(6): 483–494.
- Al-Tarhouni, M., Simms, P., and Sivathayalan, S., 2011. Cyclic behaviour of reconstituted and desiccated–rewet thickened gold tailings in simple shear. *Canadian Geotechnical Journal*, 48(7): 1044–1060.
- Amer, M.I., Aggour, M.S., and Kovacs, W.D., 1986. Testing using a large-scale cyclic simple shear device. *Geotechnical Testing Journal*, 9(3): 140–146.
- ASTM D7181-20.2020. Standard Test Method for Consolidated Drained Triaxial Compression Test for Soils. *ASTM International*. 12.
- Atkinson, J.H., Lau, W.H.W., and Powell, J.J.M., 1991. Measurement of soil strength in simple shear tests. *Canadian Geotechnical Journal*, 28(2): 255–262.
- Bernhardt, M.L., Biscontin, G., and O’Sullivan, C., 2016. Experimental validation study of 3D direct simple shear DEM simulations. *Soils and Foundations*, 56(3): 336–347.
- Bolton, M.D., 1986. The strength and dilatancy of sands. *Géotechnique*, 36(1): 65–78.
- Bowman, E.T., and Soga, K., 2003. Creep, ageing and microstructural change in dense granular materials. *Soils and Foundations*, 43(4): 107–117.
- Budhu, M., 1985. Lateral stresses observed in two simple shear apparatus. *Journal of Geotechnical Engineering*, 111(6): 698–711.
- Castro, G., 1969. *Liquefaction of sands*. Ph.D. Thesis, Harvard University, Harvard soil mechanics series, 81, Cambridge, Massachusetts, USA.
- DeGregorio, V.B., 1990. Loading systems, sample preparation, and liquefaction. *Journal of Geotechnical Engineering*, 116(5): 805–821.

- Duku, P.M., Stewart, J.P., Whang, D.H., and Yee, E., 2008. Volumetric strains of clean sands subject to cyclic loads. *Journal of Geotechnical and Geoenvironmental Engineering*, 134(8):1073–1085.
- Dyvik, R., and Suzuki, Y., 2018. Effect of Volume Change in Undrained Direct Simple Shear Tests. *Geotechnical Testing Journal*, 42(4): 1075–1082.
- Dyvik, R., Berre, T., Lacasse, S., and Raadim, B., 1987. Comparison of truly undrained and constant volume direct simple shear tests. *Géotechnique*, 37(1): 3–10.
- Finn, W.D.L, Pickering, D.J., and Bransby, P.L., 1971. Sand liquefaction in triaxial and simple shear tests. *Journal of Soil Mechanics & Foundations Div.*, 97(4): 639–659.
- Frost, J. D., and Park, J. Y., 2003. A Critical Assessment of the Moist Tamping Technique. *Geotechnical Testing Journal, ASTM*, 26(1): 57–70.
- Guo, P., 2008. Modified direct shear test for anisotropic strength of sand. *Journal of Geotechnical and Geoenvironmental Engineering*, 134(9): 1311–1318.
- Ishihara, K., 1993. Liquefaction and flow failure during earthquakes. *Géotechnique*, 43(3): 351–451.
- Ishihara, K., Tatsuoka, F., and Yasuda, S., 1975. Undrained deformation and liquefaction of sand under cyclic stresses. *Soils and Foundations*, 15(1): 29–44.
- Jefferies, M., and Been, K., 2016. *Soil liquefaction: a critical state approach*. Second edition, CRC press. New York.
- Kjellman, W., 1951. Testing the shear strength of clay in Sweden, *Géotechnique*, 2(3): 225–232.
- Kuo, C.Y., and Frost, J.D., 1996. Uniformity evaluation of cohesionless specimens using digital image analysis. *Journal of Geotechnical Engineering*, 122(5): 390–396.

- Ladd, R.S., 1978. Preparing test specimens using undercompaction. *Geotechnical Testing Journal*, 1(1): 16–23.
- Li, Y., Yang, Y., Yu, H.S., and Roberts, G., 2018. Effect of sample reconstitution methods on the behaviors of granular materials under shearing. *Journal of Testing and Evaluation*, 46(6): 2718–2725.
- Lings, M.L., and Dietz, M.S., 2004. An improved direct shear apparatus for sand. *Géotechnique*, 54(4): 245–256.
- Loukidis, D., and Salgado, R., 2011. Effect of relative density and stress level on the bearing capacity of footings on sand. *Géotechnique*, 61(2): 107–119.
- Miura, S., and Toki, S., 1982. A sample preparation method and its effect on static and cyclic deformation-strength properties of sand. *Soils and Foundations*, 22(1): 61–77.
- Monkul, M.M., Gültekin, C., Gülver, M., Akın, Ö., and Eseller-Bayat, E., 2015. Estimation of liquefaction potential from dry and saturated sandy soils under drained constant volume cyclic simple shear loading. *Soil Dynamics and Earthquake Engineering*, 75: 27–36.
- Mulilis, J.P., Arulanandan, K., Mitchell, J.K., Chan, C.K., and Seed, H.B., 1977. Effects of sample preparation on sand liquefaction. *Journal of the Geotechnical Engineering Division*, 103(2): 91–108.
- Mulilis, J.P., Townsend, F.C., and Horz, R.C., 1978. Triaxial testing techniques and sand liquefaction. *Dynamic Geotechnical Testing, American Society for Testing and Materials, ASTM STP 654*. 265–279.
- Oda, M., 1972a. Initial fabrics and their relations to mechanical properties of granular material. *Soils and Foundations*, 12(1): 17–36.

- Oda, M., 1972b. The mechanism of fabric changes during compressional deformation of sand. *Soils and Foundations*, 12(2): 1–18.
- Oda, M., 1972c. Deformation mechanism of sand in triaxial compression tests. *Soils and Foundations*, 12(4): 45–63.
- Oda, M., Nemat-Nasser, S., and Konishi, J., 1985. Stress-induced anisotropy in granular masses. *Soils and Foundations*, 25(3): 85–97.
- Peacock, W.H., and Seed, B., 1968. Sand liquefaction under cyclic loading simple shear conditions. *Journal of Soil Mechanics & Foundations Div.*, 94(3): 689–708.
- Rad, N.S., and Tumay, M.T., 1987. Factors affecting sand specimen preparation by raining. *Geotechnical Testing Journal*, 10(1): 31–37.
- Riemer, M.F., and Seed, R.B., 1997. Factors affecting apparent position of steady-state line. *Journal of Geotechnical and Geoenvironmental Engineering*, 123(3): 281–288.
- Roscoe, K.H., 1953. An apparatus for the application of simple shear to soil samples. *Proceedings, 3rd International Conference on Soil Mechanics and Foundation Engineering*, Zurich, Switzerland, (1): 186–191.
- Rousé, P.C., 2018. Relation between the critical state friction angle of sands and low vertical stresses in the direct shear test. *Soils and Foundations*, 58(5): 1282–1287.
- Roy, K., Hawlader, B., Kenny, S., and Moore, I., 2018. Upward Pipe–Soil interaction for shallowly buried pipelines in dense sand. *Journal of Geotechnical and Geoenvironmental Engineering*, 144(11): 04018078.
- Seed, H. B., and Silver, M. L., 1972. Settlement of Dry Sands during Earthquakes. *Journal of the Soil Mechanics & Foundations Div., ASCE*, 98(4): 381–397.

- Silver, M.L., and Seed, H.B., 1971. Volume changes in sands during cyclic loading. *Journal of Soil Mechanics & Foundations Div., ASCE*, 97(9): 1171–1182.
- Silver, M.L., Tatsuoka, F., Phukunhaphan, A., and Avramidis, A.S., 1980. Cyclic undrained strength of sand by triaxial test and simple shear test. In *Proceedings of the 7th World Conference on Earthquake Engineering*, 281–288.
- Sivathayalan, S., and Ha, D., 2011. Effect of static shear stress on the cyclic resistance of sands in simple shear loading. *Canadian Geotechnical Journal*, 48(10): 1471–1484.
- Sze, H.Y., and Yang, J., 2014. Failure modes of sand in undrained cyclic loading: impact of sample preparation. *Journal of Geotechnical and Geoenvironmental engineering*, 140(1): 152–169.
- Terzaghi, K., Peck, R.B., and Mesri, G., 1996. *Soil mechanics in engineering practice*. Second edition, John Wiley & Sons, Inc.
- Thomas, J., 1992. *Static, cyclic and post liquefaction undrained behaviour of Fraser River sand*. Master's Thesis, University of British Columbia, Vancouver, Canada, 117.
- Tong, Z., Fu, P., Zhou, S., and Dafalias, Y.F., 2014. Experimental investigation of shear strength of sands with inherent fabric anisotropy. *Acta Geotechnica*, 9(2): 257–275.
- Vaid, Y.P., and Finn, W.D.L., 1979. Static shear and liquefaction potential. *Journal of Geotechnical and Geoenvironmental Engineering*, 105(ASCE 14909 Proc Paper), 105(GT10):1233.
- Vaid, Y.P., and Negussey, D., 1984. Relative density of pluviated sand samples. *Soils and Foundations*, 24(2): 101–105.

- Vaid, Y.P., and Negussey, D., 1988. Preparation of Reconstituted Sand Specimens. *Advanced Triaxial Testing of Soil and Rock*, ASTM STP 977, R. Donaghe, R. Chaney, and M. Silver, Eds., ASTM International, 405–417.
- Vaid, Y.P., and Sivathayalan, S., 2000. Fundamental factors affecting liquefaction susceptibility of sands. *Canadian Geotechnical Journal*, 37(3): 592–606.
- Vaid, Y.P., Byrne, P.M., and Hughes, J.M.O., 1981. Dilation angle and liquefaction potential. *First International Conferences on Recent Advances in Geotechnical Earthquake Engineering & Soil Dynamics*. 3. Apr 26th - May 3rd. St. Louis, Missouri, USA. 161–165.
- Vaid, Y.P. and Chern, J.C., 1985. Cyclic and monotonic undrained response of saturated sands, *Proc. Advances in the art of testing soils under cyclic loading conditions*, Detroit, 120–147.
- Vaid, Y.P., Chung, E. K. F., and Kuerbis, R. H., 1990. Stress path and steady state. *Canadian Geotechnical Journal*, 27(1): 1–7.
- Vaid, Y.P., Sivathayalan, S., and Stedman, D., 1999. Influence of specimen-reconstituting method on the undrained response of sand. *Geotechnical Testing Journal*, 22(3): 187–195.
- Wan, R.G., and Guo, P.J., 2001. Effect of microstructure on undrained behaviour of sands. *Canadian Geotechnical Journal*, 38(1): 16–28.
- Wijewickreme, D., Dabeet, A., and Byrne, P., 2013. Some observations on the state of stress in the direct simple shear test using 3D discrete element analysis, *Geotechnical Testing Journal*, 36(52): 1–8.
- Wijewickreme, D., Sriskandakumar, S., and Byrne, P., 2005. Cyclic loading response of loose air-pluviated Fraser River sand for validation of numerical models simulating centrifuge tests. *Canadian Geotechnical Journal*, 42(2): 550–561.

- Yamamuro, J.A., and Wood, F.M., 2004. Effect of depositional method on the undrained behavior and microstructure of sand with silt. *Soil Dynamics and Earthquake Engineering*, 24(9-10): 751–760.
- Yamashita, S., and Toki, S., 1993. Effects of fabric anisotropy of sand on cyclic undrained triaxial and torsional strengths. *Soils and Foundations*, 33(3): 92–104.
- Yang, Z.X., Li, X.S., and Yang, J., 2008. Quantifying and modelling fabric anisotropy of granular soils. *Géotechnique*, 58(4): 237–248.
- Yoshimine, M., and Ishihara, K., 1998. Flow potential of sand during liquefaction. *Soils and Foundations*, 38(3): 189–198.
- Yoshimine, M., Ishihara, K., and Vargas, W., 1998. Effects of principal stress direction and intermediate principal stress on undrained shear behavior of sand. *Soils and Foundations*, 38(3): 179–188.
- Yoshimine, M., Robertson, P.K., and Wride, C.E., 1999. Undrained shear strength of clean sands to trigger flow liquefaction. *Canadian Geotechnical Journal*, 36(5): 891–906.

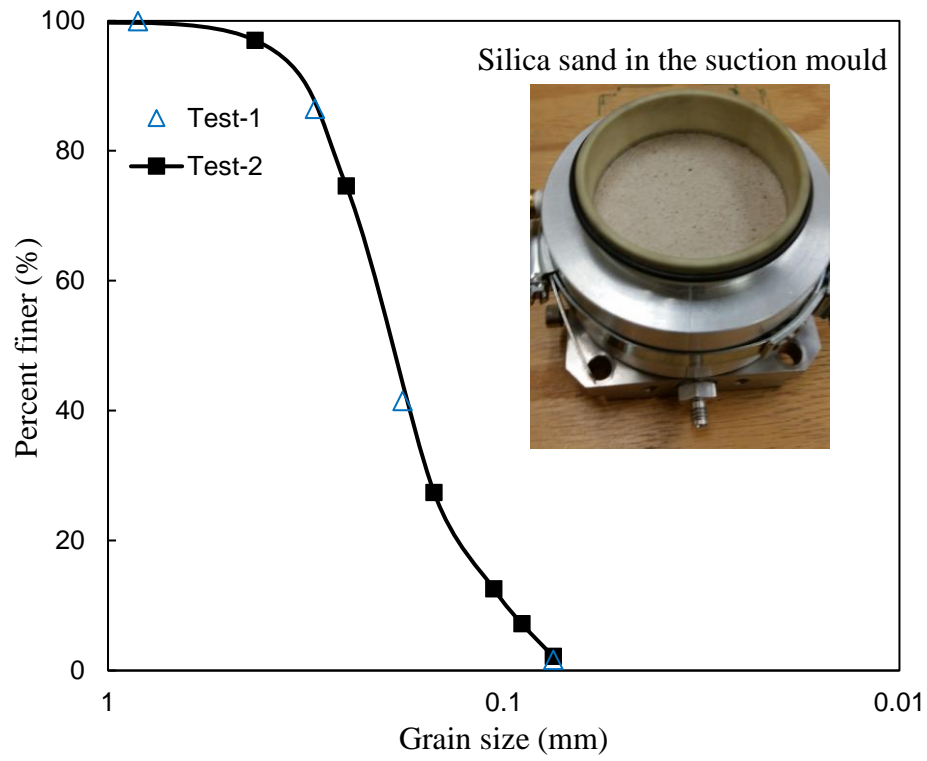


Fig. 5.1. Grain size distribution of silica sand

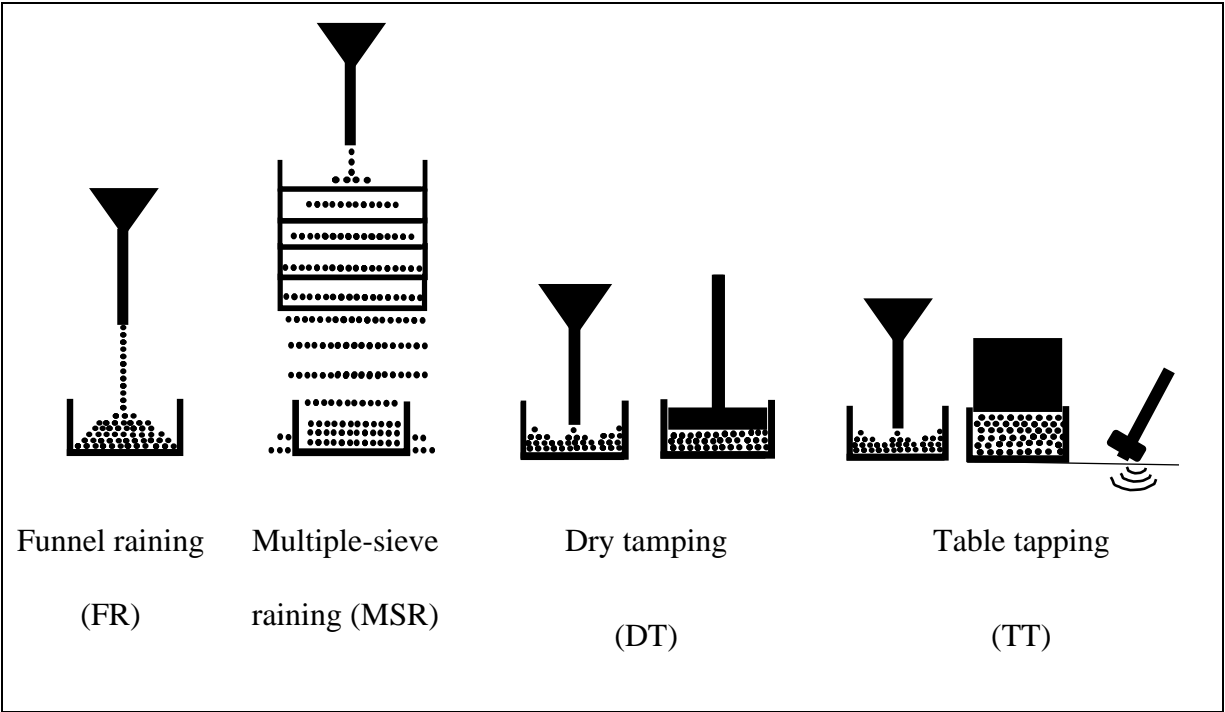


Fig. 5.2. Sample preparation methods

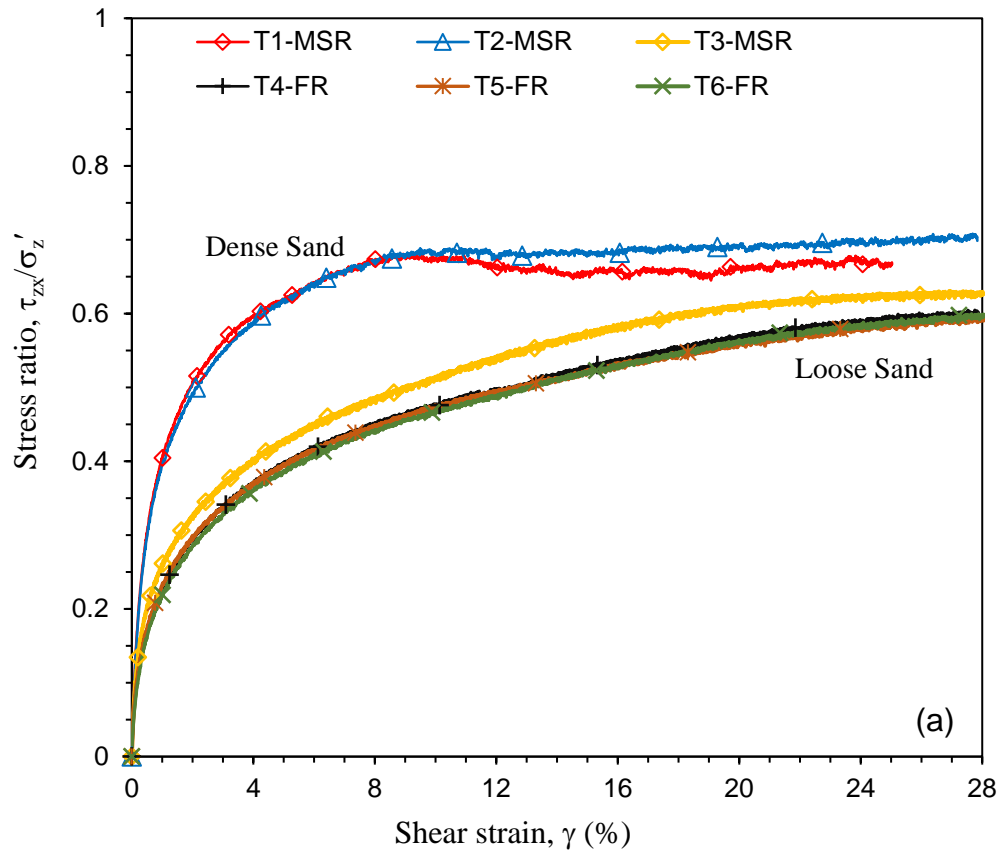


Fig. 5.3. Constant stress tests on loose and dense repeatable samples: (a) stress–strain behaviour; (b) volume change behaviour

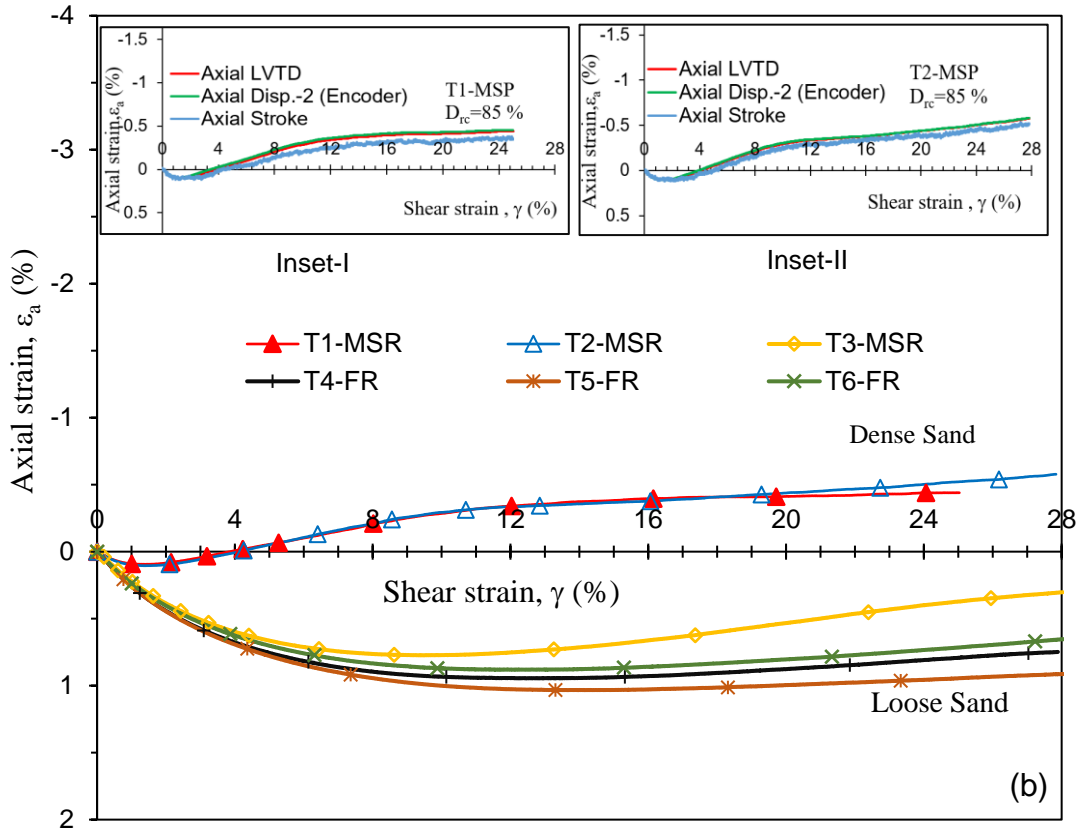


Fig. 5.3. Constant stress tests on loose and dense repeatable samples: (a) stress–strain behaviour; (b) volume change behaviour

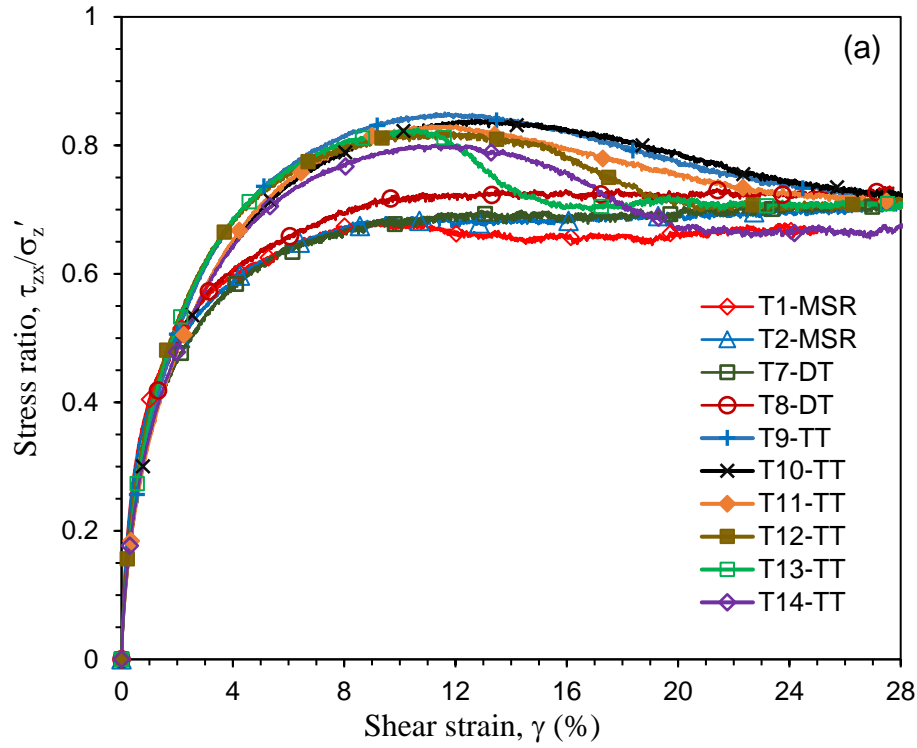


Fig. 5.4. Effects of sample preparation: (a) stress–strain behaviour; (b) volume change behaviour

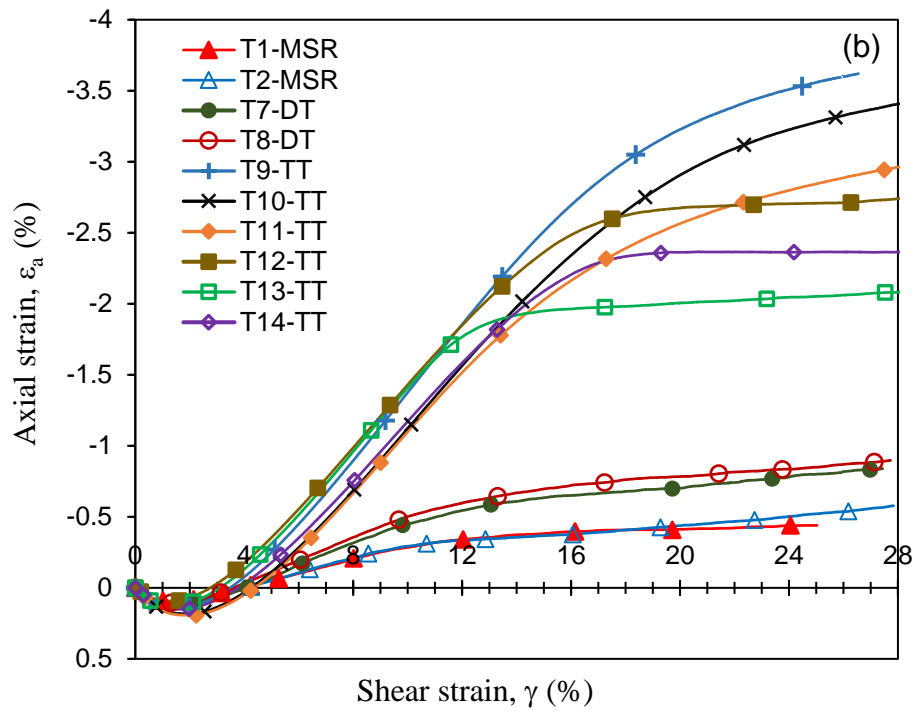


Fig. 5.4. Effects of sample preparation: (a) stress–strain behaviour; (b) volume change behaviour

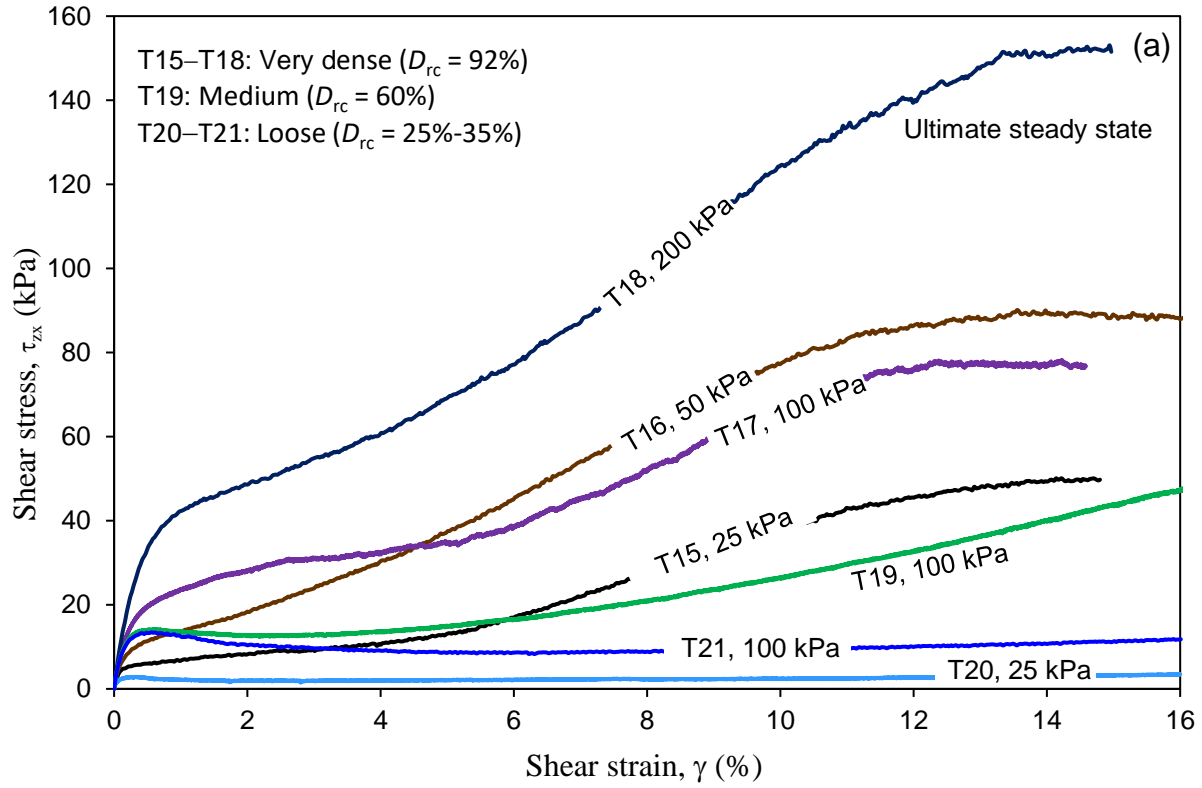


Fig. 5.5. Constant height tests: (a) Stress–strain behaviour; (b) Normalized stress–strain behaviour; (c) Variation of stress ratio of very dense specimens prepared by dry tamping and table tapping; (d) Stress path

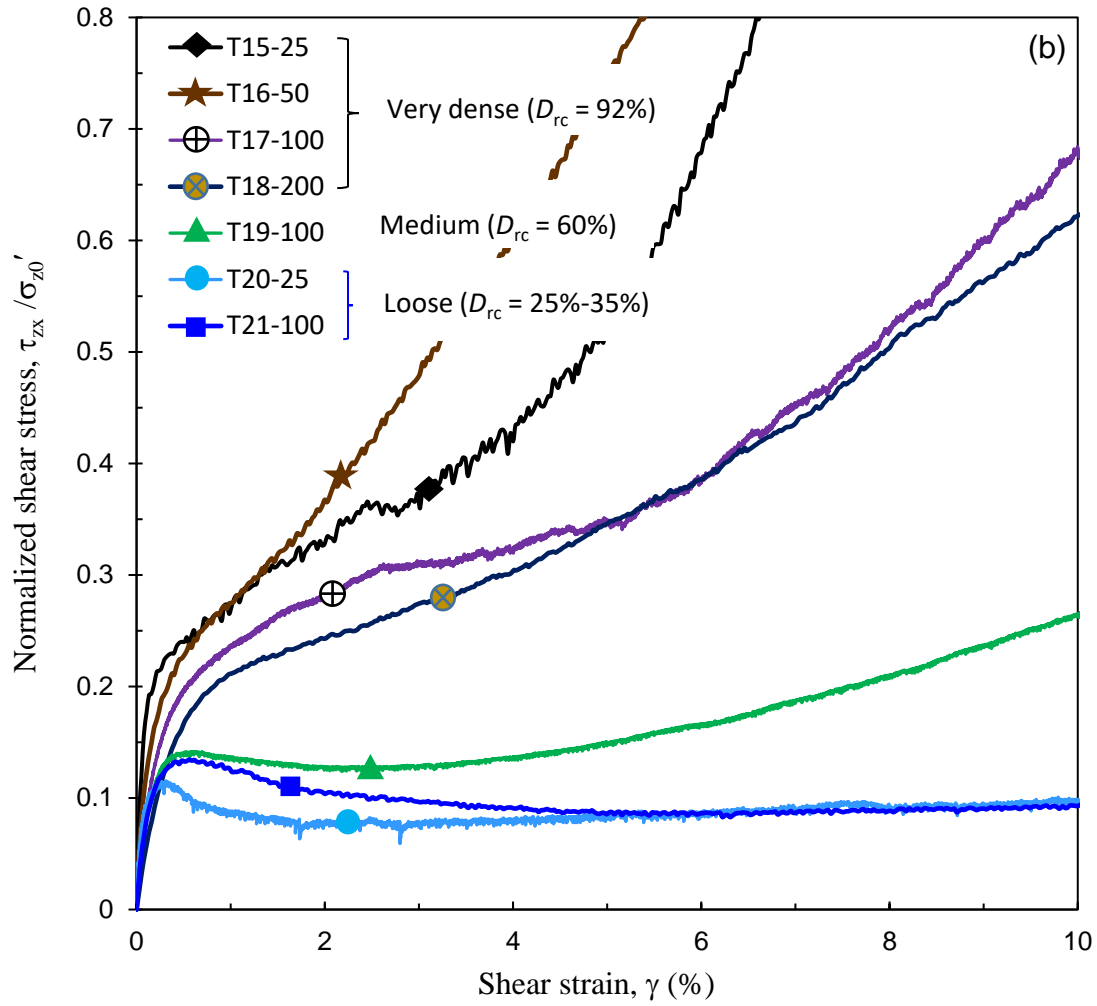


Fig. 5.5. Constant height tests: (a) Stress–strain behaviour; (b) Normalized stress–strain behaviour; (c) Variation of stress ratio of very dense specimens prepared by dry tamping and table tapping; (d) Stress path

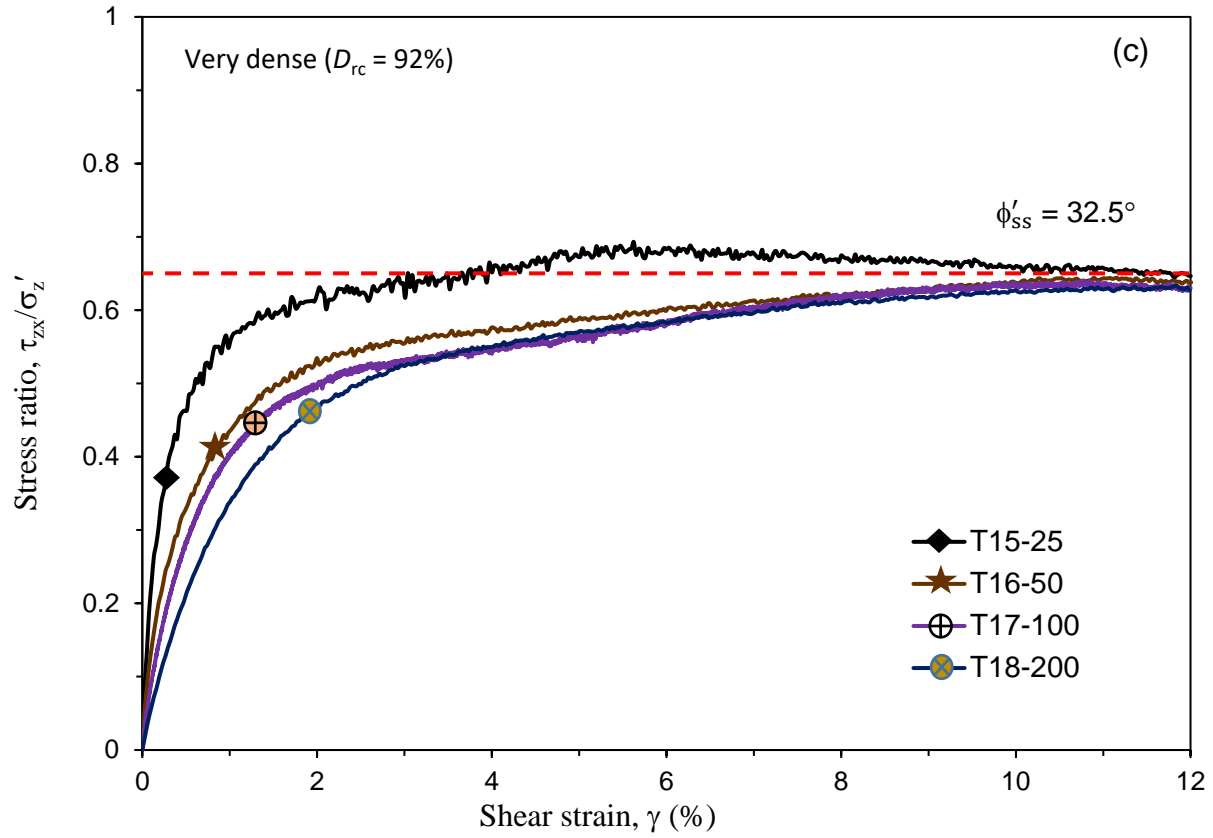


Fig. 5.5. Constant height tests: (a) Stress–strain behaviour; (b) Normalized stress–strain behaviour; (c) Variation of stress ratio of very dense specimens prepared by dry tamping and table tapping; (d) Stress path

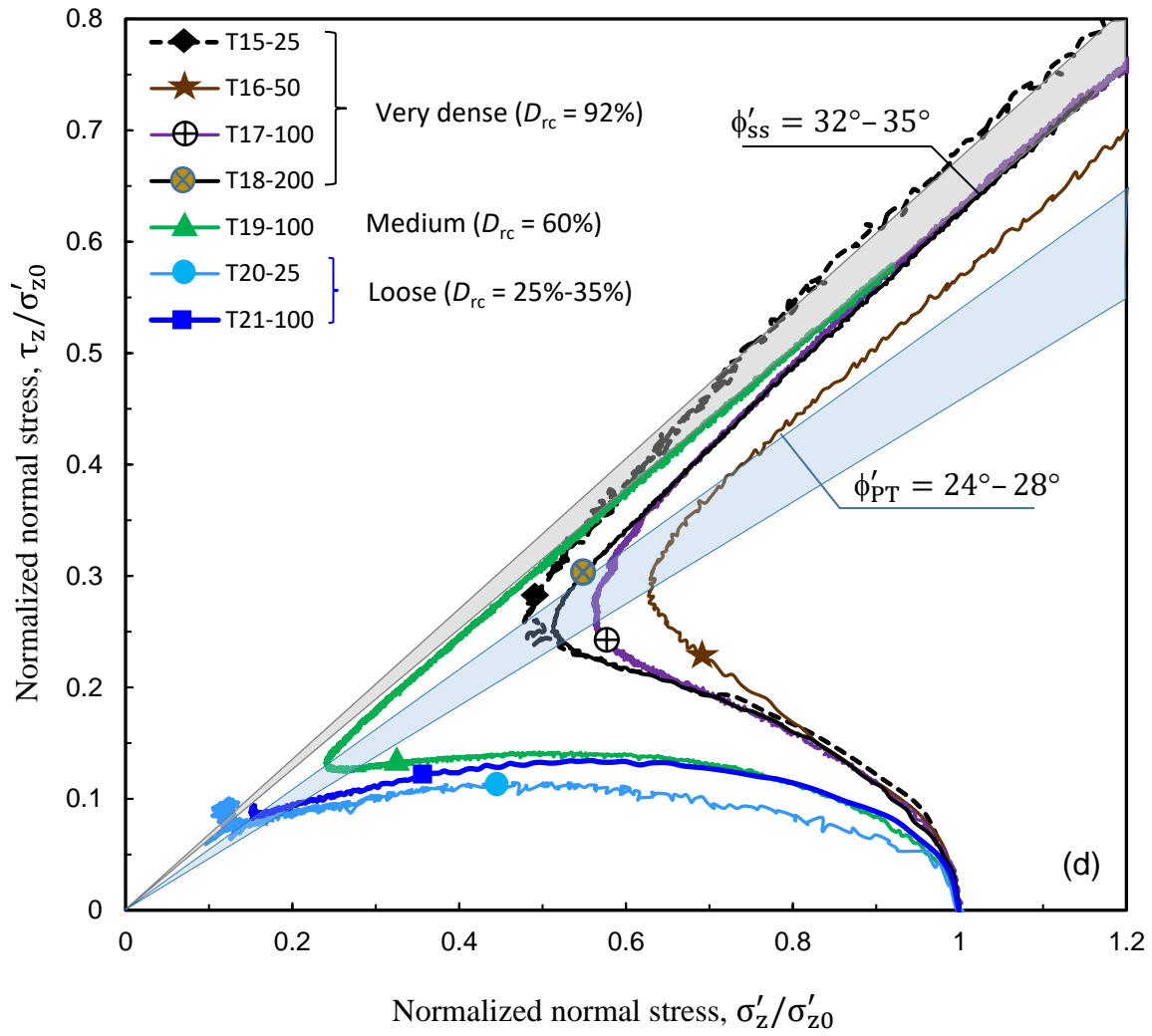


Fig. 5.5. Constant height tests: (a) Stress–strain behaviour; (b) Normalized stress–strain behaviour; (c) Variation of stress ratio of very dense specimens prepared by dry tamping and table tapping; (d) Stress path

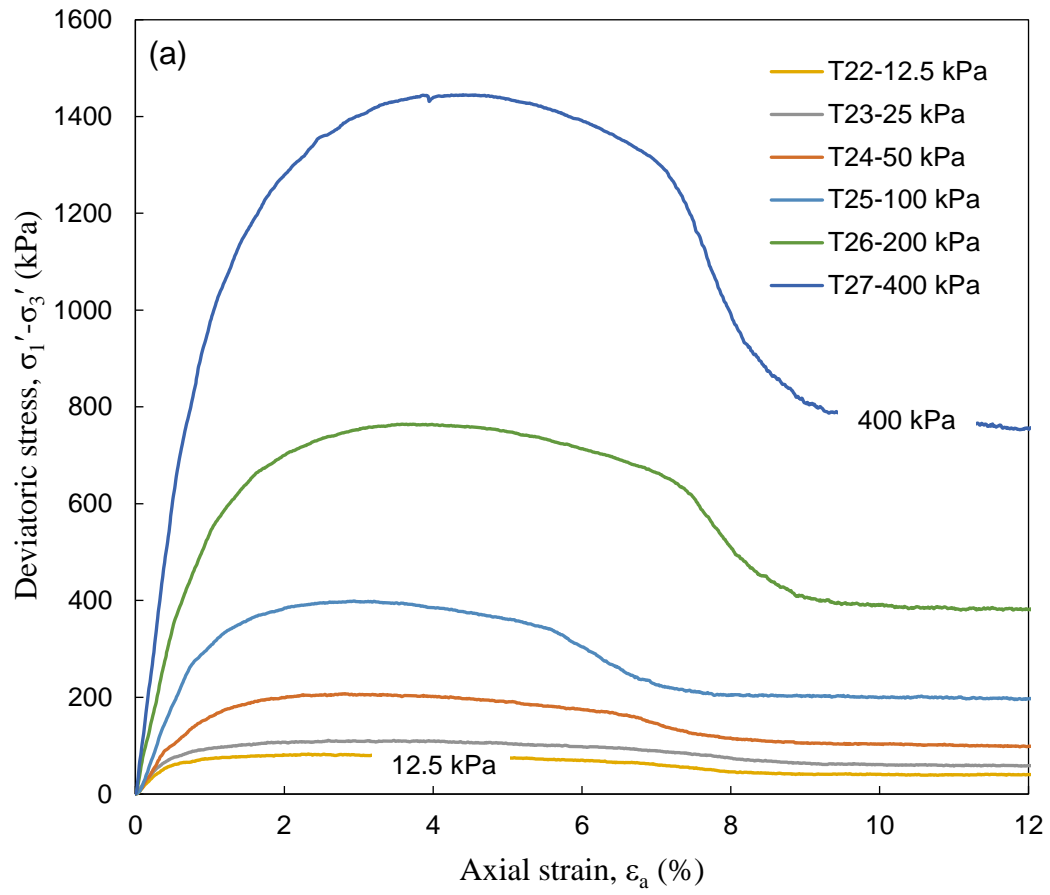


Fig. 5.6. Drained triaxial test results: (a) Stress–strain behaviour; (b) Stress ratio; (c) volume change

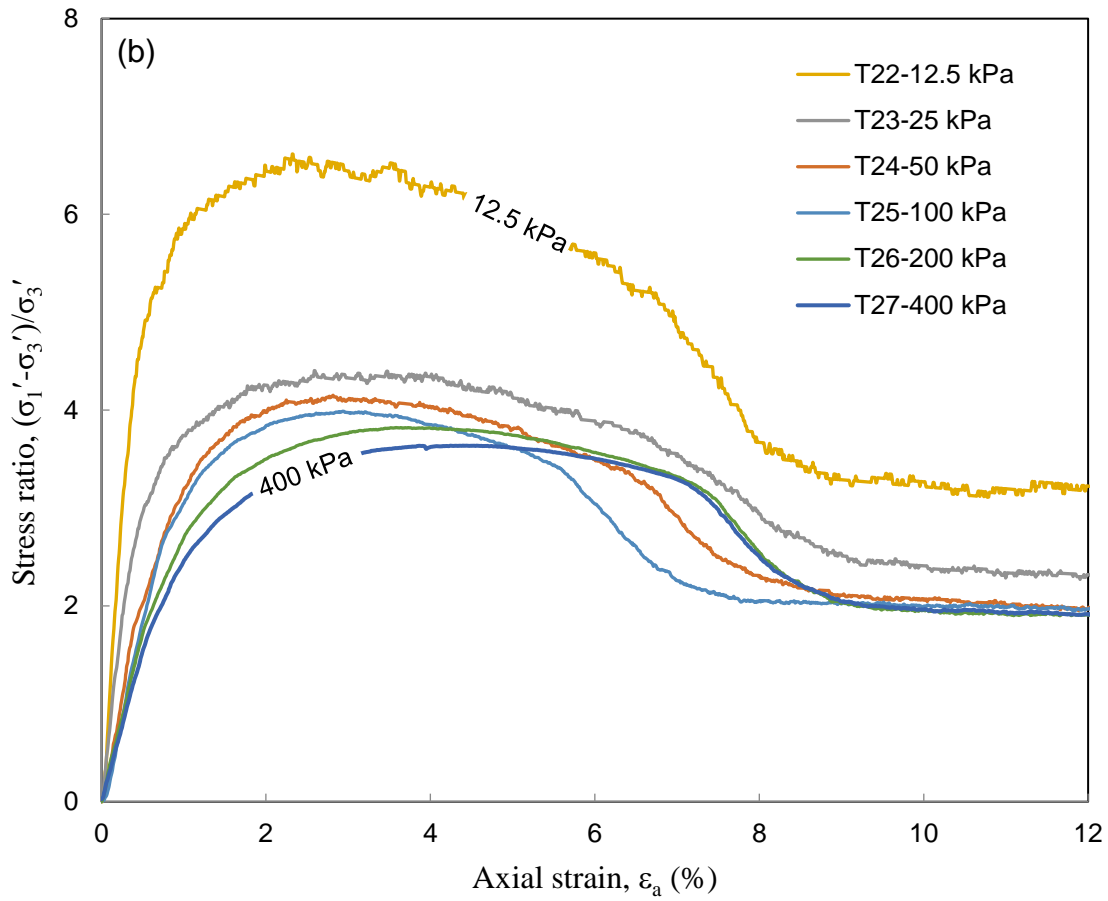


Fig. 5.6. Drained triaxial test results: (a) Stress–strain behaviour; (b) Stress ratio; (c) volume change

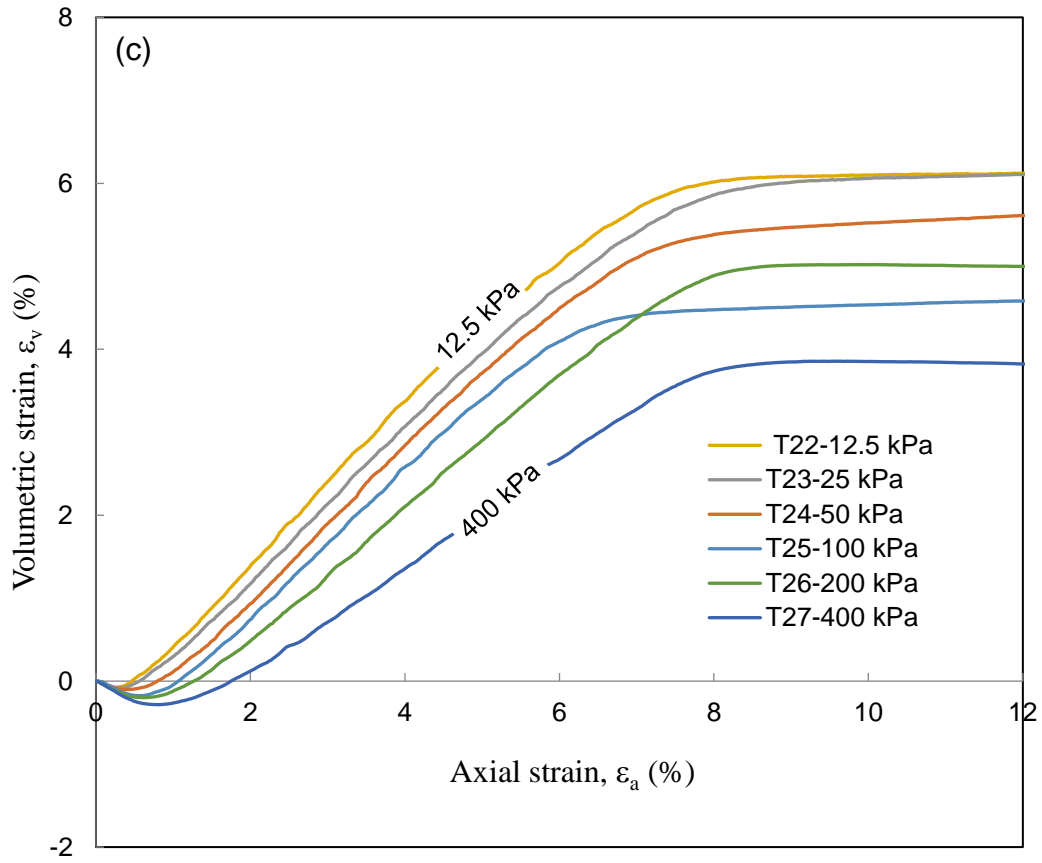


Fig. 5.6. Drained triaxial test results: (a) Stress–strain behaviour; (b) Stress ratio; (c) volume change

Table 5.1 Summary of direct simple shear and triaxial test conditions

Test no.	Consolidation pressure (kPa)	Relative density after consolidation, D_{rc} (%)	Specimen preparation methods
a) Constant stress DSS			
T1		85 ± 1	
T2	80		Multiple- sieve raining
T3		40	
T4			
T5	80	38 ± 2	Funnel raining
T6			
T7		78	
T8	80		Dry tamping
T9			
T10			
T11	80	80 ± 2	Table tapping
T12			
T13			
T14			

b) Constant height DSS

T15	25		
T16	50	92	Dry tamping & Table tapping
T17	100		
T18	200		
T19	100	60	Dry tamping
T20	25	25	Funnel raining
T21	100	35	Funnel raining

c) Drained triaxial compression

T22	12.5		
T23	25		
T24	50	85 ± 2	Dry Tamping
T25	100		
T26	200		
T27	400		

CHAPTER 6

Conclusions and Recommendations for Future Research

6.1 Conclusions

Sand might be subjected to various types of loading—from monotonic to cyclic loading, at a wide range of amplitudes, frequencies and durations under drained and undrained conditions. Geotechnical properties of sand are generally obtained from laboratory tests on reconstituted samples because of difficulties in collecting undisturbed sand samples from the field. The process of deposition and methods of compaction might give a different fabric in sand in the field. Also, in the field, sometimes the effective stress could be very low, in the order of 10–30 kPa, such as for the soil around the buried pipelines and near the seabed. Therefore, the monotonic and cyclic behaviour of sand at a low-stress level is required.

The aim of this research is to advance the understanding of the monotonic and cyclic behaviour of sand at a low-stress level. A new simple shear apparatus called Combined Advanced Dynamic Cyclic Simple Shear (ADVDCSS), which was supplied by GDS Instruments Ltd. and developed for Memorial University of Newfoundland (Canada), is used to conduct experiments. The apparatus has a high-precision feedback system for controlling and measuring forces and displacements while maintaining a high level of accuracy.

The general conclusions of the entire thesis are presented in this section. The problem-specific conclusions are presented in each chapter (Chapters 3–5).

Chapter 3 presents the monotonic and cyclic test results of sand under constant stress simple shear loading. Tests were conducted for a wide range of normal stresses and the response at low-stress

level is compared with that at the typical stress level used in laboratory tests. The monotonic testing result demonstrates that the peak and critical state friction angle increase with the decrease in normal stress, especially when the normal stress is less than 50 kPa. Less significant effects of normal stress on the critical state friction angle in the tests on loose sand and the steady-state friction angle in constant height tests are found. In monotonic DSS tests on dense sand, the dilation angle decreases with an increase in normal stress. The dilation angle also decreases with shear strain (γ) after the peak; however, ψ is not always zero at the typical large strain generally applied in laboratory tests (e.g., $\gamma = 20\%$), although it is small ($\psi < 2^\circ$). The cyclic test results showed that cyclic compaction occurs when the applied shear strain amplitude is greater than the threshold value, γ_{tv} . Although a clear relation was not found from the limited number of tests, γ_{tv} at high normal stress is larger. Magnitude of cyclic compaction is significantly influenced by normal stress, especially at a low-stress level. In strain-controlled (constant strain amplitude) tests, cyclic compaction decreases with the increase in normal stress. However, the opposite trend is found for stress-controlled (constant stress amplitude) tests. Axial strain at 15 cycles can be expressed as a power function of shear strain amplitude. An approximate loglinear relation exists between normalized axial strain at 15 cycles ($\varepsilon_{z,15}$) and number of cycles (N). However, it is nonlinear at low and high cycles, depending upon normal stress and shear strain amplitude.

The results of Chapter 4 contribute to the understanding of the factors that influence the cyclic stress–strain behaviour, dynamic properties and cyclic stress–dilatancy relationship of sand. Tests were conducted on dry sand specimens by stress- and strain-controlled loading. Multi-stage and single-stage tests were performed under a wide range of shear strain amplitudes to understand the effects of the strain history on the cyclic behaviour of sand. The results show that the stress ratio–strain behaviour for low and high-stress levels are different at various shear strain amplitudes—

the stress ratio increases with decreases in the stress level. The shape of the hysteresis loops for both levels is also different, which affects the damping ratio. The dynamic properties are highly influenced by the stress level and shear strain amplitude, and less influenced by the strain history. The shear modulus increases with a decrease in the cyclic shear strain amplitude. For a given shear strain amplitude, the damping ratio increases with a reduction of the stress level, but the opposite trend is seen for the shear modulus. The damping ratio is more affected by the strain history than the shear modulus. However, this dependency increases at a low-stress level. The axial strain generation due to cyclic loading could involve both compaction and dilation at the same cycle, depending upon the shear strain amplitude and cyclic loading history of the soil element. In multi-stage tests on medium dense and dense sand, the axial strain increases with shear strain amplitude and becomes almost flat for a low-stress level at lower γ_a compared to the high stress level. However, the effects of strain history on the axial strain were not significant in dense sand. The stress–dilatancy relationships produced by the cyclic constant stress direct simple shear test in this study show excellent agreement with the experimental results available in the literature, using the hollow cylinder torsional simple shear test. For a conventional stress level ($\sigma'_z = 100$ kPa), after a few cycles, the cyclic stress ratio–dilatancy relationships generally consist of two inclined parallel segments and two nearly vertical segments. However, the stress ratio–dilatancy relationships of the first few cycles are different.

Chapter 5 presents the effects of confining stress and sample preparation methods on the behaviour of direct simple shear (DSS) and triaxial tests (TXC). The stress–strain behaviour of loose and dense sands in direct simple shear (DSS) and triaxial compression (TXC) is investigated. In the present study, constant stress (drained) direct simple shear tests were conducted on silica sand samples prepared by four different methods: funnel raining (FR), multiple-sieve raining (MSR),

dry tamping (DT) and table tapping (TT). In addition, constant height (undrained) DSS and triaxial compression (TXC) tests were performed to compare the soil parameters obtained from different modes of shearing. The experimental program covers a wide range of confining pressures, including low stresses. The constant stress DSS test results show that the repeatable dense samples prepared by table tapping give similar response until the peak; however, the stress–strain curves are somewhat different at large strains. The samples prepared by table tapping show a stronger behaviour than the samples prepared by the other three methods. The former one shows a peak stress ratio, while in the latter three, the shear stress continuously increases with shear strain. In constant stress DSS tests, at given effective stress levels, the stress ratio at a large shear strain is almost the same and is independent of the sample preparation method. Considerable initial contractive followed by dilative behaviour has been observed in the constant height DSS tests on medium to very dense sand specimens. The phase transformation and ultimate steady-state lines in the stress space change by 3° – 4° due to specimen preparation methods, relative density, and the initial consolidation pressure. The steady-state friction angle slightly increases (up to 4°) in low-stress level tests. Post-peak softening is more pronounced in the drained triaxial compression tests than in DSS tests. A clear constant volume/critical state condition is achieved at a relatively small shear strain in TXC as compared to the drained DSS tests.

In terms of practical applications, the findings of this research will help better understand the monotonic and cyclic behaviour of sand at a low-stress level. One of the principal findings of this research is that the monotonic and cyclic behaviour of sand at low- and high-stress levels might be considerably different. The influence of the stress level on cyclic behaviour was not fully understood, and contradictory results were found in previous studies. This study would also help

to estimate geotechnical parameters, such as friction angle and dilation angle, for geotechnical problems at low-stress levels, such as for shallow buried pipelines.

6.2 Recommendations for Future Studies

This study primarily presents the direct simple shear test results. The apparatus used in this study has a wide range of capacities, including the ability to conduct monotonic and cyclic tests in triaxial mode and bender element tests for soil properties at low strain levels. Tests could also be done for these conditions and then constitutive models could be developed for three-dimensional loading conditions, incorporating the low to high stress and strain behaviour.

One of the major challenges is the interpretation of the direct simple shear test results, because the lateral stresses on the vertical face are not known. Numerical simulations could be performed to identify the effects of the stress change on this surface during shearing and the resulting non-uniformities in stresses and strains.

Additional comprehensive experimental studies are required to investigate the influence of sand type, relative density and initial static shear stress on the cyclic behaviour.

REFERENCES

- Adams, R.K., 2017. *Near-surface response of beach sand: An experimental investigation*. Master's Thesis, Oregon State University, Oregon, USA.
- Al Tarhouni, M., Fouzder, A., Hawlader, B., and Dhar, A., 2017. Direct simple shear and triaxial compression tests on dense silica sand at low effective stress. *GeoOttawa 70th Canadian Geotechnical Conference*, Ottawa, Canada, Oct. 1–4, 7p.
- Al Tarhouni, M., Hawlader, B., Fouzder, A., and Dhar, A., 2019. Dynamic behaviour of dry sand in simple shear loading at a wide range of normal stresses. *GeoSt.John's, 72nd Canadian Geotechnical Conference*, St. John's, Canada, Sep. 29–Oct. 2, 7p.
- Alarcon-Guzman, A., Chameau, J.L. Leonards, G.A., and Frost, J.D., 1989. Shear modulus and cyclic undrained behavior of sands. *Soils and Foundations*, 29(4): 105–119.
- Alshibli, K.A., Batiste, S.N., and Sture, S., 2003. Strain localization in sand: plane strain versus triaxial compression. *Journal of Geotechnical and Geoenvironmental Engineering*, 129(6): 483–494.
- Al-Tarhouni, M., Simms, P., and Sivathayalan, S., 2011. Cyclic behaviour of reconstituted and desiccated–rewet thickened gold tailings in simple shear. *Canadian Geotechnical Journal*, 48(7): 1044–1060.
- Amer, M.I., Aggour, M.S., and Kovacs, W.D., 1986. Testing using a large-scale cyclic simple shear device. *Geotechnical Testing Journal*, 9(3): 140–146.
- Andersen, K.H., 2009. Bearing capacity under cyclic loading—offshore, along the coast, and on land. The 21st Bjerrum Lecture presented in Oslo, 23 November 2007. *Canadian Geotechnical Journal*, 46(5): 513–535.

- Ao, Y., Kodikara, J., and Robert, D., 2014. Cyclic direct simple shear test on soft clay at low normal stress-As applicable to offshore pipeline axial walking problems. Proceedings of the 8th Australasian Congress on Applied Mechanics (ACAM 8), Melbourne, Australia, 24–28 November. 519–528.
- Arshad, M., and O’Kelly, B.C., 2013. Offshore wind-turbine structures: a review. *Proceedings of the Institution of Civil Engineers-Energy*, 166(4): 139–152.
- ASTM D7181-20.2020. Standard Test Method for Consolidated Drained Triaxial Compression Test for Soils. *ASTM International*. 12.
- Atkinson, J.H., Lau, W.H.W., and Powell, J.J.M., 1991. Measurement of soil strength in simple shear tests. *Canadian Geotechnical Journal*, 28(2): 255–262.
- Been, K., Jefferies, M.G., and Hachey, J., 1991. The critical state of sands. *Géotechnique*, 41(3): 365–381.
- Bernhardt, M.L., Biscontin, G., and O’Sullivan, C., 2016. Experimental validation study of 3D direct simple shear DEM simulations. *Soils and Foundations*, 56(3): 336–347.
- Bjerrum, L., and Landva, A., 1966. Direct simple shear tests on a Norwegian quick clay. *Géotechnique*, 16(1): 1–20.
- Blaker, Ø., and Andersen, K.H., 2019. Cyclic properties of dense to very dense silica sand. *Soils and Foundations*, 59(4): 982–1000.
- Bolton, M.D., 1986. The strength and dilatancy of sands. *Géotechnique*, 36(1): 65–78.
- Bolton, M.D., 1987. Discussion: The strength and dilatancy of sands. *Géotechnique*, 37(2): 219–226.

- Boulanger, R.W., Chan, C.K., Seed, H.B., Seed, R.B., and Sousa, J.B., 1993. A low-compliance bi-directional cyclic simple shear apparatus. *Geotechnical Testing Journal*, 16(1): 36–45.
- Bowman, E.T., and Soga, K., 2003. Creep, ageing and microstructural change in dense granular materials. *Soils and Foundations*, 43(4): 107–117.
- Budhu, M., 1984. Nonuniformities imposed by simple shear apparatus. *Canadian Geotechnical Journal*, 21(1): 125–137.
- Budhu, M., 1985. Lateral stresses observed in two simple shear apparatus. *Journal of Geotechnical Engineering*, 111(6): 698–711.
- Budhu, M., 1988. Failure state of a sand in simple shear. *Canadian Geotechnical Journal*, 25(2): 395–400.
- Budhu, M., and Britto, A., 1987. Numerical analysis of soils in simple shear devices. *Soils and Foundations*, 27(2): 31–41.
- Casagrande, A., 1975. Liquefaction and Cyclic Deformation of Sands; a Critical Review. *Proceedings of the Pan-American Conference on Soil Mechanics and Foundation Engineering*, (5): 79–133.
- Castro, G., 1969. *Liquefaction of sands*. Ph.D. Thesis, Harvard University, Harvard soil mechanics series, 81, Cambridge, Massachusetts, USA.
- Chakraborty, T., and Salgado, R., 2010. Dilatancy and shear strength of sand at low confining pressures. *Journal of Geotechnical and Geoenvironmental Engineering*, 136(3): 527–532.
- Chern, J.-C., 1985. *Undrained response of saturated sands with emphasis on liquefaction and cyclic mobility* (Doctoral dissertation, University of British Columbia).

- Clukey, E.C., Jackson, C.R., Vermersch, J.A., Koch, S.P. and Lamb, W.C., 1989. Natural densification by wave action of sand surrounding a buried offshore pipeline. *In Offshore Technology Conference*. Offshore Technology Conference, January 1989, OTC 6151, 291–300.
- Dabeet, A., 2014. *Discrete element modeling of direct simple shear response of granular soils and model validation using laboratory tests*. Ph.D. Thesis, University of British Columbia. Canada.
- de Josselin de Jong, G., 1988. Elasto–plastic version of the double sliding model in undrained simple shear tests. *Géotechnique*, 38(4): 533–555.
- De Silva, L.I.N., Koseki, J., Wahyudi, S., and Sato, T., 2014. Stress–dilatancy relationships of sand in the simulation of volumetric behavior during cyclic torsional shear loadings. *Soils and Foundations*, 54(4): 845–858.
- DeGregorio, V.B., 1990. Loading systems, sample preparation, and liquefaction. *Journal of Geotechnical Engineering*, 116(5): 805–821.
- DeGroot, D.J., Germaine, J.T., and Ladd, C.C., 1993. The multidirectional direct simple shear apparatus. *Geotechnical Testing Journal*, 16(3): 283–295.
- Dobry, R., Ladd, R. S., Yokel, F. Y., Chung, R. M., and Powell, D., 1982. Prediction of pore water pressure buildup and liquefaction of sands during earthquakes by the cyclic strain method. *National Bureau of Standards Building Science Series 138*, Washington, D.C.
- Doroudian, M., and Vucetic, M., 1995. A direct simple shear device for measuring small-strain behavior. *Geotechnical Testing Journal*, 18(1): 69–85.
- Duku, P.M., Stewart, J.P., Whang, D.H., and Venugopal, R., 2007. Digitally controlled simple shear apparatus for dynamic soil testing. *Geotechnical Testing Journal*, 30(5): 368–377.

- Duku, P.M., Stewart, J.P., Whang, D.H., and Yee, E., 2008. Volumetric strains of clean sands subject to cyclic loads. *Journal of Geotechnical and Geoenvironmental Engineering*, 134(8): 1073–1085.
- Dyvik, R., and Suzuki, Y., 2018. Effect of Volume Change in Undrained Direct Simple Shear Tests. *Geotechnical Testing Journal*, 42(4): 1075–1082.
- Dyvik, R., Berre, T., Lacasse, S., and Raadim, B., 1987. Comparison of truly undrained and constant volume direct simple shear tests. *Géotechnique*, 37(1): 3–10.
- Dyvik, R., Zimmie, T.F., and Floess, C.H.L., 1981. Lateral stress measurements in direct simple shear device. In Laboratory shear strength of Soil. *ASTM International*. ASTM STP 740: 191–206.
- Finn W., Bhatia S., and Pickering D., 1982. The Cyclic Simple Shear Test. In Pande N., and Zienkiewicz O. (Eds), *Soil Mechanics–Transient and Cyclic Loading*. John Wiley & Sons Ltd. Northern Ireland, 583–607.
- Finn, W.D.L, Pickering, D.J., and Bransby, P.L., 1971. Sand liquefaction in triaxial and simple shear tests. *Journal of Soil Mechanics & Foundations Div.*, 97(4): 639–659.
- Franke, E., Kiekbusch, M., and Schuppener, B., 1979. A new direct simple shear device. *Geotechnical Testing Journal*, 2(4): 190–199.
- Frost, J. D., and Park, J. Y., 2003. A Critical Assessment of the Moist Tamping Technique. *Geotechnical Testing Journal, ASTM*, 26(1): 57–70.
- Fukushima, S. and Tatsuoka, F., 1984. Strength and deformation characteristics of saturated sand at extremely low pressures. *Soils and Foundations*, 24(4): 30–48.

- Georgiannou, V.N., Tsomokos, A., and Stavrou, K., 2008. Monotonic and cyclic behaviour of sand under torsional loading. *Géotechnique*, 58(2): 113–124.
- Guo, P., 2008. Modified direct shear test for anisotropic strength of sand. *Journal of Geotechnical and Geoenvironmental Engineering*, 134(9): 1311–1318.
- Guo, P.J., and Stolle, D.F., 2005. On the failure of granular materials with fabric effects. *Soils and Foundations*, 45(4): 1–12.
- Hardin, B.O., and Black, W.L., 1966. Sand stiffness under various triaxial stresses. *Journal of Soil Mechanics & Foundations Div., ASCE*, 92(2): 27–42.
- Hardin, B.O., and Drnevich, V.P., 1972. Shear modulus and damping in soils: design equations and curves. *Journal of Soil Mechanics & Foundations Div.*, 98(sm7).
- Houlsby, G.T., 1991. *How the dilatancy of soils affects their behaviour*. Oxford: University of Oxford, Department of Engineering Science. Soil Mechanics Report No. 121/91, 1189–1202.
- Hsu, C.-C., and Vucetic, M., 2004. Volumetric threshold shear strain for cyclic settlement. *Journal of Geotechnical and Geoenvironmental Engineering*, 130(1): 58–70.
- Hsu, S.T. and Liao, H.-J., 1998. Uplift behaviour of cylindrical anchors in sand. *Canadian Geotechnical Journal*, 35(1): 70–80.
- Ishihara, K., 1993. Liquefaction and flow failure during earthquakes. *Géotechnique*, 43(3): 351–451.
- Ishihara, K., 1996. *Soil Behaviour in Earthquake Geotechnics*, Clarendon Press, Oxford, UK.
- Ishihara, K., and Yamazaki, F., 1980. Cyclic simple shear tests on saturated sand in multi-directional loading. *Soils and Foundations*, 20(1): 45–59.

- Ishihara, K., Tatsuoka, F., and Yasuda, S., 1975. Undrained deformation and liquefaction of sand under cyclic stresses. *Soils and Foundations*, 15(1): 29–44.
- Iwasaki, T., Tatsuoka, F., and Takagi, Y., 1978. Shear moduli of sands under cyclic torsional shear loading. *Soils and Foundations*, 18(1): 39–56.
- Japanese Geotechnical Society (JGS), 2009. Method for cyclic undrained triaxial test on soils, JGS0541-2009. Japan
- Jefferies, M., and Been, K., 2016. *Soil liquefaction: a critical state approach*. Second edition, CRC press. New York.
- Jung, J.K., O'Rourke, T.D., and Olson, N.A., 2013. Uplift soil–pipe interaction in granular soil. *Canadian Geotechnical Journal*, 50(7): 744–753.
- Kang, X., and Kang, G.-G., 2015. Modified monotonic simple shear tests on silica sand. *Journal of Marine Georesources and Geotechnology*, 33(2): 122–126.
- Kang, X., Ge, L., Chang, K.-T., and Kwok, A.O.-L., 2016. Strain-controlled cyclic simple shear tests on sand with radial strain measurements. *Journal of Materials in Civil Engineering*, 28(4): 04015169.
- Kjellman, W., 1951. Testing the shear strength of clay in Sweden, *Géotechnique*, 2(3): 225–232.
- Kokusho, T., 1980. Cyclic triaxial test of dynamic soil properties for wide strain range. *Soils and Foundations*, 20(2): 45–60.
- Kramer, S.L., 1996. *Geotechnical Earthquake Engineering*. Prentice-Hall, New Jersey, USA.
- Kuo, C.Y., and Frost, J.D., 1996. Uniformity evaluation of cohesionless specimens using digital image analysis. *Journal of Geotechnical Engineering*, 122(5): 390–396.

- Ladd, R.S., 1978. Preparing test specimens using undercompaction. *Geotechnical Testing Journal*, 1(1): 16–23.
- Lee, C.-J., 1991. Deformation of sand under cyclic simple shear loading. *Second International Conferences on Recent Advances in Geotechnical Earthquake Engineering and Soil Dynamics*. 13. St. Louis, Missouri. 33–36.
- Lee, K.L., and Seed, H.B., 1967. Drained strength characteristics of sands. *Journal of Soil Mechanics & Foundations Div.*, ASCE, 93(6): 117–141.
- Li, Y., Yang, Y., Yu, H.S., and Roberts, G., 2018. Effect of sample reconstitution methods on the behaviors of granular materials under shearing. *Journal of Testing and Evaluation*, 46(6): 2718–2725.
- Lings, M.L., and Dietz, M.S., 2004. An improved direct shear apparatus for sand. *Géotechnique*, 54(4): 245–256.
- López-Querol, S., and Coop, M.R., 2012. Drained cyclic behaviour of loose Dogs Bay sand. *Géotechnique*, 62(4): 281–289.
- Loukidis, D., and Salgado, R., 2011. Effect of relative density and stress level on the bearing capacity of footings on sand. *Géotechnique*, 61(2): 107–119.
- Miura, S., and Toki, S., 1982. A sample preparation method and its effect on static and cyclic deformation-strength properties of sand. *Soils and Foundations*, 22(1): 61–77.
- Monkul, M.M., Gültekin, C., Gülver, M., Akın, Ö., and Eseller-Bayat, E., 2015. Estimation of liquefaction potential from dry and saturated sandy soils under drained constant volume cyclic simple shear loading. *Soil Dynamics and Earthquake Engineering*, 75: 27–36.

- Mortezaie, A.R., and Vucetic, M., 2012. Small-strain cyclic testing with standard NGI simple shear device. *Geotechnical Testing Journal*, 35(6): 935–948.
- Mulilis, J.P., Arulanandan, K., Mitchell, J.K., Chan, C.K., and Seed, H.B., 1977. Effects of sample preparation on sand liquefaction. *Journal of the Geotechnical Engineering Division*, 103(2): 91–108.
- Mulilis, J.P., Townsend, F.C., and Horz, R.C., 1978. Triaxial testing techniques and sand liquefaction. *Dynamic Geotechnical Testing, American Society for Testing and Materials, ASTM STP 654*. 265–279.
- National Research Council (NRC), 1985. *Liquefaction of soils during earthquakes*. National Academy Press, Washington, D.C., <https://doi.org/10.17226/19275>.
- Nemat-Nasser, S., and Takahashi, K., 1984. Liquefaction and fabric of sand. *Journal of Geotechnical engineering, ASCE*, 110(9): 1291–1306.
- Nikitas, G., Arany, L., Aingaran, S., Vimalan, J., and Bhattacharya, S., 2017. Predicting long term performance of offshore wind turbines using cyclic simple shear apparatus. *Soil Dynamics and Earthquake Engineering*, (92): 678–683.
- Nishimura, S., 2002. *Development of three dimensional stress–strain model of sand undergoing cyclic undrained loading and stress-axes rotation*. M. Eng. thesis. Dept. of Civil Engineering, University of Tokyo, Japan.
- Oda, M., 1972a. Initial fabrics and their relations to mechanical properties of granular material. *Soils and Foundations*, 12(1): 17–36.
- Oda, M., 1972b. The mechanism of fabric changes during compressional deformation of sand. *Soils and Foundations*, 12(2): 1–18.

- Oda, M., 1972c. Deformation mechanism of sand in triaxial compression tests. *Soils and Foundations*, 12(4): 45–63.
- Oda, M., Nemat-Nasser, S., and Konishi, J., 1985. Stress-induced anisotropy in granular masses. *Soils and Foundations*, 25(3): 85–97.
- Oh-oka, H., 1976. Drained and undrained stress-strain behavior of sands subjected to cyclic shear stress under nearly plane strain condition. *Soils and Foundations*, 16(3): 19–31.
- Park, S.-S., Byrne, P.M., and Wijewickreme, D., 2005. A swinging plane model for soil liquefaction analysis. *Proceedings of the 16th International Conference on Soil Mechanics and Geotechnical Engineering*, 845–850.
- Peacock, W.H., and Seed, B., 1968. Sand liquefaction under cyclic loading simple shear conditions. *Journal of Soil Mechanics & Foundations Div.*, 94(3): 689–708.
- Pradhan, T.B., and Tatsuoka, F., 1989. On stress-dilatancy equations of sand subjected to cyclic loading. *Soils and Foundations*, 29(1): 65–81.
- Rad, N.S., and Tumay, M.T., 1987. Factors affecting sand specimen preparation by raining. *Geotechnical Testing Journal*, 10(1): 31–37.
- Ramadan, J.I., 2007. *Settlement of dry cohesionless soil deposits under earthquake induced loading*. Ph.D. Thesis, University of Southern California, California, USA.
- Randolph, M.F., Jamiolkowski, M.B., and Zdravkovic, L., 2004. Load carrying capacity of foundations. *Proc. Skempton Memorial Conf.*, London 1, 207–240.
- Razeghi, H.R., and Romiani, H.M., 2015. Experimental investigation on the inherent and initial induced anisotropy of sand. *KSCE Journal of Civil Engineering*, 19(3): 583–591.

- Riemer, M.F., and Seed, R.B., 1997. Factors affecting apparent position of steady-state line. *Journal of Geotechnical and Geoenvironmental Engineering*, 123(3): 281–288.
- Roscoe, K.H., 1953. An apparatus for the application of simple shear to soil samples. *Proceedings, 3rd International Conference on Soil Mechanics and Foundation Engineering*, Zurich, Switzerland, (1): 186–191.
- Roscoe, K.H., Bassett, R.H., and Cole, E.R.L., 1967. Principal Axes Observed During Simple Shear of a Sand. In *Proceedings of the Geotechnical Conference on Shear Strength Properties of Natural Soils and Rocks*, Oslo, Norway, 19–22 September. 213–237.
- Roscoe, K.H., Schofield, A., and Thurairajah, A., 1963. Yielding of clays in states wetter than critical, *Géotechnique*, 13(3): 211–240.
- Rousé, P.C., 2018. Relation between the critical state friction angle of sands and low vertical stresses in the direct shear test. *Soils and Foundations*, 58(5): 1282–1287.
- Rowe, P.W., 1962. The stress-dilatancy relation for static equilibrium of an assembly of particles in contact. *Proceedings of the Royal Society of London. Series A. Mathematical and Physical Sciences*, London, 269(1339): 500–527.
- Roy, K., Hawlader, B., Kenny, S., and Moore, I., 2016. Finite element modeling of lateral pipeline–soil interactions in dense sand. *Canadian Geotechnical Journal*, 53(3): 490–504.
- Roy, K., Hawlader, B., Kenny, S., and Moore, I., 2018. Upward Pipe–Soil interaction for shallowly buried pipelines in dense sand. *Journal of Geotechnical and Geoenvironmental Engineering*, 144(11): DOI: 10.1061/(ASCE)GT.1943-5606.0001957.
- Rutherford, C.J., and Biscontin, G., 2013. Development of a multidirectional simple shear testing device. *Geotechnical Testing Journal*, 36(6): 858–866.

- Sadrekarimi, A., and Olson, S.M., 2011. Critical state friction angle of sands. *Géotechnique*, 61(9): 771–783.
- Seed, B., 1979. Soil Liquefaction and Cyclic Mobility Evaluation for Level Ground During Earthquakes. *Journal of Geotechnical and Geoenvironmental Engineering, ASCE*, 105(2): 201–255.
- Seed, H.B. and Silver M.L., 1972. Settlement of Dry Sands during Earthquakes. *Journal of the Soil Mechanics & Foundations Div., ASCE*, 98(4): 381–397.
- Shahnazari, H., and Towhata, I., 2001. Prediction of volumetric strain for sand under cyclic loading. *4th International Conference on Recent Advances in Geotechnical Earthquake Engineering and Soil Dynamics*, Missouri University of Science and Technology, December. 13. Paper no. 1.16, 8p.
- Shahnazari, H., and Towhata, I., 2002. Torsion shear tests on cyclic stress-dilatancy relationship of sand. *Soils and Foundations*, 42(1): 105–119.
- Silver, M.L., and Seed, H.B., 1971. Volume changes in sands during cyclic loading. *Journal of Soil Mechanics & Foundations Div., ASCE*, 97(9): 1171–1182.
- Silver, M.L., Tatsuoka, F., Phukunhaphan, A., and Avramidis, A.S., 1980. Cyclic undrained strength of sand by triaxial test and simple shear test. In *Proceedings of the 7th World Conference on Earthquake Engineering*, 281–288.
- Sivathayalan, S., and Ha, D., 2011. Effect of static shear stress on the cyclic resistance of sands in simple shear loading. *Canadian Geotechnical Journal*, 48(10): 1471–1484.

- Stephenson, R.W., Stringer, S.K., and Sutterer, K., 1991. The influence of large prestrains on dynamic properties of sand. *Second International Conferences on Recent Advances in Geotechnical Earthquake Engineering and Soil Dynamics*. Louis, Missouri, 1921–1926.
- Stroud, M.A., 1971. *The behaviour of sand at low stress levels in simple shear apparatus*. Ph.D. Thesis, University of Cambridge, Cambridge, England.
- Sze, H.Y., and Yang, J., 2014. Failure modes of sand in undrained cyclic loading: impact of sample preparation. *Journal of Geotechnical and Geoenvironmental engineering*, 140(1): 152–169.
- Tatsuoka, F., Iwasaki, T., and Takagi, Y., 1978. Hysteretic damping of sands under cyclic loading and its relation to shear modulus. *Soils and Foundations*, 18(2): 25–40.
- Tatsuoka, F., Iwasaki, T., Fukushima, S., and Sudo, H., 1979. Stress conditions and stress histories affecting shear modulus and damping of sand under cyclic loading. *Soils and Foundations*, 19(2): 29–43.
- Tatsuoka, F., Ochi, K., Fujii, S., and Okamoto, M., 1986. Cyclic undrained triaxial and torsional shear strength of sands for different sample preparation methods. *Soils and Foundations*, 26(3): 23–41.
- Taylor, D., 1948. *Fundamentals of soil mechanics*. Chapman and Hall, Limited., New York.
- Terzaghi, K., Peck, R.B., and Mesri, G., 1996. *Soil mechanics in engineering practice*. Second edition, John Wiley & Sons, Inc.
- Thomas, J., 1992. *Static, cyclic and post liquefaction undrained behaviour of Fraser River sand*. Master's Thesis, University of British Columbia, Vancouver, Canada, 117.
- Tokimatsu, K., and Seed, H.B., 1987. Evaluation of settlements in sands due to earthquake shaking. *Journal of Geotechnical Engineering*, 113(8): 861–878.

- Tong, Z., Fu, P., Zhou, S., and Dafalias, Y.F., 2014. Experimental investigation of shear strength of sands with inherent fabric anisotropy. *Acta Geotechnica*, 9(2): 257–275.
- Tong, Z.-X., Zhang, J.-M., Yu, Y.-L., and Zhang, G., 2010. Drained deformation behavior of anisotropic sands during cyclic rotation of principal stress axes. *Journal of Geotechnical and Geoenvironmental Engineering*, 136(11): 1509–1518.
- Ueng, T.-S., and Lee, C.-J., 1990. Deformation behavior of sand under shear—particulate approach. *Journal of Geotechnical Engineering*, 116(11): 1625–1640.
- Uthayakumar, M., 1992. *Dynamic properties of sands under cyclic torsional shear*. Ph.D. Thesis, University of British Columbia, Canada.
- Uthayakumar, M., and Vaid, Y.P., 1998. Static liquefaction of sands under multiaxial loading. *Canadian Geotechnical Journal*, 35(2): 273–283.
- Vaid, Y.P. and Chern, J.C., 1985. Cyclic and monotonic undrained response of saturated sands, *Proc. Advances in the art of testing soils under cyclic loading conditions*, Detroit, 120–147.
- Vaid, Y.P., and Finn, W.D.L., 1979. Static shear and liquefaction potential. *Journal of Geotechnical and Geoenvironmental Engineering*, 105(ASCE 14909 Proc Paper), 105(GT10):1233.
- Vaid, Y.P., and Negussey, D., 1984. Relative density of pluviated sand samples. *Soils and Foundations*, 24(2): 101–105.
- Vaid, Y.P., and Negussey, D., 1988. Preparation of Reconstituted Sand Specimens. *Advanced Triaxial Testing of Soil and Rock*, ASTM STP 977, R. Donaghe, R. Chaney, and M. Silver, Eds., ASTM International, 405–417.

- Vaid, Y.P., and Sivathayalan, S., 1996. Static and cyclic liquefaction potential of Fraser Delta sand in simple shear and triaxial tests. *Canadian Geotechnical Journal*, 33(2): 281–289.
- Vaid, Y.P., and Sivathayalan, S., 2000. Fundamental factors affecting liquefaction susceptibility of sands. *Canadian Geotechnical Journal*, 37(3): 592–606.
- Vaid, Y.P., Byrne, P.M., and Hughes, J.M.O., 1981. Dilation angle and liquefaction potential. *First International Conferences on Recent Advances in Geotechnical Earthquake Engineering & Soil Dynamics*. 3. Apr 26th - May 3rd. St. Louis, Missouri, USA. 161–165.
- Vaid, Y.P., Chung, E. K. F., and Kuerbis, R. H., 1990. Stress path and steady state. *Canadian Geotechnical Journal*, 27(1): 1–7.
- Vaid, Y.P., Sivathayalan, S., and Stedman, D., 1999. Influence of specimen-reconstituting method on the undrained response of sand. *Geotechnical Testing Journal*, 22(3): 187–195.
- Vaid, Y.P., Uthayakumar, M., Sivathayalan, S., Robertson, P.K., and Hofmann, B., 1995. Laboratory testing of Syncrude sand. In *Proceedings of the 48th Canadian Geotechnical Conference, 25–27 Sep. 1995, Vancouver*, (1): 223–232.
- Vucetic, M., 1994. Cyclic threshold shear strains in soils. *Journal of Geotechnical engineering*, 120(12): 2208–2228.
- Vucetic, M., Lanzo, G., and Doroudian, M., 1998. Damping at small strains in cyclic simple shear test. *Journal of Geotechnical and Geoenvironmental Engineering*, ASCE, 124(7): 585–594.
- Wahyudi, S., and Koseki, J., 2012. Stress-dilatancy characteristics of sand in drained cyclic torsional shear tests, *Institute of Industrial Science, University of Tokyo Japan, Bulletin of ERS*, No. 40. 131–140.

- Wahyudi, S., Chiaro, G., De Silva, L.I.N, and Koseki, J., 2010. Stress-dilatancy behavior of loose sand during drained cyclic torsional shear loading, *12th International Summer Symposium of JSCE*, Tokyo, Japan. 183–186.
- Wan, R.G., and Guo, P.J., 2001. Effect of microstructure on undrained behaviour of sands. *Canadian Geotechnical Journal*, 38(1): 16–28.
- White, D.J., Cheuk, C.Y., and Bolton, M.D., 2008. The uplift resistance of pipes and plate anchors buried in sand. *Géotechnique*, 58(10): 771–779.
- Wichtmann, T., and Knittel, L., 2020. Behaviour of Granular Soils Under Uni-and Multidimensional Drained High-Cyclic Loading. In *Recent Developments of Soil Mechanics and Geotechnics in Theory and Practice*, Springer, Cham, 136–165.
- Wijewickreme, D., Dabeet, A., and Byrne, P., 2013. Some observations on the state of stress in the direct simple shear test using 3D discrete element analysis. *Geotechnical Testing Journal*, 36(52): 1–8.
- Wijewickreme, D., Sriskandakumar, S., and Byrne, P., 2005. Cyclic loading response of loose air-pluviated Fraser River sand for validation of numerical models simulating centrifuge tests. *Canadian Geotechnical Journal*, 42(2): 550–561.
- Wu, Z.-X., Yin Z.-Y., Dano C., and Hicher P.-Y., 2020. Cyclic volumetric strain accumulation for sand under drained simple shear condition. *Applied Ocean Research*, 101(2020): 102200. <https://doi.org/10.1016/j.apor.2020.102200>.
- Yamamuro, J.A., and Wood, F.M., 2004. Effect of depositional method on the undrained behavior and microstructure of sand with silt. *Soil Dynamics and Earthquake Engineering*, 24(9-10): 751–760.

- Yamashita, S., and Toki, S., 1993. Effects of fabric anisotropy of sand on cyclic undrained triaxial and torsional strengths. *Soils and Foundations*, 33(3): 92–104.
- Yang, L.-T., Li, X., Yu, H.-S., and Wanatowski, D., 2016. A laboratory study of anisotropic geomaterials incorporating recent micromechanical understanding. *Acta Geotechnica*, 11(5): 1111–1129.
- Yang, Z.X., Li, X.S., and Yang, J., 2008. Quantifying and modelling fabric anisotropy of granular soils. *Géotechnique*, 58(4): 237–248.
- Yee, E., Stewart, J.P., and Duku, P.M., 2012. Seismic compression behavior of sands with fines of low plasticity. In *GeoCongress 2012: State of the Art and Practice in Geotechnical Engineering*, ASCE, 839–848.
- Yoshimine, M., and Ishihara, K., 1998. Flow potential of sand during liquefaction. *Soils and Foundations*, 38(3): 189–198.
- Yoshimine, M., Ishihara, K., and Vargas, W., 1998. Effects of principal stress direction and intermediate principal stress on undrained shear behavior of sand. *Soils and Foundations*, 38(3): 179–188.
- Yoshimine, M., Robertson, P.K., and Wride, C.E., 1999. Undrained shear strength of clean sands to trigger flow liquefaction. *Canadian Geotechnical Journal*, 36(5):891–906.
- Youd, L.T., and Craven, T.N., 1975. Lateral stress in sands during cyclic loading. *Journal of Geotechnical Engineering Division*, ASCE, 101(2): 217–221.
- Youd, T.L., 1972. Compaction of sands by repeated shear straining. *Journal of Soil Mechanics & Foundations Div.*, 98(SM7): 709–725.

Zimmie, T.F., and Floess, C.H., 1979. *Simple Shear Behavior of Fine Grained Soils Subjected to Earthquake and Other Repeated Loading*. Department of Civil Engineering, Rensselaer Polytechnic Institute. New York. Report No. NSF/RA-790094. 132 p.